Biological applications of designed hairpin peptides: as antimicrobials and as inhibitors of amyloidogenesis

Kalkena Sivanesam

A dissertation
submitted in partial fulfillment of the
requirements for the degree of

Doctor of Philosophy

University of Washington
2017

Reading Committee:
Niels H. Andersen, Chair
Pradipsinh K. Rathod
Stefan Stoll

Program authorized to offer degree:
Department of Chemistry

University of Washington

Abstract

Biological Applications of Designed Hairpin Peptides: As antimicrobials and as inhibitors of amyloidogenesis

Kalkena Sivanesam

Chair of Supervisory Committee:

Professor Niels H. Andersen

Department of Chemistry

More than 40 diseases have been associated with the misfolding of peptides (or proteins) that form fibrils with a very specific morphology. These peptides classified as amyloidogenic peptides have been implicated in the development of Alzheimer's Disease, Parkinson's Disease, Type II Diabetes, Hungtinton's Disease etc. To date, these diseases have no cure, only therapies that can ameliorate the symptoms to a degree. Inhibition of the amyloidogenesis of these peptides has been proposed as a possible treatment option. While small molecules have been heavily tested as inhibitors of amyloidogenesis, peptides have emerged as potential inhibitors. In this work, the ability of a set of designed hairpin peptides to inhibit the amyloidogenesis of two different systems, α-synuclein (implicated in Parkinson's Disease) and human amylin (implicated in Type II Diabetes) is tested. Using circular dichroism and thioflavin T fluorescence, the ability of these peptides to inhibit amyloidogenesis is tested. The binding loci of these inhibitors to α-synuclein are also explored.

The use of peptides as antimicrobials on the other hand is not a novel concept. However, most antimicrobial peptides, both natural and designed, rely heavily on covalent stabilizations in order

to maintain secondary structure. In this study, non-covalent stabilizations are applied to a couple of natural as well as designed antimicrobials in order to study the effects of secondary structure stabilization on biological activity.

Table of Contents

List of Figures

List of Tables

List of Abbreviations

AMP: AntiMicrobial Peptide

CD: Circular Dichroism

CSD: Chemical Shift Deviation

DMF: DiMethyl Formamids

DSS: 2,2-Dimethyl-Silapentane-5-Sulfonic acid

EtF: Edge-to-Face

Fmoc: Fluorenylmethyloxycarbonyl

FTIR: Fourier Transform Infrared Spectroscopy

Gdn.HCl: Guanidinium Hydrochloride

hAM: Human Amylin

HFIP: Hexafluoroisopropanol

HPLC: High Performance Liquid Chromatography

HSQC: Heteronuclear Single Quantum Coherence

IAPP: Islet Amyloid PolyPeptide

MD: Molecular Dynamics

NAC: Non-Amyloid Component

NMR: Nuclear Magnetic Resonance

NOESY: Nuclear Overhauser Spectroscopy

PD: Parkinson's Disease

T2D: Type II Diabetes

TEM: Transmission electron microscopy

TFA: trifluoroacetic acid

ThT: Thioflavin T

TOCSY: Total Correlation Spectroscopy

UV-Vis: UltraViolet-Visible Spectroscopy

α-syn: alpha-synuclein

List of Publications

The following is a list of papers based on some of the research presented in this dissertation:

Sivanesam, K., Byrne, A., Bisaglia, M., Bubacco, L. & Andersen, N. (2015) Binding interactions of agents that alter α-synuclein aggregation. *RSC Advances*, **5**, 11577–11590.

> The research published in this paper is described in Chapter 3, Sections 3.4.1, 3.4.2, 3.4.3 and 3.4.5.

Sivanesam, K. & Andersen, N.H. (2016) Modulating the Amyloidogenesis of α-Synuclein. *Current Neuropharmacology*, **14**, 226–237.

> The above paper is a review of inhibitors of the amyloidogenesis of α-synuclein. The information presented in this review is also present in Chapter 3, Section 3.2.

Sivanesam, K., Shu, I., Huggins, K.N.L., Tatarek-Nossol, M., Kapurniotu, A. & Andersen, N.H. (2016) Peptide Inhibitors of the amyloidogenesis of IAPP: verification of the hairpin-binding geometry hypothesis. *FEBS letters*, **590**, 2575–2583.

> The research published in this paper is described in Chapter 4, Section 4.4.1.

Sivanesam, K., Kier, B.L., Whedon, S.D., Chatterjee, C. & Andersen, N.H. (2016) Hairpin structure stability plays a role in the activity of two antimicrobial peptides. *FEBS letters*, **590**, 4480–4488.

> The research published in this paper is described in Chapter 4, Section 5.3.1.

Acknowledgements

I consider myself extremely lucky to have had Dr. Niels Andersen as my graduate advisor. His patience and guidance has allowed me to develop as a scientist and his ever positive attitude has helped me soldier on when research results or a lack thereof have been demoralizing. His willingness to explain even simple concepts with care has helped me understand so much more about chemistry. In the end, it will be his youthful spirit and ever inquisitive nature that I will carry with me as I continue down my path as a scientist.

I am also very fortunate to have had the privilege to work with excellent lab mates. Jordan Anderson was instrumental in the early years, teaching me the ropes of peptide synthesis and NMR experiments. Now he serves as the perfect person to run ideas by, be they good or bad. Dr. Brandon Kier, whose enthusiasm for peptides always leaves me smiling, was crucial in coming up with ideas for my antimicrobial project and providing support when my data looked strange. I was also glad to have worked with Dr. Aimee Byrne, who passed on the torch for the amyloidogenesis project and helped me navigate the experiments in the early stages. I have also had the pleasure of working with supportive and helpful lab members, Katherine Graham and Alex Shcherbakov.

My good friends in grad school and my dear family have also been a constant pillar of strength, motivating me to keep going. Finally I would like to thank my husband, Chris Compeggie, for always believing in me, for letting me go crazy and for never giving up. Without you, I would not have made it this far.

Dedication

To my mother, my brother and my husband, the three people in the world I could not live without. Everything I do, I do for you.

Chapter 1: Introduction

1.1 Protein folding

Proteins represent one of the building blocks of life and play a role in almost every reaction in the cell. The activity of proteins depends heavily upon the final structure of the protein, making this characteristic of proteins an important focus of research. Protein structure can be classified into four levels: a) primary structure, the amino acid sequence that makes up the protein, b) secondary structure which arises from the interactions of the amino acids to form local structures such as α-helices, loops, β-turns and β-strands, c) tertiary structure which is a more complex interaction of the various secondary structures within a protein and d) quaternary structure which is only present when multiple domains or proteins interact to form an even more complex structure.

The most important question about protein folding was posed by Levinthal in the late 1960s. Levinthal observed that the sampling of every possible conformational state by a protein would be highly inefficient and is in direct opposition to the speed with which unfolded proteins achieve their native state. His question (how can proteins fold so fast?) known as Levinthal's paradox, has led to a number of theories. The most common of which is the theory that proteins have folding pathways resulting from the cooperating interactions of the secondary and tertiary structures of the proteins. (Dill & Chan, 1997; Bai, 2003) This cooperative pathway limits the conformational space that a protein can sample thus reducing the time taken to reach the native state. The protein folding landscape, represents the configurational entropy of a protein which progressively decreases as the protein samples multiple folded states before finally arriving at the lowest energy state, also known as the native state (Figure 1.1). (Onuchic *et al.*, 1997) Therefore, studying the secondary structure of proteins can reveal valuable information regarding the cooperative folding of proteins.

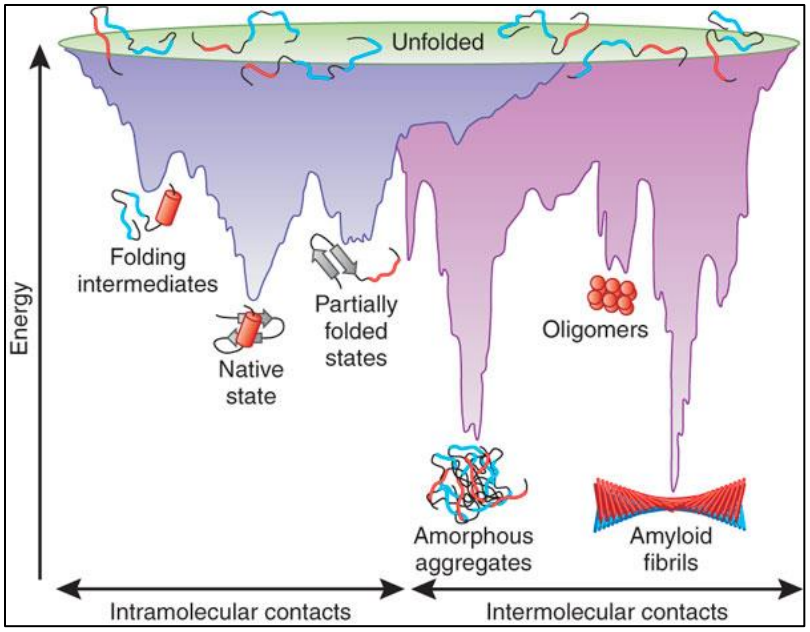

Figure 1.1. Protein folding landscape. The purple "funnel" shows the intramolecular contacts that a protein can make to form the native state. The pink "funnel" shows the potential intermolecular contacts that a protein can make which could lead to misfolding. *(Image adapted from Hartl & Hayer-Hartl, 2009)*

However, the study protein folding is limited by the large number of interactions in each protein that is difficult to elucidate and individual contributions to the final structure is harder to determine. To overcome this problem, research has focused on small peptides that are capable of forming secondary structures such as α-helices and β-turns. Using small peptides, peptide folding timescales can be studied along with the role of specific sequences in the formation of stable secondary structures. These results have led to the improved a priori design of proteins and peptides as well as an increased understanding of the protein folding landscape.

1.1.1. β-hairpin peptides

While the study of α-helices has resulted in much useful information, (Serrano & Fersht, 1989; Andersen & Tong, 1997; Petukhov *et al.*, 2009) including the helical propensities of individual residues outside of the protein context, using β-hairpins as a tool to study the folding pathways of larger proteins has been hampered by their, typically poor, folding once excised from the larger protein. (Blanco *et al.*, 1994; Searle *et al.*, 1995) The lack of stabilizing motifs that are usually

present in larger proteins results in aggregation-prone sequences. (Richardson & Richardson, 2002) In order to overcome this, stabilizing motifs such as disulfide bonds have been used in order to maintain the secondary structure of small β-hairpin peptides.(Kier *et al.*, 2015) However, the dependence on covalent stabilization limits the biomedical application of designed peptides in reductive conditions while constraining the number of conformations a peptide sequence can adopt. As such, non-covalent stabilizations have become an important tool to design peptides that can have biomedical applications.

1.1.2 Designing hairpin peptides

The design of stable β-hairpin peptides focuses on three different aspects: the residues within the strands, the turn, and the ends. In order to design stable hairpin peptides, amino acids that favor the β-sheet register are used. These amino acids have a high intrinsic β propensity, which is described as the ability of a residue to stabilize a β-sheet relative to alanine. β-branched aliphatic residues such as Val, Ile, and aromatic residues such as Phe, Trp and Tyr have been shown to exhibit high β-sheet propensities (Minor & Kim, 1994) and are often used in designed β-hairpin peptides.

The other consideration given to hairpin design is in creating a favorable hairpin turn. The initial classification of hairpin turns was done in 1968 and relied on the ϕ,ψ angles of the amino acids within the turn. (Venkatachalam, 1968) Using a Ramachandran plot, one would be able to compare the favorability of a particular amino acid at specific positions within a hairpin turn as well as determine the kind of turn that a residue was likely to form. The initial classification of hairpin turns into type I and type II along with their enantiomers, type I' and type II' can be done using ^{1}H-^{1}H Nuclear Overhauser Effect spectroscopy (NOESY) experiments. This type of NMR experiment allows for the determination of distances between different hydrogen nuclei. This

information can be used to determine the conformation of residues within a turn since the difference between a type I and type II turn lie in the orientation of the peptide bond between the residues, which consequently affects the orientation of the turn residues' side chains. (Marcelino & Gierasch, 2008)

However, while the classification of turns as type I or type II is still very useful, it is limited to turns that have only have two residues. A more comprehensive nomenclature and classification was proposed by Sibanda and Thornton in 1991. (Sibanda & Thornton, 1991) This new nomenclature describes the turn based on the number of residues in the turn which can vary greatly. The nomenclature used is [x:y] where x represents the number of residues in the turn while y represents the total number of residues before the first instance of full pairwise cross-strand hydrogen bonding. Residues in a turn can be differentiated from those in a loop because they are more rigid and exhibit less flexibility in their ϕ,ψ angles.

Total Correlation spectroscopy (TOCSY) experiments can be used to determine which residues within a peptide are located in the hairpin turn thus determining the values of x and y for the [x:y]-turn designation. Chemical shift deviations (CSD) of backbone H_N are affected by the electron cloud of the peptide bond, created by anisotropy (Figure 1.2). All residues within the strand of a β-sheet peptide are in the same plane as the backbone and so experience some amount of deshielding resulting in positive CSDs. Residues within the turn however, have slightly different ϕ,ψ angles that forces backbone H_N out of the plane resulting in interaction with the electron cloud. This interaction shields the protons resulting in a negative CSD. (Fesinmeyer *et al.*, 2005)

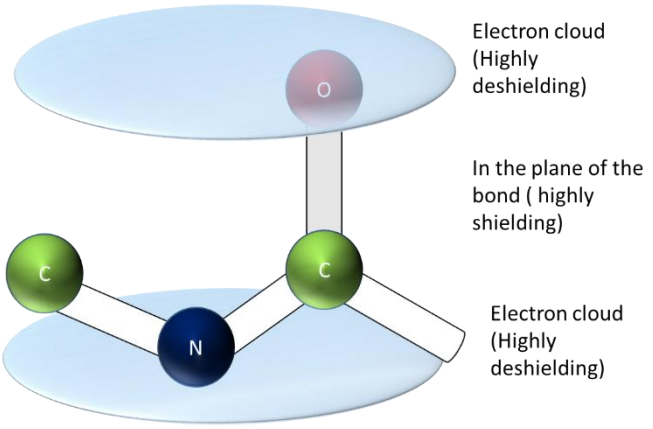

Figure 1.2. Cartoon depiction of the anisotropy experienced by peptide bonds due to the resonance of nitrogen lone pair with the adjacent carbonyl bond

The most prominent, and effective, non-covalent stabilization that the Andersen lab has developed is the use of cross strand Trp residues at non-H bonded positions to stabilize the ends of β-strands as well as hairpin turns. (Andersen *et al.*, 2006; Eidenschink *et al.*, 2009; Kier *et al.*, 2010; Anderson *et al.*, 2014; Anderson, Kier, *et al.*, 2016) The Trp side chain can form an edge-to-face (EtF) interaction when placed in this position. The interaction arises from the coulombic attraction between the electron poor edge of one ring with the electron rich π-cloud of another. This results in a T-shaped orientation, known as the EtF interaction. (Guvench & Brooks, 2005) The EtF interaction is particularly useful in stabilizing long β-strands and can be used to prevent fraying on the ends of short peptides.

Another useful motif that can prevent fraying at the ends of a peptide is the β-cap, which incorporates an EtF Trp/Trp interaction: Ac-W…. WTG-NH_2. (Kier *et al.*, 2010) In this motif, the Gly-H_N interacts with the indole ring of the C-terminus Trp while the Thr side chain-OH forms a hydrogen bond with the carbonyl group of the Ac-W peptide bond in the N-terminus. (Figure 1.3) The stability afforded by this cap is approximately 2 kJ/mol more than the stability conferred by a disulfide bridge, making this a very prominent non-covalent stabilization. Further studies into

possible alternatives to the β-cap led to the development of a coulombic cap; RW…WE. (Anderson *et al.*, 2014) Studies showed that the coulombic cap had a higher fraction fold than the β-cap at both high and low pH environments providing a more versatile alternative to the β-cap.

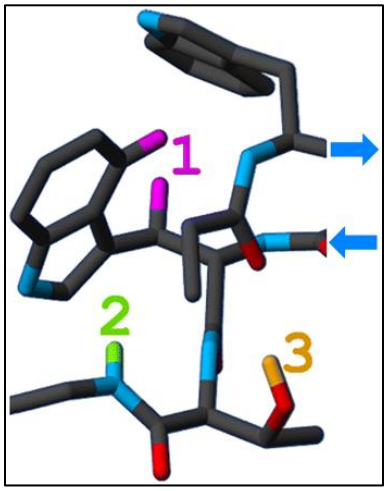

Figure 1.3. Structural representation of the interactions within a β-cap motif. Interaction (1) is the edge-to-face interaction between the cross strand Trp/Trp pair. Interaction (2) is the interaction of the Gly-H_N with the indole ring of the C-terminal Trp. Interaction (3) is the interaction of the hydroxyl group of Thr with the carbonyl group of the N-terminal Trp-Ac peptide bond. *(Image adapted from Kier* et al.*, 2010)*

1.2. Protein misfolding

Since the final structure of a protein is responsible for a majority of its function, the proper folding of a protein to its native state is crucial. However, proteins are capable of falling into kinetic traps while sampling different conformations. (Hartl & Hayer-Hartl, 2009) These traps result in protein misfolding and can favor intermolecular interactions over intramolecular ones (see Figure 1.1). Protein misfolding, with the formation of oligomeric β-structures within the body, has been linked to the onset of a class of over 40 diseases known as the amyloid diseases. For example, Alzheimer's Disease, (Glenner & Wong, 1984; Masters, Multhaup, *et al.*, 1985; Masters, Simms, *et al.*, 1985; Murphy & LeVine, 2010) Parkinson's Disease, (Polymeropoulos *et al.*, 1997) Type II Diabetes, (Cooper *et al.*, 1987) and Huntington's disease (Zheng & Diamond, 2012) have all been traced back to a common misfolding pathway, the formation of amyloid fibrils that have a similar

morphology regardless of the protein composition. Amyloid fibrils are typically characterized as having long, unbranched ribbon-like morphology. Each fibril typically has a distinct, well ordered, cross-β-sheet geometry with strands running perpendicular to the long axis of the fibril. (Petkova *et al.*, 2002; Vilar *et al.*, 2008) (Figure1.4)

Many amyloidogenic proteins adopt a random-coil conformation in their native state but amyloidogenesis can also occur from the partially unfolded states of proteins that have a defined tertiary structure. Amlyoidogenesis is said to have happened when proteins adopt a β-sheet conformation and begin to self-associate forming soluble oligomers that eventually become protofibrils, followed by mature fibrils that can be visualized as plaques. Studies suggest that that this process is a nucleation dependent process that begins with a lag phase, followed by a rapid growth phase and ending with a plateau. (Rochet & Lansbury, 2000; Padrick & Miranker, 2002; Ruschak & Miranker, 2007) In the past, amyloid plaques have been found in patients with these diseases and have been identified as the cause of the disease. (Glenner & Wong, 1984; Masters, Multhaup, *et al.*, 1985; Masters, Simms, *et al.*, 1985; Luk *et al.*, 2012; Pieri *et al.*, 2012) However, recent studies have shown that the mature fibrils may not be the main cause of cytotoxicity, instead, soluble oligomers have been posited as being the most toxic species. (Karpinar *et al.*, 2009; Winner *et al.*, 2011) This is due to the discovery that the amount of amyloid plaques found in patients had no correlation to the severity of the disease. (DaRocha-Souto *et al.*, 2011) This has led to research targeting the formation of soluble oligomers as a way of inhibiting the cytotoxicity of amyloidogenesis.

1.2.1. Alpha-synuclein and Parkinson's disease

Alpha-synuclein (α-syn), a 140 amino acid peptide that is the primary component in Lewy Bodies and has been implicated in the development of Parkinson's Disease, a chronic progressive disease that results in the death of dopamine producing cells in the brain. Alpha-syn is found predominantly in neural tissue, but the exact function of the peptide is not fully understood. A role in dopamine homeostasis has been suggested (Perez *et al.*, 2002) and the association of α-syn with synaptic vesicles stabilizes the vesicles and inhibits neurotransmitter release. (Nemani *et al.*, 2010) Conformation-specific interaction between α-syn and a number of proteins have been detected (Woods *et al.*, 2007) and a role in the assembly of a soluble NSF attachment protein receptor has been reported. (Burré *et al.*, 2010) Interactions with mitochondrial membranes have also been detected. (Nakamura *et al.*, 2008, 2011)

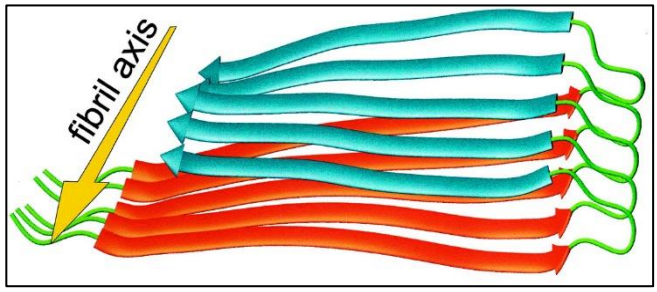

Figure 1.4. Structural model of the fibrils formed by Aβ $_{1\text{-}40}$. Yellow arrow shows the long axis of the fibril. *(Image adapted from Petkova* et al.*, 2002)*

This largely unstructured protein has 3 regions: residues 1-60 make up the N-terminal region. This region contains a nearly conserved KTKEGV hexameric motif that repeats itself several times within the sequence of the peptide. Residues 61-99 of α-syn is known as the Non-amyloid β Component (NAC) region of α-syn. This nomenclature was developed when these residues were found to be a part of the plaques in patients with Alzheimer's disease but were not found in the amyloid-β protein that was determined to be the main component of these plaques. (George &

Clayton, 1996) It was later discovered to be a region within the α-syn peptide. (Culvenor *et al.*, 1999) Interestingly, the NAC region of α-syn has been shown to be the most amyloidogenic region of the protein and has additional units like the previously mentioned repeat. The minimum sequence of amino acids that can aggregate into amyloid fibrils is found within this region. The C-terminal segment of α-syn, comprising residues 100-140 is a highly acidic, proline-rich segment that is the least structured region of α-syn. Even in the soluble oligomeric state, this part of the protein remains mobile and can be observed by solution state NMR. (Sivanesam *et al.*, 2015) The truncation of this segment of α-syn has been shown to increase the rate of amyloid formation by the peptide. (Murray *et al.*, 2003) In fact, a percentage of the plaques found in patients with PD contain the C-terminally truncated form of α-syn. (Liu *et al.*, 2005)

In aqueous solution, monomeric α-syn adopts a predominantly random-coil conformation but some transient long-range contacts have been detected. Upon binding to lipids, the N-terminal region of the peptide adopts a helical conformation that has been mimicked in vitro in the presence of membranes and membrane-like environments. (Eliezer *et al.*, 2001; Georgieva *et al.*, 2008; Jao *et al.*, 2008) These results have been confirmed by NMR studies that show avid lipid vesicle binding by the N-terminal region. (Fusco *et al.*, 2016)

1.2.2. Human Amylin and Type II Diabetes

Human amylin (hAM), also known as islet amyloid polypeptide, IAPP, is a 37-residue peptide that has been implicated in the development of Type II Diabetes. (Kapurniotu, 2001) Co-secreted with insulin by the pancreatic β-cells of the Islet of Langerhahns (Moore & Cooper, 1991), hAM has been known to play a role in inhibiting glucagon secretion, slowing down stomach emptying and inducing a feeling of satiety after a meal. (Samsom *et al.*, 2000; Westermark *et al.*, 2011; Lutz, 2012) In its monomeric state, hAM has been shown to adopt a random-coil conformation with a

disulfide bridge between Cys 2 and Cys 7 (inducing partial helicity from residue 5 – 20) and an amidated C-terminus. (Roberts *et al.*, 1989) Upon binding to membranes, hAM has been shown to adopt a helical conformation spanning residues 5 to 28 while the rest of the peptide remains unstructured. (Patil *et al.*, 2009) There is also some evidence that hAM may adopt an α-helical intermediate structure during amyloidogenesis. (Abedini & Raleigh, 2009)

1.3. Antimicrobial activity

Antimicrobial peptides (AMPs) are highly cationic, amphipathic peptides that are able to selectively bind to host invaders such as bacteria, viruses and fungi. AMPs appear to have a variety of conformations: α-helix, β-sheet, extended or loop. (Powers & Hancock, 2003; Jin *et al.*, 2005; Hancock & Sahl, 2006; Midura-Nowaczek & Markowska, 2014) The human body produces a number of natural AMPs such as defensins, cathelicidins and histadins. Increasing numbers of drug resistant bacteria has made the design and development of novel antimicrobial peptides (AMP) a rapidly growing area of research.

1.3.1. Antibiotic resistance

While some bacteria have innate resistance to certain AMPs and antibiotics, it is the developed resistance of bacteria that has become a cause for concern. Bacteria can develop resistance to antibiotics through one of two ways: genetic mutation or through acquiring resistance from another bacterium. Mutation occurs in bacterial DNA at about the same rate as mutation in human DNA. Some of these mutations have the ability to confer upon a bacterium the ability to resist the actions of antibiotics through the production of chemicals that degrade the antibiotics. Other possible forms of resistance are through the elimination of antibiotic targets within the cell, closing up of

ports through which antibiotics enter the cell and the development of pumps that are able to remove antibiotics from the cell. (Blair *et al.*, 2015)

Similarly, bacteria can develop antibiotic resistance by obtaining genetic material from other bacterium through the process of conjugation, or by picking up "naked" DNA in their surrounding environment. Viruses are also capable of transporting bacterial DNA from one bacterium to another. (Alanis, 2005) These forms of bacterial resistance are becoming more problematic because bacteria are capable of developing resistance to multiple classes of antibiotics leading to the development of "super bugs" that cannot be treated. (Wright, 2000) This is one of the reasons that AMPs are gaining prominence. A lot of research postulates that most AMPs do not act on targets within the cell, rather they target the cell membrane of bacteria. This, coupled with the non-specific peptide-peptide interaction that a lot of AMPs seem to have with bacterial membranes, makes it harder for bacteria to develop resistance to AMPs thus making it a viable alternative to small molecule antibiotics which have specific intracellular targets.

1.3.2. Mechanism of Antimicrobial Peptide activity

The greatest hurdle in this field remains the lack of an understanding of the mechanism by which these peptides disrupt the membranes of bacteria. The two most prevailing hypotheses are the pore formation hypothesis and the carpet hypothesis. In the pore formation hypothesis, the AMPs are attracted to the negatively charged membrane of a bacterial cell and form a pore within the membrane of the cell. The formation of the pore causes the contents of the bacterial cell to leak out resulting in the apoptosis of the cell. (Silvestro *et al.*, 2000)

Two types of pores have been observed; the barrel-stave pore and the toroidal pore. (He *et al.*, 1996; Matsuzaki, Yoneyama, Fujii, *et al.*, 1997; Matsuzaki, Yoneyama, & Miyajima, 1997)

Formation of the barrel-stave pore has been posited to happen when the AMP reaches a threshold concentration on the membrane of a bacterial cell and begins to dissociate from the lipid head groups. This causes the peptides to sink into the membrane and form a pore with the hydrophobic face of the peptide facing outwards towards the membrane and the hydrophilic face forming the inside of the "barrel". (He *et al.*, 2013) The toroidal pore on the other hand does not show dissociation from the lipid head group. Instead, the peptide causes curvature of the bacterial membrane resulting in a pore. (Melo *et al.*, 2009) The carpet hypothesis proposes that the AMP does not form a pore but rather causes a more uniform disruption of the bacterial membrane. (Pouny *et al.*, 1992) The membrane destabilization then results in cell death.

Beta-sheet AMPs that have been isolated in other organisms have shown a high dependence on disulfide stabilization in order to maintain their β-hairpin structures. This reduces the versatility of the peptide as well as making it sensitive to oxidative environments. Designing peptides that are not reliant on these covalent stabilizations could therefore be a useful tool to study the importance of the hairpin structure for bioactivity.

1.4. Techniques employed

1.4.1. Circular Dichroism

Circular dichroism is a useful technique for elucidating the secondary structure of proteins and peptides due to the inherent chirality of peptides. A circular dichroism spectrum arises from the differential absorption of left and right circularly polarized light. Typically, the far-UV region is used to determine the secondary structure of proteins since the protein backbones absorb in the 180-230 nm range. The dihedral angles (ϕ,ψ) of peptide and protein backbones differ depending

on the structural conformation of the peptide and cause the intensities and energies of a peptide amide bond n→π* and π→π* transitions in the CD spectrum to change. This is what allows the elucidation of different secondary structures. A CD signal represents the sum of all the secondary states within a protein and can be used to calculate the fraction of α-helix (characteristic maximum at 190 nm and two minima at 208 nm and 222 nm) and β-sheet populations (characteristic maximum at 198 nm and minimum at 216-220 nm). (Figure 1.5)

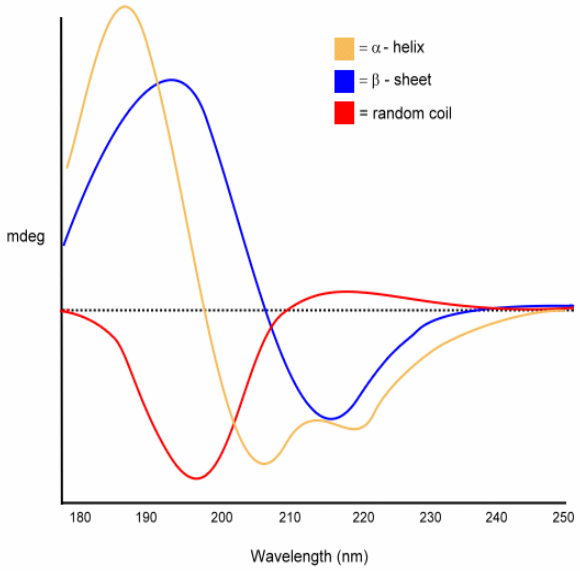

Figure 1.5. The expected CD spectra for peptides with pure α-helix, β-sheet and random-coil. (Image adapted from http://www.proteinchemist.com/cd/cdspec.html)

Amyloidogenic proteins and peptides have been determined to be in a random-coil conformation in their native state but begin to aggregate into β-sheets at the beginning of amyloidogenesis. The transition from random-coil to β-sheet can be observed by monitoring the change in CD signal (measured in deg, θ) of a peptide at 198 nm. In the random-coil conformation, the CD spectra shows a minimum at 198 nm that transitions to a maximum as the peptide organizes into the β-sheet conformation. The development of a new minimum at 216-220 nm can also be used to monitor the formation of β-sheet secondary structure.

CD can also be used to determine the stability of the secondary structure of a peptide by comparing the CD spectra of a peptide at various temperatures. The addition of heat will cause non-covalent interactions to break from the weakest to the strongest resulting in a progressive loss of secondary structure. Therefore, the change in secondary structure from a folded β-sheet or α-helix to random-coil can determine the stability of the folded state of a peptide through the calculation of a melting point, T_m.

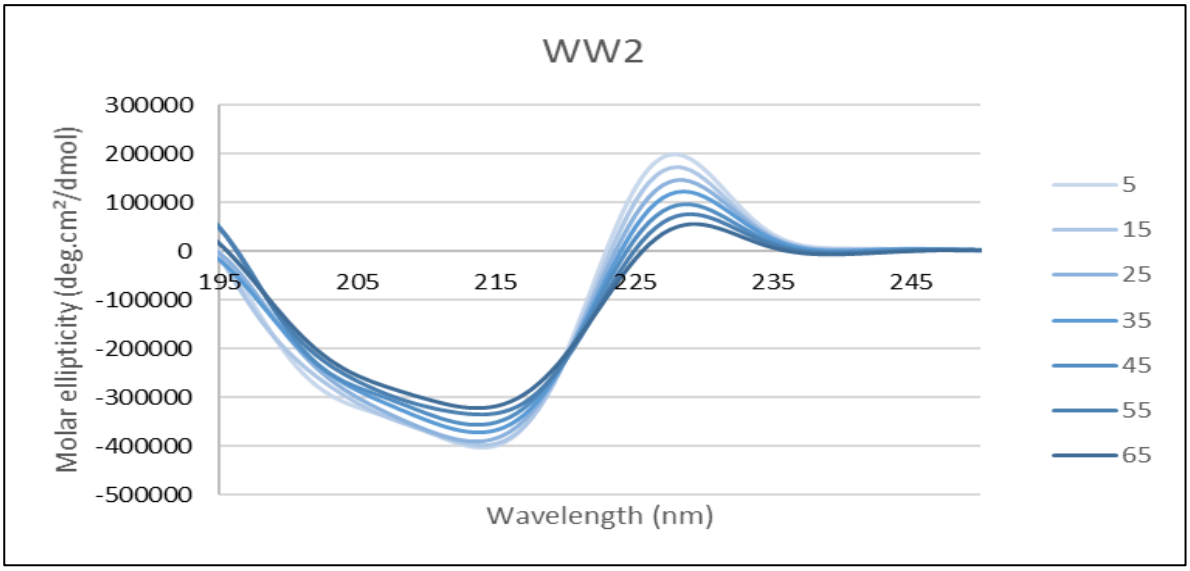

Figure 1.6. A typical series of CD spectra that can be used to track the melting of a peptide over a range of temperatures. The presence of the bisignate curve indicates that an edge-to-face interaction is present. The interaction dominates the spectrum despite the presence of β-sheet and turn structure. The peptide shown above is WW2 (Sequence of WW: KKLTVWIpGKWITVSA)

Another common feature that is observed in this study is the formation of an exciton couplet in peptides that have aromatic amino acids with an edge-to-face interaction. An exciton couplet results from the coupling of two of the same chromophores, with similar ΔEs, that are in close proximity to one another and the strength and chirality of the interaction is dependent on the

relative orientation of the chromophores. When chromophores are in proximity to one another, the electronic transition that resulted from the absorption of a photon becomes delocalized over all the chromophores. (Telfer *et al.*, 2011) This phenomenon results in one excited state being at a higher energy than the original excited state while the other excited state is at a lower energy than the original. This difference in energy states can be visualized as a bisignate curve by CD, centered at the absorption maxima of the chromophore with a positive curve at longer wavelengths (red shift) and a negative curve at shorter wavelengths (blue shift). The strength of the interaction can be measured by the intensity of the CD signal. (Figure 1.6)

1.4.2. Nuclear Magnetic Resonance

While CD is a useful tool for determining the overall structure of a peptide, the summary nature of the spectrum prevents the identification of the contribution of specific residues to the structure. In order to study the secondary structure of a peptide in detail, one has to obtain more precise local measurements. To this end, two-dimensional NMR spectroscopy has proven to be a very useful tool, in particular, total correlation spectroscopy (TOCSY) and nuclear Overhauser effect spectroscopy (NOESY) can be used to study amino acids within a peptide or protein by observing the chemical shifts of ^{1}H nuclei and spin transfer between sites within residues and between residues.

TOCSY experiments probe the spin-spin coupling interaction of ^{1}H- ^{1}H nuclei within a single spin system while NOESY experiments show the through-space dipolar interactions between $^{1}H/^{1}H$ nuclei. The close proximity required for the transfer of magnetization between nuclei in a NOESY experiment allows for the determination of amino acid sequence in peptide as well as the determination of some aspects of peptide secondary (and if present, tertiary) structure.

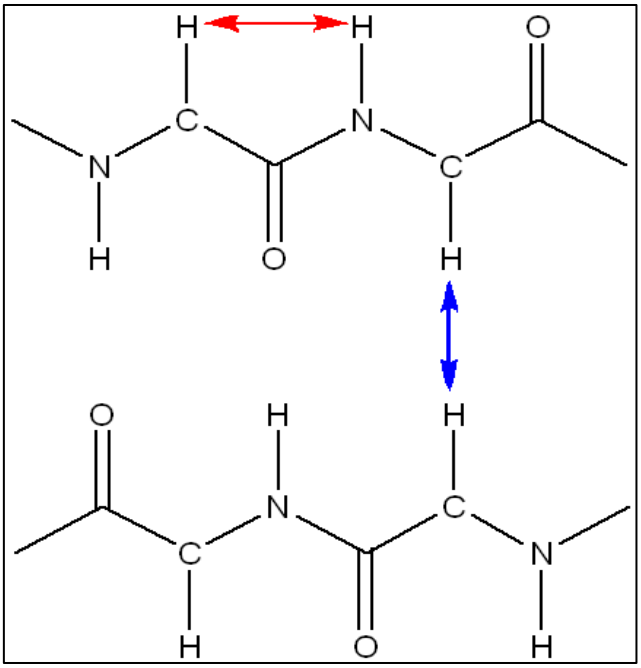

Figure 1.7. β-sheet pattern illustrating some of the through-space interactions that can be observed in a NOESY experiment. The red arrow depicts the interaction of adjacent amino acids which can be used to verify the sequence of a peptide by NOESY. The blue arrow depicts a cross-strand Hα-Hα interaction that can be visualized in β-strands.

Chemical shifts (δ) are the main information obtained from a single NMR spectrum and are a result of ^{1}H nuclei being in unique environments in a molecule. The proximity of a nucleus to an electron-withdrawing or -donating environment can affect the chemical shift of the nuclei resulting in increased shielding (electron-rich environment) or decreased shielding (electron-withdrawing) of the nucleus. Diamagnetic anisotropy that results from resonance (Figure 1.2) is also capable of affecting the chemical shift of a nucleus. These electron cloud modifications are what leads to the differences in chemical shifts of a nucleus.

Chemical shifts can be determined for each proton in each amino acid residue in any particular solution state. These values, when compared to random-coil chemical shifts (δ_{rc}) can provide the secondary-structure preference of a peptide at each amino acid. These differences are called chemical shift deviations (CSDs). These deviations can be calculated using the following equation:

$$Chemical\ Shift\ Deviation\ (CSD) = measured\ chemical\ shift\ (\delta) - \delta_{rc}$$

Since the chemical shift of a nucleus is also affected by interactions such as hydrogen bonds, the presence of a hydrogen bond in a peptide can also produce CSDs. Hydrogen bonds are formed when a hydrogen atom attached to a fluorine, nitrogen, sulfur, or oxygen atom interacts with another nitrogen, fluorine, sulfur, or oxygen atom through space. In a β-hairpin peptide, hydrogen bonds occur when a cross-strand residue H_N is in close proximity to a backbone carbonyl oxygen. This occurs in the area between the antiparallel aligned strands. While one might expect the hydrogen bond to result in the shielding of that H_N in an NMR spectrum, the opposite effect is observed. This is due to the anisotropy of the peptide bond. (Figure 1.2) This anisotropy creates an electron cloud "sandwich" with an electron poor middle. Therefore, all backbone H_N that lie in the plane of the peptide bond experience some deshielding by the electron cloud. Hydrogen bonded H_N, by virtue of their position in the middle of both β-strands, experience a larger amount of deshielding due to their sequestered nature.

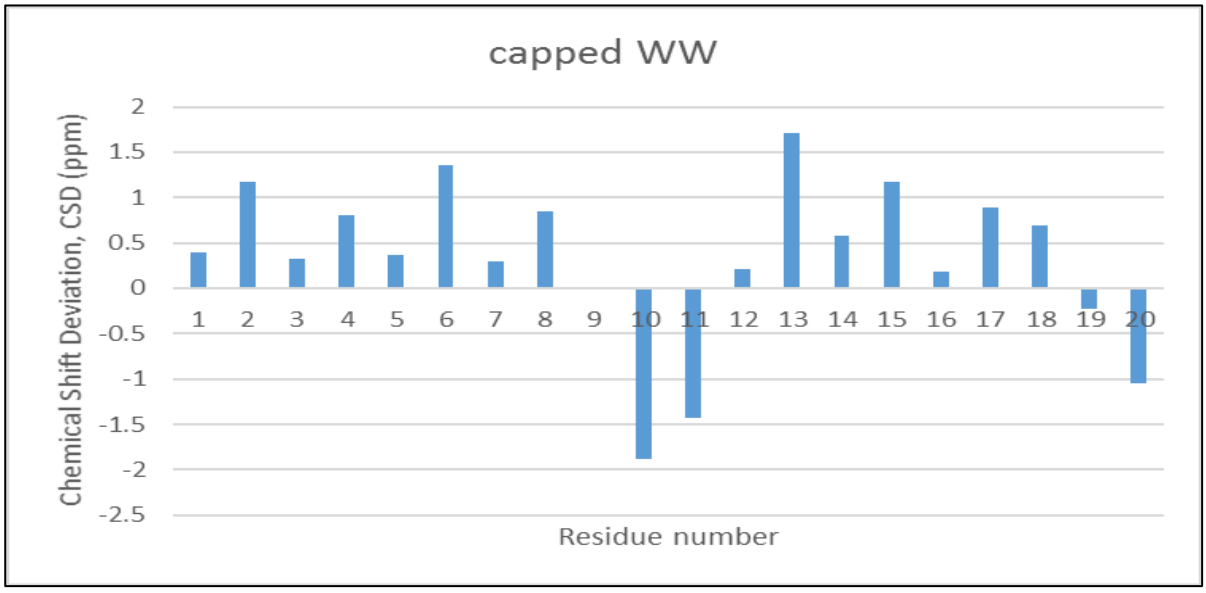

Figure 1.8. A graph that demonstrates the β-hairpin register of the strands of a peptide, cappedWW. The alternate high and low positive CSDs represent the presence of hydrogen bonds at alternate positions while the negative CSDs show the position of the turn. (*see 1.1.2. for explanation)* (Sequence of capped-WW: Ac-WKKLTVWIpGKWITVSAWTG-NH_2)

CSDs can therefore be used to determine the secondary structure of a peptide by observing the chemical shifts of the backbone hydrogen atoms which has a distinct register in the β-sheet conformation. (Figure 1.8) The increase in deshielding of hydrogen bonded H_N correlates to an increase in the magnitude of CSDs and can be used to quantify the β-fold of a peptide.

CSDs can also be used to determine the presence of edge-to-face (EtF) interactions. The preferred EtF geometry of interacting aromatics places some of the hydrogens of the edge-ring deep within the shielding cone of the other aromatic ring (face-ring). (Figure 1.9) This allows for the determination of which amino acid is in the edge position and which amino acid is in the face position.

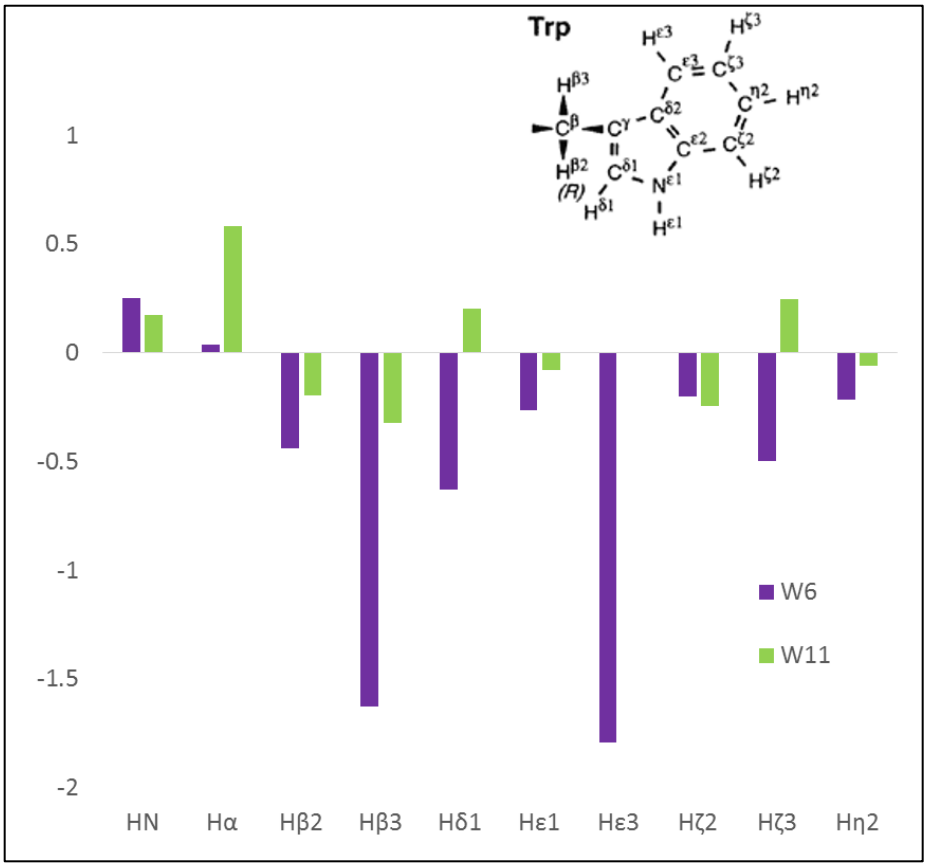

Figure 1.9. The graph shows a comparison of the CSDs of all the tryptophan protons in a peptide, WW. (Tryptophan proton IUPAC naming given inset) Note that the dramatically increased shielding experienced by Hβ3 and Hε3 of W6 indicate that this tryptophan is the edge-ring while the lower CSDs of W11 indicate that this tryptophan is the face-ring.

(Sequence of WW: KKLTVWIpGKWITVSA)

NMR can also be used to study the binding loci of two peptides using heteronuclear 2D NMR. Heteronuclear single quantum coherence (HSQC) spectroscopy can be used to determine the chemical shifts of a peptide or protein with universal ^{13}C or ^{15}N labelling. In this experiment, there is a magnetization transfer between a hydrogen atom and a heteronuclear atom (either nitrogen or carbon) via an INEPT (insensitive nuclei enhanced by polarization transfer) step. The magnetization is then transferred back to the hydrogen via a retro-INEPT step after a specified time delay that results in signal that can be recorded. In peptides, this experiment demonstrates the interaction between nitrogen atoms and amide protons. This technique is particularly useful to study the binding of two peptides where one peptide is isotopically labeled and the other is not. If binding is occurring between the two peptides, then the chemical shifts of the amino acids that are bound will be altered due to the change in environment in the bound complex. This change in chemical shift can then be observed through HSQC NMR experiments.

1.4.3. Fluorescence Spectroscopy

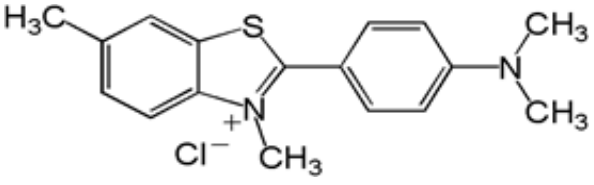

Figure 1.10. Molecular structure of Thioflavin T

While the transition of amyloidogenic peptides from random-coil to β-sheet is typically indicative of the initial phase of amyloidogenesis, confirmation that fibrils (or protofibrils) have formed and have the features of "amyloid" requires the use of microscopy to visualize the fibrils or fluorescence spectroscopy with dyes that show a high specificity for the amyloid structural motif. Fluorescence spectroscopy monitors the excitation and emission of light from a fluorophore that may be intrinsic to the fluorophore or a product of the external environment of the fluorophore. In this study, the

change in emission spectrum signal intensity of the dye Thioflavin T (ThT) is used to monitor the development of the soluble β-oligomers during amyloidogenesis.

Thioflavins are benzathiol salts that are often used to determine the presence of amyloid fibrils in solution. Since its discovery in 1959, (Vassar & Culling, 1959) ThT has been widely used because it has an increased emission at 482 nm and experiences a red shift of approximately 100 nm (from 350 to 450 nm) in its excitation spectrum when bound to β-sheet rich structures, (Naiki *et al.*, 1989; LeVine, 1993, 1995) unlike the analog Thioflavin S (ThS). ThS's lack of red shift results in fluorescence spectra that have too much background interference, making it unsuitable for the quantification of amyloid fibrils. (LeVine III, 1999) Instead it is more commonly used for histological staining.

The fluorescence enhancement of ThT upon binding to amyloid fibrils most likely arises from the decrease in the free rotation about the carbon-carbon bond between the benzylamine and benzathiole rings of ThT. In solution, ThT is predicted to behave like a "molecular rotor" that rapidly quenches excited states that are generated by photon excitation. However, upon binding to a rigid structure such as amyloid fibrils or soluble β-oligomers, the molecule is unable to freely rotate resulting in enhanced fluorescence. Since ThT binding does not depend on the sequence of the peptide or protein forming the amyloid fibrils, the current theory is that the dye binds to channel-like motifs along the surface of the fibrils formed by the side chains of amino acids in the cross β-sheet structure of amyloids. (Wu *et al.*, 2008) Polarized fluorescence microscopy also revealed that the dye is most likely aligned parallel to the long axis of the fibers. (Krebs *et al.*, 2005)

1.5. Overview of research

The research presented in this dissertation expands on the use of peptides as inhibitors of amyloidogenesis and the application of hairpin stabilization techniques to native AMPs. The first part of this work focuses on the use of designed hairpin peptides as inhibitors of amyloidogenesis of two distinct systems; α-syn and hAM. With the exception of being capable of forming amyloid fibrils, both of these systems bear no similarity, including no stretches of sequence similarity. However, the amyloidogenesis of both of these systems can be inhibited by the same peptides. My studies have also validated the hypothesis that self-self recognition of amyloid systems can be overcome by inhibitors that already have a stable hairpin fold, eliminating the dependence on peptide inhibitors that are modified fragments of the target systems.

For hAM, I developed protocols for the efficient synthesis and purification of full-length hAM. Reproducible assay conditions were developed and the effects of multiple inhibitors were tested against hAM. Results indicated that there was a definite correlation between hairpin stability and the potency of the peptide as an inhibitor of amyloidogenesis. I was also able to verify that the α-helix conformation may be an on-pathway intermediate in hAM amyloidogenesis.

My studies with α-syn were building upon conditions developed by Dr. Aimee Byrne and Dr. Kelly Huggins. I also developed conditions for an NMR titration assay in order to study the binding loci of my most potent inhibitors. Through these studies, I have also been able to isolate a secondary binding locus for my most prominent inhibitors that is outside the C-terminus. This secondary locus is gaining prominence as the location for an early folding event in the amyloidogenic pathway. I also confirmed that α-syn has a slight preference for the phenolic amino acid residue and that this preference can overcome small deficiencies in fold stability of the inhibitor. However, my examination of hairpin peptides with and without the phenolic residue,

Tyr, showed that at very stable β-folds, the presence of the Tyr residue does not contribute to increased inhibitory activity. I was also able to establish that the addition of known small- molecule inhibitors to peptide inhibitors did not necessarily guarantee a synergistic effect.

The second part of this study focuses on the application of hairpin stabilization techniques in antimicrobial peptides. Using prior knowledge with regards to non-covalent stabilization techniques, I have progressively modified two native antimicrobials, tachyplesin I and gomesin, to reduce and or eliminate their dependence on disulfide stabilization. As a result, I have made mutants that have the same or better antimicrobial activity than the native antimicrobials they were derived from.

These experiments have also led to the development of a class of peptides known as acyclins, non-covalently-stabilized derivatives of a previously cyclized AMP, that are capable of inhibiting the antimicrobial activity of gram-negative *E. coli.* The results of this study could help with the *a priori* design of new antimicrobial peptides in the future. Finally, I was able to enhance the β-fold of a completely novel AMP, I-RW, demonstrating once again that non-covalent stabilizations can increase the β-folding propensity of relatively random-coil peptides. However, the increased stabilization does not, necessarily, translate to increased antimicrobial activity providing an interesting perspective on the relationship between fold and activity.

Chapter 2: Methods and Materials

2.1. Solid phase peptide synthesis and purification

Peptide hairpins and controls were synthesized by standard Fmoc Solid Phase Peptide Synthesis methods on a CEM Liberty Blue microwave peptide synthesizer. Wang resin preloaded with C-terminal amino acids and Rink Amide-MBHA resin were employed. DIC/Oxyma was used as coupling reagents and 20% piperidine in DMF was used for deprotection of Fmoc-groups. N-terminal acetylation or benzoylation was accomplished using a 1:10:10 ratio of peptide: anhy-dride (acetic anhydride or benzoic anhydride): triethylamine in 5 mL DMF. The mixture under-went shaking for 1 hour at room temperature before cleavage.

Peptide cleavage was done using 95:2.5:2.5 trifluoroacetic acid (TFA):triisopropylsilane (TIPS): water mixture where water and TIPS served as radical scavengers. Disulfide bonds were formed by diluting the peptide in minimal amounts of DMSO (500μL) and 3 mL of water. The peptides were allowed to oxidize overnight at room temperature. All peptides were purified by reverse-phase HPLC (Varian ProStar 220 HPLC, Agilent 21.2 × 50 mm C18 column, 10 mL/min, eluent A: water with 0.1% TFA, eluent B: acetonitrile with 0.085% TFA) on a 10-60% gradient over 25 minutes and visualized at 215 nm and 280 nm. Fractions that were collected to an excess of 97% purity, were lyophilized and characterized using a Bruker Esquire Ion Trap ESI mass spectrometer before use in experiments.

2.1.1. Backbone cyclization of peptides

Peptides that needed to be backbone cyclized were made using 2-Cl-Trt resin that was preloaded with isoleucine or glycine. The protected peptide was cleaved from the resin using 3x30 mins treatment with 1% TFA in dichloromethane (DCM). The peptide was then dissolved in 10 mL of

N,N-dimethylformamide (DMF) and titrated into 30 mL of DMF with 5 eq. PyAoP/HATU and 3 eq. diisopropyl ethyl amine (DIEA). The mixture was allowed to cyclize overnight with constant stirring. DMF was then removed via rotavap (using toluene to form an azeotrope) and the product was precipitated with nanopure water. The cyclic protected peptide (precipitate) was then deprotected by dissolving the peptide in a 20 mL mixture of 95:2.5:2.5 TFA:triisopropylsilane:water. The cyclic deprotected peptide was purified using reverse-phase HPLC as described above.

2.1.2. Synthesis and purification of hAM

Synthesis of human amylin and its derivatives employed the use of pseudo-prolines. Fmoc-Ala-Thr ($\Psi^{Me,Me}$Pro)-OH was used to substitute for Ala-8 and Thr-9 while Fmoc-Leu-Ser ($\Psi^{Me,Me}$Pro)-OH was used to for Leu-27 and Ser-28. (Abedini & Raleigh, 2005) Each pseudo-proline was coupled at 50°C for 10 mins. The crude product from peptide synthesis, presumably a solely cysteine-containing peptide mixture, was dissolved in 30% acetonitrile solution and lyophilized. This step was repeated 6 times. The resulting mixture was then dissolved in 6 M guanidinium chloride before being purified by reverse-phase HPLC as described above. The central peak from HPLC, concentrated by lyophilization, was dissolved in a solution of 30 % DMSO and allowed to oxidize in air overnight. The mixture was then centrifuged and the supernatant was removed. Any precipitate was re-dissolved in 6 M guanidinium chloride, and both solutions were purified by reverse-phase HPLC. The purity of the lyophilizate of the collected fractions was verified by Bruker Esquire Ion Trap mass spectrometry.

2.2. Nuclear Magnetic Resonance

All NMR experiments were carried out on Bruker instruments: DRX499, AV700 and AV800 with 500, 700 and 800 MHz respectively.

2.2.1 Proton NMR

For proton spectra collection, peptide samples were made using 1 mM lyophilized peptide (by weight) dissolved in 90% phosphate buffer at varying concentrations and pHs with 10% 1 mM sodium 2,2-dimethyl-2silapentane-5-sulfonate (DSS) in D_2O. D_2O served as a lock signal and DSS was used as an internal chemical shift reference that was set to 0 ppm. Due to the proton signal of peptides in aqueous solution being obscured by the large proton signal of water, a solvent suppression technique known as excitation sculpting was employed to better visualize the proton peaks of the peptide.

The two NMR techniques used to characterize the sequence and structure of peptides were Total Correlation Spectroscopy (TOCSY) and Nuclear Overhauser Effect Spectroscopy (NOESY). The TOCSY experiment allowed the determination of protons within the same spin system that were interacting through bond connectivity while the NOESY allowed for the characterization of proton interactions through space. The raw NMR spectra were processed using nmrDraw and the peaks were assigned using Sparky.

Chemical shift deviations (CSDs) were calculated and compiled using an in-house algorithm developed to correct for the neighboring inductive effects, temperature and pH fluctuations, available at http://andersenlab.chem.washington.edu/CSDb. The chemical shifts of the assigned peptides were extracted from Sparky and uploaded into the Chemical Shift Database (CSDb).

Chemical shifts were calculated based upon the following equation:

$$CSD = \delta_{observed} - \delta_{reference}$$

Where the $\delta_{reference}$ is the statistically and experimentally determined random-coil value of each amino acid.

2.2.2. HSQC NMR

All HSQC spectra were recorded on Bruker AV700 (700 MHz) and AV800 (800 MHz) instruments.

Experiments with ^{15}N-labeled α-syn were carried out with two different conditions:

200 μM α-syn (by weight) was dissolved in 90% 50 mM phosphate buffer pH 6.5 and 10% 1 mM DSS in D_2O. 120 μM to 440 μM peptide inhibitors were titrated into the NMR sample. Spectrum was recorded after each addition. Hexafluoroisopropanol (HFIP) was added to afford a final concentration of 1.5% v/v. All HSQC spectra were recorded at 303K.

100 μM α-syn (by weight) was dissolved in 90% 20 mM Tris. HCl buffer, pH 7.2 and 10% 1 mM DSS in D_2O. Peptide inhibitors were titrated into the NMR sample to 60 μM, 120 μM, and 200 μM final concentrations. HFIP was added to a final concentration of 2.0 vol-%. After each addition, HSQC spectra was recorded at 280K. Once HFIP had been added and a spectrum was recorded at 280K, the temperature of the sample was increased to 300K and another spectrum was recorded. After a 22- to 24-hour incubation, a final spectrum is recorded at 300K.

2.3. Aggregation Assays

2.3.1. Human amylin

Two different assays were developed to measure the amyloidogenesis of full-length human amylin. The first assay, employed the use of 2 vol-% HFIP. Lyopholized human amylin was dissolved in neat HFIP to afford a human amylin stock with a final concentration of 5 mM hAM by mass. The peptide mixture was vortexed for 5 minutes to ensure complete dissolution of peptide. The hAM stock solution is employed to make CD assay samples with a final concentration of 50 μM hAM, with or without 5 – 200 μM inhibitor, in 50 mM pH 2.0 phosphate buffer containing 25 mM NaCl and 2 vol-% HFIP.

The second assay employed the use of 1 % HFIP. 5 mM human amylin stocks in neat HFIP was diluted with buffer, to make a sample with a final concentration of 50 μM hAM with or without 5-200 μM inhibitor, in 50 mM pH 2.0 phosphate buffer containing 25 mM NaCl and 1 vol-% HFIP.

For each assay, a 400 μL sample in a 2 mL vial with a screw cap closure and a 7 mm stirbar is warmed to 37 °C in a water bath with constant stirring. Periodically, 40 μL aliquots of sample are removed and diluted with 50 mM phosphate pH 2.0 buffer for a CD sample with a final concentration of 10 μM hAM (final volume 200 μL). To make the sample ready for ThT, 10 μL of 1.6 mM ThT is added to the CD sample.

2.3.2. Alpha-synuclein

Alpha-synuclein samples were provided by Dr. Marco Bisaglia (University of Padua, Italy) in lyophilized form. The peptide was dissolved in 50 mM phosphate pH 6.5 containing 50 mM NaCl to make a stock solution. The concentration of the stock solution was determined using UV absorbance measured at 280 nm.

The following Beer's Law equation was employed:

$$A = \varepsilon c l$$

Where A=absorbance, ε=sum of the molar extinction coefficients for all tryptophans (ε=5690 M^{-1} cm^{-1}) and tyrosines (ε=1280 M^{-1} cm^{-1}) present in peptide, *l*=length of the cell.

The α-syn stock was then diluted with 50 mM phosphate pH 6.5 containing 50 mM NaCl to afford an assay sample with a final concentration of 90 µM α-syn. Samples were incubated in a 2 mL vial with a 7 mm stir bar and warmed in a 37°C water bath with constant stirring. Aliquots of 10 µL were removed periodically and diluted with 190 µL of 2 vol-% HFIP in 50 mM phosphate pH 6.5 buffer (without NaCl) for CD measurements. For ThT measurements, 10 µL of 720 µM ThT was added to the sample.

2.4. Circular Dichroism

All spectra were recorded on a Jasco J-720 Circular Dichroism instrument. Typical spectral accumulation parameters were as follows: scan rate of 100 nm/min with a 2 nm bandwidth and a 0.1 nm step resolution over the wavelength range of 190−270 nm with eight scans averaged for each spectrum. Raw ellipticity data (θ_{obs}, in degrees), were converted into molar ellipticity ([θ], with units of $deg \cdot cm^{-1} \cdot M^{-1}$, usually given as $deg \cdot cm^2 \cdot dmol^{-1}$) or mean residue-molar ellipticity ($[\theta]_{MRW}$) when the chromophore of interest is the peptide bonds in a peptide or protein. All calculation employed the Jasco software with the CD spectra corrected for a blank after reverse FT smoothing of both. The pathlength of the CD cell used in all cases was 1 cm.

Thus molar ellipticities were calculated as:

$$[\theta] = 100\ (\theta_{obs} / c \cdot l) \quad \text{with c = molarity and the pathlength (l) in cm.}$$

and $[\theta]_{MRW}$ was obtained as $[\theta] / N - 1$ where N is the number of amino acid residues.

$[\theta]_{MRW}$ values are reported for all α-syn and hAM samples.

In order to obtain the melting temperature of peptides, spectra were accumulated for peptides with a concentration by UV of 30 μM at 10 °C intervals from 5 °C to 95 °C, allowing 300 seconds between spectral accumulation in order to allow peptide sample to equilibrate to the temperature.

In CD-based inhibitor assays, all CD spectra were corrected for inhibitor and/or solvent contribution using the following equations:

$$CD_{final} = CD_{amyloid\ peptide+inhibitor} - CD_{inhibitor}$$

$$CD_{final} = CD_{peptide} - CD_{solvent}$$

For the 2 vol-% HFIP hAM assay, at the onset, and every 45 minutes thereafter, a 40 μL aliquot is removed and diluted to a final volume of 200 μL with 2 vol-% HFIP, 50 mM pH 2.0 phosphate buffer, producing a 10 μM hAM sample for CD measurement. At the end of 3 hours, aliquots were taken every hour up to 6 hours.

For the 1 vol-% HFIP assay, a 40 μL aliquot is removed every hour for 6 hours and diluted to a final volume of 200 μL with 1% HFIP, 50 mM pH 2.0 phosphate buffer, producing a 10 μM hAM sample for CD measurement.

For the α-syn assay, a 10 µL aliquot is removed at t = 0hr, 2hr, 4hr, 12hr, 16hr and 18hr and diluted to a final volume of 200 µL with 2% HFIP, 50 mM pH 6.5 phosphate buffer, producing a 3.6-µM α-syn concentration sample for CD measurement.

2.5. Thioflavin T Fluorescence assay

Thioflavin T spectra were recorded on Perkin Elmer LS50B and LS55 fluorescence spectrometers. The following parameters were used: emission wavelength 482 nm and excitation wavelength 450 nm; 10 mm pathlength cells with 5 nm excitation slit width and 10 nm emission slit width, scan speed 500 nm/min.

The excitation and emission wavelengths were chosen to monitor the increase in the fluorescence of the Thioflavin T dye upon the onset of fibril formation. The measurement was done in arbitrary units (AU).

For all hAM assays, 10 µL of ThT was added to the CD sample, to give a final concentration of 80 µM ThT before the fluorescence measurement was taken. For all α-syn assays, 10 µL of 720 µM ThT was added to the CD sample and measurements were taken.

2.6. Antimicrobial Assay

2.7.1. Gram-negative assays

E. coli (Dh5α) were grown overnight at 37 ˚C in sterile LB media. From the overnight culture 1 mL was removed and spun for 5 mins at 3000 rpm. Supernatant was removed and the cell pellet was resuspended in 5 mL fresh, sterile LB, followed by return to a 37 ˚C shaking incubator. Growth was tracked by measuring the absorbance at 600 nm (OD_{600}) until an absorbance between 0.5-0.8

was reached. From this culture two sequential dilutions were made: the first dilution to >0.1, and the second to the desired 0.001. From the culture with OD_{600} of 0.001, 90 µL was combined with 10 µL of peptide stock solution in a 96-well plate. Plate lids were sealed on three sides with parafilm to reduce evaporation. Peptide stock solutions with concentrations from 3.9 µM to 1 mM, obtained by serial dilution were used and each concentration was tested in triplicate. The control wells for 100% growth include 10 µL of water in place of the peptide solution; the background controls (no growth) consist of 100 µL of the LB broth alone. OD_{600} is measured for each well after incubation at 37 °C with gentle agitation for 24 hours using a Thermo Labsystems Multiskan Spectrum UV/Visible microplate reader. The %-inhibition is given as 1 – [(ODsample – ODback) / (ODcontrol – ODback)].

2.7.2. Gram-positive assay

Corynebacterium glutamicum (ATCC 13032) were grown at 30 ˚C in sterile LBG media (LB supplemented with 0.5% sterile filtered glucose). Overnight cultures were pelleted by spinning 5 min at 3000 rpm. Supernatant was removed and the pellet was resuspended in 5 mL fresh, sterile LBG, followed by return to a 30 ˚C shaking incubator. Growth was tracked until an OD_{600} of >0.5 was reached. From this culture two sequential dilutions were made: the first dilution to >0.05, and the second to the desired 0.001. From the culture with OD_{600} of 0.001, 180 µL was combined with 20 µL of peptide stock solution in a 96 well plate. Plate lids were sealed on three sides with parafilm to reduce evaporation. Peptide stock solutions with concentrations from 0.06 µM to 7.81 µM, obtained by serial dilution were used and each concentration was tested in triplicate. The control wells for 100% growth include 20 µL of 20 mM phosphate, pH 6.5 buffer in place of the peptide solution; the background controls (no growth) consist of 200 µL of the LB broth alone. OD_{600} is measured for each well after 24 and 48 hrs of incubation at 30 °C with gentle agitation

using a Thermo Labsystems Multiskan Spectrum UV/Visible microplate reader. The %-inhibition is given as 1 – [(ODsample – ODback) / (OD-control – ODback)].

Chapter 3: α-Synuclein

3.1 Introduction

Alpha-synuclein (α-syn) is a 140-amino acid cytoplasmic protein, found in the pre-synaptic terminal of neuronal cells, that has been implicated in the development of Parkinson's disease and Dementia with Lewy Bodies. The sequence of the peptide is given below (Figure 3.1) and shows the three distinct regions of the peptide, the N-terminus region (residues 1-60), the NAC region (residues 61-100) and the C-terminus region (residues 101-140). Of the three, only the N-terminus region- and in some cases extending into the NAC region- show specific secondary structures in the native state. The N-terminal region of α-syn contains 5 nearly conserved 11-residue repeats of the hexamer motif –KTKEGV- while the NAC region contains 2 slightly less conserved equivalents. The less conserved repeats within the NAC region may play a role in the amyloidogenesis of α-syn because reordering of the sixth repeat, in particular, with any of the other repeats leads to a lack of fibril formation. Instead amorphous aggregates, similar to those formed by β-synuclein are detected. (Rao *et al.*, 2009; Suk *et al.*, 2010)

N-terminal region	^{1}MDVFMKGLSK ^{11}AKEGVVAAAE ^{21}KTKQGVAEAA ^{31}GKTKEGVLYV ^{41}GSKTKEGVVH ^{51}GVATVAEKTK
NAC region	^{61}EQVTNVGGAV ^{71}VTGVTAVAQK ^{81}TVEGAGSIAA ^{91}ATGFVKKDQL
C-terminal region	^{101}GKNEEGAPQE ^{111}GILEDMPVDP ^{121}DNEAYEMPSE ^{131}EGYQDYEPEA

Figure 3.1. The full sequence of α-syn separated into the three distinct regions.

Native α-syn is typically post-translationally acetylated at the N-terminus. (Anderson *et al.*, 2006) This modification has often been identified as the reason α-syn does not aggregate in healthy systems. This may be due to the enhanced helical character of residues 1-9 in the presence of an acetylated N-terminus. (Georgieva *et al.*, 2008; Kang *et al.*, 2012) HSQC NMR experiments have

been used to show that the effect of N-acetylation on α-syn is confined to these residues and comparisons between the acetylated and non-acetylated peptides have shown a decreased propensity to form β-sheets by the acetylated peptide. (Kang *et al.*, 2012, 2013)

Even without the α-helix promoting modification, native α-syn adopts a helical conformation when in contact with membranes. (Eliezer *et al.*, 2001; Jao *et al.*, 2004; Bisaglia *et al.*, 2005, 2006; Ulmer *et al.*, 2005) However, there is a lack of consensus on the type of helix formed. Studies have shown the formation of both elongated helices from residues 1-102 (Ramakrishnan *et al.*, 2003; Georgieva *et al.*, 2008; Jao *et al.*, 2008) and antiparallel helices that are broken around residues 43 and 44. (Chandra *et al.*, 2003) It is possible that α-syn is capable of forming both helices, the type formed dependent on the type of vesicle it is binding to. (Rao *et al.*, 2009) Most likely, α-syn is capable of adopting a broken helix state when binding to small vesicles and the elongated helix state when binding to larger vesicles. There is also some ambiguity as to whether or not the helix formed merely results in surface contacts with the vesicle membrane or if the peptide is actually capable of inserting itself into the membrane. (Bisaglia *et al.*, 2005, 2006)

As has been mentioned before, the C-terminal tail of α-syn does not adopt a defined secondary structure, even in the early stages of amyloidogenesis. The presence of multiple Pro (P) residues in this segment could be causing the lack of secondary structure since Pro causes kinking in peptide chains that breaks up α-helix as well as prevents the formation of elongated β-sheets. Despite its lack of secondary structure, studies have shown that there are long-range interactions between the C-terminus of α-syn and other parts of the peptide. For instance, aromatic residues in the C-terminus have been shown to interact with the NAC region of α-syn. This is further confirmed by studies that show interactions between residues 120-140 of the C-terminus and residues 30-100 of the peptide, (Dedmon *et al.*, 2005), between residues 110-130 of the C-terminus with residues 85-

95 of the NAC region, (Bertoncini *et al.*, 2005) and between residues 121-140 of the C-terminus with residues 1-20 of the N-terminus. (Bernadó *et al.*, 2005) The strong contacts between the C-terminus of α-syn and multiple other regions of the peptide could explain why α-syn has a more compact structure than that of other random-coil peptides of the same size. The interactions could also have some protective effects that prevent α-syn from aggregating. Studies have demonstrated that truncation of the C-terminus of α-syn results in an increased rate of amyloidogenesis.(Hoyer *et al.*, 2004) Progressive truncation of α-syn further proves the protective effects of residues 120-140 since deletion of these residues results in increased rates of amyloidogenesis. (Murray *et al.*, 2003) In fact, plaques found in the brains of Parkinson's patients are made up of a significant amount of truncated α-syn. (Liu *et al.*, 2005) *In vitro* studies have also shown that C-terminal truncated α-syn aggregates faster than full-length α-syn and is capable of seeding the aggregation of full-length α-syn even at sub-stoichiometric concentrations. (Li *et al.*, 2005) The high acidity (and thus negative charge) of this segment of the peptide due to the increased number of Glu, E residues could also be playing a role in reducing the amyloidogenic propensity of native α-syn.

3.1.1. α-Syn and amyloidogenesis

Viewed by microscopy, α-syn fibrils are typically made up of multiple filaments forming a helical ultrastructure. Each filament is found to have a diameter of approximately 3-4 nm resulting in fibrils with 15-20 nm diameters. (Vilar *et al.*, 2008; Nakamura *et al.*, 2015) These unbranched fibrils are the hallmark of all amyloid fibrils. (Serpell *et al.*, 2000)

α-Syn has been determined to undergo amyloidogenesis in a nucleation-dependent manner. *In vitro* studies have shown that a typical amyloidogenesis curve for α-syn contains a lag phase, growth phase and a stationary phase. (Ghosh & Maji, 2015) Studies have tracked the transition of α-syn from random-coil to amyloid fibrils using a variety of spectroscopic methods including CD

and the enhanced fluorescence observed upon thioflavin-T (ThT) binding. One such study conducted by Ghosh *et al.* proposes that α-syn adopts a helix-rich intermediate before transitioning to β-sheets that form the amyloid fibrils. (Ghosh, Singh, *et al.*, 2015)

In amyloid plaques, α-syn has been shown to adopt a typical fibrillary conformation of cross β-sheet geometry whereby each individual strand runs perpendicular to the fibril axis. A number of techniques used, including solid-state NMR has shown that the amyloid fibrils of α-syn form predominantly in residues 30 to 110. Vilar *et al.* have shown through quenched deuterium/hydrogen exchange NMR that α-syn may be forming five distinct β-strands from residues 35 to 96; β1 (35-41), β2 (49-56) β3 (62-68), β4 (70-79 or 70-83) and β5 (90-96). They propose that the five strands, with a short unstructured loop between each strand, forms a β-strand sandwich that runs perpendicular to the amyloid fibril axis (Figure 3.2). (Vilar *et al.*, 2008)

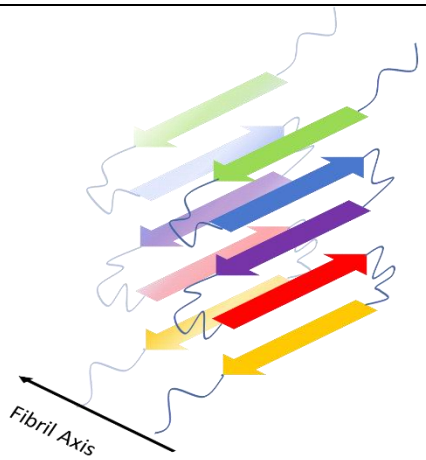

Figure 3.2. Fold of α-syn fibrils as proposed by Vilar *et al.*, 2008. The five β-strands are shown as $\beta1_{35\text{-}41}$(green), $\beta2_{49\text{-}56}$ (blue) $\beta3_{62\text{-}68}$ (purple), $\beta4_{70\text{-}79 \text{ or } 70\text{-}83}$ (red) and $\beta5_{90\text{-}96}$ (orange).

While some studies still contend that the fibrils of α-syn are responsible for toxicity, (Luk *et al.*, 2012; Pieri *et al.*, 2012) most research now views a soluble oligomeric form of α-syn as the toxic species of associated with amyloidogenesis. (Karpinar *et al.*, 2009; Winner *et al.*, 2011) Therefore, a lot of work has been focused on studying this form of α-syn both to discover how it causes

cytotoxicity as well as learning how to inhibit its formation or build-up. It has recently been proposed that the oligomeric form of α-syn adopts an antiparallel β-sheet structure as opposed to the parallel β-sheets seen in mature plaques. (Celej *et al.,* 2012) Mirecka *et al.* have also demonstrated that α-syn may in fact adopt individual β-strands (or hairpins) on the pathway to amyloidogenesis. (Mirecka *et al.,* 2014) Their studies using a protein inhibitor led to the identification of a binding locus within α-syn which happens to coincide with strands β1 and β2 that were identified in the studies done by Vilar *et al.* The same hairpin was studied by Salveson *et al.* and was shown to form higher-order structures that showed high levels of cytotoxicity in neuronal cells. (Salveson *et al.,* 2016) These results are further bolstered by the fact that residue H50 is one of the first residues that displays peak attenuation by solution NMR during amyloidogenesis leading to a possible nucleating role for this portion of α-syn in amyloidogenesis. (Sivanesam *et al.,* 2015)

A prominent role has also been posited for the aromatic residues within α-syn. Alpha-syn contains one Tyr residue in the N-terminus and three more Tyr residues in the C-terminal tail. A mutational analysis of these residues showed that the replacement of all three Tyr residues in the C-terminal tail resulted in complete elimination of α-syn amyloid formation. Point mutation of each Tyr residue showed that of the three residues Y133 played the most important role in amyloid formation. This conclusion arose because Y125A and Y136A mutations only showed limited inhibition while Y133A resulted in complete inhibition. It can be further concluded that Y133 may have an important interaction with Y39 since the Y39A-mutation also demonstrated substantial inhibition of amyloid formation. (Ulrih *et al.,* 2008)

Of all the post-translational modifications that α-syn is said to undergo, the most controversial has to be the phosphorylation of Ser-129. Since its discovery in 2002, by Fujiwara *et al.* in Lewy Body

inclusion, this modification has yielded highly conflicting results. (Fujiwara *et al.*, 2002) It is a common observation that approximately 90% of α-syn in Lewy Bodies are phosphorylated while only 5% of α-syn is phosphorylated in healthy individuals. (Sato *et al.*, 2011) However, whether or not, the phosphorylation plays a role in amyloidogenesis or if it just a result of amyloidogenesis is unclear. It is also unclear whether or not the phosphorylation affects the rate of aggregation. The initial study done by Fujiwara *et al.* would seem to indicate that this modification does increase the rate of amyloid formation. (Fujiwara *et al.*, 2002) However, there are studies that produce conflicting results. (Paleologou *et al.*, 2008) Paleologou *et al.* also conclude that the S129 phosphorylation increases the flexibility of α-syn, making it less compact. This is concomitant with long range interactions between the C-terminus and N-terminus of α-syn being disrupted by the presence of the phosphoryl group.

It is becoming more evident however that the phosphorylation of S129 may play a role in the membrane binding affinity of α-syn. A recent study showed that phosphorylation increased the membrane binding of A30P, a pathogenic mutant of α-syn but decreased the membrane binding of A53T, another pathogenic mutant. (Samuel *et al.*, 2016) Along with membrane binding, the study suggested that phosphorylation results in a higher rate of endocytic vesicle rupture. This could be an important result because the rupturing of endocytic vesicles carrying misfolded α-syn could be how the oligomers recruit more monomers upon entering adjacent neurons. But even these results are a contradiction of earlier studies that show phosphorylated S129 has a reduced membrane binding affinity with phospholipids. (Pronin *et al.*, 2000) The only conclusion one can draw from these results so far is that the phosphorylation of S129 of α-syn plays some role in disease pathogenesis.

3.1.2. Mutations in the α-syn gene

Until the late 90's, Parkinson's disease (PD), especially late-onset PD, had been viewed as a sporadic disease caused by point mutations in the gene encoding α-syn, with no genetic inheritance. (Gwinn-Hardy & Farrer, 2002) However, a study done in Iceland showed that a large number of people who were diagnosed with this disease were "significantly more related to each other than were subjects in matched groups of controls". (Sveinbjörnsdottir *et al.*, 2000) This led to the conclusion that PD, regardless of age of onset, is caused in part by genetic factors. The initial discovery of SNCA whole gene multiplication occurred when investigation into the cause of PD in a large family yielded no point mutations in the SNCA gene. Quantitative real-time PCR amplification of the SNCA gene was used to determine that whole gene triplication was the common factor among family members exhibiting PD pathology. (Singleton *et al.*, 2003; Singleton *et al.*, 2004) While whole gene triplication has been linked to early onset PD, Chartier-Harlin *et al.* showed that whole gene duplication could also be causing PD but at a later age. (Chartier-Harlin *et al.*, 2004)

Point mutations within the SNCA gene have also been linked to autosomal dominant forms of PD. To date, 6 mutations have been discovered and studied. The first point mutation linked to a genetic inheritance of PD was A53T, discovered in 1997 by Polymeropoulos *et al.* in an Italian-American family, known as the Contursi family. (Polymeropoulos *et al.*, 1997) Interestingly, their discovery of this mutation is what led to the conclusion that α-syn is the primary component of Lewy body inclusions. The discovery of A53T was quickly followed by the discovery of the mutant A30P in a German family displaying autosomal dominant PD. (Krüger *et al.*, 1998) Biophysical studies into the fibril formation of these two mutations led to the conclusion that A53T was aggregating at a much higher rate than wild-type (WT) α-syn. (Giasson *et al.*, 1999; Conway, Harper, *et al.*,

2000; Conway, Lee, *et al.*, 2000; Li *et al.*, 2001; Choi *et al.*, 2004; Greenbaum *et al.*, 2005; Ghosh *et al.*, 2014) However, conflicting results were initially found for A30P. The earliest studies, initially indicated that A30P formed spherical aggregates and took longer to form the elongated fibrils typical of WT. (Conway *et al.*, 1998) However, Narhi *et al.*, using sedimentation experiments came to a different conclusion, indicating that both A30P and A53T aggregated faster than WT. (Narhi *et al.*, 1999) Subsequent studies discovered that while A30P did in fact oligomerize at an equal rate or slightly faster than WT (Conway, Lee, *et al.*, 2000), it stayed in the oligomer phase of amyloidogenesis for much longer. This conclusion led to the theory that it was in fact the oligomer phase that plays a role in cell cytotoxicity. An important support to this conclusion is that the fibrils formed by either mutation shows no morphological difference to fibrils formed by WT. However, studies have shown that the A30P, and to some extent the A53T, mutants of α-syn display less avid binding to membranes. (Choi *et al.*, 2004; Ghosh *et al.*, 2014) The lack of binding could be due to the location of this mutation in the region where helix-2 is known to form when in the presence of membranes. The presence of a Pro, P residue in place of helix-favoring Ala could play a significant role in preventing helix formation. The inability to form helices could result in the abrogation of normal α-syn functions which could be another factor that causes disease.

In 2004, a third mutation, E46K was discovered in a Spanish family. (Zarranz *et al.*, 2004) This mutation showed very similar pathology to the A53T mutation and in *in vitro* studies, it had higher rates of fibrillation similar to that of A53T. (Choi *et al.*, 2004; Greenbaum *et al.*, 2005) However, liposome binding assays indicated that the E46K mutation resulted in almost two-fold higher binding to liposomes. The difference in binding for A30P as well as E46K, may be related the fact that both these residues are highly conserved in the α-syn of all species. However, A53T shows no

similar conservation with A53 being present in humans while T53 is present in other species. (Hamilton, 2004) This difference in residue conservation across species could point to an important role being played by those two residues in α-syn function while A53T, which shows no difference in binding assay, may not be playing an important functional role. It is also important to note that the A53T and E46K mutations, which result in faster amyloid formation, are also part of a β-hairpin-forming region of α-syn that has been proposed to be an early event in amyloidogenesis. (Mirecka *et al.*, 2014)

Following the discovery of E46K, no new mutations of α-syn were discovered until 2013, when two more mutations, H50Q (Appel-Cresswell *et al.*, 2013) and G51D (Kiely *et al.*, 2013) were found. H50Q was shown to have a higher rate of aggregation than WT and was displaying pathology very similar to A53T. Proukakis *et al.* suggested that the reason H50Q was disease causing could be related to its interaction with Cu^{2+} ions that are known to be elevated in PD patients. (Proukakis *et al.*, 2013) Studies have shown that in WT α-syn, the H50 imidazole ring binds to Cu^{2+} by "wrapping around to participate in the Cu^{2+} coordination environment." This results in α-syn having to leave the α-helix conformation. However, in H50Q this is not necessary, leading to a stabilization of the helix state and more conformational freedom. The increased freedom could play a role in increasing the rate of aggregation of this mutant *in vivo*. Ghosh *et al.* showed that the lack of His at position 50, rather than the presence of Q is the cause for the increase in aggregation. (Ghosh *et al.*, 2013) Their mutational analysis of H50A showed similar aggregation rate as H50Q. They were also able to ascertain that the H50Q led to perturbations in the residues around it (residues 44-56) as well as perturbation further down in the C-terminus (residues 113-135). These results further validate the studies that point to long-range interactions between the C-terminus and other parts of α-syn resulting in a more compact structure.

The discovery of G51D however has given rise to more questions about what role α-syn may play in the synucleinopathies. This mutation seems to have a slower rate of aggregation than WT and forms amorphous aggregates similar to A30P. However, G51D seems to trigger apoptotic cell death by caspace-3 more than WT. (Lesage *et al.*, 2013) Fares *et al.* also made some interesting observations about G51D. This mutation is able to form a helix in helix-promoting environments such as TFE but shows lower membrane binding affinity than WT. (Fares *et al.*, 2014) The lower binding affinity is most likely due to a lesser extent of helix formation by residues 45-55, as seen by NMR. This reduced helical propensity in the presence of lipids could possibly be negating the inhibitory effects that high lipid:α-syn ratios have against aggregation. (Bodner *et al.*, 2009, 2010) The study also showed that G51D mutants were secreted more rapidly in mammalian cells and they were more localized in the nucleus as well as having more Ser-129 phosphorylation. The presence of G51D also seemed to result in abnormal mitochondrial structures in cells but this did not result in cell death. Taken together, the effect of the G51D mutant as a disease-causing mutation may not be related to amyloid formation but could instead point to a different mechanism by which α-syn causes disease. (Fares *et al.*, 2014)

The final known mutation, A53E, was discovered in 2014 by Pasanen *et al.* in a Finnish family. (Pasanen *et al.*, 2014) The pathology of the patients showing this mutation was similar to that of the G51D mutation but there was less consensus on whether the mutation resulted in early onset PD. Biophysical studies of the mutation showed that this mutant had a slower rate of fibril formation than WT α-syn. (Ghosh *et al.*, 2014) To determine if the mutation of a hydrophobic residue to an acidic residue was the cause for the change in aggregation rates, a mutational study with A53K was done. The results of this study showed that a charged residue at this position slows down aggregation. Time-dependent AFM studies and dynamic light scattering experiments

revealed that the mutant was spending a longer time in the oligomer state, similar to the observations made about A30P. The mutation was shown to cause perturbations of chemical shifts for the residues surrounding it as expected. It also showed perturbations in the C-terminus, once again pointing to long-range interactions between this region and the C-terminus of α-syn. Similarly to A53T, the A53E mutation shows no difference in helix-formation in TFE buffers. However, the dissociation constant from membrane binding studies indicate that the mutant has a lower binding affinity than WT which is a different result as that shown by A53T mutants.

3.2. Inhibitors of α-syn toxicity

Since its implication as the possible underlying cause of Parkinson's disease, α-syn has been heavily studied; particularly with respects to inhibitors that could possibly serve to ameliorate the negative effects of α-syn soluble oligomers that are prevalently accepted as the most toxic species. A number of inhibitory strategies can be envisioned: a) maintaining the random-coil structure of α-syn and never allowing it to form toxic oligomers; b) increasing the rate of amyloidogenesis so that α-syn does not linger as a soluble oligomer (the presumed toxic state) but quickly forms non-toxic fibrils and plaques; c) redirecting α-syn amyloidogenesis to form non-toxic off-pathway aggregates, or d) signaling the mechanisms within the body to promote clearance of toxic forms of α-syn. Numerous classes of inhibitors have emerged as possible therapeutics for α-syn amyloidogenesis but the problem remains, developing small molecules or peptides that are capable of penetrating the blood-brain barrier in order to be most effective against α-syn.

3.2.1. Small molecule inhibitors

The most common motif of small molecules that have been tested successfully as inhibitors of α-syn amyloidogenesis is the presence of the phenol moiety. From this category, a number of natural products have been discovered to inhibit α-syn. Among them, resveratrol is a popular test subject. Resveratrol is extracted from the skin of grapes, blueberries, raspberries, and mulberries. This polyphenol has been shown to be an antioxidant and has been tested extensively *in vivo* as a potential therapeutic for PD. Rat models have shown that resveratrol can confer neuroprotective effects on 6-hydroxydopamine induced PD, showing results as early as 48 hours after administration. (Jin *et al.*, 2008) Dopaminergic neuron degradation by the neurotoxin 1-methyl-4-phenyl-1,2,3,6-tetrahydropyridine (MPTP) has also been reduced by the protective effects of resveratrol. (Blanchet *et al.*, 2008) Unlike most small-molecule inhibitors, the *in vitro* activity of resveratrol has been shown to be quite modest. (Caruana *et al.*, 2011) This is most likely due to the fact that the neuroprotective effects of resveratrol may be a result of activation of human sirtuin 1 (SIRT1) that is known to promote the autophagy of proteins in the nucleus and cytoplasm. (Albani *et al.*, 2009) These results were confirmed when the activity of resveratrol was eliminated in the presence of sirtinol, an inhibitor that is specific for SIRT1. Up-regulation of autophagy by resveratrol is particularly relevant since it has been shown that patients with PD typically demonstrate down-regulated autophagy in the brain. (Cheung & Ip, 2009) Resveratrol is also able to upregulate the clearance of mutant α-syns, A30P and A53T in PC12 cells, further singling this molecule out as a potential therapeutic for PD. (Wu *et al.*, 2011)

While resveratrol action depends on indirect effects on α-syn, gallic acid, another small molecule extracted from grape skins, gallnuts, tea leaves and other plants has been shown to act directly on α-syn amyloidogenesis *in vitro*. This small molecule has been shown to inhibit the formation of

fibrils and reduce the amount of oligomers formed by wild-type α-syn. (Ardah *et al.*, 2014) However, this effect was only observed at high doses of gallic acid. At low doses, gallic acid instead seemed to promote the formation of oligomers. However, these oligomers were found to be non-toxic to cells giving rise to the conclusion that gallic acid redirects α-syn amyloidogenesis to off-pathway aggregates. ^{15}N-HSQC NMR studies have revealed that gallic acid may not have specific binding loci on α-syn monomers, even though some protection from peak attenuation has been observed in the N-terminal and NAC binding regions. (Liu *et al.*, 2014) Instead, it is proposed that gallic acid binds to an oligomer form of α-syn and stabilizes it. (Ardah *et al.*, 2014) This has been confirmed by size-exclusion chromatography and UV scanning that shows oligomers formed in the presence of gallic acid contain gallic acid.

In vitro studies that test the activity of gallic acid against α-syn mutant, A53T, showed that it was capable of inhibiting the amyloidogenesis of this mutant. (Liu *et al.*, 2014) This is despite the fact that A53T has been shown to have a faster rate of amyloidogenesis than wild-type α-syn. Similarly to wild-type, studies into the interaction of gallic acid with A53T resulted in no specific binding loci. Instead, the study concluded that gallic acid may be binding non-specifically to the random-coil state and stabilizing it.

A derivative of gallic acid, (-)-epigallocatechin gallate (EGCG), has also been heavily tested as an inhibitor of α-syn amyloidogenesis. This small molecule, extracted from green tea, has shown promise as an inhibitor of other amyloidogenic systems such as Aβ and tau as well as α-syn. Experimental data shows that EGCG may be redirecting α-syn to form non-toxic off-pathway spherical aggregates. (Ehrnhoefer *et al.*, 2008) The proposed mechanism involves the binding of EGCG to α-syn, presumably to the C-terminal tail of α-syn, in order to prevent the formation of intermolecular β-sheets and fibrils. (Ehrnhoefer *et al.*, 2008; Lorenzen *et al.*, 2014) However, my

^{15}N-HSQC studies, reported herein, suggest that the binding may be less specific. (Sivanesam *et al.*, 2015) There have also been studies that suggest EGCG is capable of binding to the toxic oligomeric state of α-syn and destabilizing, thus preventing these oligomers from exerting cytotoxicity by interacting with membranes. (Lorenzen *et al.*, 2014) Other studies have also proposed that EGCG can interact with mature fibrils and convert them into spherical aggregates. (Bieschke *et al.*, 2010)

Figure 3.3. The chemical structure of select small molecule inhibitors of α-syn amyloidogenesis.

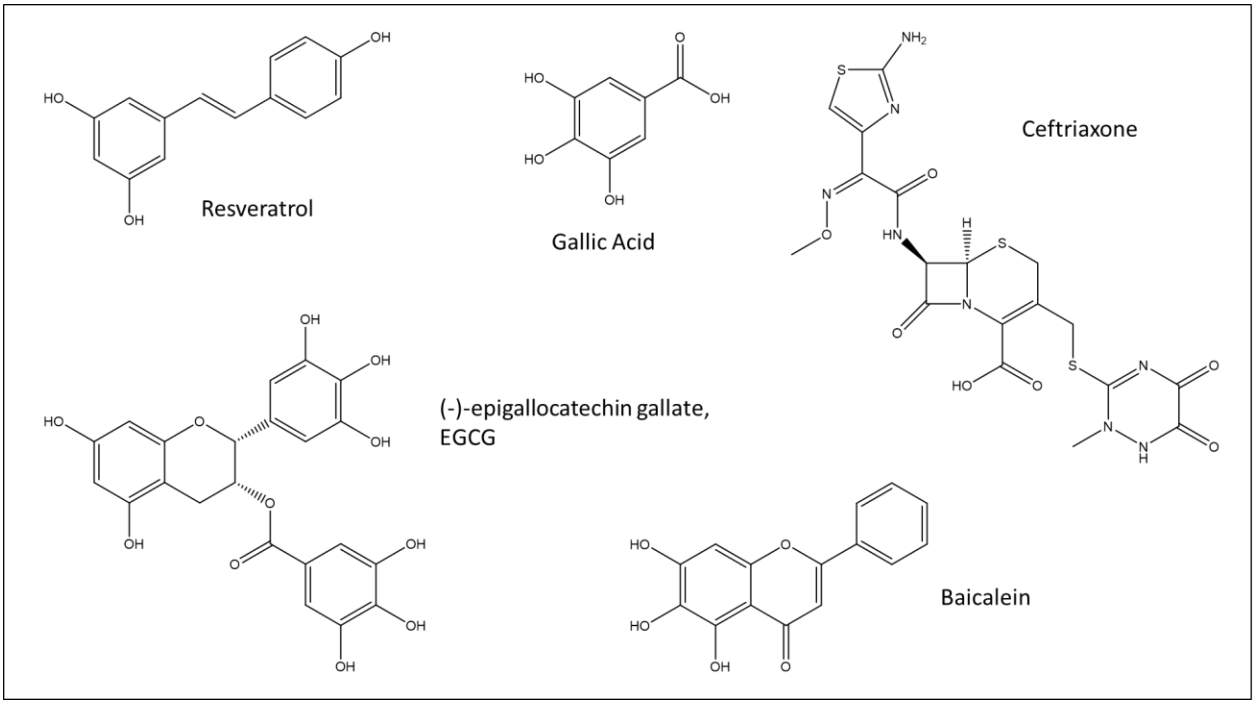

The significance of the phenols on these and other polyphenolic inhibitors has given rise to multiple studies attempting to determine how the phenol group interacts with α-syn. Studies that explored the effects of the phenol group on a benzoic acid template concluded that there is a strong correlation between the number of hydroxyl groups, their placement relative to the carboxyl unit and the inhibitory activity of the polyphenol. Ardah *et al.*'s study indicated that three hydroxyl groups positioned in the ortho and para positions relative to the carboxyl group where most

efficient at inhibiting α-syn amyloidogenesis. (Ardah *et al.*, 2014) This is interesting because gallic acid and EGCG both have 3 hydroxyl groups that are meta- and para- to the carboxyl group. The study showed that benzoic acid molecules with hydroxyl groups in this conformation had 72% activity while having three groups at ortho and para had 99% activity.

The most prevalent theory regarding the efficacy of polyphenols as inhibitors of α-syn amyloidogenesis, is the ability of polyphenols to form quinones. This is an accepted hypothesis, particularly for the polyphenol baicalein that demonstrated increased levels of inhibition in its oxidized state. (Zhu *et al.*, 2004) This may be due to the increased stability of the quinone when binding to α-syn since it is no longer susceptible to oxidation. (Taniguchi *et al.*, 2005) It has been proposed that the quinone interacts with aromatic residues and inhibits the π-π stacking of these residues. In particular, the quinone is most likely interacting with one of the three Tyr residues in the C-terminal tail since truncation of the C-terminus eliminates the activity of oxidized baicalein. (Meng *et al.*, 2009) These results further support the theory that the Tyr residues in the C-terminal tail play a role in amyloidogenesis as previously mentioned.

It is also consistent with the fact that the C-terminal tail of α-syn remains exposed even in the soluble oligomer form, making it an easier target for inhibitors. This may serve as further explanation for why an increasing number of inhibitors that are shown to bind to this region of α-syn. For example, ceftriaxone, a β-lactam antibiotic, (that has been shown *in vivo* to modulate the motor deficits of PD rats, (Leung *et al.*, 2012) and *in vitro* to completely inhibit the formation of soluble oligomers of α-syn,) has been computationally determined as binding the C-terminal tail. (Ruzza *et al.*, 2014)

3.2.2. Antibody inhibitors

The finding that α-syn is not confined to neuronal cells and is in fact secreted into the blood and cerebrospinal fluid by exocytosis in all individuals, regardless of PD development, (Borghi *et al.*, 2000; El-Agnaf *et al.*, 2003) led to the development of monoclonal antibodies. These antibodies were intended to localize and quantitate α-syn in the body (Lee *et al.*, 2011) but were later shown to promote the clearing of extracellular α-syn before it could result in cytotoxicity. (Desplats *et al.*, 2009; Lee *et al.*, 2010) Ab274, a monoclonal antibody has emerged as a strong inhibitor of α-syn cytotoxicity by promoting the lysosomal 'digestion' of toxic states of α-syn. (Bae *et al.*, 2012) This antibody has been determined to bind to the C-terminus of α-syn and could be interacting with the Fcγ receptor on microglial cells, promoting the macrophagy of these toxic forms of α-syn. Mouse studies showed that this antibody was capable of rescuing PD mice from the motor deficits associated with PD through inoculation. Another monoclonal antibody, 9E4, was also able to ameliorate the memory and learning deficits in mice models by increasing the clearance of α-syn aggregates in the cortex and hippocampus of the subject. (Masliah *et al.*, 2011) This is an interesting development since one of the most prominent hurdles to developing therapies that reduce α-syn related cytotoxicity is the ability to cross the blood-brain barrier.

Another class of antibodies that has emerged as potential therapeutics are single-chain antibody fragments (scFv). In the past, studies have identified scFvs that are capable of targeting the huntingtin protein and inhibiting its amyloidogenesis while protecting cells from the neurotoxic effect of the protein. (Lecerf *et al.*, 2001; Murphy & Messer, 2004) This information was used to identify an scFv that had nanomolar binding affinity to α-syn and reduced the rate of oligomer formation *in vitro*. (Emadi *et al.*, 2004) Intracellular testing of another scFv, D10, showed that this antibody was capably of identifying monomeric α-syn and binding to it thus preventing

amyloidogenesis. (Zhou *et al.*, 2004) However, the selectivity for monomeric α-syn could lead to the prevention of α-syn natural functions. This led to the development of an scFv, D5, that was capable of selectively binding to the oligomeric form of α-syn. (Emadi *et al.*, 2007) scFv D5 was capable of rescuing human neuroblastoma cells from the toxic effects of aged α-syn at sub-stoichiometric concentrations.

3.2.3. Protein and Peptide inhibitors

The concept of selectively targeting the oligomeric form of α-syn while ignoring the monomeric form of α-syn was utilized in the development of a short peptide that is capable of eliciting an immune response in the body. The peptides, known as AFFITOPES, were designed to mimic the C-terminus of α-syn but share no sequence similarity with α-syn. (Schneeberger *et al.*, 2010) This is an important feature of AFFITOPES since it prevents deadly autoimmune responses which have been known to hinder the development of vaccines for PD treatment. As a result of their study, Mandler *et al.* identified an AFFITOPE peptide, AFF1 that was able to elicit an immune response against oligomeric α-syn but not monomeric α-syn. (Mandler *et al.*, 2014) The peptide was further shown to be specific to only α-syn and not to the other types of synuclein such as β-syn that share some sequence similarity to α-syn. Mice studies showed that the vaccination with AFF1 was successful at reducing the pathological behaviors associated with PD. The success of the *in vivo* studies has led to the development of a vaccine, PDO1A, that has been tested in clinical trials. Preliminary results indicate that the vaccine is safe and tolerable at both doses administered. At least half the patients in the study demonstrated α-syn antibodies and showed less worsening of the disease compared to the control group. (Kuhl, 2014) However, the antibody levels began to drop over time which has led to the second phase of the trial, the administering of a booster dose which has so far shown positive results. (Kuhl, 2016)

While clearance of the toxic form of α-syn is an attractive prospect for study, there are still a number of other peptides and proteins that focus on inhibiting the amyloidogenesis of α-syn. One such protein, β-wrapin AS69, was developed from a ZAB_3, a protein that binds to Aβ. (Mirecka *et al.*, 2014) AS69, differs from ZAB_3 at four residues in each subunit resulting in a complete change in selectivity. The protein was also determined to be an inhibitor of α-syn cytotoxicity at equimolar concentration, rescuing human neuroblastoma cells from α-syn cytotoxicity. Crystallographic studies of the inhibitor when bound to α-syn revealed an interesting binding motif in the N-terminal region of α-syn. (see section 3.4.5 for further discussion)

Another common approach to designing inhibitors of α-syn has been to use segments of α-syn itself that are shown to bind to the monomer and prevent self-self recognition that leads to amyloidogenesis. Typically, these segments are modified in order to increase solubility and prevent the segment from aggregating on its own. El-Agnaf *et al.* chose to study residues 64-100 of α-syn in one such effort. (El-Agnaf *et al.*, 2004) These residues were chosen most likely due to the fact that this spans the NAC region that has been postulated as the most amyloidogenic portion of the protein. They synthesized a series of six-residue peptides that span this region and included hydrophilic residues at both termini in order to increase the solubility of the peptide inhibitors. Of all the peptides tested, one peptide was determined to be a good inhibitor of α-syn amyloidogenesis. This conclusion was drawn based on ThT fluorescence experiments that showed inhibition when incubated with α-syn at 1:2, 1:1 and 2:1 ratios. However, my own attempts to replicate these results were unsuccessful: the difference in reaction conditions for the assay may have played a role in this failure. (Sivanesam *et al.*, 2015)

Other studies have shown that N-methylation of certain residues within the inhibitor segment or the insertion of proline residues into the inhibitor segment can also be useful in preventing self-

aggregation. This is because aggregation depends on the ability of the peptide backbone to hydrogen bond to form stable intermolecular β-sheets. The presence of a methyl group at the backbone nitrogen or the lack of primary nitrogen at that position can eliminate hydrogen bonding thus preventing self-aggregation of the inhibitor. (Gordon *et al.*, 2002; Adessi *et al.*, 2003; Kokkoni *et al.*, 2006) This is also the proposed mechanism by which aggregation of α-syn is inhibited. The short segment is recognized by α-syn due to sequence homology, however, the presence of the secondary nitrogens on the other face of the inhibitor, prevents the continued addition of monomers, thus preventing amyloidogenesis.

Multiple N-methylated peptides have been synthesized based on the minimum sequence of α-syn required for aggregation. Bodles *et al.* determined that the 10-residue span ^{68}GAVVTGVTAVA^{78} of α-syn was capable of forming toxic aggregates in rat PC12 cells. (Bodles *et al.*, 2000, 2001) The N-methylation of G73 however, prevented aggregation *in vitro* and at equimolar concentrations, reduced toxicity of full-length α-syn *in vivo*. (Bodles *et al.*, 2004) Madine *et al.* identified a shorter self-aggregating sequence spanning residues 77-82. The N-methylated inhibitor that they synthesized, VAQKT$_m$V showed high levels of inhibition at equimolar concentrations *versus* full-length α-syn in *in vitro* experiments. (Madine *et al.*, 2008)

The dependence on sequence homology to facilitate recognition by α-syn, while convenient, poses a problem for therapeutic development. These peptides are more susceptible to degradation within the cell and may not be able to reach their targets intact. The overreliance on sequence homology also prevents the understanding of common features α-syn may have with other amyloidogenic systems. This knowledge paved the way for the Andersen lab to develop peptide inhibitors that had no sequence homology to α-syn but were still capable of inhibiting amyloidogenesis. My studies are based on the hairpin hypothesis that states the pre-amyloid state of any protein would

form more favorable interactions with stable β-hairpins, thus overcoming their propensity to undergo self-self recognition and amyloidogenesis.

3.3. Assay development

3.3.1. CD and ThT assay

The conditions for this assay were developed by Dr. Kelly Huggins and were successfully replicated for all the studies done below.

Calculation of percent inhibition by CD was done using the following formula:

$$Percent\ inhibition = 100 - (\frac{In\ the\ presence\ of\ inhibitor\ (\Delta_{198} - \Delta_{217})}{In\ the\ absence\ of\ inhibitor\ (\Delta_{198} - \Delta_{217})}\ x\ 100)$$

where Δ_{198} = difference in mean residue-molar ellipticity ($[\theta]_{MRW}$) at 198 nm between t=0 and t=18 hours

Δ_{217} = difference in mean residue-molar ellipticity ($[\theta]_{MRW}$) at 217 nm between t=0 and t=18 hours

Calculation of percent inhibition by ThT was done using the following formula:

$$Percent\ inhibition = 100 - (\frac{signal\ at\ t = 18\ hours\ in\ the\ presence\ of\ inhibitor}{signal\ at\ t = 18\ hours\ in\ the\ absence\ of\ inhibitor}\ x\ 100)$$

3.3.2. HSQC NMR assay

The initial studies done for α-syn were done using conditions developed by Dr. Aimee Byrne in a phosphate buffer system that more closely mimicked the conditions for the CD and ThT assays.

However, these conditions were later modified to perform the experiments in a different buffer system, Tris.HCl. The conditions for the new NMR assay required only 100μM α-syn instead of the 200μM α-syn that was used in the past. Under these conditions, I found that α-syn aggregation could be induced almost immediately, in the presence of 2% v/v HFIP, by increasing the temperature of the experiment from 280K to 300K.

3.4. Results and discussion

3.4.1. Examining previously discovered inhibitors

In an effort to verify that known inhibitors of α-syn would show activity in our assay, I tested two inhibitors: a small molecule, (-)-epigallocatechin gallate (EGCG) and a peptide, RGAVVTGR-NH_2. The peptide inhibitor was first discovered by El-Agnaf *et al.* and was shown to inhibit α-syn aggregation at sub-stoichimetric concentrations. (El-Agnaf *et al.*, 2004) Under my conditions however, RGAVVTGR-NH_2 failed to show any activity even at 4 eq peptide to α-syn. EGCG on the other hand did show approximately 65% inhibition at 2 eq inhibitor. In the initial study conducted by Ehrnhoefer *et al.*, they found increasing peak broadening at the C-terminus of α-syn that was most evident at five- and ten-fold excess inhibitor to peptide. (Ehrnhoefer *et al.*, 2008) The peaks, D119, S129, E130, and D135 that disappeared at equimolar concentration of inhibitor were determined to be the strongest binding positions.

At a 10:1, EGCG: α-syn ratio, I observed immediate precipitation that prevented me from examining the sample by NMR. Spectra taken at a 5:1, EGCG: α-syn ratio, showed binding shifts that were much lower ($\Delta\delta(^1H)$ = 0.007 - 0.010 ppm) than those reported in the literature. (Appendix B1) I also saw several shifts in regions outside of the C-terminus which could be a secondary

binding locus of EGCG. To investigate this further, I performed a titration at lower concentrations of EGCG. The results showed a number of shifts in the N-terminus, half of which were located in the β1 and β2 hairpin region identified by Vilar *et al.* (Vilar *et al.*, 2008) (Appendix B2) The remaining shifts were in the C-terminus of α-syn. However, none of these shifts approached the magnitude of the shifts that was seen for our peptide inhibitors, WW and cp-WW that have been tested in this lab. (Appendix B4)

Incubation of the inhibitor with α-syn over a 6-hour time period revealed few residues showing peak attenuation, which contradicts the results shown by the earlier studies of Ehrnhoefer *et al.* (Ehrnhoefer *et al.*, 2008) The only peaks that showed attenuation, S9, K10, A11, K43 and H50, were also among the first peaks to show attenuation in the absence of inhibitor (see Figure 3.5). Upon addition of 1.5 vol-% HFIP and incubation for 96 hours, three observations were made: 1. Peak attenuation continued to increase for almost all residues, with peaks in the N-terminus and NAC region completely disappearing at this point. 2. Time-dependent chemical shifts that went in the opposite direction of shifts observed upon EGCG addition began occurring in the C-terminal segment. 3. No precipitation was observed. (Appendix B3) All of the attenuated peaks that were observed, corresponded to the same peaks that disappeared in the absence of inhibitor. The reversal of binding shifts over the course of time could be attributed to a decrease in binding affinity of EGCG to α-syn in the presence of HFIP. This could also be used to explain why the activity of EGCG in the CD and ThT assay did not show the same level of potency as that in the literature. All in all, our studies show that EGCG did not redirect α-syn to off-pathway aggregates as reported, instead it was most likely slowing down the rate of oligomer formation.

3.4.2. Fold stability and inhibition – the WW series

The use of non-sequence-homologous peptides as inhibitors of amyloidogenesis is not an entirely novel concept. Gramicidin S, an antibacterial cyclic peptide has been shown to inhibit the aggregation of Aβ42, a protein implicated in Alzheimer's disease. A designed peptide with a tryptophan zipper motif, Trpzip-3 was shown to inhibit the amyloidogensis of Aβ as well as transthyretin, another known amyloidogenic protein. (Hopping *et al.*, 2013) Also, the B1 domain of protein G had previously been shown to inhibit the aggregation of Aβ40. Unlike gramicidin S, the protein-G-related inhibitors did not contain unnatural amino acids. However, the final inhibitor did have several mutations of non-aromatic residues to the aromatic residues, W and Y. (Smith *et al.*, 2006) This led to the initial idea to test aryl-rich hairpin peptides as inhibitors of amyloidogenesis in the Andersen laboratory. Dr. Kelly Huggins performed that initial studies that led to the discovery of hairpin, WW (KKLTV**W**-IpGK-**W**ITVSA) that was capable of inhibiting the amyloidogenesis of α-syn. (Huggins *et al.*, 2011)

My studies built upon this discovery and aimed to further examine the hairpin hypothesis by testing more peptides as potential inhibitors of amyloidogenesis. While all the peptides previously tested demonstrated high fold populations under assay conditions, there was no way to determine if unfolding occurred prior to association with the target. Therefore, our first aim was to determine if confining the β-hairpin fold of WW would result in changes in antiaggregatory activity. To test this, we synthesized two "cyclic" peptides: WW-DS – had a disulfide bond between C residues at non-H-bonded positions, and cyclo-WW – had backbone cyclization by including an –IpPK- turn at the termini. The precursor to cyclo-WW was the circular permutant of WW, cp-WW. Circular permutation refers to the moving of a Trp/Trp pair from its original position (in the case of WW, as a turn flanking pair) to a new position (in the case of WW, to an end capping position). This is

typically done in order to study the effect of the Trp/Trp pair at various positions, on the folding of the peptide.

Another stabilization technique that has been developed in the lab (as previously discussed), the β-cap, was also employed to further stabilize the hairpin fold of WW. This peptide, Ac-cap-WW contained an acetyl group at the N-terminus that interacts with the hydroxyl group of the Thr residue at the C-terminus, thus reducing the fraying of the termini. This acetyl group can be replaced with other carboxylic acids. To determine if small molecules at this position could increase the activity of WW, we studied two mutants of capped-WW: gal-cap-WW – acetyl group was replaced with a gallate group, and bz-cap-WW – acetyl group was replaced with a benzoyl group. An additional set of "hairpin" peptides were also tested including a peptide (mWWhp) and its circular permutant (cp-mWWhp) that were mutated from Pin1 of the WW domain. I also tested the highly-truncated version of WW, uPro1 (C_2H_5CO-**W**-IpGK-**W**TG-NH_2) that had previously been shown to be a good inhibitor of α-syn amyloidogenesis despite the lack of β-strands. A list of all the peptides in the WW series tested, is given in Table 3.1.

Table 3.1. The amino acid sequence for all the peptides tested in the WW series. Edge-to-face aryl/aryl pairs are denoted in bold.

Peptide name	Peptide sequence
WW	KKLTV**W**-IpGK-**W**ITVSA
WW-DS	KCLTV**W**-IpGK-**W**ITVCA
Cyclo-WW	cyclo-(GK-**W**ITVS-IpPK-KLTV**W**-Ip)
cp-WW	GK**W**ITVS-IpPK-KLTV**W**Ip
Ac-cap-WW	CH_3CO-**W**-KKLTV**W**-IpGK-**W**ITVSA-**W**TG-NH_2
Gal-cap-WW	$C_7H_5O_4$ - **W**-KKLTV**W**-IpGK-**W**ITVSA-**W**TG-NH_2
Bz-cap-WW	C_7H_5O - **W**-KKLTV**W**-IpGK-**W**ITVSA-**W**TG-NH_2
mWWhp	RWEKR**W**-DRGSGR-**W**FYFND
Cp-mWWhp	R**W**FYFN-DRGSGK-WEKR**W**D

RAVWW	RAVT**W**-NPATGK-**W**ITVWE
µPro1	C_2H_5CO-**W**-IpGK-**W**TG-NH_2
YY-µPro1	CH_3CO-**Y**-IpGK-**Y**TG-NH_2

A typical CD spectrum for uninhibited α-syn shows a random-coil signal ($[\theta]_{198}$ = -16000 deg·cm^2·dmol^{-1}) at time 0 and a β-sheet signal at t=18 hours ($[\theta]_{217}$ = -16000 deg·cm^2·dmol^{-1}; $[\theta]_{198}$ = 22000 to 35000 deg·cm^2·dmol^{-1}) under my assay conditions. As shown in Figure 3.4A, the transition from random-coil to β-sheet can be observed in the changing of the minimum at 198 nm to a maximum while the minimum at 217 nm grows. These spectra are reproducible and correspond to spectra that have been reported in the literature. (Nath *et al.*, 2010) Spectra of samples containing both α-syn and the peptide inhibitor are processed by subtracting a blank measurement that contains the appropriate amount of inhibitor. This is done to ensure that the final spectrum is only showing the structural changes of α-syn. However, the measurements taken for some peptide inhibitors are complicated by the fact that a precipitate is formed upon addition of the peptide to α-syn samples. This prevents the effective quantification of the amount of α-syn remaining in solution which could affect the molar ellipticity calculations for CD as well as the ThT fluorescence measurements. To study this effect, all samples were incubated for 2 hours without HFIP following addition of peptide inhibitor. Figure 3.4B shows the ThT measurements taken at t=0, t=4 hours, t=12 hours and t=18 hours. Each point on the graph is an average of three runs and the error bars represent the standard deviation of the three runs. The data shows that the amyloid character of the sample grows over time with a steep increase between t=12 hours and t=18 hours, which most likely represents the growth phase of the amyloid fibril curve.

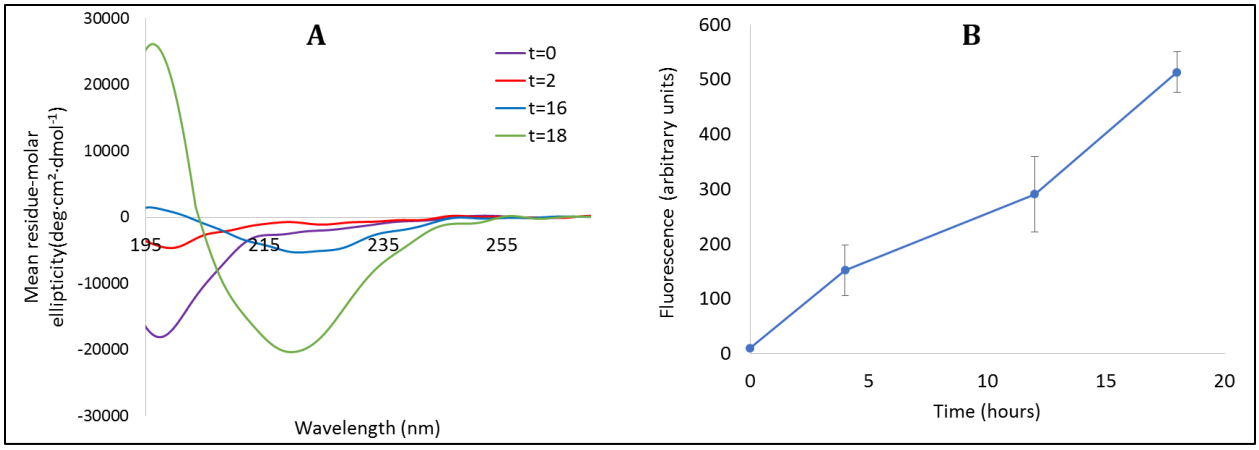

Figure 3.4. Panel A- CD spectra of uninhibited α-syn. Panel B- ThT measurements taken at t=0, t=4, t=12 and t=18 hours of uninhibited α-syn. The error bars represent the standard deviation of each measurement. (n=3)

Typically, the inhibitors that we have studied in this series have acted on α-syn by increasing the amount of time spent in the random-coil state. Over the course of 18 hours, most of the peptides prevent the transition from random-coil to β-sheet to some extent (Table 3.2). Of the three WW peptides initially tested, cp-WW showed the least inhibitory activity, followed by WW. The most potent inhibitor to emerge from my studies is cyclo-WW. The peptide can maintain α-syn in a random-coil state for up to 18 hours at substoichiometric concentrations. The less effective disulfide cyclized peptide, WW-DS did not exhibit the same level of potency as cyclo-WW. These results can serve to affirm the hairpin hypothesis since the most folded peptide, cyclo-WW is showing the highest levels of inhibition.

An interesting comparison emerged between Trp/Trp pairs and Tyr/Tyr pairs in this study. The activity of μPro1 was determined to be approximately 50% when 2 eq of the peptide was co-incubated with α-syn. However, the Try/Tyr analog of the peptide, YY-μPro had an 85% inhibitor activity at the same concentrations. This increase in activity despite a decrease in peptide fold stability could be pointing to a role played by the phenol side chain of Tyr.

Table 3.2. Compilation of ThT data as well as CD data for peptides tested in this series. Each ThT measurement and CD measurement is an average of 3 repeats.

	2 eq			1 eq		
	% inhibition			% inhibition		
	ThT	CD	Average	ThT	CD	Average
WW2	73 ± 11	80 ± 14	~ 75	60 ± 16	43 ± 31	~ 50
WW2-DS	51 ± 21	36 ± 9	~ 50	35 ± 16	16 ± 1	< 30
cyclo-WW	92 ± 4	91 ± 7	> 90	74 ± 13	78 ± 14	~ 75
cp-WW2	66 ± 19	67 ± 16	~ 65	24 ± 15	48 ± 22	~ 35
ac-cap-ww	86 ± 10	75 ± 2	~81	93 ± 2	73 ± 1	~83
gal-cap-ww	94 ± 3	75 ± 3	~85	88 ± 1	71 ± 3	~80
bz-cap-ww	95 ± 4	78 ± 1	~87	82 ± 7	71 ± 2	~76.5
mWWhp	56 ± 9	49 ± 10	~ 50			
cp-mWWhp	11 ± 13	20 ± 7	< 20			
RAVWW	63 ± 7	54 ± 10	~ 60			
μPro1	63 ± 10	44 ± 10	~ 50			
YY-μPro1	92 ± 7	96, 95	~ 90	89 ± 5	84 ± 8	~ 85

Investigating the role of phenols was done by using gal-cap WW. This peptide contains a known α-syn inhibitor, gallic acid as the N-acyl cap for the peptide. NMR data (Appendix A4) indicates that the different groups used as N-acyl caps of the peptide did not have a significant effect on stability, with CSDs throughout the peptide showing minor variations among the three peptides. The CD data (Appendix A1, A2 & A3) however indicates that the presence of a benzoyl group at the N-terminus affords the strongest exciton couplet at 5°C (519 853 deg·cm^2·dmol^{-1}) followed by the acetyl group (391 612 deg·cm^2·dmol^{-1}). The presence of the gallate group appears to afford the least amount of stabilization for the β-cap (269 012 deg·cm^2·dmol^{-1}).

The activity of the other two capped-WWs was compared to the activity of gal-cap-WW. CD data indicates that all three are potent inhibitors of α-syn, even at substoichiometric concentrations.

Unfortunately, the CD data did not allow for distinguishing of one inhibitor as more potent than the other. The ThT data, on the other hand, would indicate that ac-cap-WW has a higher level of inhibition than gal-cap-WW at 0.5 eq. This result contradicts the initial assumption that the presence of a known inhibitor of α-syn would increase the potency of the peptide inhibitor due to the synergism of the two moieties. Polyphenols are thought to form quinones prior to interaction with α-syn. Per a number of investigators (Porat *et al.*, 2006; Ebrahimi & Schluesener, 2012; Hamley, 2012), quinones' planar structure allows the small molecules such as gallic acid to align with the hydrophobic grooves found in α-syn fibrils. However, my results indicate that the addition of a peptide may be too bulky and could be preventing the quinone moiety from exerting its effects, resulting in a lack of synergism between the peptide and quinone motif. This could possibly explain why gal-cap-WW shows no prominent difference in activity from ac-cap-WW.

Table 3.3. The activity of ac-cap-WW and derivatives at 0.5 eq peptide to α-syn. Each ThT measurement and CD measurement is an average of 3 repeats.

	% inhibition by ThT Fluorescence	% inhibition by CD signal	Average % inhibition
ac-cap-ww	13 ± 7	60 ± 6	~48
gal-cap-ww	29 ± 6	42 ± 15	~54
bz-cap-ww	51 ± 18	59 ± 7	~64

3.4.3. Fold stability and inhibition – the turnless series

We also tested turnless β-sheet models. These peptides are dimers that have an antiparallel strand alignment due to a disulfide linkage at the middle of the peptide and edge-to-face aryl/aryl clusters at both termini. To further stabilize these peptides, a coulombic interaction between positively charged R and negatively charged E is introduced at both termini. These peptides can be used as evidence for the effects of minor residue changes at certain positions to fold stability. Replacing Trp/Trp pairs with Tyr/Tyr pairs decreases the β-sheet population of the peptide by approximately 66% at 300K. Changing the residues flanking the C in the middle of the peptide from HCH to VCI significantly improved the fold population of the peptide, with AcY-VCI-YTG showing an 88%-fold population at 300K. A complete list of all the peptides tested in the turnless series is given in Table 3.4.

Table 3.4. Amino acid sequence of the peptides in the turnless series.

Peptide name	Peptide sequence
RW-HCH-WE	(R**W**TTHCHRK**W**E)$_2$
RY-HCH-YE	(R**Y**TTHCHRK**Y**E)$_2$
RY-VCI-YE	(R**Y**TTVCIRK**Y**E)$_2$
AcY-VCI-YTG	(Ac-**Y**TTVCIRK**Y**TG)$_2$

RW-HCH-WE emerged as a strong inhibitor in this series (Table 3.5). The CD spectra for this inhibitor with α-syn showed a minimum at 228 nm instead of at 217 nm as is typical for a β-sheet signal. This is most likely attributed to the decrease in RW-HCH-WE in solution over the course of time. The minimum at 228 nm is most likely a decrease in the exciton couplet that would typically be present at this wavelength. Since my CD processing includes the subtraction of a blank

containing the initial concentrations of the peptide inhibitor, the growing minimum at 228 nm can be used to track the decrease in inhibitor concentration over time.

To further test the hairpin hypothesis, I compared the activity of RY-HCH-YE and RY-VCI-YE; the latter forms a significantly more stable hairpin fold. The results showed that at the same concentrations, RY-VCI-YE showed a modest increase in inhibitor activity compared to RY-HCH-YE. However, when comparing the activity of RY-HCH-YE to its Trp/Trp counterpart, there did not seem to be much of a difference in activity. This lack of difference may be due to the presence of Tyr residues that can, somehow compensate for the decrease in fold stability compared to RW-HCH-WE.

Table 3.5. The activity of all the turnless series peptides that were tested. Each ThT measurement and CD measurement is an average of 3 repeats.

	2 eq			1 eq		
	% inhibition			% inhibition		
	ThT	CD	Average	ThT	CD	Average
RW-HCH-WE	84 ± 11	75 ± 7	≥ 75	66 ± 10	64 ± 9	~ 65
RY-HCH-YE	63 ± 8	77, 74	~ 70			
RY-VCI-YE	81 ± 7	78 ± 9	~ 80	72, 66	45 ± 9	~ 50
AcY-VCI-YTG	73 ± 6	70 ± 11	~ 70			

3.4.4. The Tyr effect and cyclic peptides

The effects of phenols on α-syn inhibition has been widely studied. As has been previously discussed, a lot of the small molecule inhibitors of α-syn activity show a dependence on the phenol moiety to act. My own studies thus far have shown that there are boosts in activity related to the replacement of Trp residues with Tyr residues. To investigate this boost further, I have studied the effect of Trp → Tyr replacement in the most potent inhibitor to date, cyclo-WW. Four more cyclic peptides were synthesized to determine if Tyr residues would further increase the potency of this inhibitor as well as to examine the effects of the position of the Tyr residues on activity.

Table 3.6. Cyclic peptides and their sequences. Edge-to-face aryl/aryl pairs are denoted in bold.

Peptide	Sequence
Cyclo-WY	cyclo- (GK-**W**ITVS-IpPK-KLTV**Y**-Ip)
Cyclo-YW	cyclo-(GK-**Y**ITVS-IpPK-KLTV**W**-Ip)
Cyclo-YY	cyclo-(GK-**Y**ITVS-IpPK-KLTV**Y**-Ip)
Cyclo-YS	cyclo- (GK-YITVS-IpPK-KLTVS-Ip)
SY	KKLTV**S**-IpGK-**Y**ITVSG

In terms of stability, the backbone cyclization ensured that all the iterations of these cyclic peptides are fully-folded and show little to no melting up to 95°C (by CD). The cyclization also negated some of the effects of using Tyr instead of Trp in the edge-to-face interaction that would have typically resulted in a larger difference in β-sheet structure. In Figure 3.5, one notable pattern of difference between the peptides was at the point of mutation itself. Having a non-Trp residue at the edge position (position 16) yielded the lowest CSDs, however the same pattern did not hold true at the face position (position 3). It is also worth noting that the Trp/Trp pair yielded the most shielding at the turn residues for the -^{17}I^{18}p^{1}G^{2}K- turn. Side chain protons, Hβ3 and aromatic

protons [Hδ -tyrosine residues; Hε3 - tryptophan residues] can be used to identify the edge-ring and the face-ring for each of the cyclic peptides.

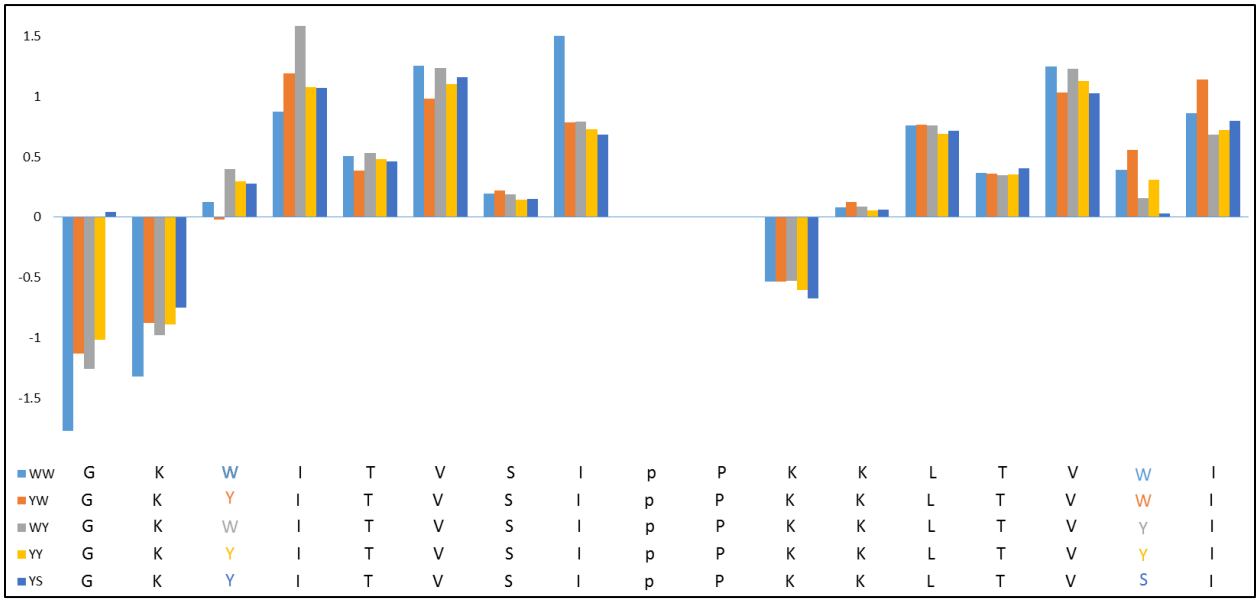

Figure 3.5. The graph depicts the chemical shift deviations (CSDs) of backbone H_N for all the cyclic peptides in this series.

Appendix A10 shows that a Trp/Tyr pair is capable of forming a strong EtF interaction with highly shielded edge protons while a Tyr/Trp pair is not as shielded. The data also shows that switching the positions of Trp and Tyr does not switch the orientation of the EtF interaction; the edge-ring remains the aromatic residue at the C-terminus while the face-ring remains the aromatic residue at the N-terminus regardless of the fact that the Trp indole ring has higher anisotropy than Tyr phenol ring.

Peptide SY, the uncyclized, non-circularly permuted iteration of cyclo-YS was synthesized to serve as a control. In Figure 3.6, the chemical shift deviation of this peptide is compared to WW, its closest analog. The data showed that while there is a good amount of β-sheet structure in the strands, most likely induced by the favorable –IpGK- turn, the lack of Trp/Trp residues flanking

the turn results in an approximately 0.5 ppm (about 50% to 66%) decrease in chemical shift deviation. Examining the melting of this peptide from 280K to 320K showed that there was very little change in CSD at H-bonded positions between residues V5 and V14. (Appendix A9) This indicates that the peptide is relatively stable and does not denature much up to 320K.

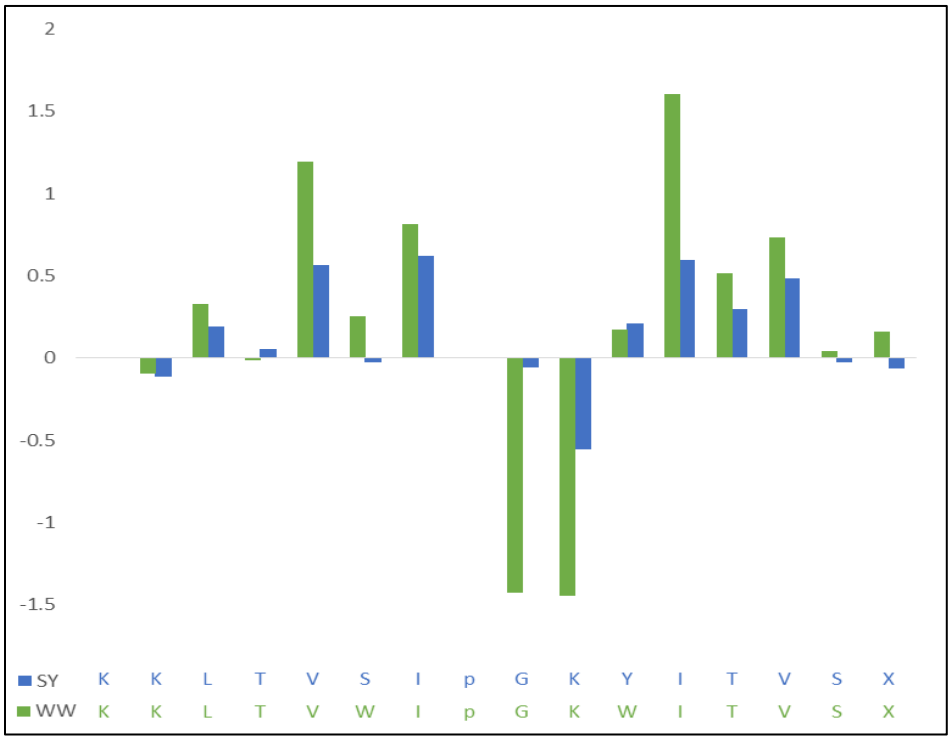

Figure 3.6. The graph shows the chemical shift deviation comparison of backbone H_N for WW and SY. The much larger CSD at V5 and I12 for WW demonstrate the extra stabilization provided by the EtF interaction of the W/W residues flanking the turn.

Testing each of these peptides at various concentrations yielded the results in Table 3.7. Unfortunately, the expected increase in activity due to the presence of phenol moiety in Tyr residues was not evident at sub-stoichiometric levels (0.5 eq inhibitor). The activity of these peptides seems to rely more heavily on the stability of the β-structure, rather than the specific residues. This is evidenced by the fact that cyclo-YS, that is lacking one aromatic residue, is still showing a high level of inhibitory activity comparable to the others. However, the importance of

the hairpin structure was validated by the reduced activity of peptide SY that had a similar sequence to cyclo-YS but did not have a stable hairpin fold.

Table 3.7. Activity of cyclic peptides. Each ThT measurement and CD measurement is an average of 3 repeats.

	2 eq			1 eq			0.5 eq		
	% inhibition			% inhibition			% inhibition		
	ThT	CD	Average	ThT	CD	Average	ThT	CD	Average
cyclo-WW	69	70	~70	81	60	~70	33	66	~50
cyclo-WY	82	63	~73	82	82	~82	73	67	~70
cyclo-YY	75	63	~70	85	77	~81	66	54	~60
cyclo-YW	65	65	~65	58	62	~60	15	50	~33
cyclo-YS	76	71	~73						
SY	36	50	~43						

3.4.5. Observing the binding of peptide inhibitors – Phosphate buffer conditions

While CD studies and ThT studies provide insight into the general activity of these peptides, it is not able to elucidate the mechanism of inhibition. Neither can it provide insight into the amyloidogenic pathway taken by α-syn. In order to study this, I performed ^{15}N-HSQC experiments with universally ^{15}N-labeled α-syn.

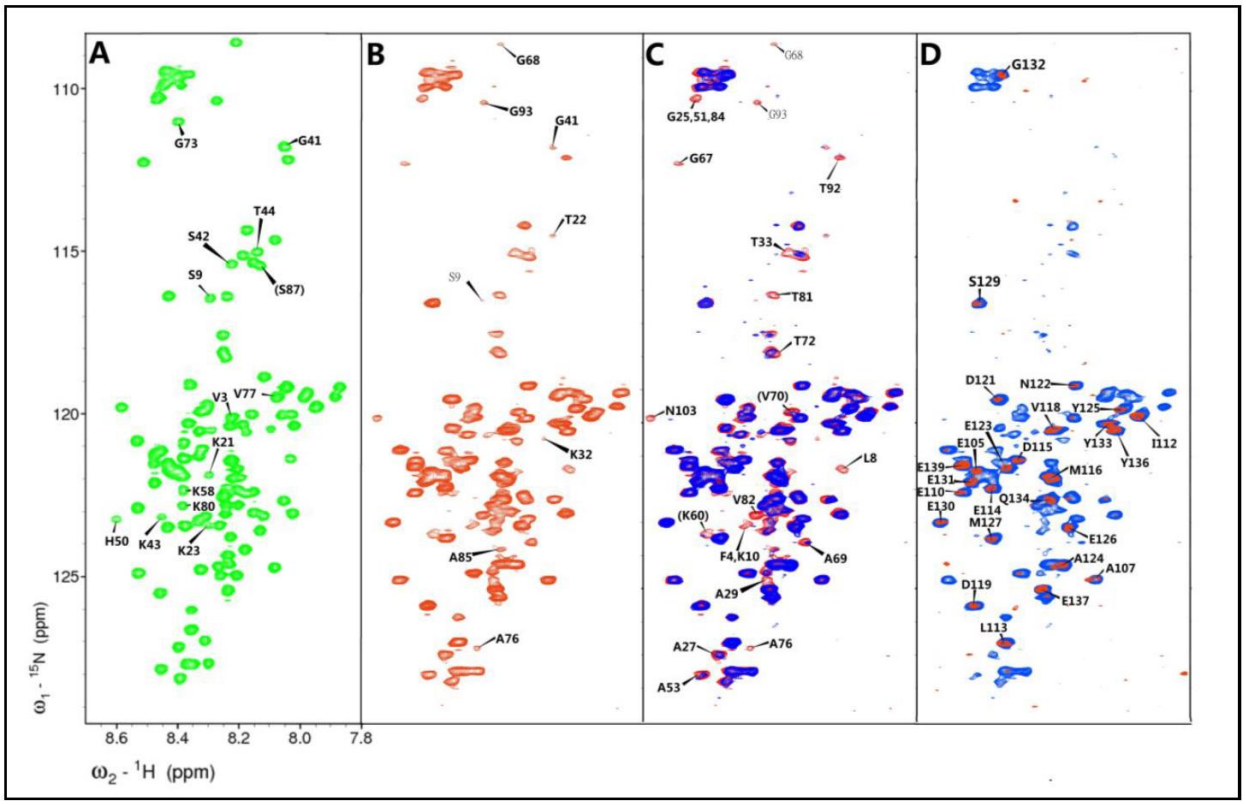

Figure 3.7. Alpha-syn spectra collected over a 24 hour time period. Panel A- 400μM α-syn in the absence of HFIP, in 50 mM pH 6.5 phosphate buffer. Panel B –D: The changes that occur to 100μM α-syn (20 mM Tris.HCl, pH 7.2 buffer) in the presence of 1.5 vol-% HFIP at t=1hour (B), t=6.5 hour (blue) over laid on the t=1 hour spectrum (C) and t=12 hours (red) overlaid on the t=6.5 hour spectrum (D). All spectra were zeroed using the peak for A140 at 130.6 ppm (ω_1-^{15}N) and 7.942 ppm (ω_2-^{1}H) since this peak showed no signs of peak attenuation throughout the course of the experiment. [*Image adapted from Sivanesam* et al., *2015]*

Dr. Aimee Byrne had previously demonstrated that α-syn amyloidogenesis can be monitored by observing the attenuation of peaks by this NMR experiment. (Figure 3.7) In those studies, α-syn

was prepared as a 100μM sample in 20 mM Tris. HCl, pH 7 buffer and allowed to incubate at 303K in the presence of 1.5 vol-% HFIP. The most rapid peak attenuation resulted in a complete broadening of signal by t=1 hour. These peaks, labelled in panel A were of residues V3, S9, K21, K23, G41, S42, K43, T44, H50, K58, G73, V77, and K80.

This peak broadening was followed by the residues labelled in panel B (T22, K32, G68, A76, A85, G93) that were already showing a decrease in peak intensity by t=1 hour. By the 6-hour time point, peaks F4, L8, K10, G25, A27, A29, T33, G51, A53, T72, G84, T92, and N103 had disappeared as well. After a 12-hour incubation, the only peaks that could still be seen by NMR were located in the C-terminus of the protein. (Panel D) The fact that C-terminal peaks remain flexible enough to produce a signal by NMR while the rest of the protein is more ordered is in line with the general lack of secondary structure in this region even in the native state of the protein. (Davidson *et al.*, 1998)

Dr. Byrne's results showed that, with the exception of 3 peaks, the earliest amyloid event was occurring in the extreme N-terminus (V3, F4, L8, S9, and K10), the well-known amyloidogenic patch between residues G67 to V82 as well as a then lesser known patch between residues V37 and T54. These results were very interesting because these residues are outside the NAC region of α-syn. Lately, however, other research has been concluding that this span of residues may be playing an important role in pre-amyloid oligomer formation. Mirecka *et al.*, through crystallizing their protein inhibitor in the presence of α-syn, determined that their inhibitor was binding to α-syn in the V^{37}LYVGSK^{43}-TKEG-V^{48}VHGVAT^{54} span. (Mirecka *et al.*, 2014) The inhibitor studies by Mirecka *et al.* also reported that this region of α-syn adopts a hairpin structure in the presence of their inhibitor. A number of studies support this conclusion. (Celej *et al.*, 2012; Salveson *et al.*, 2016) Of note is the fact that these residues represent the β1 and β2 strands that

were first characterized by Vilar *et al.* and determined to be a part of the mature fibrils formed by α-syn. (Vilar *et al.*, 2008) Also, these residues happen to be the location of many of the familial mutations that are implicated in PD, including A53T, H50Q, G51D and E46K. Finally, the only Tyr residue outside of the C-terminal region of α-syn is located in this span. Taken together, this information points to an important role being played by this hairpin in the early amyloid formation of α-syn.

Using Dr. Byrne's assay conditions, I could perform titration experiments that allowed me to monitor the binding of some of the best inhibitor peptides to α-syn from the WW series as well as the turnless series. Inhibitor binding to be peptide can be determined by monitoring the changes in α-syn backbone chemical shifts.

Cyclo-WW was titrated into a 200μM sample of ^{15}N-labeled α-syn with spectra taken prior to inhibitor addition and with 0.6, 1.2, and 2.0 eq of inhibitor added. (Appendix B5 & B6) The titration was carried out in the absence of HFIP to allow for the determination of binding loci before monitoring the inhibitor's effects on amyloidogenesis. The initial two concentrations of cyclo-WW showed binding shifts in the C-terminus that had previously been observed for WW and cp-WW. These shifts, located between Q109 and E137, had similar magnitudes and were all moving in the same direction. However, unlike the WW and cp-WW spectra, there were shifts discernible in a secondary span of residues: G41, V48, H50, V52, and T54. These residues are part of the soluble hairpin that was discussed previously.

Cyclo-WW's secondary binding locus could be a reason this peptide demonstrates a higher level of inhibitor activity compared to its un-cyclized counterpart, cp-WW. Since both these peptides have the exact same sequence, the secondary binding could be attributed to the increased fold stability of cyclo-WW. The span of residues that cyclo-WW recognizes is also important because

it is the same span that has been receiving increased attention as a possible nucleator of α-syn aggregation. By interacting with this region, cyclo-WW may be inhibiting some of the earliest events of oligomerization. This is further supported by the fact that H50 is always the first residue to broaden out in α-syn NMR spectra and yet remains visible in the presence of cyclo-WW for extended periods of time.

Upon addition of 1.5 vol-% HFIP, I observed a general upfield shift for all residues of α-syn. This same observation had been made in previous inhibition studies and could be attributed to an increased solubilizing environment for the hydrophobic side chains of α-syn. The general upfield shift could also be caused by a conformational change since peaks that had been attenuated before the addition of HFIP seem to return, albeit with a low intensity. It is, however, difficult to envision a conformational preference change that would move peaks throughout the sequence upfield and by a similar amount.

I also tested the binding capabilities of RW-HCH-WE. This peptide was one of the best inhibitors to come out of the turnless series, and showed precipitation upon co-incubation with α-syn. Similar to all the inhibitors tested so far, most of the binding shifts were located in the C-terminus. (Appendix B7) However, not all of these shifts were in the same direction as those seen in the presence of the WW series inhibitors. Some of the shifts observed were even larger than those observed in the presence of WW series inhibitors. (Appendix B4) This could be due to an increased affinity of peptide to α-syn due to the higher concentration of Trp residues in the turnless-β-sheet. This is in line with the theory that interfering with the π-π stacking of C-terminal Tyr residues could be the mechanism by which quinones inhibits α-syn amyloid formation (as previously discussed). Further support for this conclusion can be seen in the largest binding shift of RW-HCH-WE occurring at Y125 and E126.

The final binding study conducted under phosphate buffer conditions was with YY-μPro. YY-μPro had demonstrated up to 90% inhibition with only 1 eq peptide added and demonstrated increased inhibition over its Trp/Trp counterpart. Unfortunately, HSQC studies did not reveal any specific binding shifts upon addition of YY-μPro to α-syn (Appendix B8). There was however a notable increase in peak intensity of some peaks that had been attenuated before the addition of inhibitor. The general upfield shift that has been observed for other peptides after the addition of HFIP was evident in this study as well. (Appendix B8 & B9) The NMR study confirmed that YY-μPro was still an inhibitor despite the apparent lack of a binding loci. This conclusion was drawn because peak attenuation was minimal at the 24-hour mark indicating that a large amount of α-syn remains in the flexible, monomeric random-coil state.

3.4.6. Observing the binding of peptide inhibitors – Tris.HCl buffer conditions

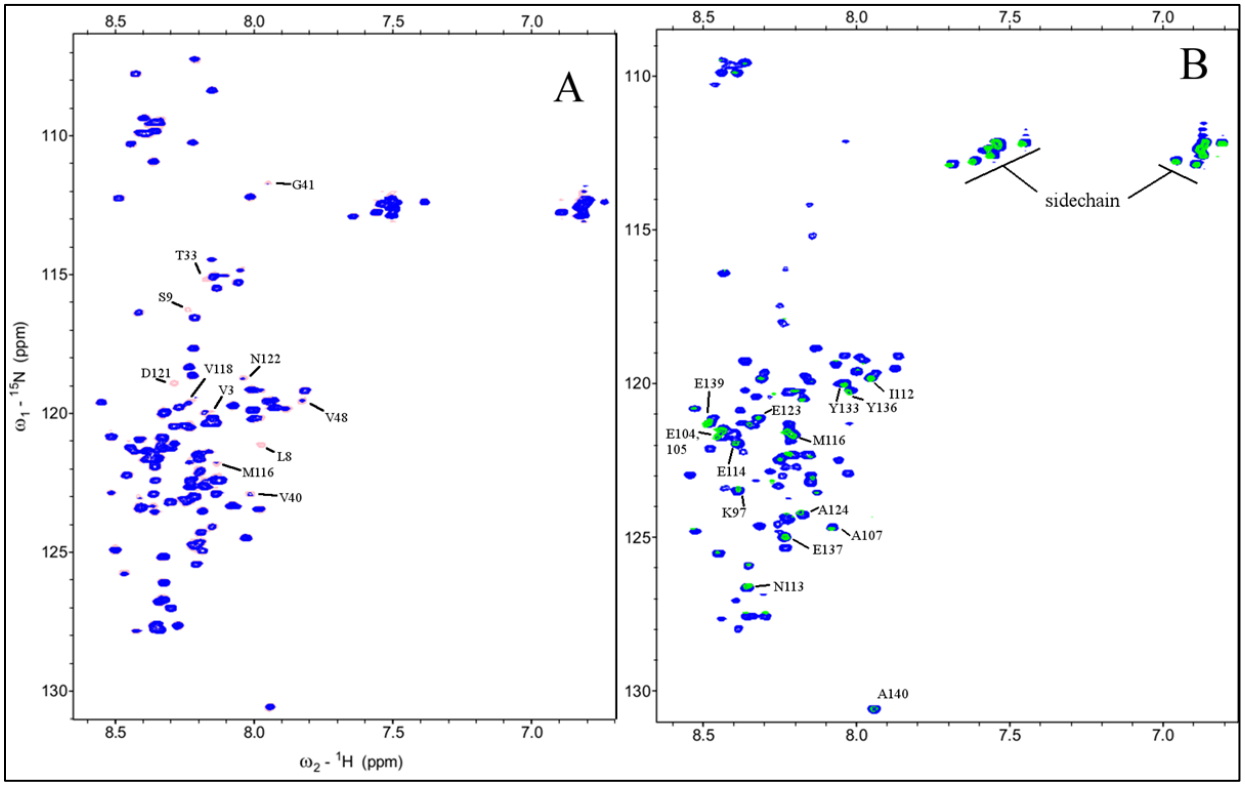

Figure 3.8. Panel A- Spectrum of 100µM α-syn in 20 mM Tris. HCl, pH 7.2 buffer in the presence of 2.0 vol-% HFIP (pink) overlaid with the spectrum of the same sample after incubation at 280K for 22 hours. Peaks that are no longer visible at t=22 hours are labeled. Panel B – Spectrum of 100µM α-syn in 20 mM Tris. HCl, pH 7.2 buffer in the presence of 2.0 vol-% HFIP at 280K overlaid with the spectrum of the same sample taken immediately after the temperature was increased to 300K.Peaks that are still visible at 300K are labeled.

My attempts to replicate Dr. Aimee Byrne's aggregation results in the Tris buffer system yielded no results. This led to the development of new conditions to observe α-syn aggregation in this buffer system by NMR. Under my new conditions, aggregation happened almost instantly upon the addition of 2 vol-% HFIP at 300K (Figure 3.8). The temperature was significant because addition of HFIP at 280K followed by 22-hour incubation does not result in the same observation. Instead only a few peaks show any attenuation: V3, L8, S9, T33, V40, G41, V48, M116, V118,

D121, and N122. (Figure 3.8A) For the most part, peaks that are showing attenuation are those that have been observed previously under Dr. Byrne's assay condition. However, there were some peaks in the C-terminus that were also showing attenuation which is contrary to our previous results. The spectrum taken immediately after the addition of HFIP at 300K (Figure 3.8B) showed only peaks from the C-terminus as well as the side chain ^{15}N-^{1}H peaks of asparagine and glutamine residues in α-syn, with the remaining peaks having disappeared most likely due to the formation of higher order structures that display less segmental motion and longer tumbling times.

Under these new conditions, inhibitor studies were repeated for cyclo-WW. NMR spectra were recorded at 0 eq inhibitor, 0.6 eq, 1.2 eq and 2.0 eq followed by a spectrum immediately after the addition of 2 vol-% HFIP. The binding shifts obtained under Tris buffer conditions were in good agreement with the shifts observed previously. (Appendix B10) As shown in Figure 3.8A, the shifts in the N-terminal region, V3 and L8 were very prominent, especially at 2.0 eq inhibitor. The secondary binding locus (Y39 – T54) was prominent as well, leading to the conclusion that the previous results were due to a defined complex formation between this inhibitor and α-syn. Notably, the peak for H50, that was previously attenuated is once again visible after the addition of 2.0 eq cyclo-WW. (Figure 3.9A)

The same set of tests were carried out in the presence of three other cyclic inhibitors as well. For cyclo-WY, the inhibitor binding in the C-terminus was very prominent as expected (Appendix B11). Most of the shifts were moving to the right (ω_2-^{1}H) and/or upward (ω_1-^{15}N). However, peaks E126 and D135 were moving in the opposite direction in the ω_2-^{1}H axis. There were also generally less binding shifts observed for cyclo-WY compared to cyclo-WW. Of note is the lack of any binding shifts for Y133 and Y136 that is very prominent in cyclo-WW. For cyclo-YW, however, the inhibitor binding was markedly weaker, compared to the other cyclic inhibitors (Appendix

B12). Even at 2.0 eq peptide to α-syn, there were few large or very large binding shifts. However, there were a few more peaks in the C-terminus demonstrating binding shifts than in the presence of cyclo-WY. It was also noted that some peaks did not demonstrate shifting, instead, peaks G106 and M116 decreased in intensity as cyclo-YW was titrated in. I also observed that E126 and D135 were demonstrating shifting in the opposite direction as the other shifts, moving to the left in the ω_2-^{1}H axis instead of to the right. The fact that this anomaly occurs in all three cyclic inhibitors could indicate that the binding to these residues is not related to the aromatic residues.

Figure 3.9 compares the binding shifts of cyclo-WW, -WY and -YW at 2 eq inhibitor to α-syn that occur outside of the C-terminus at positions V3, L8, V40, G41, V48, H50, V52, A53 and T54. With the exception of V3 and L8, these residues correspond to the hairpin that was first proposed by Mirecka *et al.* as a possible initial event in the amyloidogenesis of α-syn. (Mirecka *et al.*, 2014) Cyclo-WY had some very weak shifts in the secondary binding locus, at residues A53 and T54. Among the binding shifts that were observed for cyclo-YW, there were small to very small shifts at V40, G41, V48, V52, A53 and T54. Despite the general reduced magnitude of binding shifts in the presence of cyclo-YW, there are a larger number of residues in the secondary binding locus that are demonstrating shifting. This could be pointing to an importance of the position of the Trp residue in the peptide. Another interesting observation that may further prove the importance of the position of the Trp residue is the shifting at V3 and L8 that is evident in cyclo-WW and cyclo-YW experiments, but not in cyclo-WY experiments. Coincidentally, these residues are two of the four residues that showed early signal attenuation in the uninhibited control (under Dr. Byrne's assay conditions).

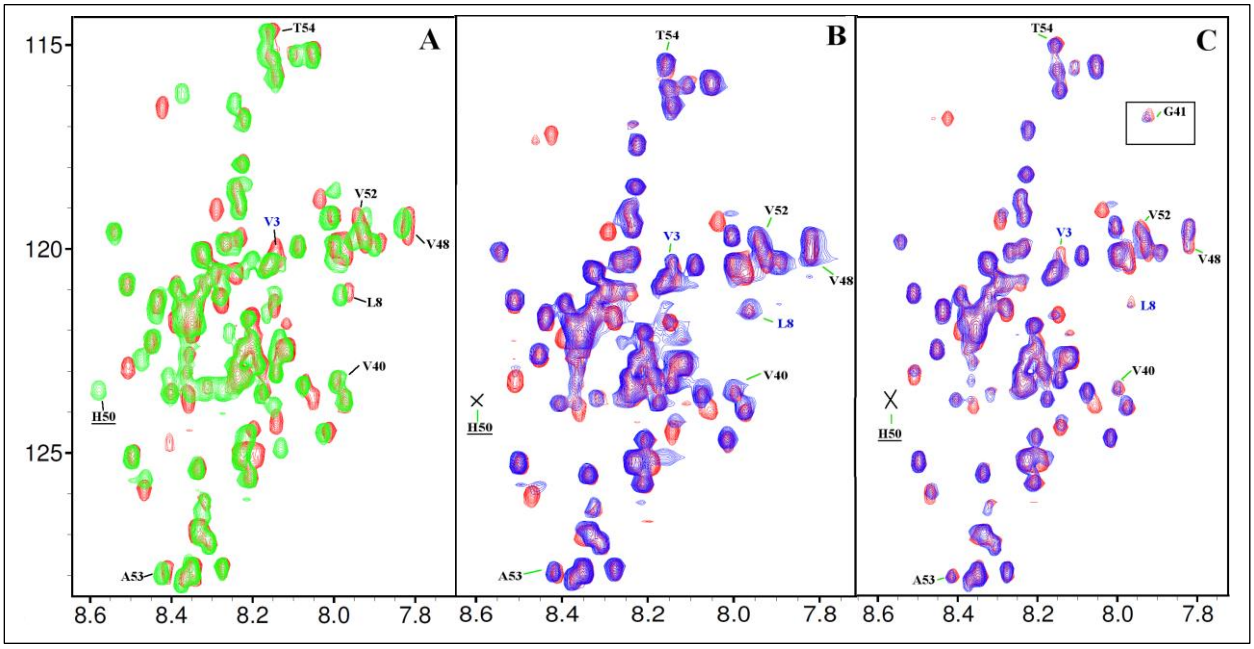

Figure 3.9. Panel A- 0 eq cyclo-WW (red) overlaid with 2.0 eq cyclo-WW (green). Panel B – 0 eq cyclo-WY (red) overlaid with 2.0 eq cyclo-WY (blue). Panel C- 0 eq cyclo-YW (red) overlaid with 2.0 eq cyclo-YW (blue). Peaks within the secondary binding locus, between residues V48-T54 are labeled. Residues V3 and L8 are labeled in blue. The position of the missing H50 peak is indicated with an 'X'.

Cyclo-YY on the other hand showed different results than the other cyclic hairpins. While peak attenuation never occurred in the presence of the other three hairpin inhibitors before HFIP addition, the titration of cyclo-YY into α-syn resulted in large amounts in peak attenuation, especially in the C-terminus of the peptide at just 0.6 eq peptide. Peak attenuation continued to increase as inhibitor concentration increased. Figure 3.10A shows the spectra of α-syn as cyclo-YY was titrated in. Several peaks in the C-terminus had completely disappeared with addition of 1.2 eq cyclo-YY. Even A140 that is typically visible even in the soluble oligomeric state had been almost completely attenuated with the addition of 1.2 eq cyclo-YY.

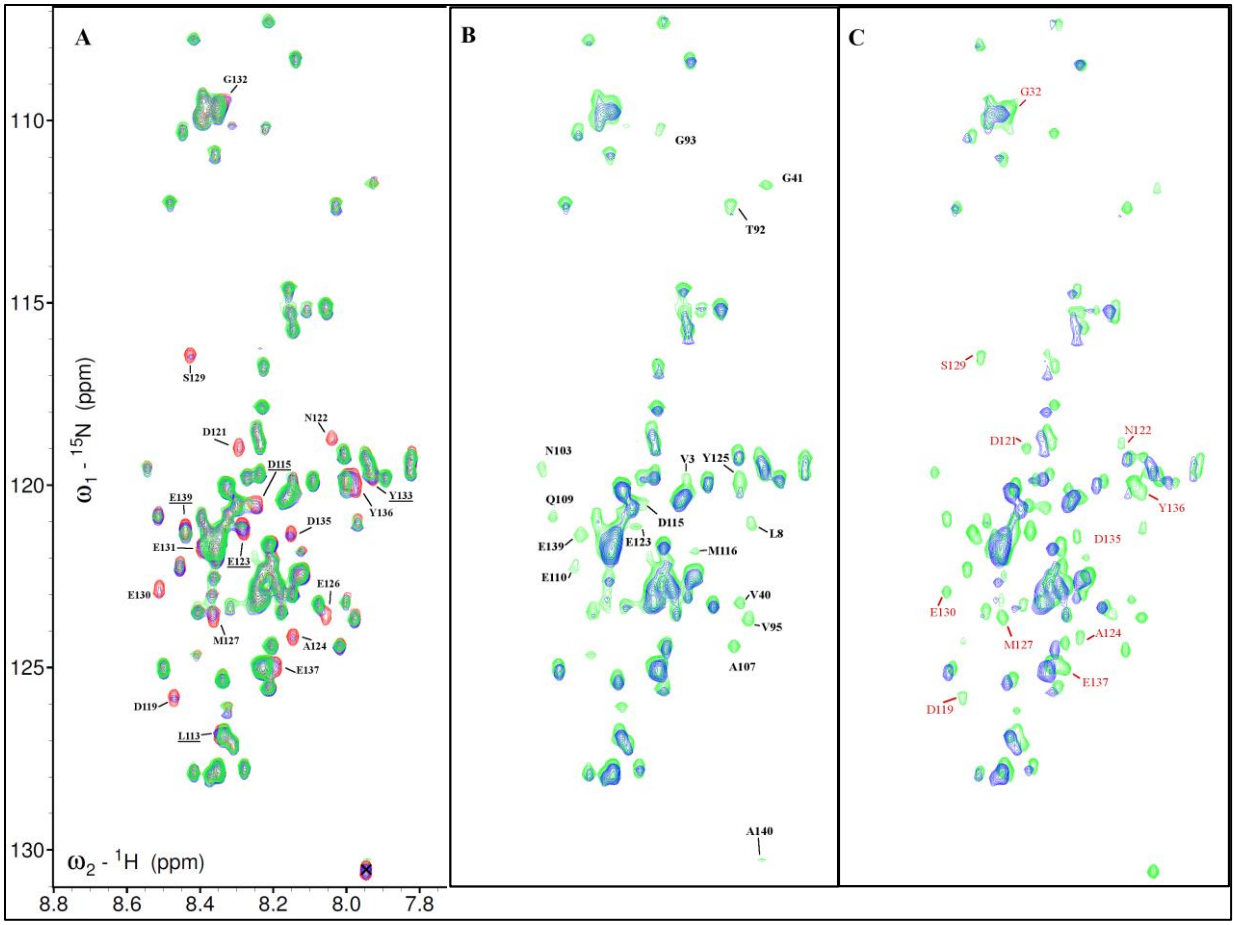

Figure 3.10. Panel A – Overlay of α-syn spectra in the presence of 0 eq cyclo-YY (red), 0.6 eq cyclo-WY (blue) and 1.2 eq cyclo-YY (green). Underlined labels indicate peaks have disappeared in the presence of 1.2 eq cyclo-YY. Panel B – Overlay of α-syn spectra in the presence of 1.2 eq cyclo-YY (green) and 2.0 eq cyclo-YY (blue). Peaks that are no longer present in 2.0 eq cyclo-YY are labeled. Panel C – Overlay of α-syn spectra that contains 2.0 eq cyclo-YY in the presence (green) and absence (blue) of 2 vol-% HFIP. Peaks that were absent even in the presence of 1.2 eq cyclo-YY but have reappeared after the addition of HFIP are labeled in red.

Panel B shows that even more peaks in the C-terminus have disappeared with the addition of 2.0 eq cyclo-YY. Peaks V3, L8, V40, G41, G93, T92, and V95 that are outside of the C-terminus also disappeared with the addition of more cyclo-YY. One rationale for the peak attenuation would be slow exchange between the monomeric α-syn and a complex with cyclo-YY. It is noteworthy that the disappearance of some peaks, when inhibitor levels were increased from 1.2 eq to 2.0 eq, was instantaneous and was not observable at inhibitor concentrations below 2.0 eq. (V3, L8, V40, G41,

T92, V95, N103, A107, E110, M116, and Y125) The addition of HFIP, however, resulted in a lot of the peaks returning along with the general upfield shift that is always observed in the presence of HFIP. Even peaks that were attenuated with the addition of 1.2 eq cyclo-YY had returned. (Figure 3.10C) This dramatic change in peak intensity upon the addition of HFIP could be due to a decreased binding affinity between the peptide and inhibitor. The difference in inhibitor effect on chemical shifts between cyclo-YY and the other three cyclic inhibitors could point to a possible π-π stacking interaction between the peptide and α-syn. This conclusion is supported by the subsequent study, done with gal-cap-WW.

Like cyclo-YY, gal-cap-WW also shows peak attenuation at 0.6 eq inhibitor. Unlike cyclo-YY that showed no significant binding shifts, gal-cap-WW shows binding shifts for certain residues at the C-terminus as shown in Figure 3.11 (S129, E126, A124, M127, Y136, E123, and E130). Additionally, gal-cap-WW does show very strong peak attenuation at the secondary binding locus (V40, V48, V52, A53, G41, T54, and T44) possibly indicating strong binding at this position. Gal-cap-WW also shows binding at V3 and L8, the same peaks that are shifted in the presence of cyclo-WW and cyclo-YW. The implications of these similarities are still unclear but could point to another location within α-syn that plays a role in amyloid formation. Upon the addition of HFIP, most of the attenuated peaks return, as was observed in the case of cyclo-YY. (Appendix B13) A notable peak that returned upon HFIP addition is H50, which is always the first peak to disappear, sometimes even before the first spectrum of α-syn can be recorded. This observation is similar to the one made in the presence of 2.0 eq cyclo-WW. However, in the case of cyclo-WW, the H50 peak is visible even in the absence of HFIP.

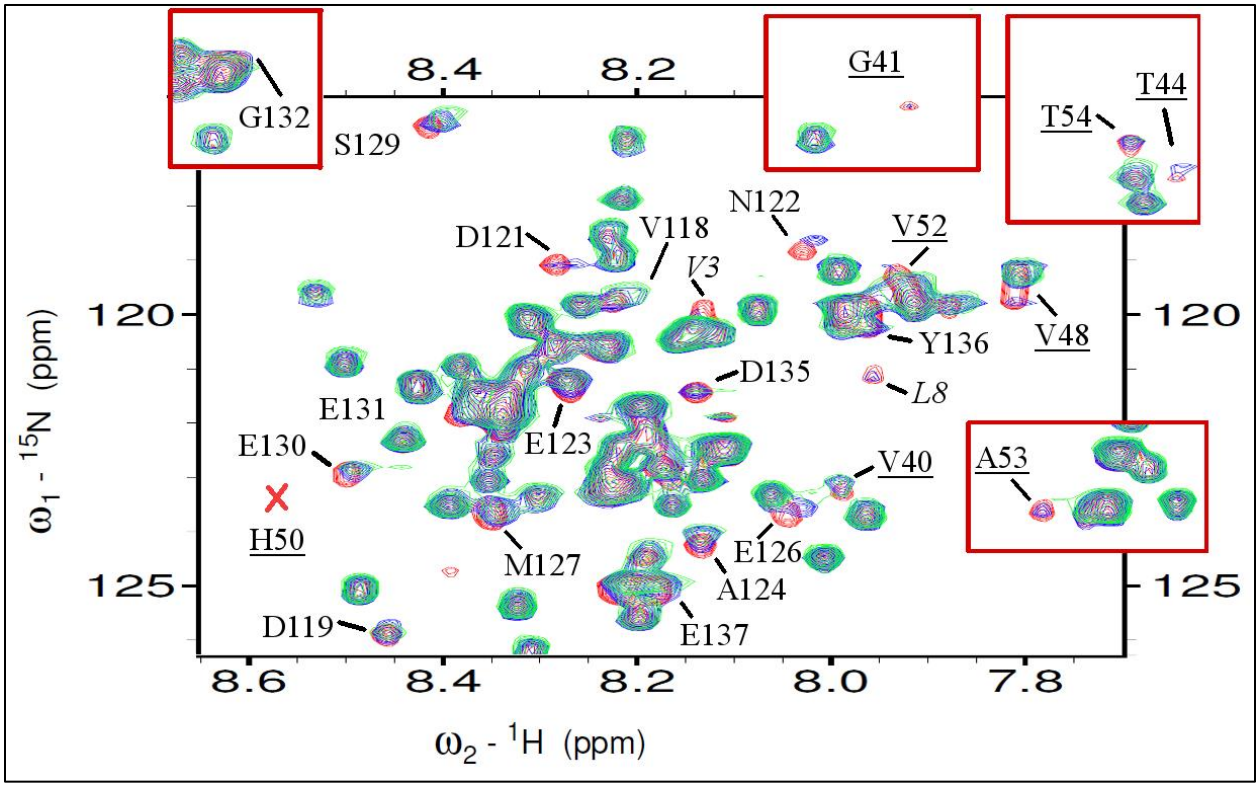

Figure 3.11. The figure shows the spectrum taken for α-syn in the absence of inhibitor (red) overlaid with the spectrum taken in the presence of 0.6 eq gal-cap-WW (blue) and 1.2 eq gal-cap-WW (green). Peaks outside of the main spectral window that demonstrated binding shifts are given inset. Shifts that occur in the soluble hairpin region between residues V37-T54 are underlined. The H50 peak which is not visible in any of the spectra is indicated with a red 'X'.

A final observation of note is the significant movement of the S129 peak in the presence of all inhibitors, even at sub-stoichiometric concentrations. As discussed previously, this residue is the sole site of phosphorylation of α-syn *in vivo*. Since the actual effects of S129 phosphorylation is unclear, it would be premature to speculate on whether or not the large shift at S129 is significant to inhibition but these results confirm that this site plays an important role in α-syn amyloid formation.

Table 3.8. List of residues that are shifted in the presence of 2 eq inhibitors (based on comparison with spectrum of α-syn with no inhibitor). The shifts are categorized from very large to very small based on the magnitude of the change in their chemical shifts. Residues outside the C-terminus are underlined.

Inhibitor induced shift	Very large	Large	Medium	Small	Very small
WW	E137, E126, E130, V3, N122, D121, S129	A53, D119, A107, A124, M127, M116, L8, Y136, Y133, V52	L113, Q134, E131, E123, D135, V48, T54, T22	V40, G41, G106	
WY	D119, E137, E126, E130, D121, N122, S129, A124	M127, E131, D115	Q109, E104	T54, A53	
YW	N122, S129, G106	E126, M127, E130, D121, D135	D119, E137, A124, E131, V3	E123, D115, V48, Y136, I112, V40	T54, G41, A53, V52
YY*	D119, E137, A124, E126, M127, E130, D121, N122, Y133, Y136, S129 **V3, L8, V40, G41, T92, V95, N103, A107, E110, M116, and Y125**	E139, DII5, G132, E123	E110, I112, G109		
Gal*	V3, L8, V26, V48,A53, G41, T54, T44, V71, N122, D121, M116, K21, E126, G106	V40, D135, E131, E130, M127, A124, D119, S129			

**Due to high amounts of peak attenuation, the inhibitor effects (binding shifts and peak attenuation) for these peptides are listed as a comparison between 0 eq inhibitor and 1.2 eq inhibitor. The peaks that disappeared only at 2.0 eq inhibitor are given in bold for cyclo-YY.*

3.5. Summary and Conclusion

In summary, these studies have confirmed that the hairpin hypothesis is valid when it comes to α-syn inhibition by non-sequence homologous peptides. This is shown by the increasing activity of peptides in the WW series as they become more structured. My results also demonstrate that the presence of phenol groups alone is not enough to boost inhibitor activity since replacing Trp residues with Tyr or Ser did not have a significant effect on aggregation. Finally, my results showed that cooperativity between two known inhibitors of aggregation is not guaranteed as evidenced by the lack of increase in the inhibitor activity of ac-cap-WW when gallic acid is replaced as the N-acyl-cap of the peptide.

One of the most interesting discoveries that has come out of this study is the importance of the hairpin first shown by Mirecka *et al.* as a possible early event in the formation of α-syn amyloid fibrils. My results confirm that most of my potent inhibitors have a secondary binding locus that corresponds to the residues of this hairpin, serving as confirmation that targeting this hairpin could result in novel therapeutics for PD and other synucleinopathies.

Chapter 4: Human Amylin

4.1. Introduction

4.1.1. Discovering human amylin

In 1901, Eugene L. Opie noticed that patients with diabetes shared a common degeneration of their islet cells in the pancreas. (Opie, 1901) He was the first to connect the presence of amyloid in the islet cells with the development of diabetes. His discovery came close on the heels of the findings by Oscar Minkowski, which showed the pancreas being affected in patients with diabetes. (Hayden & Tyagi, 2001) However, Opie was unable to unequivocally confirm that the albuminoid substance (hyaline) he was observing was in fact amyloid. It would be 60 years before the hyaline in islet cells was confirmed to be amyloid, with the aid of Congo Red. (Ehrlich & Ratner, 1961) In 1973, Westermark *et al.* identified these amyloid plaques to be made up of fibrils (Westermark, 1973) and more than a decade later, he was able to determine that a 37-amino acid peptide he termed islet amyloid polypeptide (IAPP) was the main component of the fibrils. (Westermark *et al.*, 1986) However, Westermark's characterization of the peptide was incomplete: one residue was incorrectly sequenced and the C-terminal amidation was not detected. At around the same time, Cooper *et al.* separately identified the same peptide and accurately sequenced it. Cooper termed the peptide amylin, (Cooper *et al.*, 1987) and this 37-amino acid peptide has been known interchangeably as IAPP and amylin ever since.

Human amylin (hAM) comes from an 89-amino acid precursor peptide. A 22-amino acid signal peptide is cleaved to give the 67-amino acid proform of the peptide. In the Golgi apparatus and in the insulin secretory granule, amino acids in the N- and C-terminus are cleaved by proprotein convertase 2 (PC2) and proprotein convertase 1/3. Peptidyl amidating mono-oxygenase complex

(PAM) then amidates the C-terminus of the peptide giving the final form of amylin. (Sanke *et al.*, 1988; Nishi *et al.*, 1989)

4.1.2. The role of hAM in the body

In healthy individuals, hAM plays an important role in the digestive system. It was found that the signal (increased blood glucose) that triggers the secretion of insulin, also triggers the release of hAM from the pancreas. It has been shown that hAM is co-secreted with insulin at a 20:1 (insulin: hAM) ratio. (Martin, 2006) The initial research into the function of hAM in the digestive system posited a function that was in opposition to the function of insulin. (Kogire *et al.*, 1991; Dégano *et al.*, 1993; Rink *et al.*, 1993) However, it is now believed that that hAM's role in digestion is complementing the role of insulin by preventing the release of glucagon, decreasing gastric emptying and stimulating satiety centers of the brain. (Cooper, 1994; Scherbaum, 1998; Kruger *et al.*, 1999; Silvestre *et al.*, 2001; Akesson *et al.*, 2003; Martin, 2006)

When hAM begins to misfold, it becomes toxic to cells, particularly the β-cells from which it originates. The basis of hAM toxicity has been linked to multiple actions including a receptor mediated mechanism, stress on the endoplasmic reticulum and defects in autophagy within the system. (Cao *et al.*, 2013) The most prominently studied effect has been the membrane permeabilization characteristic of the peptide. Several studies have shown that hAM can cause damage through pore or channel formation in the lipid bilayer. Mirzabekov *et al.* have shown that channels formed by hAM are capable of promoting the influx of calcium ions and the efflux of sodium and potassium ions. (Mirzabekov *et al.*, 1996) This was supported by a study by Kayed *et al.* that showed calcium levels being disturbed by the action of hAM on plasma membranes. (Kayed *et al.*, 2004)

hAM has also been shown to cause the generation of reactive oxygen species (ROS). (Mattson & Goodman, 1995) Schubert *et al.* observed increased accumulation of hydrogen peroxide in B12 cells in the presence of hAM which leads to free-radical induced lipid peroxidation and eventually cell death. (Schubert *et al.*, 1995) Further support to this toxicity pathway is the ability of ROS scavengers to inhibit the cytotoxicity of hAM. Rifampicin and its analogues, p-benzoquinone and hydroquinone were able to inhibit the toxicity of hAM. (Tomiyama *et al.*, 1997) However, the study that discovered these inhibitors also showed that rifampicin was able to bind to hAM oligomers and prevent interaction with cell surface. This led to the conclusion that the action of these inhibitors were two-fold: inhibiting oligomer-membrane interaction as well as ROS scavenging.

Another possible basis of hAM cytotoxicity is the triggering of apoptosis. (Lorenzo *et al.*, 1994) Multiples studies have shown that hAM is able to promote the expression of tumor suppressor genes - p21 and p53, upregulate c-Jun expression, as well as increase the levels of Fas/Fas ligand and Fas-associated death domain (FADD). (Zhang *et al.*, 1999, 2002, 2008) All these actions promote the apoptosis of cells and could be one of the causes of β-cell death in Type II Diabetes (T2D). It has also been proposed that apoptosis can be triggered by elevated levels of calcium ions in the cell. This could be a downstream effect of the aforementioned channels formed by hAM in the plasma membrane. (Huang *et al.*, 2010)

4.1.3. hAM fibrils: Formation and Morphology

In its monomeric form, hAM adopts a random-coil structure with a disulfide bond between the cysteine residues at positions 2 and 7, and an amidated C-terminus. The sequence of hAM can be broken up into three sections, the helix favoring N-terminus between residues 1-19 (Nanga *et al.*, 2008), the middle section between residues 20-29 that has been shown to form amyloid

independently (Westermark *et al.*, 1990; Tenidis *et al.*, 2000) and the C-terminal tail. The first proposal, that the residues within the 20-29 region of hAM were the most amyloidogenic, came from Westermark *et al.* in 1990. However, over the years, different studies have shown that different parts of the peptide are capable of forming amyloid fibrils. It is also worth noting that studies have shown that the 20-29 region of hAM may not be the only important region for hAM aggregation. One study that created random point mutations along hAM found that there were multiple mutants that did not aggregate. Of these mutants, many had mutations in the 20-29 region but a significant number also contained mutations at residues 13, 15 and 17, pointing to a possible role being played by these positions in amyloidogenesis. (Fox *et al.*, 2010)

As with other amyloidogenic peptides, the final fibril form of hAM was initially proposed to be the most toxic form of the peptide. (Lorenzo *et al.*, 1994; Mattson & Goodman, 1995; Mirzabekov *et al.*, 1996; Tomiyama *et al.*, 1997; Janciauskiene & Ahrén, 1998; Bai *et al.*, 1999; Hiddinga & Eberhardt, 1999; Jaikaran & Clark, 2001; Yan *et al.*, 2007) However, there is a significant amount of research that supports the theory that, similar to the other amyloid peptides, a soluble oligomeric form of hAM is more toxic. (Janson *et al.*, 1999; Anguiano *et al.*, 2002; Kayed *et al.*, 2004; Ritzel *et al.*, 2007; Aitken *et al.*, 2010) Using thioflavin T fluorescence, transmission electron microscopy and circular dichroism, Konarkowska *et al.* showed that the fibril form of hAM was not toxic to cells. (Konarkowska *et al.*, 2006) Inhibitor studies with rifampicin have also shown that inhibiting the fibril formation does not necessarily decrease cytotoxicity, leading to multiple inhibitor studies focused on earlier stages of amyloidogenesis. (Meier *et al.*, 2006)

The amyloidogenesis of almost all amyloid forming peptides is believed to begin with a monomer undergoing self-self recognition, followed by hydrophobic interactions that result in β-sheet oligomer formation. The oligomers continue to grow through monomer addition and eventually

become protofibrils and finally fibrils. (Dobson, 2003) Experimental observation of hAM dimers shows that hAM forms an extended β-sheet by electro-spray ionization mass spectroscopy as well as MD simulation supporting the formation of β-sheets as part of the amyloidogenesis pathway. (Dupuis *et al.*, 2011) However, there is a prominent hypothesis that hAM monomers may undergo an intermediate secondary structure before β-sheet formation: that an α-helical species may form prior to β-structuring. Numerous studies using circular dichroism (CD), two-dimensional infrared spectroscopy and NMR have observed an increase in the α-helical character of hAM just prior to β-sheet formation. (Kayed *et al.*, 1999; Goldsbury *et al.*, 2000; Lopes *et al.*, 2007; Yonemoto *et al.*, 2008; Ling *et al.*, 2009) Williamson and Miranker first put forth the hypothesis that the α-helical form of hAM may be an on-pathway intermediate in fibril formation. (Williamson & Miranker, 2007) They showed that the N-terminal region of hAM had helical propensity even in the monomeric state; this has been established in our laboratory (Cort *et al.*, 2009; Huggins *et al.*, 2011; Sivanesam, Shu, *et al.*, 2016) as well as by Raleigh and coworkers (Abedini & Raleigh, 2009). They posited that this secondary structure may be important for the hormonal function of hAM since a large portion of this sequence is highly conserved in hAM and CGRP, both of which bind to a common receptor.

Crystal structures of hAM fused to maltose-binding protein (MBP) showed that the N-terminus of hAM forms a helix that is capable of forming a dimer with itself or with a molecule of insulin. (Wiltzius *et al.*, 2009) The dimer formed showed prominent aromatic stacking between the F15 residues of each monomer at the dimer interface. Replacing the phenylalanine at this position with residues that are favored or tolerated in helices - such as serine, alanine and aspartic acid - resulted in increased amyloidogenesis, whereas lysine resulted in reduced amyloidogenesis. Mutations of residues outside of the dimer interface had a much smaller effect on amyloid formation supporting

the helical intermediate hypothesis. The results of this study were supported by data from position 15 mutations with leucine and isoleucine, as well as the unnatural amino acids, tert-leucine and norleucine. (Tu & Raleigh, 2013) The data showed a positive correlation between helical propensity and rate of aggregation since leucine, which has the highest helical propensity of the four residues, showed the highest rate of aggregation while *tert*-leucine, which has the highest β-propensity, had the lowest rate of aggregation. Random point mutations within the hAM sequence also showed that mutation of residue 13 from alanine to a glycine resulted in a marked decrease in hAM aggregation, most likely due to a disruption of the α-helix by this mutation. (Fox *et al.*, 2010) A swap-mutation between residues L12 and N14 (becoming N12 and L14) also resulted in a mutant that does not aggregate despite the fact that this mutation does not affect the formation of a β-sheet. (Williamson *et al.*, 2009) However, the mutation would disrupt the formation of an α-helix, providing further credence to the helical intermediate hypothesis.

Studies that manipulate the amount of helix formed by the monomer also demonstrate a correlation between helicity and amyloid formation. For example the presence of lipid membranes, particularly anionic lipids, have been shown to promote hAM aggregation. Evers *et al.* propose that the lipids induce the nucleation of hAM which leads to oligomerization followed by the detachment of larger aggregates that eventually become the plaques that are observed in T2D patients. (Evers *et al.*, 2009) The increased ability of hAM to form amyloid in the presence of membranes is well studied (Zhang *et al.*, 2017), however studies are showing that the ability to disrupt model membranes may not correlate directly with cytotoxicity. (Brender *et al.*, 2008; Cao *et al.*, 2013) One study used computational methods to identify compounds that can alter the structure and behavior of membrane-bound hAM. Experimental studies of the identified

compounds showed that the compounds that were predicted to enhance membrane binding did not enhance cytotoxicity. (Nath *et al.*, 2015)

On the other hand, interactions that "overstabilize" the helix formed by hAM are capable of inhibiting aggregation. Hexafluoroisopropanol (HFIP) at high concentrations has been shown to promote helicity and can be used to inhibit the aggregation of hAM. (Higham *et al.*, 2000) This type of interaction has also been proposed to be the mechanism by which insulin inhibits hAM aggregation in the secretory granule. (Wiltzius *et al.*, 2009) The insulin interaction with hAM is much stronger than the hAM-hAM interaction due to a larger buried surface area, resulting in inhibition of aggregation. The same mechanism has been proposed for the inhibition of hAM aggregation by rat amylin (rAM). One study mutated two residues (A13P and F15D) within the N-terminal region of rAM, creating a peptide that formed a far less stable α-helix. This mutant was unable to inhibit hAM aggregation at the same level as wild type rAM leading to the conclusion that rAM stabilizes the helical region of hAM thus reducing amyloidogenesis. (Cao *et al.*, 2010) Therefore, stabilization of the N-terminal α-helix of hAM may be a viable target for inhibitor design. Thus far, most peptidic hAM amyloidogenesis inhibitors have been related to the demonstrably most aggregation prone segment, ^{21}NNFGAILSS^{29}, of the hAM sequence. (see section 4.2.2)

The final conformation of the fibrils has been studied by multiple groups and has resulted in a number of structures being proposed. In 2005, Kajava *et al.* created a model of hAM in the protofibril state using a yeast prion model they had previously proposed. (Kajava *et al.*, 2005) Their structure had 3 β-strands that were antiparallel to one another. Strand 1 (12-17), stand 2 (22-27) and strand 3 (28-30) were all connected via short loops between them. Their structure provided an explanation for why rAM does not aggregate readily, since the proline residue at positions 25,

28 and 29 would inhibit the hydrogen bond formation between the strands. It was also noted that the histidine at position 18 in hAM (arginine in rAM) is more favorable for parallel in-register stacking which could further explain the solubility of rAM when compared to hAM. A molecular dynamics (MD) simulation also shows that hAM monomers form stable β-sheets with a loop in the trimer and pentamer stage of aggregation while rAM does not. (Liang *et al.*, 2013)

In 2007, Luca *et al.* used solid-state NMR to elucidate the structure of the amyloid fibrils formed by hAM. (Luca *et al.*, 2007) Their data showed that hAM fibrils were striated ribbons that had a cross-β strand structure which is typical of amyloid fibrils. Each fibril is made up of 2 twisted columns of peptide and each column of peptide is made up of multiple layers of peptide monomer that form parallel intermolecular β-sheets, another hallmark of amyloid fibrils. Each monomer unit is then made up of 2 β-strands (not including residues 1-7 in the N-terminus that is connected by the disulfide bridge between C2 and C7) with a loop between them from residues 18-27. (Figure 4.1) The structure proposed here was further supported by a separate study that used the crystal structures of 2 fragments of hAM (NNFGAIL and SSTNCG) to model a structure for the full-length peptide monomer in the fibril conformation. (Wiltzius *et al.*, 2008) Their data showed that SSTNVG oligomers form a class I steric zipper, similar to that formed by other amyloidogenic peptides. (Sawaya *et al.*, 2007) NNFGAIL oligomers on the other hand, have a bend at the glycine residue that allows the asparagine side chain to interact with the backbone carbonyl of glycine. In their deduced structure for full-length hAM monomers in amyloid fibrils, they proposed that SSTNVG is forming a steric zipper with other monomers of the peptide while NNFGAIL is part of the hairpin turn, similar to what was suggested by the solid state NMR data.

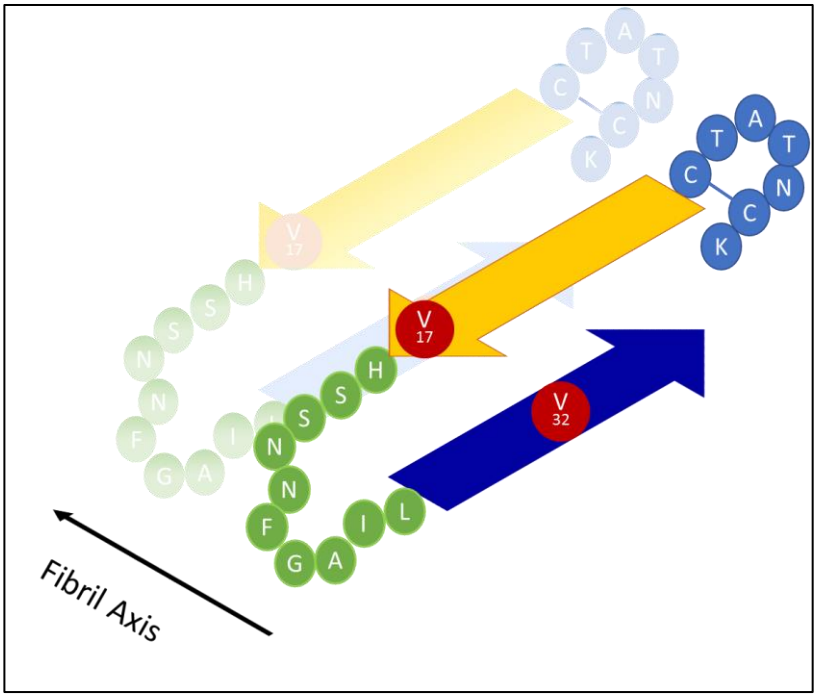

Figure 4.1. The structure of two monomers of hAM forming parallel β-sheets in the fibril state as proposed by Luca *et al.* No cross-strand H-bonding is implied, this is not a hairpin of β-sheet. The loop residues, shown in green circles, are between position 18 and 27. The first 7 N-terminal residues that are not part of the N-terminal β-strand are shown in blue circles. V17, the fastest position to become immobile and V32, the slowest position (as proposed by Shim *et al.*, 2009) are shown in red circles.

The results of both these studies stand in contrast to most conclusions: that the 20-29 region of hAM is the most amyloidogenic portion of the peptide. However, a study done by Shim *et al.* using 2D infrared spectroscopy showed that the formation of the 2 β-strands in hAM may be nucleated by residues within the loop. (Shim *et al.*, 2009) Their study, done using strategically labeled amino acids showed that V17 was one of the fastest residues to transition from random-coil to β-sheet while V32 was the slowest. They concluded that the formation of the two β-strands was independent from one another with the N-terminal strand forming faster than the C-terminal strand.

4.1.4. hAM and the amino acid proline: the rise of pramlintide

Other species have been found to have analogues of amylin including cats and non-human primates. (Howard, 1978; Yano *et al.*, 1981; Spear *et al.*, 1984; Westermark, Wernstedt, O'Brien, *et al.*, 1987; Westermark, Wernstedt, Wilander, *et al.*, 1987; Nishi *et al.*, 1989) Some of these species, i.e. rats, show no evidence of islet amyloid deposits. Rat amylin (rAM) differs from human

amylin (hAM) by six residues at positions 16, 18, 23, 25, 28, and 29. Of these six positions, three positions, 25, 28 and 29 are of particular interest. In rAM these positions replace an alanine and two serines with proline residues. The presence of prolines at these residues has been implicated as the reason rAM maintains solubility and does not have a tendency to aggregate. The prolines at positions 25 and 29 may be important because in cats the presence of one proline at position 29 does not preclude amyloid formation. In the degu, a small caviomorph rodent, amylin has two prolines at positions 28 and 29, yet this variant is also capable of forming amyloid deposits. However, hamsters, that have two prolines at positions 25 and 29, do not form amyloid fibrils. (Westermark *et al.*, 1990)

Peptide	Sequence
Human amylin (hAM)	KCNTATCATQRLANFLVHS^{20}<u>SNNFGAILSS</u>^{30}TNVGSNTY-NH_2
Rat amylin (rAM)	KCNTATCATQRLANFLV**R**S^{20}SNN**L**G**PV**L**PP**^{30}TNVGSNTY-NH_2
Pramlintide (prAM)	KCNTATCATQRLANFLVHS^{20}SNNFG**P**IL**PP**^{30}TNVGSNTY-NH_2

Figure 4.2. The sequences of full-length hAM as well as the analogue of amylin found in rats, rat amylin is given above. The sequence of a synthetic analogue of hAM, pramlintide is also shown. The residues in rAM and prAM that differ from hAM are shown in bold. The region of hAM generally considered to be the most amyloidogenic portion of hAM is underlined.

One important study showed that the presence of proline at all three of these positions has no effect on the function of amylin since rAM and hAM have the same levels of biological activity. (Cooper *et al.*, 1988; Chantry *et al.*, 1991) This most likely indicates that the structural consequences of having proline residues at those positions does not affect the active conformation of the peptide. This information led to the development of a synthetic form of human amylin, with three proline substitutions (at positions 25, 28, and 29), designated as pramlintide. Pramlintide (prAM)'s

receptor binding and biological activity was tested in rats and found to be comparable to that of rAM and hAM in the same situation. (Young *et al.*, 1996) In humans, prAM was first tested in the late 1990's as a potential companion to insulin administered to patients with Type I and Type II diabetes. Results from early drug trials showed that prAM could reduce the postprandial hyperglycaemia in patients with diabetes. (Kolterman *et al.*, 1995; Kolterman, 1997) Studies also showed that the infusion of prAM with insulin resulted in a significant reduction in the glucose, insulin, C-peptide and lactate concentrations in patients with diabetes four hours after a meal. (Thompson *et al.*, 1997) At present, prAM is a commercially available drug that is administered with insulin to patients with Type I and Type II diabetes.

In vitro examination of the amyloidogenic propensity of prAM has led to mixed results. One study found that prAM showed approximately 10% the aggregation capacity of hAM. The aim of the study had been to determine the role of the six residues in hAM that differ in rAM, on the aggregation propensity of the peptide. The results of the study showed that the presence of the proline residues alone was not enough to completely eliminate aggregatory activity. Instead, the three other mutations contribute in some degree to rAM's propensity to remain monomeric. (Green *et al.*, 2003) The results of this study were supported by another study that showed prAM aggregation to be dependent on pH as well as the type of buffer being used for the *in vitro* assay. (da Silva *et al.*, 2016) prAM showed no aggregation at pH 3 and 4 and lower aggregation rates in Tris buffer systems compared to phosphate buffer systems. FTIR and X-ray diffraction data showed that prAM formed fibrils that were similar in morphology and characteristic to hAM fibrils. However, the rate of aggregation of both these peptides were different, with hAM aggregating faster than prAM under all tested conditions. Molecular dynamics simulations of hAM and prAM as well as hAM A25P and hAM S28P, S29P showed that aggregation happens more

readily when these peptides are in the β-sheet free energy state. (Chiu *et al.*, 2013) However, for prAM and to a lesser extent, hAM S28P, S29P, the free-energy state of the α-helix conformation is much lower and therefore more favorable. hAM A25P on the other hand, had a much smaller ΔG between the α-helix and β-sheet states resulting in a peptide that is more likely to aggregate.

The capabilities of prAM as an inhibitor of hAM aggregation has also been studied. Wang *et al.* compared the effects of co-incubating hAM with different amount of rAM and prAM. (Wang *et al.*, 2015) Their results showed that both rAM and prAM slowed down the aggregation of hAM in a dose dependent manner. However, prAM was more effective than rAM at increasing the lag time to aggregation. Interestingly, their studies found that prAM was not reducing the number of fibrils observed by TEM similar to rAM. Instead, there was evidence that prAM was co-precipitating with hAM upon aggregation. They also studied the effect of mutating residues H18 and F23 of prAM to arginine and leucine respectively. These mutations increase the sequence similarity between prAM and rAM and either mutation resulted in a decrease in prAM's inhibitor activity, possibly indicating an important role for these residues.

More recently prAM has been studied as a potential drug-therapy to combat obesity. There is evidence that the expression of prAM in response to lipids in transgenic mice, can reduce body weight, blood lipid levels as well as food consumption. (Rössger *et al.*, 2013) Human studies show that prAM is capable of reducing the LDL-cholesterol levels in patients with T2D and the triglyceride levels in patients with Type I diabetes. (Hoogwerf *et al.*, 2008) Clinical trials of prAM and a leptin-analogue, metreleptin, have shown promising results. (Ravussin *et al.*, 2009) Patients that were administered both drugs demonstrated significant weight loss over the course of 20 weeks with no signs of plateau in weight change.

4.1.5. hAM and aromatics

The hAM sequence contains three aromatic residues that have received a lot of attention due to their possible role in amyloid formation. In 1999, Kayed *et al.*, shows that the aromatic rings in hAM underwent stacking directly before fibril formation. (Kayed *et al.*, 1999) This was confirmed when an alanine scan of the core amyloidogenic unit of hAM (residues 22-27) highlighted the importance of residue F23. (Azriel & Gazit, 2001) The presence of phenylalanine at this position was examined by comparing the effects of NFGAILSS and NYGAILSS on aggregation of full-length hAM. The results showed that while NFGAILSS accelerated fibril formation slightly, NYGAILSS inhibited fibril formation. Mutation of residue 23 in the 22-27 fragment to any other hydrophobic residue also resulted in a decrease in amyloidogenic propensity of this peptide. (Porat *et al.*, 2004)

In 2001, Padrick and Miranker used the intrinsic fluorescence of tyrosine to study the amyloidogenesis of hAM. (Padrick & Miranker, 2001) Their results showed that in fibrils, Y37 is solvent protected; but this is not true at the earlier stages of amylodogenesis indicating that this residue may be one of the last to become structured. This was confirmed by the fluorescence anisotropy measurements that showed Y37 is highly rigid in fibrils and the aromatic ring does not rotate freely. Foerster energy resonance transfer (FRET) measurements between Y37 and the remaining two aromatic residues in hAM show that these residues are in close proximity to one another in the fibril structure, indicating that there could be a turn within the peptide monomer in fibril form. While intermolecular interaction between phenylalanine and tyrosine could also be responsible for the FRET data, the transfer efficiency observed gives rise to a distance of approximately 10.2Å, which is a lot lower than the interstrand distances of in register parallel β-

sheets. These results therefore support the generally accepted theory of strand-loop-strand of each hAM monomer in the final fibril form.

A computational study also supports an interaction between all three aromatic residues, placing each aromatic residue in one of three strands formed by hAM in the protofibril state. (Kajava *et al.*, 2005) Experimentally, the mutation of all three aromatic residues to leucine resulted in a much longer lag time for the aggregation of the peptide when compared to wild-type hAM. (Marek *et al.*, 2007) The final fibrils formed, however, did have the same fibril morphology as those from wild-type hAM as observed by transmission electron microscopy and atomic force microscopy. Mutation of individual aromatic residues to leucine showed that F15 may be playing a more significant role in inhibiting amyloid formation since the aggregation rate of F15L was two times higher than WT. Meanwhile, F23 and Y37 may be playing a role in promoting amyloid formation since F23L and Y37L had a two-fold and three-fold decrease in aggregation rates respectively. (Tu & Raleigh, 2013)

There has also been a study showing the F23L mutant in two short fragments of hAM (comprising residues 21-29 and residues 22-27) forming amyloid fibrils while the F23A mutant of these fragments does not. (Tracz *et al.*, 2004) The same study also showed that the F15L mutant of a hAM fragment (comprising residues 10-19) was also capable of forming amyloid fibrils. While these results show that the presence of aromatic residues is not required to form fibrils, it does not immediately contradict the possible role being played by these residues in promoting the high rate of aggregation nucleation observed for hAM. The aromatic interactions within hAM has garnered a lot of attention and has resulted in multiple studies proposing that these aromatic interactions be targeted in order to design inhibitors of hAM amyloidogenesis (*vide infra*). (Gazit, 2002; Porat *et al.*, 2004, 2006)

4.2. Inhibitors of hAM aggregation

4.2.1. hAM and insulin

If the supposition that hAM undergoes aggregation at certain threshold concentrations is true, then the question that must be answered is how does hAM remain monomeric in the secretory granule at the high concentrations therein? *In vitro*, hAM can form fibrils at concentrations as low as 1μM in physiological buffers; yet the concentration of hAM in the secretory granule has been found to be between 1 – 4 mM in healthy individuals. The answer to this conundrum is insulin. Insulin has been shown to inhibit hAM fibril formation in a dose-dependent manner. (Westermark *et al.*, 1996; Larson & Miranker, 2004) As previously mentioned, insulin adopts an α-helical conformation that can form a heterodimer with hAM, with prominent π-stacking between residues F15 of hAM and Y16 of the insulin B-chain. (Wiltzius *et al.*, 2009)

Examination of the individual components of insulin showed that only the B-chain of insulin was capable of inhibiting hAM aggregation while the A-chain had no effect. (Susa *et al.*, 2014) At an equimolar ratio, ion mobility studies show that the presence of the complete insulin protein or just the insulin B-chain forced hAM to adopt a more compact structure that does not transition to amyloid fibrils. These results support the conclusions of a previous study that show residues 9-20 of the insulin B-chain binding to hAM. (Gilead *et al.*, 2006)

4.2.2. Peptide inhibitors of hAM

Most peptide inhibitors of hAM are derived from sequence homologues that have been modified in some small way. The most common modification is mutation of residues, frequently making use of proline residues. Rat amylin (rAM) which differs from hAM at only 6 positions has been shown to inhibit hAM amyloid fibril formation in a dose-dependent manner. (Cao *et al.*, 2010)

However, an even more conserved peptide, hAM-I26P, was more effective at inhibiting aggregation. (Abedini *et al.*, 2007) At equimolar concentrations, hAM-I26P was able to increase the lag time of hAM aggregation by 20-fold and decrease the eventual maximum thioflavin T fluorescence observed three fold.

N-methylation of amino acid residues has also been a useful tool in designing inhibitors. The residue 23-27 span of hAM have been shown to be the shortest fragment capable of forming aggregates of similar morphology to amyloid fibrils. (Tenidis *et al.*, 2000; Mazor *et al.*, 2002) N-methylation of G24 and I26 in this segment of hAM has yielded potent inhibitors of hAM aggregation. Kapurniotu *et al.* showed that N-methylation of G24 and I26 in the NFGAIL and SNNFGAILSS fragments yielded peptides that were non-amyloidogenic as well as not cytotoxic. (Kapurniotu *et al.*, 2002) These peptides were also able to inhibit the aggregation of their non-N-methylated counterparts, providing support for a relatively novel approach to hAM inhibitor design at the time. When tested as inhibitors of full-length hAM, the N-methylated fragment, NF_mGA_mIL was able to inhibit the amyloidogenesis of full-length hAM to a small extent at substoichiometric concentrations and to a larger extent at a 1:10 molar ratio of hAM to inhibitor. It was also able to increase the viability of pancreatic β-cells when co-incubated with hAM. (Tatarek-Nossol *et al.*, 2005) Yan *et al.* showed that N-methylation of G24 and I26 in full-length hAM yields a peptide that is capable of fully blocking amyloidogenesis as well as reversing the amyloidogenesis of pre-formed fibrils. (Yan *et al.*, 2006) The N-methylation does not interfere with the activity of hAM since this mutant is able to bind to hAM receptors and activate them at approximately the same level as hAM.

While the studies above focus on the 20-29 region of hAM being a highly amyloidogenic patch, there are studies that have shown fragments from this region to be inhibitors of amyloidogeneis

under their assay conditions. Scrocchi *et al.* designed an overlapping series of hexapeptides for residues 20-29 of hAM and found that SNNFGA and GAILSS were strong inhibitors of hAM, maintaining the random-coil structure of hAM for up to 72 hours. (Scrocchi *et al.*, 2002) However, only SNNFGA was able to lower the cytotoxicity of hAM toward RIN-1056 pancreatic β-cells while GAILSS had no effect.

While peptide inhibitors of hAM are commonly derived by modifying the sequence of hAM, Ghosh *et al.* demonstrated that a small peptide with no sequence homology, TVYVYSRVK-NH_2, termed TK9 was able to inhibit the aggregation of hAM when incubated at a 2:1 (TK9:hAM) ratio. (Ghosh, *et al.*, 2015) This peptide, which was taken from the C-terminal sequence of the SARS corona virus envelope protein, was shown to be capable of forming amyloid fibrils itself *in vitro*. However, the process took several days indicating that it was a slow aggregating peptide. The inhibition of hAM by TK9 is similar to the activity of a nine-residue peptide, adopted from the same protein that is capable of inhibiting the fibrillation of insulin.(Banerjee *et al.*, 2013)

4.2.3. Small molecule inhibitors of hAM

A number of the inhibitors of hAM aggregation are also known to inhibit the aggregation of other amyloidogenic peptides. For example, I have previously described the activity of the phenols (-)-epigallocatechin gallate (EGCG) and resveratrol against α-synuclein. These small molecules have also shown high levels of activity against hAM. In 2009, Mishra *et al.* first demonstrated that resveratrol had dose-dependent activity against hAM *in vitro*. Assays done in the presence of membranes that typically promote the aggregation of hAM also showed resveratrol inhibiting amyloid formation. Finally, *in vivo* assays of hAM in pancreatic cells showed a 30% increase in cell viability in the presence of equimolar concentrations of resveratrol were co-incubated with hAM. (Mishra *et al.*, 2009)

A study of possible mechanisms of resveratrol action on hAM by computational modeling suggests that this inhibitor may be blocking the lateral growth of a single-layered β-sheet by interfering with the side-chain stacking of the monomers in the oligomer form. In particular, this phenol may be targeting the π-stacking of the aromatic side chains. (Jiang *et al.*, 2011) Experimentally, the action of resveratrol was examined using mutants of hAM at positions R11, H18, F15, and Y37. (Tu *et al.*, 2015) Mutation of any of these residues to leucine resulted in a decrease in the inhibitory activity of resveratrol. Removal of the N-terminal 7 residues also resulted in the same observations. However, the mutation of F23 to leucine did not produce a noticeable effect on resveratrol activity. The study concluded that the N-terminus as well as the aromatic residues were interacting with resveratrol in some way. The anomalous result of the F23 mutation may have been due to the fact that F23 resides in the loop in the hAM amyloid fibril and may not have interactions with other monomers of hAM with which resveratrol could interfere. Resveratrol has also been used in clinical trials to examine its effects on insulin sensitivity in patients diagnosed with insulin resistant T2D. The results were fairly promising with most patients, showing decreased insulin resistance within 4 weeks of taking the oral form of resveratrol. (Brasnyó *et al.*, 2011)

Despite these promising results, resveratrol has been found to be less effective than EGCG at disaggregating pre-formed hAM fibrils. (Tu *et al.*, 2015) Meng *et al.* found that EGCG was able to completely inhibit hAM aggregation at 1:1 ratios along with protecting pancreatic cells against the cytotoxicity associated with hAM. (Meng, Abedini, Plesner, Verchere, *et al.*, 2010) Studies examining the possible targets of EGCG within hAM revealed that EGCG did not interact specifically with any of the aromatic residues, amino groups, or the sulfhydryls within hAM. (Cao & Raleigh, 2012) Instead, the research proposed that EGCG had a non-specific interaction with monomers and intermediates. The same study also examined the most important moieties of

EGCG that were responsible for its inhibitory activity. The results showed that the gallate ester and one of the hydroxyl groups, depicted in Figure 4.3, were the most important for activity since the loss of either one of these groups resulted in decreased activity while the loss of both completely abolished the inhibitory activity of this small molecule.

The importance of the phenol and hydroxyl groups of EGCG is shared by another inhibitor of hAM: baicalein. Baicalein (5,6,7-trihydroxyflavone) is a flavonoid found in the roots of certain flowering plants. It is also one of the active ingredients in the Japanese herbal supplement, Sho-Saiko-To. This small molecule has been shown to inhibit hAM aggregation in a dose-dependent fashion. (Velander *et al.*, 2016) Structure-activity relationship studies showed that at least two hydroxyl groups were necessary for the flavone action and at least one of those groups had to be at position 6 since 5,7-dihydroxyflavone had no activity against hAM. Based on LC-MS results, the study proposed that the formation of a Schiff-Base with an *o*-quinone intermediate may be the mechanism of action.

Congo Red is an unusual inhibitor of hAM aggregation. It's a diazo dye that is used to stain amyloid materials in cells. In the presence of amyloid fibrils, Congo red emits an apple-green birefringence under polarized light. Aitken *et al.* showed that the co-incubation of Congo red at equimolar concentrations of hAM resulted in a decrease in hAM aggregation as well as an increase in the viability of RINm5F cells. (Aitken *et al.*, 2003) However, the *in vitro* results of Congo red inhibition may be dependent on assay conditions since a previous study showed that Congo red had no effect on fibril formation while *in vivo* studies showed some protection from hAM cytotoxicity. (Lorenzo & Yankner, 1994)

One common motif among the many small-molecule inhibitors of hAM amyloidogenesis is the presence of a benzene ring, often as a phenol. Besides the previously mentioned small molecules,

other inhibitors such as acid fuchsin (Meng, Abedini, Plesner, Middleton, *et al.*, 2010), tetracycline (Forloni *et al.*, 2001; Aitken *et al.*, 2010) and phenol red (Porat *et al.*, 2004) all contain at least one benzene ring within the molecule. Profit *et al.* examined the effect of the electrostatic repulsion of benzoic acids conjugated to the 22-29 fragment of hAM on hAM aggregation. (Profit *et al.*, 2017) Their results found several conjugates that were capable of increasing the rate of fibril formation thus forcing hAM to spend less time in the highly toxic soluble oligomer state. They were also able to isolate a conjugate of pyromellitic acid that was capable of inhibiting hAM amyloid formation when present in 10-fold excess. When the activities of these benzoic acids were studied without conjugation to the hAM fragment, trimesic acid emerged as a strong inhibitor of aggregation.

Finally, nanoparticles are an interesting class of hAM inhibitors that has only recently been discovered. Initial studies showed that nanoparticles made up of 1:1 N-isopropylacrylamide: N-tert-butylacrylamide (NiPAM:BAM) were able to inhibit the fibril formation of full-length hAM as well as the 20-29 fragment of hAM. (Cabaleiro-Lago *et al.*, 2010) Further examination showed that particles made up of 100% NiPAM were even more effective at inhibiting amyloidogenesis. The mechanism of action of these particles was proposed to be through the adsorption of hAM monomers onto the surface of the particle, thus reducing the monomer concentration in solution.

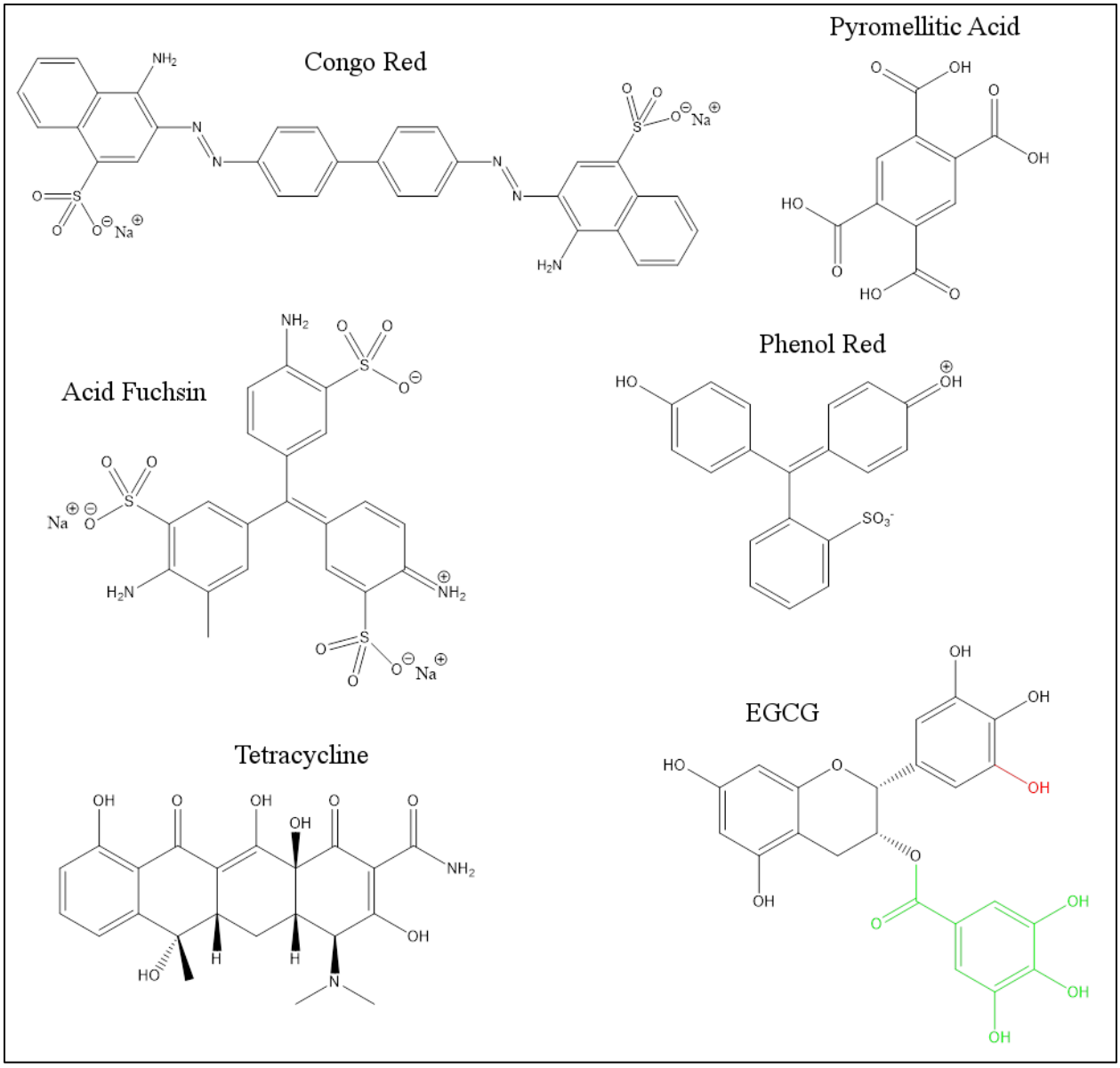

Figure 4.3. The structure of some small molecule inhibitors of hAM amyloidogenesis. For EGCG, the two most important moieties: gallate ester (green) and 3-hydroxyl group (red) of the trihydroxyl phenyl ring are highlighted.

4.3. Method Development

Developing assay conditions for hAM aggregation proved to be a balancing act between the concentration of hAM, the ionic strength of the buffer, the pH of the buffer, and the use of appropriate amounts of HFIP which is known to promote aggregation optimally at 5 vol-% at low pH. (Yanagi *et al.*, 2011) After multiple trials, the following assay conditions were found to give a reproducible aggregation course: 50µM hAM in 50 mM phosphate buffer, pH 2.0 with 25 mM NaCl and 2 vol-% HFIP. It has been shown that at lower pH, hAM aggregation is slowed down, which is useful since the concentration of hAM used in this assay was higher than the norm. (da Silva *et al.*, 2016) This yielded an assay where hAM achieved maximal β-signal by CD in 135 minutes in the presence of 25 mM NaCl and 2 vol-% HFIP. Maximal ThT fluorescence was observed between 160 and 180 mins.

Each CD and ThT measurement was taken in triplicate. For CD, in every replicate, measurements were taken at 45 minute intervals beginning with t=0 minutes. For ThT, the three replicates were staggered so that each one had the first measurement taken at a slightly later time point, allowing one to plot a graph with points at every 10 minutes for the first 180 minutes and every 20 minutes for the next 180 minutes. This was done by taking the first measurement at t=0 minutes for run 1, at t=10 minutes for run 2 and t=20 minutes for run 3. The subsequent measurements were all taken at 30 minute intervals up to 180 minutes, then 60 minute intervals up to 360 minutes.

Percent inhibition calculations for the ThT fluorescence assay used the following equations:

$$Percent\ inhibition = 100 - (\frac{S\ in\ the\ presence\ of\ inhibitor}{S\ in\ the\ absence\ of\ inhibitor}\ x\ 100)$$

where S = the average of the ThT signals at 160, 170 and 180 mins.

The average signal taken at these three points was used because in the control, the maximum ThT appeared at one of these three time points.

4.4. Results

4.4.1. The WW series

As described previously, the use of non-sequence homologous peptides as inhibitors of amyloidogenesis has been successful for inhibiting the aggregation of two other amyloidogenic peptide: Aβ that is implicated in Alzheimer's disease and in the present work α-synuclein. (Chapter 3.4.2) However, little work has been done to study peptide inhibitors of hAM aggregation that are not derived from the sequence of hAM. Dr. Kelly Huggins' initial discovery of peptide WW, which is capable of inhibiting the amyloidogenesis of α-synuclein as well as hAM gave rise to the hairpin hypothesis. The hairpin hypothesis proposes that a combination of aryl side-chains and pre-structured β-strands will interact more favorably with the pre-amyloid state of hAM thus preventing self-self recognition and the subsequent formation of amyloid fibrils.

The uninhibited control for hAM aggregation showed a transition from random-coil to a maximum β-signal by CD at 135 minutes. (Figure 4.4A) However, when monitored by ThT fluorescence, maximal amyloid formation is not detected until approximately 160 minutes at which point the fluorescence remains constant up to 300 minutes before beginning to decrease. (Figure 4.4B) The decrease is most likely occurring due to insoluble aggregate formation indicating a transition from the soluble-oligomer/small-protofibril phase to larger protofibrils and the extended fibril stages of amyloidogenesis.

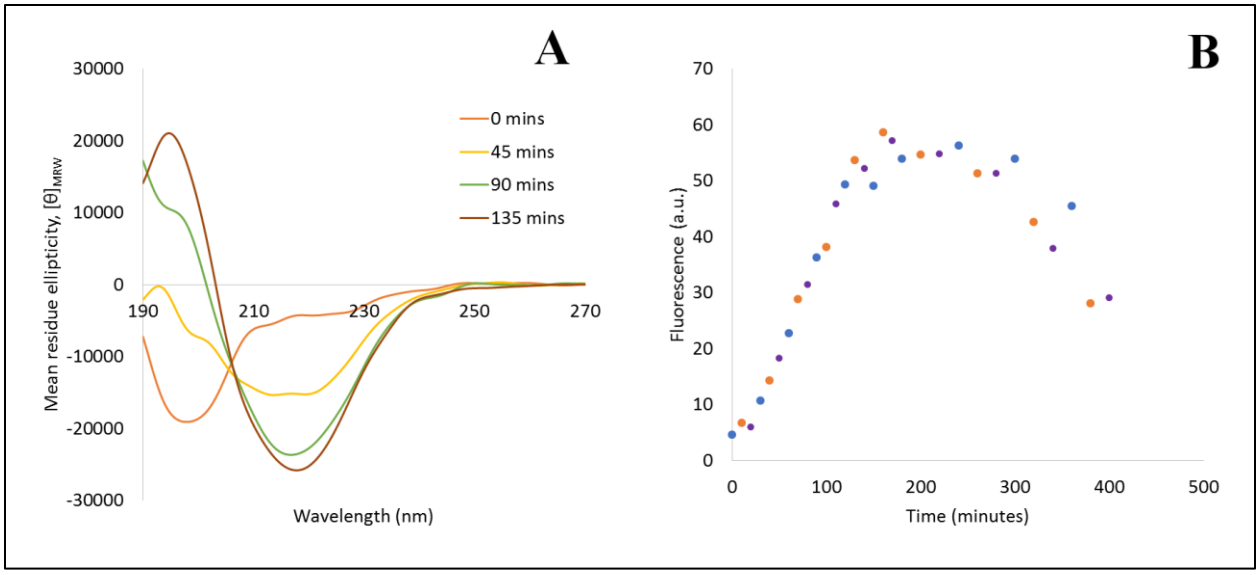

Figure 4.4. Panel A- CD spectra for the hAM in the absence of inhibitor. Panel B- Staggered ThT spectrum representing three replicates of hAM aggregation in the absence of inhibitor.

Building on the ground work of Dr. Huggins, my initial studies in hAM inhibition involved testing the peptide WW and variants with different degrees of hairpin structuring in order to examine if the hairpin fold played the previously suggested role in inhibitor activity. Of the peptides tested, the most well folded variant was cyclo-WW. This cyclized version of the peptide WW has proven to be a potent inhibitor of α-synclein aggregation as well. The other variants tested were capped-WW and cp-WW. cp-WW is the circularly permuted variant of WW as well as the uncyclized variant of cyclo-WW. A cartoon representation of the three peptides is shown in Figure 4.5A. Circular permutation involves changing the location of the termini of a peptide while preserving all other aspects of the sequence. For cp-WW, this is done by adding a favorable hairpin turn –IpPK- connecting the N- and C-terminus while the original turn is-IpGK- is severed. Connecting the original turn gives rise to cyclo-WW.

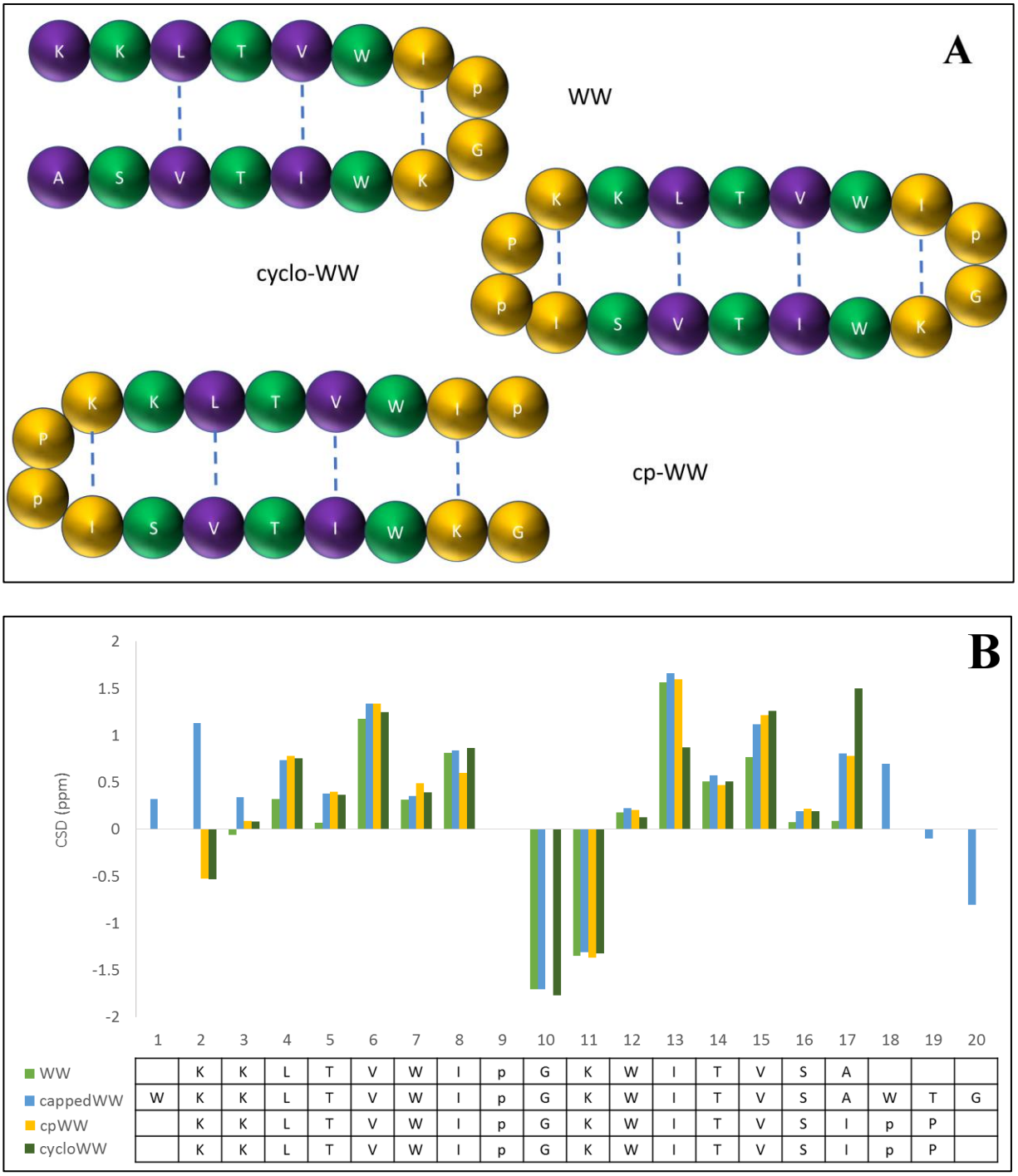

Figure 4.5. (A) - Cartoon representation of three peptides: WW, cyclo-WW and cp-WW. The cross-strand hydrogen bonds are indicated as blue dashed lines. (B) - Comparison of backbone H_N chemical shift deviation of 4 peptides.

The graph in Figure 4.5B compares the backbone H_N values for the residues of these 4 peptides. The residues for cp-WW are reordered to match that of the other three peptides so that a comparison can be made. The proper ordering of amino acids for cp-WW is given in Figure 4.5A. All four peptides show the characteristic structuring of a β-hairpin with a prominent hairpin register. The chemical shift deviation of G20 in capped-WW demonstrates that this hydrophobic cap is not fully formed since a well formed cap has been known to have CSDs of up to 3.0 ppm for the Gly-H_N in the unit. Since the termini of these peptides vary due to circular permutation of one peptide and backbone cyclization of another, the most useful tool to compare the fold of these peptides is a strand residue CSD comparison. For this the H-bonded strand residues at positions 4, 6, 13 and 15 ,as shown in Figure 4.5B, can be used. The data shows that at positions 4 and 15, peptide WW is the least structured variant, especially since these residues are further away from the turn-flanking Trp/Trp stabilization. In the case of capped-WW, cp-WW and cyclo-WW, the stability offered by the β-cap, the end-capping Trp/Trp interaction and the backbone cyclization stabilizes positions 4 and 15 resulting in similar CSDs.

At position 6 however, all 4 peptides seem to share similar CDSs, while at position 13, cyclo-WW seems to have the lowest CSD, indicating weaker hydrogen bonding than the other 3 peptides. This discrepancy could be attributed to the strength of the EtF face interaction of the adjacent tryptophan residue. A CD comparison of WW, capped-WW and cyclo-WW shows that the exciton couplet of cyclo-WW at 5°C is very weak, only 68,000 $deg \cdot cm^2 \cdot dmol^{-1}$ while those of capped-WW and WW are 5-fold and 2-fold larger respectively at the same temperature. This data indicates that the Trp/Trp interaction is not as strong in cyclo-WW as the other peptides which could be why the hydrogen bonding of adjacent residues is affected.

In inhibition studies with these 4 peptides, cyclo-WW emerged as the most potent inhibitor, followed by capped-WW, WW and finally cp-WW. (Table 4.1) The potency of cyclo-WW was such that even at 0.25 molar eq (*versus* hAM) of added peptide, I was able to observe a 60% inhibition of amyloid fibril formation. Capped-WW also proved to be a strong inhibitor with 0.5 eq capped-WW having a higher level of inhibition than 2 eq WW. However, increasing concentrations of capped-WW proved underwhelming with 2 eq of capped-WW only showing a 74.4% inhibition by ThT while 4 eq of WW had an 88.3% inhibition. The peptide, cp-WW was the least effective with no concentration dependent increase in inhibitor activity between 4 eq and 1 eq.

	4 eq	2 eq	1 eq	0.5 eq	0.25 eq	0.1 eq
WW	88.3	50.4	9.7			
capped-WW		74.4	61.7	63.0		
gal capped-WW	74.1	76.8	70.7			
bz-capped-WW	81.6	68.7	72.8			
cp-WW	49.0	45.1	47.7			
cyclo-WW		91.1	89.4	88.4	58.8	~0

Table 4.1. The percent inhibition of each peptide in the WW series at different concentrations based on ThT measurements.

The results so far support the hairpin hypothesis since cyclo-WW, with the most stable hairpin folded, is the most potent inhibitor of hAM amyloidogenesis. The data also allows me to draw one further conclusion: the mechanism of inhibition by the WW series does not involve the unfolding and restructuring of the peptide to other conformations, including linear conformations. If restructuring were involved, the rigidity of cyclo-WW would prevent any change in the structure thus making this inhibitor the least potent of the 4 peptides tested. The potency of cyclo-WW in

the *in vitro* assay is supported by *in vivo* testing in rat insulinoma cells. The assays, performed in the lab of a collaborator, Dr. Aphrodite Kapurniotu, show that this peptide is also able to mitigate hAM related toxicity in cells when present in concentrations as low as 0.5 eq relative to hAM. Taken together, the *in vitro* and *in vivo* results show a peptide with strong inhibitor activity that may be safe from proteolytic digestion due its cyclic nature making this an interesting peptide for further studies.

Cell culture studies were also done for capped-WW. The results showed that this peptide was as potent as cyclo-WW in maintaining the viability of cells in the presence of hAM. The results of this study contradict my *in vitro* results that show 2 eq capped-WW not having the same potency as 0.5 eq cyclo-WW. The reason for this contradiction could be the difference in buffer pH between the 2 assays. The *in vitro* studies were done at a lower pH than the *in vivo* studies and could be affecting the hairpin structure of capped-WW since it is not covalently stabilized. However, my CD comparisons of the peptide at pH 2 and pH 6.5 do not show significant differences in the molar ellipticity of the peptide, indicating that the pH has very minor effects on hairpin structure. The conflicting results cannot then be attributed to structure and may be a result of some other characteristic of the peptide under *in vivo* conditions. One possibility could be a difference in cell membrane penetration of the peptide. Capped-WW may be able to penetrate cells more easily resulting in higher concentrations within cells while cyclo-WW may be unable to enter cells as easily resulting in lower activity at high concentrations than in *in vitro* assays.

Since capped-WW was showing promising results in both assays, I decided to explore if adding benzoyl conjugates to the N-terminus of the peptide would affect inhibitor activity. I chose two conjugates, the benzoyl group and a gallate. The gallate unit has been shown to be an essential feature for hAM inhibition by EGCG. Benzoyl groups and benzene rings, on the other hand, are a

common motifs shared in a lot of non-peptidic hAM inhibitors. Unfortunately, neither conjugate provided improved inhibition, compared to capped-WW, at the higher concentrations. At 1 eq of added inhibitor there is about 10% greater inhibition by the conjugate-capped-WW peptides than capped-WW. These results could be indicative of a lack of synergy between the two motifs, especially at higher concentrations. It could also be an indication that the N-terminus of the peptide is not making significant contacts with hAM at higher concentrations, thus making the added moieties at this position less available for interaction.

4.4.2. New studies of hAM sequence fragments

Following my non-sequence homologous peptide inhibitor studies, I studied the effect of the 22-29 fragment of hAM on aggregation. The 20-29 region of hAM had been considered the shortest sequence within hAM capable of forming amyloid fibrils. (Glenner *et al.*, 1988; Westermark *et al.*, 1990; Moriarty & Raleigh, 1999) However, Tenidis *et al.* showed that within this sequence, the pentapeptide FGAIL and the hexapeptide NFGAIL were also capable of forming fibrils. (Tenidis *et al.*, 2000) Their studies demonstrated that the fibrils formed by FGAIL were very long and broad whereas those formed by NFGAIL resembled the typical amyloid fibril morphology. *In vitro* studies of this peptide when co-incubated with hAM showed no effect on hAM aggregation.

Since hAM seeds have been known to accelerate the aggregation of hAM monomers, (Hu *et al.*, 2017) I wanted to study the effect of seeds comprised of hAM fragments on the amyloidogenesis of full-length hAM. However, since NFGAIL was expected to be extremely hydrophobic and difficult to purify by HPLC, I chose to begin my study with the 22-29 fragment of hAM: NFGAILSS. The expectation was that this fragment would seed aggregation and decrease the lag time of aggregation. In order to accommodate these potential observations, the assay conditions that were being used at the time needed to be modified. I examined the growth of β-signal over

time for various sodium chloride (NaCl) concentrations in the presence of 2 vol-% HFIP. Decreasing the salt concentration proved to be too drastic as the peptide remained random-coil for up to 6 hours. After various attempts, I finally obtained conditions that demonstrated the transitioning of hAM secondary structure from random-coil to β by CD over the course of 240 minutes in the presence of 50 mM NaCl and 1 vol-% HFIP. The lag time was approximately 50 minutes as monitored by ThT fluorescence. (Figure 4.6 B) Maximal ThT fluorescence was reached at approximately 260 minutes.

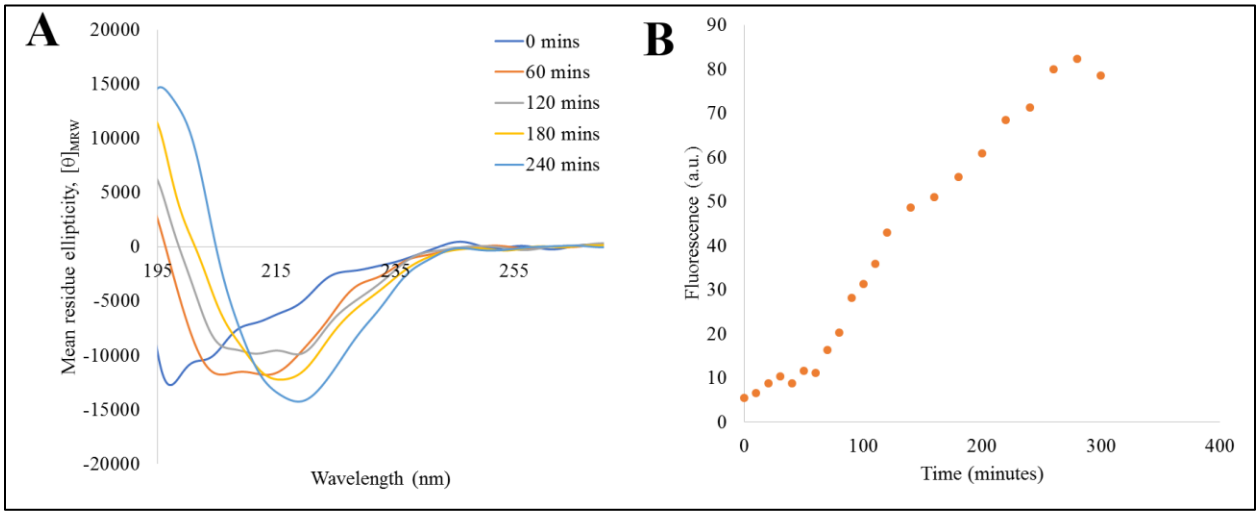

Figure 4.6. Panel A – CD spectra of hAM in the absence of peptides, under 1% assay conditions taken at hourly intervals up to 4 hours. Panel B – Staggered ThT runs representing 3 replicates of hAM under 1% assay conditions.

An interesting observation that was made under these conditions is the presence of an α-helix-like signal by CD at time points t=60 minutes and t=120 minutes. (Figure 4.6A) The signal at the second maximum, which is attributed to the n → π* transition of the peptide backbone, is blue shifted from 222 nm to approximately 214 nm at t=60 minutes. At t=120 minutes, the signal red shifts to 219 nm putting it a little closer to the expected signal for this transition. The reason for this shift is unclear. However, the α-helix structure has been proposed to be an on-pathway

intermediate in the amyloidogenesis of hAM. The data from this assay shows that a helical intermediate may be present under my assay conditions as well.

To investigate if pre-formed seeds of the 22-29 (NFGAILSS) fragment of hAM could seed hAM aggregation, I allowed a 2 mM sample of the fragment to aggregate at room temperature without shaking or stirring for 2 weeks. At this point, a precipitate was visible, indicating that aggregation had occurred. The sample was spun down and the supernatant was used in experiments containing hAM. The concentration of the fragment had to be estimated based on the initial concentration of the monomer. The results from the experiment were wholly unexpected. (Table 4.2) Instead of seeding aggregation, the addition of solution from aged NFGAILSS to the hAM sample resulted in the complete inhibition of amyloidogenesis. The inhibition of the aged sample was approaching 100% at 0.4 eq peptide (monomer based concentration) to hAM.

	1 eq	0.4 eq	0.1 eq
fresh NFGAILSS	77	66	11
aged NFGAILSS	79	85	67
NFGAILS	73	31	
NFGAIL	37	15	

Table 4.2. The percent inhibition of each fragment at different concentrations (and with different preparations) based on ThT measurements.

In order to investigate these results further, fresh samples of NFGAILSS were prepared and tested. The data showed that even fresh NFGAILSS was able to inhibit aggregation at 0.4 eq peptide to hAM. However, the activity of the fragment decreases dramatically at 0.1 eq peptide to hAM. Figure 4.7 shows the ThT fluorescence time course for hAM aggregation with the aged and fresh fragments present at sub-stoichiometric concentrations. The inhibitory activity of fresh at 0.4 equiv matches that of aged NFGAILSS at 0.1 eq. There is a possibility that, since the concentration of

the aged sample is estimated based on the initial monomer concentration, what was assumed to be 0.1 eq could in fact be a significantly lower concentration of peptide aggregate or peptide remaining in the supernatant, given that the aged sample was allowed to aggregate and form a precipitate. These results point to a role being played by the oligomers formed by the NFGAILSS fragment in inhibiting hAM aggregation. It is also possible that the presence of two serine residues affects the way this peptide interacts with full-length hAM. Supporting an hypothesis that that the serine residues play a role in inhibiting hAM aggregation, Scrocchi *et al.* have previously shown that the peptide GAILSS is a potent inhibitor of hAM aggregation.

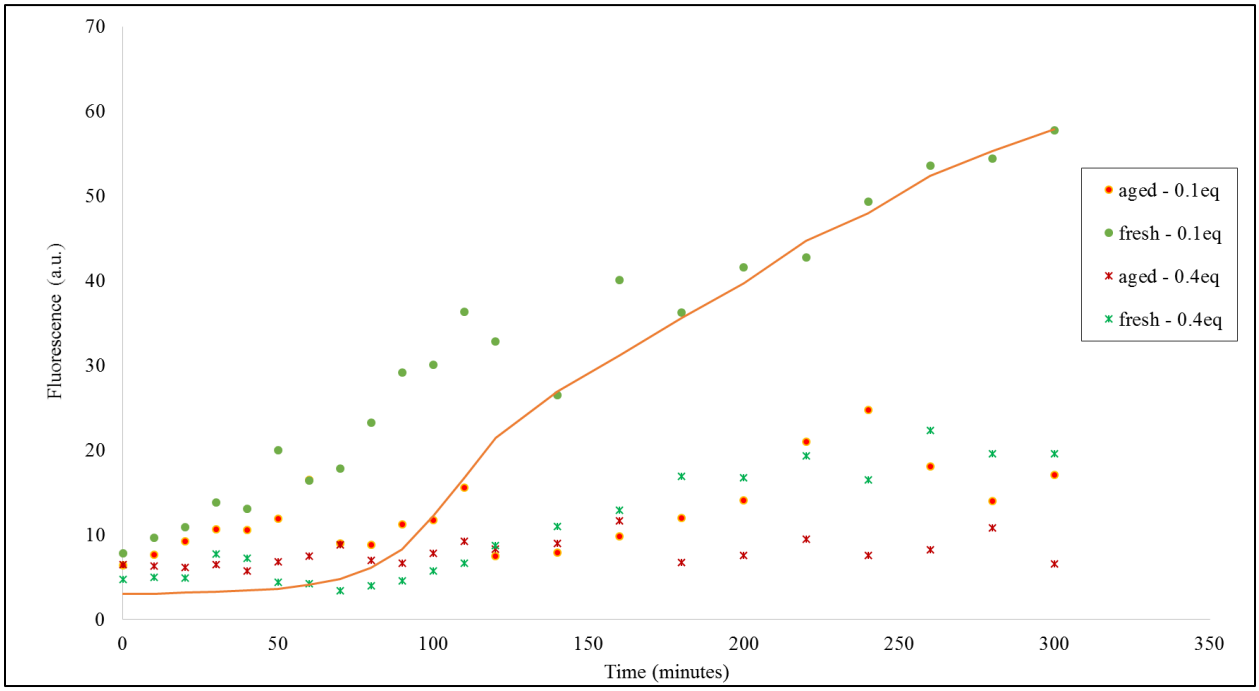

Figure 4.7. The graph represents the 3 staggered measurement of ThT fluorescence of substoichiometric aged and fresh NFGAILSS in the presence of hAM. The solid line represents the change in ThT fluorescence over time for hAM in the absence of inhibitor.

Given that these results stand in contrast to the results observed by Tatarek-Nossol *et al.* with NFGAIL, I decided to systematically examine whether the addition of the two serine residues to the hexapeptide had any effect on the fragment's ability to inhibit hAM aggregation. In order to

do this, I synthesized two more peptides, NFGAILS and NFGAIL. As shown in Table 4.2, the percent inhibition by NFGAILS at 1 eq mirrored that of NFGAILSS at the same concentration but at substoichiometric concentrations, the activity of NFGAILS begins to decrease. The removal of all serines, results in a peptide that has very little activity at equimolar concentrations *versus* hAM. This result is more in keeping with previously reported studies that show immediate change in conformation of hAM upon the addition of 10- or 20- fold NFGAIL. (Scrocchi *et al.*, 2002) The CD results shown in Figure 4.8A confirm that there is little to no change in random-coil structure of hAM throughout the time course of the assay in the presence of 1 eq NFGAILS. On the other hand, incubation with NFGAIL results in a distinct α-helix signal. (Figure 4.8B) This signal was also observed by Scrocchi *et al.* immediately upon the addition of 10-fold NFGAIL to a sample of hAM. (Scrocchi *et al.*, 2002) A similar α-helix signal can be seen in the uninhibited control at 120 minutes. (Figure 4.6A) This could be an indication that NFGAIL binds to full-length hAM and delays the formation of the α-helix conformer thus slowing down aggregation to a certain extent. This would explain why the random-coil state seems to be more populated at 120 mins in the presence of NFGAIL than in an uninhibited control. This could also be an indication that the 2 serine residues are solubilizing and play a role in maintaining the random-coil structure of hAM.

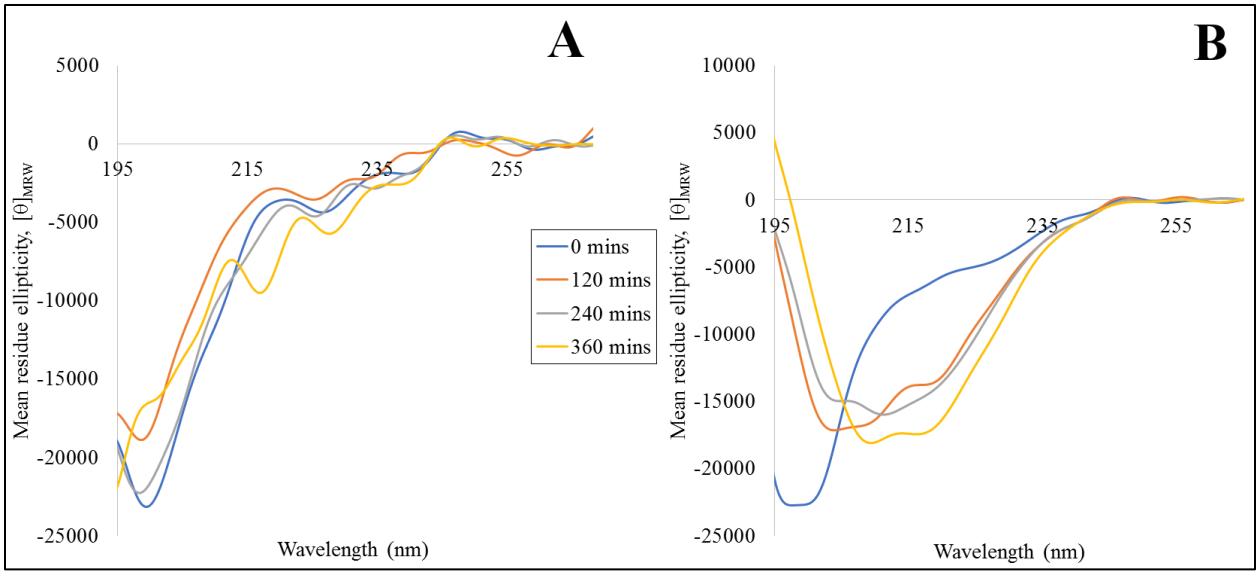

Figure 4.8. CD spectra of hAM when co-incubated with equimolar concentrations of (A) NFGAILS and (B) NFGAIL. The legend for both spectra is in the middle. The spectra in panel B provide another instance in which hints of helical structuring are evident.

4.5. Summary and Conclusions

The present study has served to validate the hairpin hypothesis first developed from the work of Dr. Kelly Huggins. My results have yielded a peptide, cyclo-WW that is very potent against hAM aggregation and is able to inhibit amyloidogenesis at substoichiometric cocentrations. This result is even more exciting considering that the same peptide is able to inhibit another amyloidogenic system, α-synuclein at low concentrations as well. The ability of cyclo-WW to inhibit two peptides that share no sequence similarity to the inhibitor or with each other also serves as proof that there are common steps in the amyloid pathway that can be targeted by inhibitors. Cyclo-WW may be emerging as a universal inhibitor of amyloidogenesis.

My analysis of the effect of a hAM fragment on aggregation proved very interesting. Contrary to initial expectations, aged samples of NFGAILSS were strongly inhibitory toward hAM amyloidogenesis instead of acting as seeds that increase the rate of amyloidogenesis. Sequential removal of the C-terminal serine residues showed that these residues play a role in the inhibition observed for peptide and its aged solutions. The data from these studies also supported the hypothesis that hAM forms an α-helix structure prior to β-oligomer formation that is typically expected of amyloidogenic peptides.

Future work for these studies must include NMR experiments that could help elucidate the secondary structure adopted by hAM during amyloidogenesis. These experiments could serve to determine if the residues within hAM are indeed forming an α-helix intermediate during amyloidogenesis. Binding experiments should also be done to determine if cyclo-WW binds to hAM monomers, thus providing a mechanism for the inhibition of these peptides. It would also

provide information on the positions within hAM that are targeted by this peptide which could prove useful in determining residues that are important in the formation of amyloid fibrils.

Chapter 5: Antimicrobial Peptides

5.1. Introduction

The advent of antibiotics was celebrated as one of the greatest discoveries of the 20th century and Alexander Fleming was touted as a hero for his discovery of penicillin. Yet almost a century later, the use of antibiotics has led to a completely different problem altogether: the evolution of the antibiotic-resistant bacteria. Medical research has discovered over 20,000 potential genes expressed by bacteria that are capable of antibiotic resistance. (Liu & Pop, 2009) To date, some of the major pathogens in the world have developed antibiotic resistance such as *M. tuberculosis*, *Escheria coli*, *Staphylococcus aureus* and *Streptococcus pneumoniae.* (Davies & Davies, 2010) The main methods of developing antibiotic resistance are from the horizontal acquisition of resistance genes, recombination of foreign DNA into the chromosome, or by mutations in the chromosomes. (Martinez & Baquero, 2000) Antibiotic resistance can be caused by a single spontaneous mutation but more often is caused by a misuse of antibiotics that results in a gradual increase in mutations resulting in resistance. Developing antibiotic resistance is a slow process and occurs over multiple generations. This is due to the fact that the expression of antibiotic resistant phenotypes is often not limited to one mutation and frequently require the expression of several mutated proteins before complete antibiotic resistance is conferred. (Martinez-Freijo *et al.*, 1998; Hooper, 1999) Horizontal acquisition of resistance genes, on the other hand, is a faster way for bacteria to develop and spread resistance. Since bacteria can acquire multiple genes, this often results in resistance to multiple antibiotics. Consequently, there is an inability to fight these bacteria with available medications.

In most cases, antibiotic resistance greatly affects antibiotics that need to permeate the bacterial cell wall in order to act on targets within the cell. Therefore, the development of antimicrobial

peptides (AMPs) has garnered a lot of interest. AMPs target the lipopolysaccharide layer of bacterial cell walls, making them more effective and less likely to encounter resistance from bacteria. (Bahar & Ren, 2013) The rate at which AMPs are able to act on bacteria has also proven to be quite useful in overcoming the rapid mutation rates that could lead to antibiotic resistance. (Loeffler *et al.*, 2001). The first AMP, gramicidin, was discovered in 1939 from a soil *Bacillus* strain that showed activity against pneumococcal infections in mice. (Dubos, 1939) In 1956, the first animal originated AMP, defensin, was found in rabbit leukocytes. (Hirsch, 1956) Since then, nearly 4000 AMPs have been discovered in plants, animals, and humans and approximately 1600 more have been synthesized. (Zhao *et al.*, 2013) In humans, a wide variety of these peptides have been found to play a role in innate immunity and can be divided into three major groups: defensins, cathelicidins, and histatins. (De Smet & Contreras, 2005) All three groups of peptides have demonstrated activity against both gram-positive and gram-negative bacteria, yeasts, fungi and enveloped viruses. (Turner *et al.*, 1998; Rothstein *et al.*, 2001; Sajjan *et al.*, 2001; Joly *et al.*, 2004)

Almost all AMPs can be classified into 4 groups based on their secondary structure: α-helix, β-sheet, extended conformation, or loop conformations. (Powers & Hancock, 2003; Jin *et al.*, 2005; Hancock & Sahl, 2006; Midura-Nowaczek & Markowska, 2014) Despite the differences in secondary structure, most AMPs that act on bacterial membranes share similar characteristics. These peptides are typically amphipathic, having a polar and non-polar face. This allows AMPs to interact with the charged outer membrane of a bacterial cell through electrostatic interactions of the polar face and subsequently use the non-polar face to insert themselves into the bacterial membrane. (White *et al.*, 1995; Madani *et al.*, 2011) AMPs tend to have high positive net charges, containing large numbers of the cationic amino acids, arginine, R and lysine, K. This is because most bacterial cell walls are anionic and attract positively charged peptides. In gram-positive

bacteria, the presence of teichoic acid in the peptidoglycan is responsible for the anionic character while in gram-negative bacteria, the anionic character is derived from the lipopolysaccharides in the outer membrane. (Figure 5.1) The anionic character of bacterial cells contrasts with mammalian cells, which have more zwitterionic phospholipids on the outer leaflet and negative phospholipids on the inner leaflet of their cell membranes. (Verkleij *et al.*, 1973; Shai, 2002) This distinction allows AMPs to selectively target bacterial cells without harming surrounding mammalian cells.

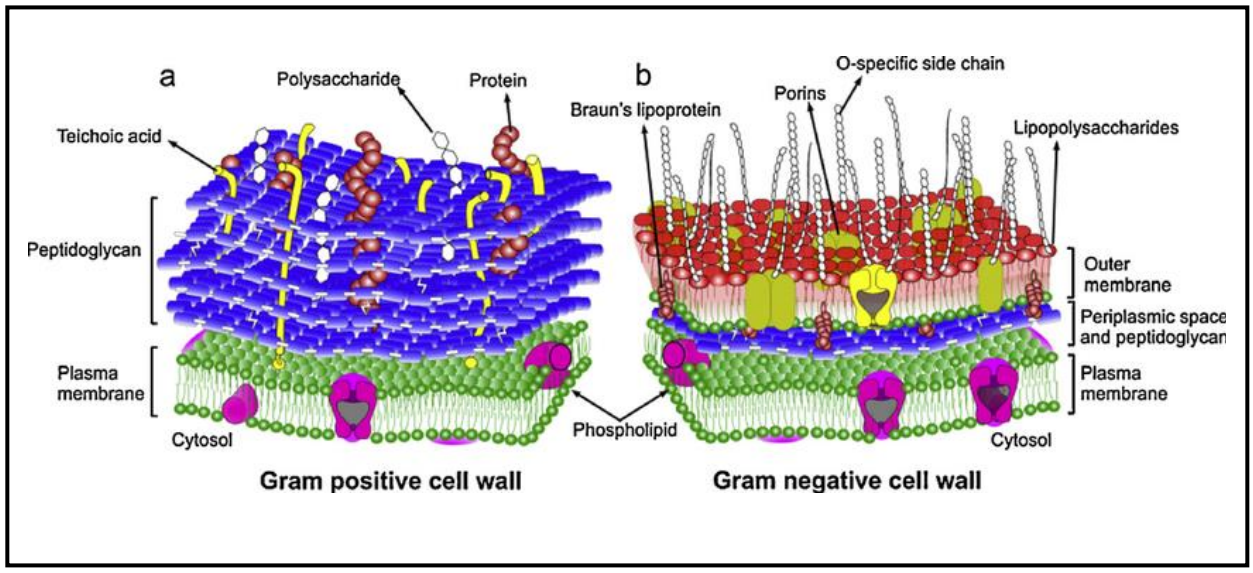

Figure 5.1. The image represents the cell wall of a) gram-positive and b) gram-negative bacteria. Gram-positive bacteria have a thick peptidoglycan layer unlike gram-negative bacteria. Instead, Gram-negative bacteria have an asymmetrical outer membrane that rests on top of a very thin peptidoglycan layer. *(Image adapted from Tripathi* et al.*, 2012*)

5.1.1. Mechanism of Action

Most AMPs that act on bacterial cell walls are thought to induce the formation of pores that cause the contents of the cell to leak out, resulting in cell death. (Silvestro *et al.*, 2000) Many different

models have been proposed, but the most common models are the pore forming model and the membrane disruption model (also known as the 'carpet' model). (Brogden, 2005) All models are typically described as beginning with the electrostatic attraction of the positively charged peptide to the anionic bacterial cell wall. Once peptides have identified their target, they typically bind to the membrane. This state is known as the surface state (or S-state). For most AMPs, once a threshold concentration is reached, the peptide begins to insert itself into the membrane resulting in membrane permeabilization, known as the I-state. It is in the transition from the S-state to the I-state where the differences in the proposed mechanisms of action lie. (Figure 5.2)

Figure 5.2. The image depicts the three different mechanisms by which antimicrobial peptides can act on membranes of bacterial cells. A) Barrel-stave pore formation B) Toroidal pore formation C) Carpet membrane disruption *(Image adapted from Park* et al.*, 2011)*

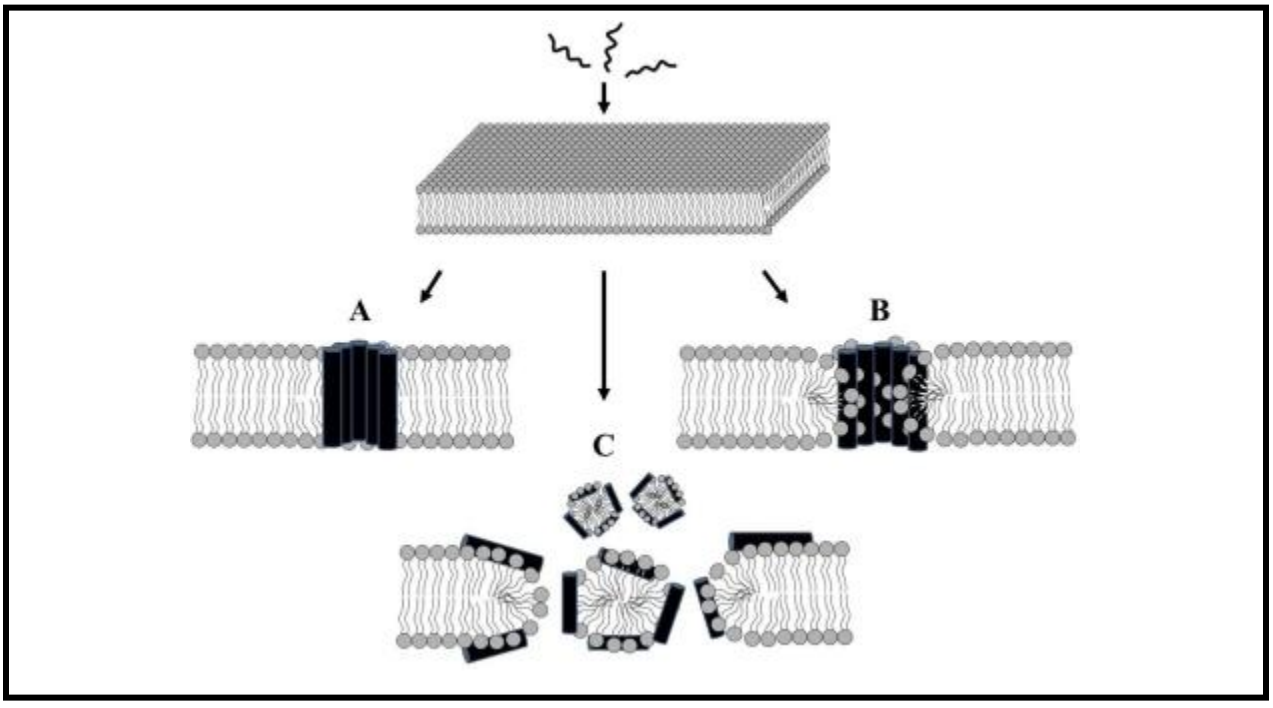

AMPs that form pores are found to form two different types of pores, the less common barrel-stave pore and the toroidal pore. The barrel-stave pore is characterized by a dissociation of the peptide

from the lipid head group of the cell membrane to form a pore with a central lumen made up of the hydrophilic face of the peptide while the hydrophobic face is in contact with the tails of the lipid bilayer. This change in peptide orientation relative to the cell membrane can be detected using oriented circular dichroism techniques. Oriented circular dichroism relies on the energy transition of $\pi \rightarrow \pi^*$ in helical peptides. When the axis of the helix is perpendicular to the light (orientation of peptides in the S-state), the $\pi \rightarrow \pi^*$ signal transition shows a maximum negative at 205 nm. However, in the I-state when the axis of the helix is parallel to the light, the signal at 205 nm is vastly decreased. This results in a CD signal that is approaching 0. (Yang *et al.*, 2001) This technique is particularly useful in determining the threshold concentration at which AMPs transition from the S-state to the I-state.

To date, the peptide that is most commonly known to form a barrel stave pore is alamethicin. Alamethicin is an α-helical peptide produced by the fungus *Trichoderma viride*, containing multiple helix-favoring Aib (2-aminoisobutyric acid) residues. Studies have shown that when in contact with bacterial membranes, at the threshold concentration, eight alamethicin monomers aggregate to form a barrel-stave pore. This was shown by numerous neutron scattering experiments that showed the inner and outer diameter of the pore formed by alamethicin. (He *et al.*, 1995, 1996) The difference in the diameters corresponds to the thickness of the alamethicin helix (~1.1 nm), that has been determined from the crystal structure. (Fox & Richards, 1982) The consistency of the pore formed has been further shown using ion-conductance experiments. The results of these experiments show that alamethicin induces single-channel conductance with multiple discrete states that is caused by the joining or leaving of one monomer to the aggregate. (Baumann & Mueller, 1974; Latorre & Alvarez, 1981; Mak & Webb, 1995)

With the barrel-stave pore being the first pore to be characterized, all subsequent pore forming peptides were thought to form a similar pore. However, studies into the pores formed by the AMP, magainin showed that another type of pore formation was possible: the toroidal pore. The toroidal pore is formed by almost all other pore forming AMPs such as magainin (Ludtke *et al.*, 1996; Matsuzaki, Nakamura, Murase, *et al.*, 1997), protegrin (Yang *et al.*, 2000) and melittin (Yang *et al.*, 2001). Unlike the barrel-stave pore, peptides do not dissociate from the lipid head group when transitioning from the S-state to the I-state. Instead, the peptide forces the membrane to bend inwards resulting in a pore. One indication that a second type of pore could be formed came in the comparison of the size of the pore formed by magainin and alamethicin. The pore formed by magainin was much larger and was highly variable in size. The thickness of the wall of the pore was also much larger than that of alamethicin, as detected by neutron scattering. (Ludtke *et al.*, 1996; Yang *et al.*, 1999) The number of monomers in each pore, based on oriented CD, similarly did not agree with the number of monomers observed for alamethicin pores. Based on the barrel-stave model, approximately 11 magainin monomers would be required to create a pore of that size and yet only 4-7 monomers are observed in each pore. (Ludtke *et al.*, 1996) It was also theorized that a barrel-stave pore of that size would be highly destabilized and experience shape deformation, and yet the pore formed by magainin did not exhibit these abnormalities. (Yang *et al.*, 2001) This resulted in the conclusion that magainin was forming a different type of pore than alamethicin.

Further evidence of a different pore was observed in fluorescent studies that showed magainin constantly attached to the polar head group, even when pores were formed. (Matsuzaki *et al.*, 1994) Finally, the difference in ability to crystallize the pores formed by magainin and alamethicin contributed to the conclusion that the two AMPs formed different types of pores. (Yang *et al.*, 2000) Yang *et al.* postulated that the difference in charge between magainin and alamethicin may

be causing the formation of different pores. Alamethicin, as one of the few almost neutral AMPs would not have to contend with a high Coulomb energy that could interfere with the aggregation of monomers in order to form a barrel-stave pore; whereas magainin, with a net charge of +5, may need the shielding provided by the lipid head groups in order to form a pore. (Yang *et al.*, 2001) Data shows that most pore-forming AMPs form toroidal pores that have the same characteristics as those formed by magainin. (Yang *et al.*, 2001)

AMPs have also been posited to disrupt membranes by the 'carpet' model. This model was initially proposed by Pouny *et al.* as the mechanism of action of dermaseptin S. In their studies, they labeled the N-terminal residue with a fluorescent dye and studied the effects on fluorescence in the presence of small unilamellar vesicles (SUVs). The results showed a blue shift upon the addition of SUVs with a subsequent release of entrapped calcein. (Pouny *et al.*, 1992) Furthermore, their studies showed that dermaseptin S demonstrated lower aggregation rates than alamethicin. Taken together, they felt the results pointed to a different mechanism of action than the typical pore formation. FTIR data has also been used to support the carpet model. Results from experiments done with an AMP showed that the peptide remained parallel to the membrane throughout membrane rupture leading to the conclusion that pore formation was not possible. (Oren *et al.*, 1999) The 'carpet' model posits carpeting of the cell membranes with the AMP, eventually resulting in the disruption of the curvature of the lipid bilayer. This model has been proposed for a few AMPs including cecropins, (Shai, 1999) and LL-37, a human AMP in the cathelicidin family (Oren *et al.*, 1999).

Despite the focus on AMP activity against cell membranes, there is growing evidence that these peptides may also have intracellular targets. Bierbaum and Sahl demonstrated that the lantibiotic Pep 5 reactivated the autolysin, N-acetylmuramoyl-L-alanine-amidase on bacterial cell walls that

is typically inhibited by lipoteichoic acids. (Bierbaum & Sahl, 1987) There is also evidence that some AMPs inhibit cell wall synthesis by preventing the maturation of peptidoglycan precursors into peptidoglycan. (Brötz *et al.*, 1998; Islam *et al.*, 2012) Another intracellular process that is frequently targeted by AMPs is cell filamentation. This process can be a result of either blocking of DNA replication or the inhibition of septum formation. (Salomón & Farías, 1992; Subbalakshmi & Sitaram, 1998) There is also evidence that some AMPs bind to DNA and that others interfere with the synthesis of DNA, RNA, and some proteins within the bacterial cell. (Yonezawa *et al.*, 1992; Patrzykat *et al.*, 2002; Brogden, 2005)

5.1.2 β-sheet antimicrobial peptides

While α-helical AMPs are well studied and derivatives of these peptides are frequently synthesized, less is known about the relationship between structure and activity of β-sheet AMPs. Most β-sheet AMPs retain their secondary structure through the presence of disulfide bridges formed between cysteine residues across the strand or through backbone cyclization. There is a lack of information on whether non-covalent stabilizations could prove to be just as useful as covalent stabilizations in maintaining the secondary structure of a β-sheet AMP and still preserve their antibacterial activity.

In order to examine if it is possible to improve the stability of naturally occurring β-hairpin AMPs with non-covalent stabilizations, I studied two peptides, tachyplesin I and gomesin. Tachyplesin I is a 17-amino acid peptide that was first extracted from the hemocyte of the horseshoe crab, *Tachypleus tridentatus*. (Nakamura *et al.*, 1988) NMR studies have shown that this peptide adopts an antiparallel β-sheet structure with two disulfide bridges and a four-residue β-turn. (Kawano *et al.*, 1990; Laederach *et al.*, 2002; Edwards *et al.*, 2016) The importance of the disulfide bridge in tachyplesin I has been examined in several studies with varying results. Replacement of the

cysteine resides with aromatic residues has been shown to result in completely linear peptides that lack AMP activity. (Rao, 1999) Contrary results were found by Ramamoorthy *et al.* Their study, involving the deletion of all four cysteine residues changed the hairpin register but did not adversely affect the AMP activity of the peptide. (Ramamoorthy *et al.*, 2006) Yet another study that prevented the formation of disulfide bridges by protecting the cysteine residue side chains with acetamidomethyl (Acm) groups reduced the ability of tachyplesin I to permeabilize membranes. (Matsuzaki, Yoneyama, Fujii, *et al.*, 1997) These conflicting results illustrate the lack of understanding of the importance of the β-hairpin structure of tachyplesin I, making it an ideal peptide for my studies.

Another interesting β-sheet AMP that is suitable for mutational analysis is gomesin, an 18-amino acid peptide first discovered in the hemocytes of the tarantula, *Aconthoscurria gomesiana.* (Silva *et al.*, 2000) Like tachyplesin I, gomesin forms two disulfide bridges and adopts an antiparallel β-sheet structure. (Mandard *et al.*, 2002) Mutation of the cysteine residues into serine residues, which results in a disordered peptide, proved to be catastrophic for the AMP activity of gomesin. The presence of at least one disulfide bridge, however, was enough to retain some AMP activity but the activity was much lower than that of the wild type. (Fázio *et al.*, 2006)

The lack of viable alternatives to disulfide bridges to stabilize β-sheet secondary structure is a common struggle in the design of β-sheet AMPs. Protegrin I, a naturally occurring AMP found in porcine leukocytes, has been extensively studied. The importance of the disulfide bridge was highlighted by studying the activity of the peptide with universal cysteine to alanine mutations. (Harwig *et al.*, 1996) The peptide, without disulfides, lacked any β-sheet secondary structure and did not show any activity but with just one of the two disulfide bridges, the protegrin-I mutant displayed similar activity to wild type. A contrary result was found when protegrin-I disulfide

bridge formation was prevented by reducing the cysteine residues or by protecting the cysteine residue side chains with Acm groups. Both mutants showed a more potent minimum inhibitory concentration against gram-negative bacteria. Coupled with ion conductance experiments to study the formation of pores by these peptides, the study concluded that the disulfide bridges were crucial for membrane permeabilization but may not be needed for AMP activity. (Mangoni *et al.*, 1996)

Tam *et al.* attempted to further investigate the importance of the disulfide bridge by making mutants of protegrin-I that involved side chain cyclization of the peptide as well as addition and removal of disulfide bonds. Their mutants showed improved activity against both gram-negative and gram-positive bacteria while showing decreased hemolytic activity. (Tam *et al.*, 2000) This study emphasized the possible correlation between peptide fold stability and AMP activity. Protegrin-I has also been grafted onto a template for backbone cyclization that makes use of the propensity of the $_{D}$-Pro-$_{L}$-Pro motif to form a hairpin turn. (Shankaramma *et al.*, 2002) Of the peptides studied, 7 mimetics emerged as having reasonable activity against gram-positive and gram-negative bacteria. One of the mimetics also demonstrated very low hemolytic activity which made it extremely suitable for follow-up mutational studies. (Robinson *et al.*, 2005) This mimetic seemed to be a suitable starting point for my own mutational studies, aimed at discovering if non-covalent stabilizations could prove equally effective at stabilizing the β-sheet structure while maintaining activity.

Finally, I studied another peptide that was designed based on a completely engineered AMP. Frecer *et al.* had demonstrated that many membrane binding peptides have a repeating motif of cationic-hydrophobic-polar amino acids. Their attempt at utilizing this motif to design a β-sheet peptide that binds membranes yielded a peptide with multiple valine and lysine residues along with cysteine residues that were necessary to ensure the β-hairpin conformation. (Frecer *et al.*,

2004) Utilizing this concept, Yu *et al.* designed a peptide with repeating units of phenylalanine and lysine that contained a short –GSG– loop in the middle to promote secondary structure. (Yu *et al.*, 2012) Some of the peptides they designed had low hemolytic activity and good AMP activity which led to a follow-up study where they mutated all the phenylalanine and lysine residues of their most potent AMP to tryptophan and arginine respectively. (Yu *et al.*, 2015) This yielded the peptide, I-RW which is a completely novel, unnatural AMP that is ripe for mutational studies to improve the stability of the peptide fold and to examine possible correlations between structural stability and activity.

5.2. Assay development

More detailed assay protocols are provided in Chapter 2.

E.coli assay development was simple due to the ease with which the bacteria is able to grow in LB broth. Maximum turbidity of cells was reached at approximately 20 hours of incubation with few precautions taken to ensure sterile conditions. *Corynebacerium glutamicum* (*C.glu)* however is known to have difficulties growing. My initial measurements showed that *C.glu* grew at half the rate of *E.coli* and required a much more sterile environment to avoid non-specific bacterial growth interference. Due to the increased incubation period needed to grow *C.glu* to a sufficiently high turbidity, evaporation of wells was a serious issue. The problem was resolved with the parafilming of 3 out of the 4 sides of the well plate as well as the aid of wells that were used as moisture barriers on the periphery of each plate. The wells that served as moisture barriers were topped up every 20 hours or so to ensure that wells containing the sample were free from evaporation.

5.3. Results and discussion

5.3.1. Gomesin and tachyplesin I

I began my studies by making small mutations to the wild-type sequence of tachyplesin I (TP1) and gomesin (see Tables 5.1 and 5.2 for sequences). This allowed for the determination of the effects of small changes on the structure of the peptide as well as on the activity of the peptide. As discussed in Chapter 1, the Trp/Trp edge-to-face interaction (EtF) can be employed to increase the association of β-strands in a hairpin peptide. (Anderson, Kier, *et al.*, 2016) For these two peptides, I studied the effect of Trp/Trp pairs at two different locations: immediately flanking the hairpin turn and at the ends of the peptide in the form of a β-cap. The simplest β-cap employs the use of a KW/WK or a KW/WR at the N- and C-terminus of the peptide. In studies done by other members of the lab, the RW/WE pair, which serves as the closest analog to the β-cap in question, increased the stabilization of a hairpin up to 6 kJ/mol. (Anderson *et al.*, 2014; Kier *et al.*, 2015)

Table 5.1. The table shows the sequence of gomesin and its mutants along with their activity against gram-negative, *E.coli* and gram-positive, *C.glu*. The mutations made to each peptide relative to gomesin is indicated in bold. The IC_{50} represents the concentration of peptide that results in approximately 50% bacterial growth (where 100% growth is taken to be the growth of bacteria in the absence of AMP). The MIC is the lowest concentration at which bacterial growth is undetectable. N.T. = not tested.

Peptide	Sequence	*E.coli*		*C.glu*	
		IC_{50} (μM)	MIC (μM)	IC_{50} (μM)	MIC (μM)
Gomesin	--ECRRLCYKQRCVTYCRGR-NH2	14.9	25	<0.006	0.195
Gommut 1	--ECRRL**W**YK**G**R**W**VTYCRGR-NH2	72	>100	N.T.	N.T.
Gommut 2	**KWI**CRRL**W**Y**RG**R**WI**TYCR**W**R	8.6	12.5	0.10	0.780

Since the goal of the study was to eliminate dependence on disulfides and introduce non-covalent stabilizations, I began my gomesin mutations by replacing the turn-flanking cysteine residues with a Trp/Trp pair. I also mutated the glutamine residue in the turn into a glycine residue in order to promote turn formation. The mutant, gommut-1, showed a strong exciton couplet by CD (with max at 228 nm), indicating a favorable Trp/Trp EtF interaction along with a high apparent melting temperature, pointing to high fold stability. However, this mutant had lost all of the activity of the native peptide *versus E.coli.* (Table 5.1) The NMR results (Appendix C2) showed that the strands of the mutant had an incomplete alignment, especially towards the ends of the peptide, which could be the reason why activity was lost.

In an effort to improve the structure, especially around the termini, gommut-2 was made with a small change to the turn (from YKGR to YRGR) and the addition of a β-cap to the termini. By NMR, the hairpin register was evident in the backbone-H_N of residues C4 to C17. Hydrogen bonding could be seen at residues R5, L7, I14 and Y16, with a strong CSD of 1.8 ppm being observed for residue I14 (Appendix C3). But by CD, the peptide showed a slightly lower exciton couplet magnitude than would be expected of a peptide with two Trp/Trp pairs. The smaller exciton couplet is most likely an indication of distortion of the hairpin structure and could be an indication that replacing a glutamic acid in the traditional β-cap with an arginine may not be enough to confer the stability that is typical of this non-covalent interaction. However, the addition of this cap improved the activity of the peptide significantly, going from an IC_{50} of 72 μM in gommut-1 to 8.6 μM in gommut-2. This decrease in IC_{50} indicated that gommut-2 had better biological activity than wild-type gomesin in *E.coli.* Unfortunately, I was unable to show similar results with the gram-positive bacterium, *C. glu.* In this system, the mutant had a 4-fold decrease in activity compared to gomesin. (Table 5.1)

Keeping the results from the gomesin mutations in mind, I tackled TP1 by first adding a β-cap to the peptide. As a control, I also synthesized a second mutant with all four cysteine residues replaced with valine residues, see Table 5.2.

Table 5.2. The table shows the sequence of tachyplesin and its mutants. The mutations made to each peptide relative to tachyplesin are indicated in bold. The bioassay results for *E. coli* are also given. The IC_{50} represents the concentration of peptide that results in approximately 50% bacterial growth. The MIC is the lowest concentration at which bacterial growth is undetected. *(Table adapted from* (Sivanesam, Kier, *et al.*, 2016)*)*

Peptide	Sequence	IC_{50} (μM)	MIC (μM)
Tachyplesin 1 (TP1)	– KW–CFRVCYRGICYRRCR–NH_2	2.03	3.1
Tachymut 1 (TM1)	– KW**W**CFRVCYRGICYRRCR–**WK**	> 100	> 100
Tachymut 2 (TM2)	– KW**WV**FRV**V**YRGI**V**YRR**V**R–**WK**	6.5	12.5
Tachymut 3 (TM3)	– KW**WV**FRV**V**Y**pR**I**V**YRR**V**R–**WK**	2.04	3.1
Tachymut 4 (TM4)	–(KW**W**VFRV**V**Y–**C**–I**V**YRR**V**R–**WK**)$_2$	> 100	> 100
Tachymut 5-ac (TM5-ac)	**Ac**–W**W**VFRV**V**Y**pR**I**V**YRR**V**R–**WTGPKK-**NH_2	>100	>100
Tachymut 5-bz (TM5-bz)	**Bz**–W**W**VFRV**V**Y**pR**I**V**YRR**V**R–**WTGPKK-**NH_2	12.4	25
Tachymut 5-py (TM5-py)	**Py**–W**W**VFRV**V**Y**pR**I**V**YRR**V**R–**WTGPKK-**NH_2	>100	>100
Tachymut 5-my (TM5-my)	**My**–W**W**VFRV**V**Y**pR**I**V**YRR**V**R–**WTGPKK-**NH_2	>100	>100
Tachymut 6 (TM6)	**Bz**–W**W**VFRV**V**Y**pR**I**V**Y**V**R**R**R–**WTGPKK-**NH_2	21.5	100

In a reversal of the results seen with gommut-2, the addition of the β-cap completely abolished activity and conferred solubility issues to tachymut 1 (TM1). However, the valine control, named tachymut-2 (TM2) showed a reasonable IC_{50}. NMR data showed that while TP1 demonstrated a

β-sheet CSD pattern (Appendix C6), this pattern was less pronounced in tachymut 1 (TM1) (Appendix C7) and almost completely absent in TM2 (Appendix C8).

With this result, I turned my attention to the turn of the peptide. In the following mutant, the turn was improved from a –YRGI– to –YpRI– turn. The presence of a D-Pro at the T1 position of a [2,4] turn has been shown to greatly improve hairpin turn propensity.(Haque *et al.*, 1994) NMR results confirmed that this held true for this peptide since the hairpin register that was not evident in TM2, was once again observed in the N-terminal strand of tachymut-3 (TM3) between residues 3 and 8. (Appendix C8 & C9) In Figure 5.3, the CSDs of backbone H_N for TM3 is compared to that of TP1. This comparison shows that the presence of the β-cap, KW/WK provides a significant amount of stabilization at the ends of TM3 that was previously not evident (increased positive CSD at position W19 and K20 indicates that these residues have a more rigid structure than the C-terminal residues in TP1).

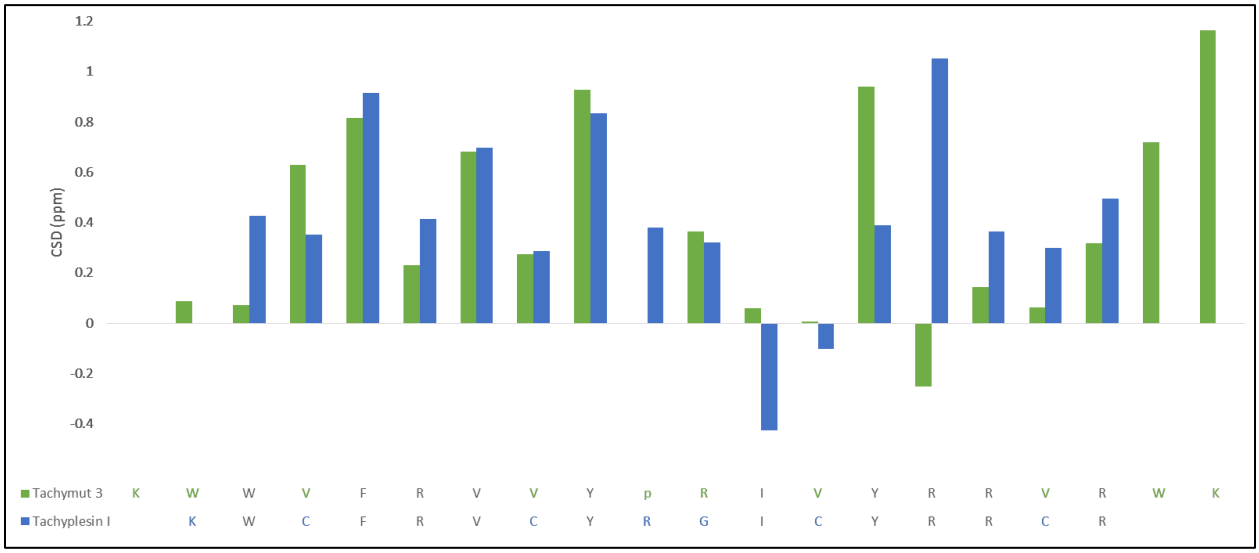

Figure 5.3. The graph depicts the CSDs of backbone H_N of TP1 and TM3.

The greater favorability of the hairpin turn is also evident in the approximately 0.6 ppm upfield shift experienced by Y14-H_N in TM3 as compared to TP1. The CD data (Appendix C15) also showed a large exciton couplet indicative of a strong EtF interaction between terminal tryptophans. Structurally, TM3 appears to adopt a similar fold as TP1 but without the aid of any covalent staples which is very encouraging. In terms of biological activity, TM3 had recovered all the activity of TP1, in both *E. coli* and *C. glu* systems, which demonstrates that the covalent stabilization is not necessary for activity. (Table 5.2 & 5.3) Instead, this data indicates that non-covalent interactions that stabilize hairpin fold, can be utilized to design effective AMPs.

Peptide	MIC (μM)
Tachyplesin I	0.195
Tachymut 3	0.195
Tachymut 5.1	No activity

Table 5.3. The table shows the results from the gram-positive assay of select peptides with *C. glu. (Table adapted from Sivanesam et al., 2016a)*

To test if the type of β-hairpin peptide mattered, I synthesized a variant of TP1 that did not have a hairpin turn. Instead, the peptide, tahcymut-4 (TM4) had a cysteine residue at the middle of the peptide that would form a dimer with a central cross-strand disulfide linkage. (Anderson *et al.*, 2014; Kier *et al.*, 2015) Along with the β-caps at the termini, these peptides form homodimeric-turnless β-sheets which proved to be more stable than TM3 by CD (Appendix C16), showing no signs of melting up to 65°C. Unfortunately, eliminating the β-turn abolished the peptide activity in *E. coli* pointing to a definite link between the presence of the hairpin turn and biological activity. (Table 5.2).

The next mutant, returned to the hairpin turn seen in TM3 and attempted to improve on the structure at the termini. For this, the simple KW/WK cap was replaced with a more hydrophobic version. (Kier *et al.*, 2010) The hydrophobic cap employed, Z-W/WTGXXX-NH_2, has an acyl

group at the N-terminus (see Chapter 1 for more details). For TM5, I used Z-W/WTGPKK-NH_2. This is because with the addition of this cap the N-terminal and C-terminal Lys residues would be removed. To avoid reducing the overall net charge by +2, two lysine residues were added to the C-terminal tail at a position where they were unlikely to play a role in the structure of the peptide. Since the positive charge of AMPs is known to play an important role in targeting bacteria, it is important to maintain the overall net charge of the peptide. As for the Z position, four different groups were used: acetyl- (from acetic anhydride), benzoyl- (from benzoic acid), myristyl- (from myristic acid) and pyrene carbonyl- (from pyrene carboxylic acid). Pyrene carboxylic acid is a polycyclic aromatic molecule made up of 4 benzene rings fused together while myristic acid is a carboxylic acid with a chain of 14 carbons. These adducts were chosen to study the effects of adding large hydrophobic groups to the AMPs and to determine if the presence of these adducts would increase the membrane binding affinity of the peptides.

The structural comparison of these peptides was complicated by the fact that TM5-ac had concentration dependent solubility issues that prevented any characterization by NMR. A CD comparison of all four Z-groups showed that the exciton couplet was severely diminished in TM5-ac and TM5-bz compared to TM3 (Appendix C15, C17 & C18). For TM5-py and TM5-my, the exciton couplet was not visible at all. Instead for TM5-py, minima at 204 nm and 241 nm were observed (Appendix C19) while the CD spectrum of TM5-my showed a strong minimum (220 nm) and maximum (200 nm) at high temperatures and three minima (193 nm, 208 nm, 218 nm) at low temperatures (Appendix C20). The CD data of TM5-py could be explained by the fluorescent character of pyrene. Typically, pyrene has been used to determine solvent environments since it is very sensitive to solvent polarity. This could be affecting the CD measurements to some degree. As for TM5-my, the CD spectra indicate that the peptide has a mixed random-coil and α-helix

structure at low temperatures. At high temperatures, however, these signals give way to what looks like a mixture of random-coil and β-sheet structures. For both peptides, the exciton couplet is so weak that all the other moieties in the peptide are overcoming the expected couplet signal by CD.

Interestingly, despite the identical sequence, only one of the four TM5 mutants, the one with the less hydrophobic and smaller benzoyl group, showed any activity against *E.coli* (Table 5.2). While we expected that the adducts would create a membrane-anchoring effect that would aid in initial binding, there is a possibility that they prevented the peptide from a) achieving the required orientation within the membrane or b) gaining access to intracellular targets. There are reports that adding fatty-acyl functional groups to known AMPs improved biological activity. (Chicharro *et al.*, 2001; Mak *et al.*, 2003; Lockwood *et al.*, 2004) However, these adducts were added to amphipathic α-helical peptides since acyl groups as N-caps are known to enhance helix formation. Since the peptides in the present study favor a β-sheet structure, the presence of an N-terminal modification that typically favors helix formation could be detrimental to structure and activity. This is shown by the slight helical character that can be detected in TM5-my by CD at low temperatures (see Appendix C20). The combination of α-helix and random-coil signatures by CD at low temperatures could be caused by the presence of the $_{D}$-Pro residue in the turn that causes a kink in a helix initiated by the N-acyl adduct. The remainder of the peptide from that point on would presumably assume a random-coil structure. It is worth noting that a benzoyl group at the N-terminus has been shown to favor helix formation to a greater extent than acetyl groups and yet, the presence of the benzoyl group in TM5-bz does not abolish biological activity. When comparing the biological activity of TM5-bz with TM3 and TP1, the data may point to a role being played by the specific location of lysine residues in TP1 since moving them to the C-terminus in TM5 results in dramatic loss of activity.

The final TP1 mutant synthesized was TM6. This mutant was meant to study the importance of residue positioning in TP1 by swapping a valine residue and an arginine residue in the C-terminus. The resulting peptide, which closely mimics TM5-bz showed a two-fold decrease in IC_{50} compared to TM5-bz. Once again, this result reaffirms the importance of specific locations of positively charged residues in TP1. However, this data appears to over-ride a hairpin stability effect. From Figure 5.4, it is clear that TM6 has a better, more populated, hairpin fold conformation. The switching of V16 (in TM5-bz) to position 14 in TM6 results in increased deshielding at this position as well as at the adjacent Y13 residue, possibly indicating stronger hydrogen bonding in this region of TM6. The β-cap also appears to be stronger in TM6 with a nearly 2-fold increase in the CSD of G20-H_N as well as W2-H_N. Overall, my studies conclude that while covalent stabilization is not necessary to maintain activity, there does not seem to be a direct correlation between hairpin stability and AMP activity.

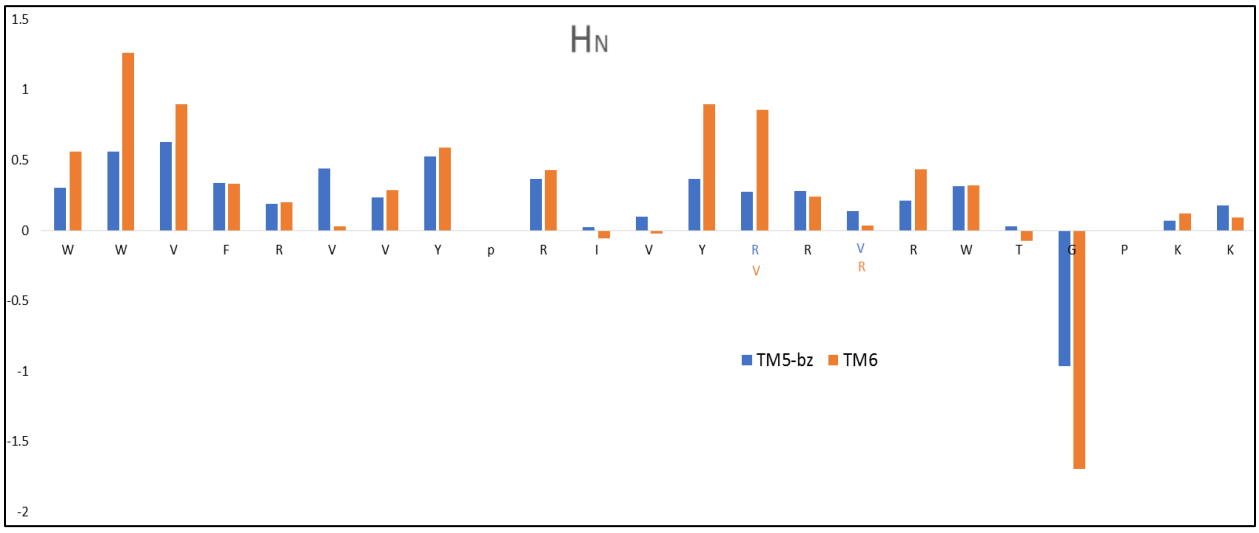

Figure 5.4. The graph depicts the CSDs of backbone H_N for TM5-bz and TM6 that only differ by the switching of positions of one valine and one arginine at position 14 and 16.

5.3.2. Acyclins

In a study conducted in 2000, Tam *et al.* showed that there was a correlation between peptide stability and antimicrobial activity for the naturally occurring AMP, protegrin I. (Tam *et al.*, 2000) This led to the design of a cyclization template that would allow for the constraining of protegrin I's β-hairpin conformation without the use of disulfide bridges. (Shankaramma *et al.*, 2002) However, this backbone cyclization poses the same problems as disulfide bridges: what if the lack of conformational freedom is limiting the activity of these peptides? From Shankaramma *et al.*'s study, mimetic 4, a cyclized analog of protegrin I, emerged as a potent antimicrobial that also had relatively low hemolytic activity. I set out to determine if non-covalent interactions could be used to stabilize the hairpin fold of mimetic 4 and if the increased conformational freedom did indeed affect antimicrobial activity.

Mimetic 4 had the following sequence: cyc(-LRLKKRRWKYRVpP-). I started my studies with an inverse variant of this sequence to study the effect of sequence inversion on activity. The first change that was made to the inverse sequence was the elimination of the $_{D}$-Pro-$_{L}$-Pro turn. In order to stabilize the termini, the hydrophobic β-cap, benzoyl-W/WTGXXX-NH_2 was added (where XXX represents residues added to the C-terminus in order to aid solubility and/or maintain the net charge of the mutants). The hydrophobic cap has been shown to provide almost 2 kJ/mol more fold stabilization than disulfide bridges, making it a highly stabilizing interaction. (Kier *et al.*, 2010) Some changes were also made to the residues within the strand (numbering based on sequence above): L1 → Y, L3 → V, ad V12 → I. These changes were made to improve the β-sheet fold of the strands. Without the aid of the backbone cyclization, the peptide sequence had no nucleating turn that would promote β-hairpin formation. In order to remedy this, the residues in the middle of the peptide, -WRRK- (in the non-inverse sequence above ^{5}KRRW^{8}) were changed

to -W-(D-R)-RK-. The presence of a D-amino acid followed by an L-amino acid has been shown to favor hairpin turn formation. (Anderson, Jurban, *et al.,* 2016) The presence of a favorable hairpin turn is important because turn nucleating sequences have been shown to increase the fold stability at adjacent residues. (Anderson, Kier, *et al.*, 2016) These mutations culminated in the synthesis of my first mutant, acyclin-1.

Table 5.4. The sequence of all the acyclin peptides and their bioactivities are shown. The mutations made to each peptide relative to acyclin-1 are indicated in bold. The IC_{50} represents the concentration of peptide that results in approximately 50% bacterial growth (where 100% growth represents the growth of bacteria in the absence of AMP). The MIC is the lowest concentration at which bacterial growth is undetected.

Peptide	Sequence	IC_{50} (μM)		MIC (μM)	
		E. coli	*C. glu*	*E. coli*	*C. glu*
Acyclin-1	Bz–WIRYK–WrRK–KVRYWTGP·–NH_2	15.85	0.06	25	0.781
Acyclin-2	Bz–WI**V**YK–WrRK–**V**VRYWTGKR–NH_2	40.00	0.03	> 100	0.049
Acyclin-3	Bz–WI**V**YK–W**p**RK–**V**VRYWTGKR–NH_2	43.50	0.04	100	0.195
Acyclin-4	Bz–WIRYK–W**p**RK–**V**VRYWTGP·–NH_2	>100	0.01	>100	0.024
Acyclin-5	Bz–WI**V**YK–W**p**RK–KVRYWTGP·–NH_2	95.00	0.13	>100	0.781
Acyclin-6	Bz–WIRYK–W**p**RK–KVRYWTGP·–NH_2	45.00	0.10	>100	0.781

The stability of acyclin-1 was examined by NMR (Figure 5.5A) and CD (Appendix C22). The CD data confirmed that an EtF interaction was occurring between the tryptophan residues nearest the peptide termini. However, NMR data showed that the hairpin fold was not fully populated, with CSDs not exceeding 0.5 ppm for residues within the strand. To improve the fold within the strand,

further mutations were made to increase the number of β-branched amino acids within the strand. The mutation of R3V and K10V however would result in a decrease in the net positive charge of the peptide, which could adversely affect the peptide's ability to bind to anionic membranes. To overcome this, the proline residue at the C-terminus was replaced with a lysine and an arginine. The addition of these residues would not adversely affect the β-cap but could be important for AMP activity. These minor changes conferred a significant increase in hairpin fold population of acyclin-2 as observed by NMR and CD (Figure 5.5 & Appendix C22, C23).

NMR showed significantly greater deshielding being experienced by the backbone-H_N's of strand residue sites of acyclin-2, as shown in Figure 5.5A. The data indicates that the turn is also well formed as can be seen by the increased shielding experienced by K9, which is predicted to be a part of the turn. By CD, the strength of acyclin-2's exciton couplet was almost double that of acyclin-1. Monitoring the molar ellipticity at 228 nm (the maximum observed in the presence of Trp/Trp exciton couplets by CD) showed that at the lowest temperature, 5°C, acyclin-2 was approaching maximum fold population while acyclin-1 was not (Figure 5.5B). This distinction can be made because the molar ellipticity of acyclin-2 does not change significantly between 5°C and 15°C, indicating that cooling cannot further increase the strength of the exciton couplet. However, at the same two temperatures, acyclin-1 demonstrates a trend that is still linear and has not reached a maximum plateau, indicating that the exciton couplet has not yet reached an optimal interaction.

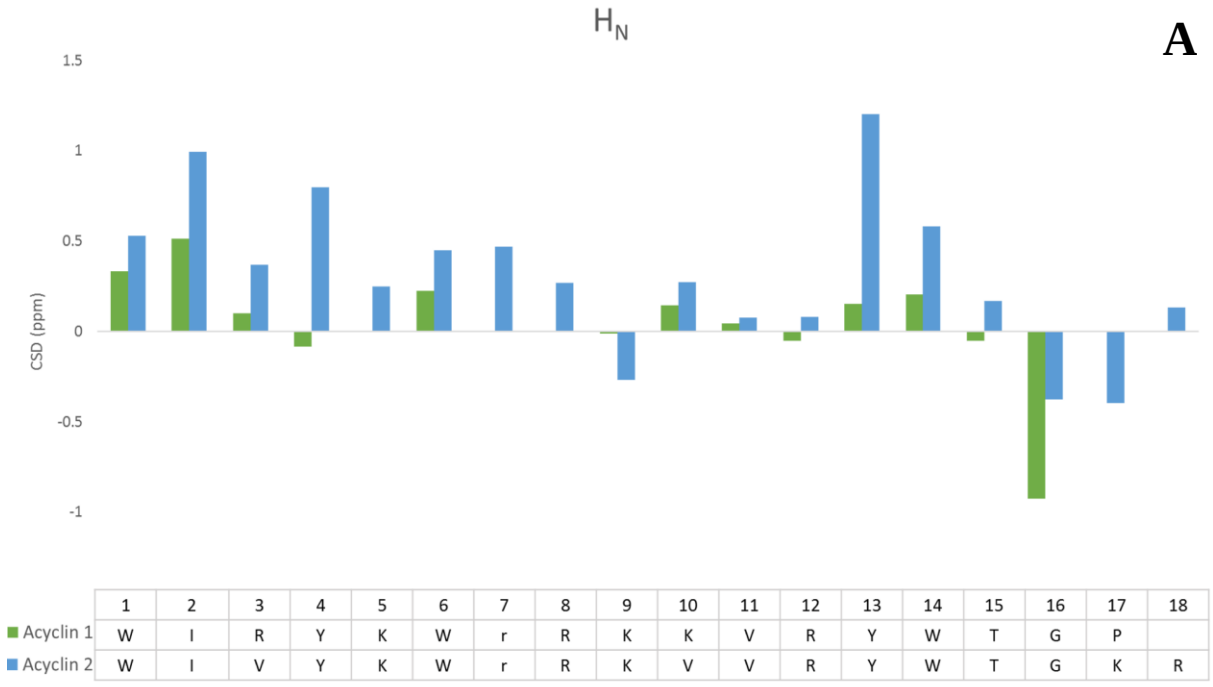

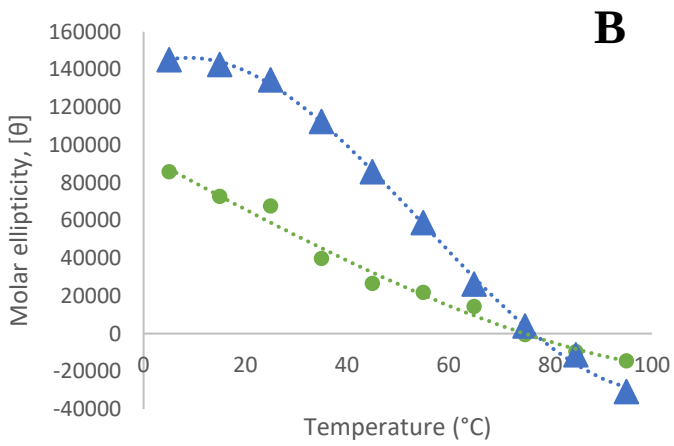

Figure 5.5. Panel A - A comparison of the chemical shift deviations of backbone H_N for acyclin-1 and -2. Panel B – The molar ellipticity of acyclin-1 (green) and acyclin-2 (blue) at 228 nm with increasing temperature. Third-degree polynomial trend line shown.

Nonetheless, there was still a lack of hairpin fold characteristics at the turn region. While having any $_D$-amino acid followed by an $_L$-amino acid can form a hairpin turn, there are definite benefits for having specific amino acids at each turn position (see Chapter 1.1.2). $_D$-Pro in particular at position T1 of a [2:4] turn has been shown to nucleate hairpin fold formation very effectively. This

knowledge led to the development of acyclin-3, which differed from acyclin-2 by one residue. The residues immediately flanking the $_{D}$-Pro most dramatically felt this change with CSDs increasing from 0.450 ppm to 0.799 ppm at W6. The β-hairpin register was also more pronounced at residue V11. CD data (Appendix C24), however, showed that the strength of the exciton couplet at low temperatures was unaffected by the change made at the middle of the peptide sequence. However, the exciton couplet did not melt as much as acyclin-2 as temperature was increased, indicating that the hairpin fold is more stable in the presence of the more favorable hairpin turn. The molar ellipticity change at 228 nm between 5°C and 95°C was 114,400 deg·cm^{2}·dmol^{-1} for acyclin-2 *versus* 108,300 deg·cm^{2}·dmol^{-1} for acyclin-3.

Antimicrobial assays were done with these three mutants to determine if this new design would have any AMP activity (Table 5.4). Acyclin-1 had an IC_{50} of 15.85 µM against *E. coli* and 0.06 µM against *C. glu.* Acyclin-2 and acyclin-3 unfortunately had a similar IC_{50} in *E.coli* as acyclin-1 which was contrary to the conclusions drawn by Tam *et al.* that correlated peptide stability and AMP activity. However, in the gram-positive *C. glu* system, acyclin-2 showed a smaller minimum inhibitory concentration (MIC) than acyclin-1 and acyclin-3. This discrepancy in MIC between acyclin-2 and -3 that differ only by one residue could be due to the fact that the replacement of a positive residue ($_{D}$-Arg) in acyclin-2 with a neutral residue ($_{D}$-Pro) in acyclin-3 resulted in the decrease of the net positive charge that was crucial to activity.

Considering the results of the gram-negative assay, I decided to determine if the positive residues that were moved to the C-terminus were in fact playing a key role in AMP activity at their initial position. To do that, I synthesized three peptides, acyclin-4 (with R3 returned), acyclin-5 (with K10 returned) and acyclin-6 (with both residues returned). For all 3 mutants, the C-terminus proline was returned. The NMR characterization data showed that acyclin-4 and acyclin-5 did not

show much difference in hairpin fold of the strands when compared to acyclin-3, except at positions 3 and 10. (Figure 5.6A) As expected, the presence of non-β-branched residues at these positions decreased the β-structure-diagnostic CSDs of the peptides. However, Figure 5.6A shows that the effect of the mutation was isolated to the specific positions and did not affect the hairpin fold of the adjacent residues.

But there were some downstream effects of the mutants on the G16-H_N CSDs with acyclin-5 showing a much higher CSD at this position than the previous mutants. This indicates that the β-cap was fully formed in this mutant but not in the others. CD data however showed that the removal of even one β-branched residue from the strand of the peptide yielded a dramatic decrease in the strength of the exciton couplet (Figure 5.6B, Appendix C24-C26), further highlighting the importance of strand association in increasing the β-cap interaction at the termini. Figure 5.6B also demonstrates that reducing strand association at either the N-terminus (acyclin-4) or the C-terminus (acyclin-5) affects the strength of the exciton couplet in a similar manner since both mutants have an approximately 50% decrease in molar ellipticity at 228 nm at 5°C compared to acyclin-3.

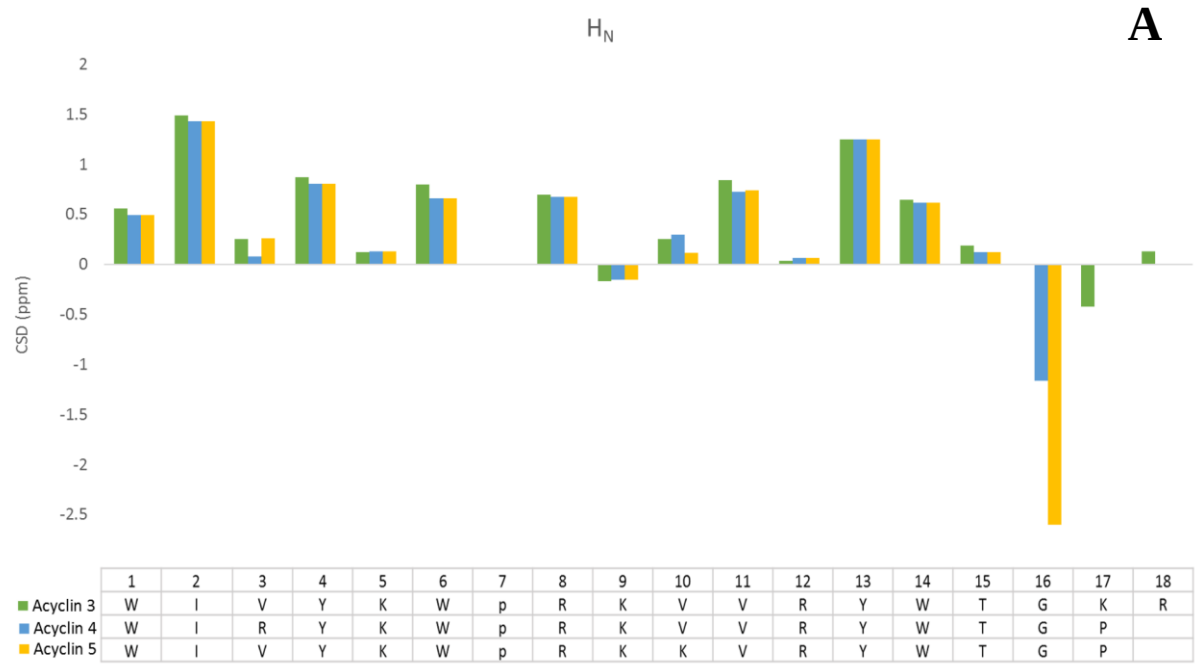

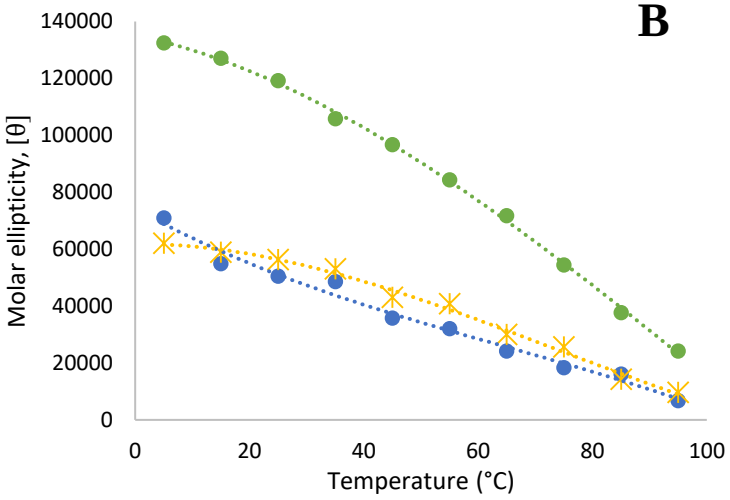

Figure 5.6. Panel A - A comparison of the chemical shift deviations of backbone H_N for acyclin-3, -4 and -5. Panel B – The molar ellipticity of acyclin -3 (green), -4 (blue) and -5 (yellow) at 228 nm with increasing temperature. Third-degree polynomial trend line shown.

Obtaining structural information by NMR for acyclin-6 proved to be challenging. The NMR resonances of this peptide were extremely broadened at low temperatures. This phenomenon could be due to the slow folding of the peptide or related to aggregation of the peptide in solution that, increases the tumbling time of the peptide which can result in peak broadening. Fortunately,

increasing the temperature of the solution provided better resolution allowing assignment. The comparison between acyclin-6 and acyclin-4 at 320 K showed that having both positive residues in the strand diminishes the β-stabilization afforded by even one β-branched valine residue. Figure 5.7 demonstrates that the effects of the mutations extend beyond the specific residue and result in a general decrease in CSD for most of the residues within the strand. The hairpin register is also less prominent with hydrogen bonded positions I2, Y4, W6, V11 and Y13 all showing decreased upfield shifts as compared to acyclin-4 indicating a weaker interaction.

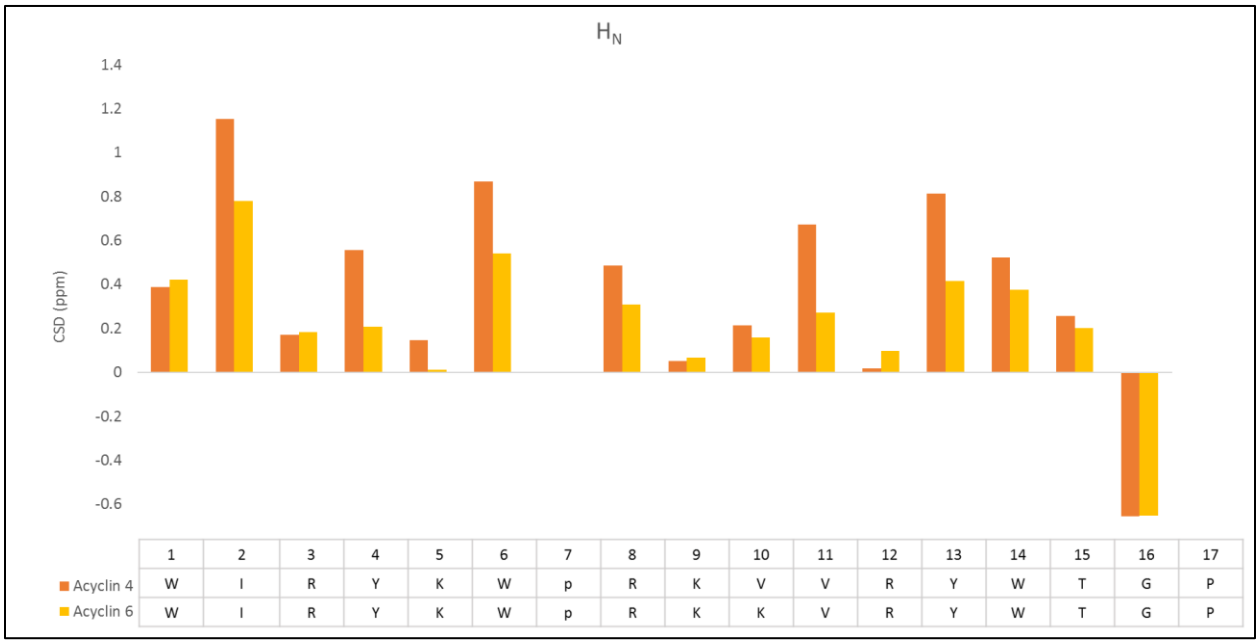

Figure 5.7. The graph depicts the comparison of the chemical shift deviations of backbone H_N for acyclin-4 and -6 at 320K.

My bioassay results proved to be even more interesting for the final three mutants (Table 5.4). In *E. coli*, acyclin-4 and acyclin-5 showed little to no AMP activity while acyclin-6 showed activity similar to that of acyclin-2 and acyclin-3. The fact that acyclin-6 differs from acyclin-1 by one residue and yet has a lower activity than acyclin-1 could point to the importance of that arginine

residue at the middle of the peptide and an overall importance of the net charge of the peptide. The lack of activity by acyclin-4 and acyclin-5 in *E. coli* conversely is hard to explain. The results would point to a major role being played by those two residues that is dependent on either having both or none of them in the strands of the peptide.

In *C. glu* however, acyclin-4 showed a high level of activity with an extremely low IC_{50} of 0.01 μM while acyclin-5 showed a much higher IC_{50} of 0.13 μM. This difference could point to an importance for having a cationic residue at position 3 but not at position 10 for gram-positive activity. On the other hand, acyclin-6 shows similar activity as acyclin-1 possibly indicating a lack of dependence on the presence of a positive residue at position 7. Taken together, the results indicate that while hairpin stabilization is possible, it does not correlate to AMP activity in the case of this peptide. Even more pertinent is the fact that the results from the gram-positive system do not always agree with the results from the gram- negative system.

5.3.3. Peptide system RW

The designing of a completely novel peptide that binds membranes was first proposed by Frecer *et al.* (Frecer *et al.*, 2004) and then co-opted by Yu *et al.* to synthesize a peptide that had activity as an AMP. After modifications and improvements, Yu *et al.* produced a peptide designated as I-RW that was capable of binding membranes as well as inhibiting the growth of bacteria at a level that is comparable to known AMP, polymyxin B. (Yu *et al.*, 2015) While this study focused on activity, there was no consideration given to the structure adopted by the peptide. Given that arginine and tryptophan residues are commonly used to stabilize the fold of β-hairpin peptides, I decided to attempt to optimize the fold of I-RW. NMR data of I-RW showed that there was no evidence of classic β-hairpin register indicating that the peptide was most likely not adopting a

specific conformation. (Figure 5.8) However CD data (Appendix C28) showed that the peptide had a small exciton couplet (131200 deg·cm^2·dmol^{-1} molar ellipticity at 228 nm), indicating that one or more pairs of tryptophans were in close proximity to one another. In order to encourage the formation of a hairpin turn, the residues at the center of the peptide -RGSG- were replaced with residues that are known to form a [3:5] hairpin turn, -NRRTG-. I also replaced both threonine residues with arginine and finally, the C-terminal arginine was replaced with a tyrosine. The pairing of RW/WY at the termini has been shown to be very favorable despite the lack of coulombic interaction typically responsible for the favorable RW/WE or KW/WE pairing. (see section 5.3.1)

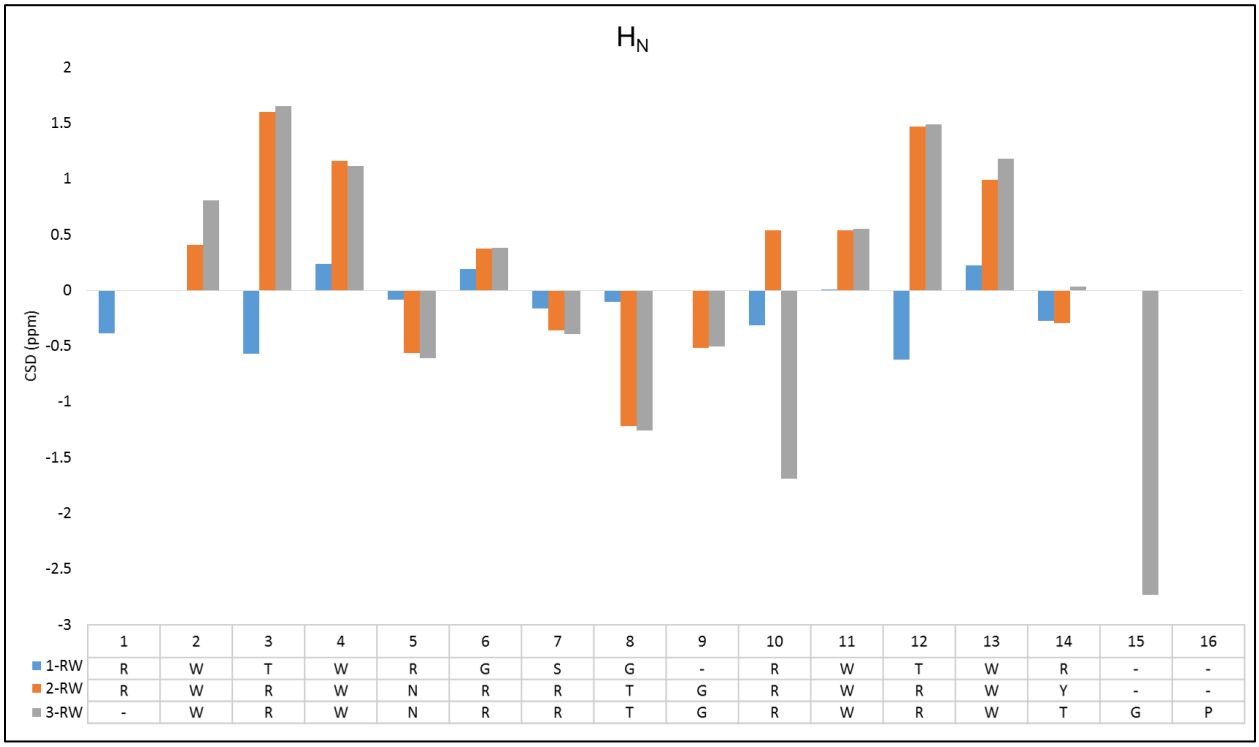

Figure 5.8. The graph depicts the CSD values for the backbone H_N of I-RW and its mutants.

This new mutant, termed 2-RW, had a strong exciton couplet by CD (Appendix C29). In figure 5.8, when compared to I-RW, 2-RW showed a prominent hairpin register throughout the peptide

with CSDs indicating that the –NRRTGR- turn was formed. Nonetheless there was still evidence of some terminal fraying at W13 and W2. This led to the synthesis of a second mutant that had the hydrophobic β-cap, benzoyl-W/WTGP-NH_2. NMR data, in Figure 5.8, shows that the new mutant, 3-RW did not have much higher stability in the strands compared to 2-RW but did show increased stability at both termini. CD data for both mutants showed a strong exciton couplet at 228 nm. (Appendix C29 & C30) Monitoring the melting of the maximum at 228 nm as temperature increased resulted in similar molar ellipticity values at all temperatures, indicating that both peptides had similar fold stability.

Table 5.5. The table shows the sequence of all the RW peptides as well as activity against *E.coli* and *C.glu*. The mutations made to each peptide relative to I-RW is indicated in bold. The IC_{50} represents the concentration of peptide that results in approximately 50% bacterial growth (where 100% growth is taken to be the growth of bacteria in the absence of AMP. The MIC is the lowest concentration at which bacterial growth is undetected.

Peptide	Sequence	IC_{50} (μM)		MIC (μM)	
		E. coli	*C. glu*	*E. coli*	*C. glu*
I-RW	Ac–RWTWRGS·GRWTWR–NH_2	12.2	0.05	25.0	0.781
2-RW	···RW**R**W**NRRT**GRW**R**W**Y**	7.8	N/A	12.5	N/A
3-RW	Bz–·W**R**W**NRRT**GRW**R**W**TGP**–NH_2	38.6	0.02	50.0	0.390

Biological data for I-RW and its mutants showed that there was little to no difference between the MIC of all 3 peptides in the *C. glu* system (Table 5.5). However, as evidenced in Figure 5.9, there is a difference in the activity of I-RW and 3-RW at concentrations below the MIC. In the gram-positive system, 3-RW showed a higher level of activity than I-RW at lower concentrations of

peptide. This may be related to the increased cationic character of 3-RW compared to I-RW. It could also be attributed to the increased β-sheet character of the mutant compared to I-RW. Unfortunately, solubility issues prevented the testing of peptide 2-RW against *C. glu*, which could have served as a way to determine if net charge or hairpin fold played a role in the slightly improved activity of 3-RW at low concentrations.

In *E. coli*, the three peptides showed similar MICs as well (Table 5.5). The IC_{50} of all three peptides however were different, indicating that 2-RW was the most active of the three at lower concentrations while 3-RW was the least active. The higher activity of 2-RW may be because it has more arginine residues than the other mutants. However, this explanation is doubtful since 3-RW, that has one more arginine residue than I-RW, has the highest IC_{50} of all three peptides. Taken together, the data indicates that increasing peptide secondary structure does not improve the activity of this designed peptide against *E. coli* significantly.

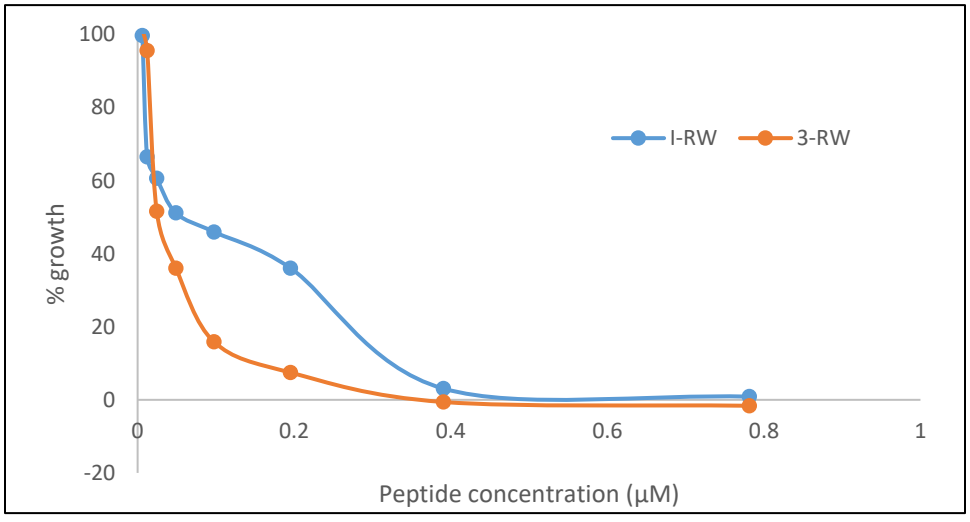

Figure 5.9. The graph depicts the growth of *C. glu* after 48 hours in the presence of increasing amounts of AMP.

5.4. Summary and Conclusion

In conclusion, my data has shown that there is not always a correlation between the structure of a peptide and its AMP activity. In the case of gomesin, increasing the hairpin fold did improve AMP activity but only against the gram- negative, *E. coli*. For the tachyplesin I series, I was able to synthesize a peptide that had no disulfide bridges but still retained the AMP activity of the native proving that non-covalent stabilizations can be used to stabilize the hairpin fold of peptides without sacrificing AMP activity. My studies with this system also showed that there is a dependence on the type of turn used to create the β-sheet conformation since a turnless homodimeric mutant was unable to inhibit the growth of *E. coli*. I also established that the addition of hydrophobic adducts could result in complete abolishment of activity possibly due to an anchoring effect that prevents the AMP from moving freely within the membrane to exert its effects. In this series, as well as the acyclin and RW series, my data confirmed that improving the hairpin fold does not guarantee an increase in activity. In fact, the results indicate that there are multiple factors that affect activity including the number of positively charged residues as well as the position of those residues within the strand.

My studies also showed that there is no guarantee that improved AMP activity against one species will translate to similar changes against another. Peptides that have strong activity against *E. coli*, i.e. gommut-2, may not have comparable activity against *C. glu*. This could be due to the difference in the membranes of the two types of bacteria. As a gram-negative bacterium, *E. coli* does not have the thick peptidoglycan layer that the gram-positive *C. glu* has. This difference may affect the binding of the AMP to the membrane. There is also the possibility that these AMPs have intracellular targets as well, and the different cell walls affect the ability of the peptide to enter the

cytoplasm. Unfortunately, without further examination of more strains of bacteria, it is difficult to determine if the effects observed here are due to the cell wall or if it is due to the specific bacterium.

Bibliography

Abedini, A., Meng, F., & Raleigh, D.P. (2007) A Single-Point Mutation Converts the Highly Amyloidogenic Human Islet Amyloid Polypeptide into a Potent Fibrillization Inhibitor. *J. Am. Chem. Soc.*, **129**, 11300–11301.

Abedini, A. & Raleigh, D.P. (2005) Incorporation of pseudoproline derivatives allows the facile synthesis of human IAPP, a highly amyloidogenic and aggregation-prone polypeptide. *Org. Lett.*, **7**, 693–696.

Abedini, A. & Raleigh, D.P. (2009) A Role For Helical Intermediates in Amyloid Formation By Natively Unfolded Polypeptides? *Phys Biol*, **6**, 015005.

Adessi, C., Frossard, M.-J., Boissard, C., Fraga, S., Bieler, S., Ruckle, T., Vilbois, F., Robinson, S.M., Mutter, M., Banks, W.A., & Soto, C. (2003) Pharmacological Profiles of Peptide Drug Candidates for the Treatment of Alzheimer's Disease. *J. Biol. Chem.*, **278**, 13905–13911.

Aitken, J.F., Loomes, K.M., Konarkowska, B., & Cooper, G.J.S. (2003) Suppression by polycyclic compounds of the conversion of human amylin into insoluble amyloid. *Biochem. J.*, **374**, 779–784.

Aitken, J.F., Loomes, K.M., Scott, D.W., Reddy, S., Phillips, A.R.J., Prijic, G., Fernando, C., Zhang, S., Broadhurst, R., L'Huillier, P., & Cooper, G.J.S. (2010) Tetracycline treatment retards the onset and slows the progression of diabetes in human amylin/islet amyloid polypeptide transgenic mice. *Diabetes*, **59**, 161–171.

Akesson, B., Panagiotidis, G., Westermark, P., & Lundquist, I. (2003) Islet amyloid polypeptide inhibits glucagon release and exerts a dual action on insulin release from isolated islets. *Regul. Pept.*, **111**, 55–60.

Alanis, A.J. (2005) Resistance to Antibiotics: Are We in the Post-Antibiotic Era? *Archives of Medical Research*, Infectious Diseases: Revisiting Past Problems and Addressing Future ChallengesInfectious Diseases: Revisiting Past Problems and Addressing Future Challenges, **36**, 697–705.

Albani, D., Polito, L., Batelli, S., De Mauro, S., Fracasso, C., Martelli, G., Colombo, L., Manzoni, C., Salmona, M., Caccia, S., Negro, A., & Forloni, G. (2009) The SIRT1 activator resveratrol protects SK-N-BE cells from oxidative stress and against toxicity caused by α-synuclein or amyloid-β (1-42) peptide. *Journal of Neurochemistry*, **110**, 1445–1456.

Andersen, N.H., Olsen, K.A., Fesinmeyer, R.M., Tan, X., Hudson, F.M., Eidenschink, L.A., & Farazi, S.R. (2006) Minimization and Optimization of Designed β-Hairpin Folds. *J. Am. Chem. Soc.*, **128**, 6101–6110.

Andersen, N.H. & Tong, H. (1997) Empirical parameterization of a model for predicting peptide helix/coil equilibrium populations. *Protein Science*, **6**, 1920–1936.

Anderson, J.M., Jurban, B., Huggins, K.N.L., Shcherbakov, A.A., Shu, I., Kier, B., & Andersen, N.H. (2016) Nascent Hairpins in Proteins: Identifying Turn Loci and Quantitating Turn Contributions to Hairpin Stability. *Biochemistry*,.

Anderson, J.M., Kier, B.L., Jurban, B., Byrne, A., Shu, I., Eidenschink, L.A., Shcherbakov, A.A., Hudson, M., Fesinmeyer, R.M., & Andersen, N.H. (2016) Aryl–aryl interactions in designed peptide folds: Spectroscopic characteristics and optimal placement for structure stabilization. *Biopolymers*, **105**, 337–356.

Anderson, J.M., Kier, B.L., Shcherbakov, A.A., & Andersen, N.H. (2014) An improved capping unit for stabilizing the ends of associated β-strands. *FEBS Letters*, **588**, 4749–4753.

Anderson, J.P., Walker, D.E., Goldstein, J.M., de Laat, R., Banducci, K., Caccavello, R.J., Barbour, R., Huang, J., Kling, K., Lee, M., Diep, L., Keim, P.S., Shen, X., Chataway, T., Schlossmacher, M.G., Seubert, P., Schenk, D., Sinha, S., Gai, W.P., & Chilcote, T.J. (2006) Phosphorylation of Ser-129 Is the Dominant Pathological Modification of -Synuclein in Familial and Sporadic Lewy Body Disease. *J. Biol. Chem.*, **281**, 29739–29752.

Anguiano, M., Nowak, R.J., & Lansbury, P.T. (2002) Protofibrillar islet amyloid polypeptide permeabilizes synthetic vesicles by a pore-like mechanism that may be relevant to type II diabetes. *Biochemistry*, **41**, 11338–11343.

Appel-Cresswell, S., Vilarino-Guell, C., Encarnacion, M., Sherman, H., Yu, I., Shah, B., Weir, D., Thompson, C., Szu-Tu, C., Trinh, J., Aasly, J.O., Rajput, A., Rajput, A.H., Jon Stoessl, A., & Farrer, M.J. (2013) Alpha-synuclein p.H50Q, a novel pathogenic mutation for Parkinson's disease. *Mov. Disord.*, **28**, 811–813.

Ardah, M.T., Paleologou, K.E., Lv, G., Abul Khair, S.B., Kazim, A.S., Minhas, S.T., Al-Tel, T.H., Al-Hayani, A.A., Haque, M.E., Eliezer, D., & El-Agnaf, O.M.A. (2014) Structure activity relationship of phenolic acid inhibitors of α-synuclein fibril formation and toxicity. *Front Aging Neurosci*, **6**.

Azriel, R. & Gazit, E. (2001) Analysis of the minimal amyloid-forming fragment of the islet amyloid polypeptide. An experimental support for the key role of the phenylalanine residue in amyloid formation. *J. Biol. Chem.*, **276**, 34156–34161.

Bae, E.-J., Lee, H.-J., Rockenstein, E., Ho, D.-H., Park, E.-B., Yang, N.-Y., Desplats, P., Masliah, E., & Lee, S.-J. (2012) Antibody-Aided Clearance of Extracellular α-Synuclein Prevents Cell-to-Cell Aggregate Transmission. *J. Neurosci.*, **32**, 13454–13469.

Bahar, A.A. & Ren, D. (2013) Antimicrobial Peptides. *Pharmaceuticals (Basel)*, **6**, 1543–1575.

Bai, J.Z., Saafi, E.L., Zhang, S., & Cooper, G.J. (1999) Role of Ca2+ in apoptosis evoked by human amylin in pancreatic islet beta-cells. *Biochem. J.*, **343 Pt 1**, 53–61.

Bai, Y. (2003) Hidden intermediates and levinthal paradox in the folding of small proteins. *Biochem. Biophys. Res. Commun.*, **305**, 785–788.

Banerjee, V., Kar, R.K., Datta, A., Parthasarathi, K., Chatterjee, S., Das, K.P., & Bhunia, A. (2013) Use of a Small Peptide Fragment as an Inhibitor of Insulin Fibrillation Process: A Study by High and Low Resolution Spectroscopy. *PLOS ONE*, **8**, e72318.

Baumann, G. & Mueller, P. (1974) A molecular model of membrane excitability. *J. Supramol. Struct.*, **2**, 538–557.

Bernadó, P., Bertoncini, C.W., Griesinger, C., Zweckstetter, M., & Blackledge, M. (2005) Defining long-range order and local disorder in native alpha-synuclein using residual dipolar couplings. *J. Am. Chem. Soc.*, **127**, 17968–17969.

Bertoncini, C.W., Jung, Y.-S., Fernandez, C.O., Hoyer, W., Griesinger, C., Jovin, T.M., & Zweckstetter, M. (2005) Release of long-range tertiary interactions potentiates aggregation of natively unstructured alpha-synuclein. *Proc. Natl. Acad. Sci.U.S.A.*, **102**, 1430–1435.

Bierbaum, G. & Sahl, H.G. (1987) Autolytic system of Staphylococcus simulans 22: influence of cationic peptides on activity of N-acetylmuramoyl-L-alanine amidase. *J. Bacteriol.*, **169**, 5452–5458.

Bieschke, J., Russ, J., Friedrich, R.P., Ehrnhoefer, D.E., Wobst, H., Neugebauer, K., & Wanker, E.E. (2010) EGCG remodels mature alpha-synuclein and amyloid-beta fibrils and reduces cellular toxicity. *Proc. Natl. Acad. Sci. U.S.A.*, **107**, 7710–7715.

Bisaglia, M., Schievano, E., Caporale, A., Peggion, E., & Mammi, S. (2006) The 11-mer repeats of human α-synuclein in vesicle interactions and lipid composition discrimination: A cooperative role. *Biopolymers*, **84**, 310–316.

Bisaglia, M., Tessari, I., Pinato, L., Bellanda, M., Giraudo, S., Fasano, M., Bergantino, E., Bubacco, L., & Mammi, S. (2005) A topological model of the interaction between alpha-synuclein and sodium dodecyl sulfate micelles. *Biochemistry*, **44**, 329–339.

Blair, J.M.A., Webber, M.A., Baylay, A.J., Ogbolu, D.O., & Piddock, L.J.V. (2015) Molecular mechanisms of antibiotic resistance. *Nat Rev Micro*, **13**, 42–51.

Blanchet, J., Longpré, F., Bureau, G., Morissette, M., DiPaolo, T., Bronchti, G., & Martinoli, M.-G. (2008) Resveratrol, a red wine polyphenol, protects dopaminergic neurons in MPTP-treated mice. *Progress in Neuro-Psychopharmacology and Biological Psychiatry*, **32**, 1243–1250.

Blanco, F.J., Rivas, G., & Serrano, L. (1994) A short linear peptide that folds into a native stable beta-hairpin in aqueous solution. *Nat. Struct. Biol.*, **1**, 584–590.

Bodles, A.M., El-Agnaf, O.M.A., Greer, B., Guthrie, D.J.S., & Irvine, G.B. (2004) Inhibition of fibril formation and toxicity of a fragment of alpha-synuclein by an N-methylated peptide analogue. *Neurosci. Lett.*, **359**, 89–93.

Bodles, A.M., Guthrie, D.J.S., Greer, B., & Irvine, G.B. (2001) Identification of the region of non-Aβ component (NAC) of Alzheimer's disease amyloid responsible for its aggregation and toxicity. *Journal of Neurochemistry*, **78**, 384–395.

Bodles, A.M., Guthrie, D.J.S., Harriott, P., Campbell, P., & Irvine, G.B. (2000) Toxicity of non-Aβ component of Alzheimer's disease amyloid, and N-terminal fragments thereof, correlates to formation of β-sheet structure and fibrils. *European Journal of Biochemistry*, **267**, 2186–2194.

Bodner, C.R., Dobson, C.M., & Bax, A. (2009) Multiple tight phospholipid-binding modes of alpha-synuclein revealed by solution NMR spectroscopy. *J. Mol. Biol.*, **390**, 775–790.

Bodner, C.R., Maltsev, A.S., Dobson, C.M., & Bax, A. (2010) Differential phospholipid binding of alpha-synuclein variants implicated in Parkinson's disease revealed by solution NMR spectroscopy. *Biochemistry*, **49**, 862–871.

Borghi, R., Marchese, R., Negro, A., Marinelli, L., Forloni, G., Zaccheo, D., Abbruzzese, G., & Tabaton, M. (2000) Full length α-synuclein is present in cerebrospinal fluid from Parkinson's disease and normal subjects. *Neuroscience Letters*, **287**, 65–67.

Brasnyó, P., Molnár, G.A., Mohás, M., Markó, L., Laczy, B., Cseh, J., Mikolás, E., Szijártó, I.A., Mérei, A., Halmai, R., Mészáros, L.G., Sümegi, B., & Wittmann, I. (2011) Resveratrol improves insulin sensitivity, reduces oxidative stress and activates the Akt pathway in type 2 diabetic patients. *Br. J. Nutr.*, **106**, 383–389.

Brender, J.R., Lee, E.L., Cavitt, M.A., Gafni, A., Steel, D.G., & Ramamoorthy, A. (2008) Amyloid Fiber Formation and Membrane Disruption are Separate Processes Localized in Two Distinct Regions of IAPP, the Type-2-Diabetes-Related Peptide. *J. Am. Chem. Soc.*, **130**, 6424–6429.

Brogden, K.A. (2005) Antimicrobial peptides: pore formers or metabolic inhibitors in bacteria? *Nat Rev Micro*, **3**, 238–250.

Brötz, H., Bierbaum, G., Leopold, K., Reynolds, P.E., & Sahl, H.G. (1998) The lantibiotic mersacidin inhibits peptidoglycan synthesis by targeting lipid II. *Antimicrob. Agents Chemother.*, **42**, 154–160.

Burré, J., Sharma, M., Tsetsenis, T., Buchman, V., Etherton, M.R., & Südhof, T.C. (2010) Alpha-synuclein promotes SNARE-complex assembly in vivo and in vitro. *Science*, **329**, 1663–1667.

Cabaleiro-Lago, C., Lynch, I., Dawson, K.A., & Linse, S. (2010) Inhibition of IAPP and IAPP(20−29) Fibrillation by Polymeric Nanoparticles. *Langmuir*, **26**, 3453–3461.

Cao, P., Abedini, A., Wang, H., Tu, L.-H., Zhang, X., Schmidt, A.M., & Raleigh, D.P. (2013) Islet amyloid polypeptide toxicity and membrane interactions. *Proc. Natl. Acad. Sci. U.S.A.*, **110**, 19279–19284.

Cao, P., Meng, F., Abedini, A., & Raleigh, D.P. (2010) The Ability of Rodent Islet Amyloid Polypeptide To Inhibit Amyloid Formation by Human Islet Amyloid Polypeptide Has Important Implications for the Mechanism of Amyloid Formation and the Design of Inhibitors. *Biochemistry*, **49**, 872–881.

Cao, P. & Raleigh, D.P. (2012) Analysis of the Inhibition and Remodeling of Islet Amyloid Polypeptide Amyloid Fibers by Flavanols. *Biochemistry*, **51**, 2670–2683.

Caruana, M., Högen, T., Levin, J., Hillmer, A., Giese, A., & Vassallo, N. (2011) Inhibition and disaggregation of α-synuclein oligomers by natural polyphenolic compounds. *FEBS Letters*, **585**, 1113–1120.

Celej, M.S., Sarroukh, R., Goormaghtigh, E., Fidelio, G.D., Ruysschaert, J.-M., & Raussens, V. (2012) Toxic prefibrillar α-synuclein amyloid oligomers adopt a distinctive antiparallel β-sheet structure. *Biochem. J.*, **443**, 719–726.

Chandra, S., Chen, X., Rizo, J., Jahn, R., & Südhof, T.C. (2003) A broken alpha -helix in folded alpha -Synuclein. *J. Biol. Chem.*, **278**, 15313–15318.

Chantry, A., Leighton, B., & Day, A.J. (1991) Cross-reactivity of amylin with calcitonin-gene-related peptide binding sites in rat liver and skeletal muscle membranes. *Biochem. J.*, **277 (Pt 1)**, 139–143.

Chartier-Harlin, M.-C., Kachergus, J., Roumier, C., Mouroux, V., Douay, X., Lincoln, S., Levecque, C., Larvor, L., Andrieux, J., Hulihan, M., Waucquier, N., Defebvre, L., Amouyel, P., Farrer, M., & Destée, A. (2004) α-synuclein locus duplication as a cause of familial Parkinson's disease. *The Lancet*, **364**, 1167–1169.

Cheung, Z.H. & Ip, N.Y. (2009) The emerging role of autophagy in Parkinson's disease. *Mol Brain*, **2**, 29.

Chicharro, C., Granata, C., Lozano, R., Andreu, D., & Rivas, L. (2001) N-Terminal Fatty Acid Substitution Increases the Leishmanicidal Activity of CA(1-7)M(2-9), a Cecropin-Melittin Hybrid Peptide. *Antimicrob. Agents Chemother.*, **45**, 2441–2449.

Chiu, C., Singh, S., & de Pablo, J.J. (2013) Effect of Proline Mutations on the Monomer Conformations of Amylin. *Biophys J*, **105**, 1227–1235.

Choi, W., Zibaee, S., Jakes, R., Serpell, L.C., Davletov, B., Crowther, R.A., & Goedert, M. (2004) Mutation E46K increases phospholipid binding and assembly into filaments of human alpha-synuclein. *FEBS Lett.*, **576**, 363–368.

Conway, K.A., Harper, J.D., & Lansbury, P.T. (1998) Accelerated in vitro fibril formation by a mutant α-synuclein linked to early-onset Parkinson disease. *Nat Med*, **4**, 1318–1320.

Conway, K.A., Harper, J.D., & Lansbury, P.T., Jr (2000) Fibrils formed in vitro from alpha-synuclein and two mutant forms linked to Parkinson's disease are typical amyloid. *Biochemistry*, **39**, 2552–2563.

Conway, K.A., Lee, S.J., Rochet, J.C., Ding, T.T., Williamson, R.E., & Lansbury, P.T. (2000) Acceleration of oligomerization, not fibrillization, is a shared property of both alpha-synuclein mutations linked to early-onset Parkinson's disease: implications for pathogenesis and therapy. *Proc. Natl. Acad. Sci. U.S.A.*, **97**, 571–576.

Cooper, G.J. (1994) Amylin compared with calcitonin gene-related peptide: structure, biology, and relevance to metabolic disease. *Endocr. Rev.*, **15**, 163–201.

Cooper, G.J., Leighton, B., Dimitriadis, G.D., Parry-Billings, M., Kowalchuk, J.M., Howland, K., Rothbard, J.B., Willis, A.C., & Reid, K.B. (1988) Amylin found in amyloid deposits in human type 2 diabetes mellitus may be a hormone that regulates glycogen metabolism in skeletal muscle. *Proc. Natl. Acad. Sci. U.S.A.*, **85**, 7763–7766.

Cooper, G.J., Willis, A.C., Clark, A., Turner, R.C., Sim, R.B., & Reid, K.B. (1987) Purification and characterization of a peptide from amyloid-rich pancreases of type 2 diabetic patients. *Proc. Natl. Acad. Sci. U.S.A.*, **84**, 8628–8632.

Cort, J.R., Liu, Z., Lee, G.M., Huggins, K.N.L., Janes, S., Prickett, K., & Andersen, N.H. (2009) Solution state structures of human pancreatic amylin and pramlintide. *Protein Eng Des Sel*, **22**, 497–513.

Culvenor, J.G., McLean, C.A., Cutt, S., Campbell, B.C.V., Maher, F., Jäkälä, P., Hartmann, T., Beyreuther, K., Masters, C.L., & Li, Q.-X. (1999) Non-Aβ Component of Alzheimer's Disease Amyloid (NAC) Revisited. *Am J Pathol*, **155**, 1173–1181.

da Silva, D.C., Fontes, G.N., Erthal, L.C.S., & Lima, L.M.T.R. (2016) Amyloidogenesis of the amylin analogue pramlintide. *Biophys. Chem.*, **219**, 1–8.

DaRocha-Souto, B., Scotton, T.C., Coma, M., Serrano-Pozo, A., Hashimoto, T., Serenó, L., Rodríguez, M., Sánchez, B., Hyman, B.T., & Gómez-Isla, T. (2011) Brain Oligomeric β-Amyloid but Not Total Amyloid Plaque Burden Correlates With Neuronal Loss and

Astrocyte Inflammatory Response in Amyloid Precursor Protein/Tau Transgenic Mice. *J Neuropathol Exp Neurol*, **70**, 360–376.

Davies, J. & Davies, D. (2010) Origins and evolution of antibiotic resistance. *Microbiol. Mol. Biol. Rev.*, **74**, 417–433.

De Smet, K. & Contreras, R. (2005) Human antimicrobial peptides: defensins, cathelicidins and histatins. *Biotechnol. Lett.*, **27**, 1337–1347.

Dedmon, M.M., Lindorff-Larsen, K., Christodoulou, J., Vendruscolo, M., & Dobson, C.M. (2005) Mapping long-range interactions in alpha-synuclein using spin-label NMR and ensemble molecular dynamics simulations. *J. Am. Chem. Soc.*, **127**, 476–477.

Dégano, P., Silvestre, R.A., Salas, M., Peiró, E., & Marco, J. (1993) Amylin inhibits glucose-induced insulin secretion in a dose-dependent manner. Study in the perfused rat pancreas. *Regul. Pept.*, **43**, 91–96.

Desplats, P., Lee, H.-J., Bae, E.-J., Patrick, C., Rockenstein, E., Crews, L., Spencer, B., Masliah, E., & Lee, S.-J. (2009) Inclusion formation and neuronal cell death through neuron-to-neuron transmission of α-synuclein. *Proc. Natl. Acad. Sci. U. S. A.*, **106**, 13010–13015.

Dill, K.A. & Chan, H.S. (1997) From Levinthal to pathways to funnels. *Nat Struct Mol Biol*, **4**, 10–19.

Dobson, C.M. (2003) Protein folding and misfolding. *Nature*, **426**, 884–890.

Dubos, R.J. (1939) STUDIES ON A BACTERICIDAL AGENT EXTRACTED FROM A SOIL BACILLUS. *J Exp Med*, **70**, 1–10.

Dupuis, N.F., Wu, C., Shea, J.-E., & Bowers, M.T. (2011) The Amyloid Formation Mechanism in Human IAPP: Dimers Have β-Strand Monomer−Monomer Interfaces. *J. Am. Chem. Soc.*, **133**, 7240–7243.

Ebrahimi, A. & Schluesener, H. (2012) Natural polyphenols against neurodegenerative disorders: potentials and pitfalls. *Ageing Res. Rev.*, **11**, 329–345.

Edwards, I.A., Elliott, A.G., Kavanagh, A.M., Zuegg, J., Blaskovich, M.A.T., & Cooper, M.A. (2016) Contribution of Amphipathicity and Hydrophobicity to the Antimicrobial Activity and Cytotoxicity of β-Hairpin Peptides. *ACS Infect Dis*, **2**, 442–450.

Ehrlich, J.C. & Ratner, I.M. (1961) Amyloidosis of the Islets of Langerhans. *Am J Pathol*, **38**, 49–59.

Ehrnhoefer, D.E., Bieschke, J., Boeddrich, A., Herbst, M., Masino, L., Lurz, R., Engemann, S., Pastore, A., & Wanker, E.E. (2008) EGCG redirects amyloidogenic polypeptides into unstructured, off-pathway oligomers. *Nat. Struct. Mol. Biol.*, **15**, 558–566.

Eidenschink, L., Kier, B.L., Huggins, K.N.L., & Andersen, N.H. (2009) Very short peptides with stable folds: Building on the interrelationship of Trp/Trp, Trp/cation, and Trp/backbone–amide interaction geometries. *Proteins*, **75**, 308–322.

El-Agnaf, O.M.A., Paleologou, K.E., Greer, B., Abogrein, A.M., King, J.E., Salem, S.A., Fullwood, N.J., Benson, F.E., Hewitt, R., Ford, K.J., Martin, F.L., Harriott, P., Cookson, M.R., & Allsop, D. (2004) A strategy for designing inhibitors of alpha-synuclein aggregation and toxicity as a novel treatment for Parkinson's disease and related disorders. *FASEB J.*, **18**, 1315–1317.

El-Agnaf, O.M.A., Salem, S.A., Paleologou, K.E., Cooper, L.J., Fullwood, N.J., Gibson, M.J., Curran, M.D., Court, J.A., Mann, D.M.A., Ikeda, S.-I., Cookson, M.R., Hardy, J., & Allsop, D. (2003) α-Synuclein implicated in Parkinson's disease is present in extracellular biological fluids, including human plasma. *FASEB J*, **17**, 1945–1947.

Eliezer, D., Kutluay, E., Bussell, R., Jr, & Browne, G. (2001) Conformational properties of alpha-synuclein in its free and lipid-associated states. *J. Mol. Biol.*, **307**, 1061–1073.

Emadi, S., Barkhordarian, H., Wang, M.S., Schulz, P., & Sierks, M.R. (2007) Isolation of a Human Single Chain Antibody Fragment Against Oligomeric α-Synuclein that Inhibits Aggregation and Prevents α-Synuclein-induced Toxicity. *Journal of Molecular Biology*, **368**, 1132–1144.

Emadi, S., Liu, R., Yuan, B., Schulz, P., McAllister, C., Lyubchenko, Y., Messer, A., & Sierks, M.R. (2004) Inhibiting aggregation of alpha-synuclein with human single chain antibody fragments. *Biochemistry*, **43**, 2871–2878.

Evers, F., Jeworrek, C., Tiemeyer, S., Weise, K., Sellin, D., Paulus, M., Struth, B., Tolan, M., & Winter, R. (2009) Elucidating the Mechanism of Lipid Membrane-Induced IAPP Fibrillogenesis and Its Inhibition by the Red Wine Compound Resveratrol: A Synchrotron X-ray Reflectivity Study. *J. Am. Chem. Soc.*, **131**, 9516–9521.

Fares, M.-B., Ait-Bouziad, N., Dikiy, I., Mbefo, M.K., Jovičić, A., Kiely, A., Holton, J.L., Lee, S.-J., Gitler, A.D., Eliezer, D., & Lashuel, H.A. (2014) The novel Parkinson's disease linked mutation G51D attenuates in vitro aggregation and membrane binding of α-synuclein, and enhances its secretion and nuclear localization in cells. *Hum. Mol. Genet.*, **23**, 4491–4509.

Fázio, M.A., Oliveira, V.X., Bulet, P., Miranda, M.T.M., Daffre, S., & Miranda, A. (2006) Structure–activity relationship studies of gomesin: Importance of the disulfide bridges for conformation, bioactivities, and serum stability. *Biopolymers*, **84**, 205–218.

Fesinmeyer, R.M., Hudson, F.M., Olsen, K.A., White, G.W.N., Euser, A., & Andersen, N.H. (2005) Chemical Shifts Provide Fold Populations and Register of β Hairpins and β Sheets. *J Biomol NMR*, **33**, 213–231.

Forloni, G., Colombo, L., Girola, L., Tagliavini, F., & Salmona, M. (2001) Anti-amyloidogenic activity of tetracyclines: studies in vitro. *FEBS Lett.*, **487**, 404–407.

Fox, A., Snollaerts, T., Errecart Casanova, C., Calciano, A., Nogaj, L.A., & Moffet, D.A. (2010) Selection for Nonamyloidogenic Mutants of Islet Amyloid Polypeptide (IAPP) Identifies an Extended Region for Amyloidogenicity. *Biochemistry*, **49**, 7783–7789.

Fox, R.O. & Richards, F.M. (1982) A voltage-gated ion channel model inferred from the crystal structure of alamethicin at 1.5-|[angst]| resolution. *Nature*, **300**, 325–330.

Frecer, V., Ho, B., & Ding, J.L. (2004) De novo design of potent antimicrobial peptides. *Antimicrob. Agents Chemother.*, **48**, 3349–3357.

Fujiwara, H., Hasegawa, M., Dohmae, N., Kawashima, A., Masliah, E., Goldberg, M.S., Shen, J., Takio, K., & Iwatsubo, T. (2002) alpha-Synuclein is phosphorylated in synucleinopathy lesions. *Nat. Cell Biol.*, **4**, 160–164.

Fusco, G., Simone, A.D., Arosio, P., Vendruscolo, M., Veglia, G., & Dobson, C.M. (2016) Structural Ensembles of Membrane-bound α-Synuclein Reveal the Molecular Determinants of Synaptic Vesicle Affinity. *Scientific Reports*, **6**, 27125.

Gazit, E. (2002) A possible role for π-stacking in the self-assembly of amyloid fibrils. *FASEB J*, **16**, 77–83.

George, J.M. & Clayton, D.F. (1996) The Non-Amyloid-β Component of Alzheimer's Disease Plaque Amyloid: Comparative Analysis Suggests a Normal Function as a Synaptic Plasticizer. In Fiskum, G. (ed), *Neurodegenerative Diseases, GWUMC Department of Biochemistry and Molecular Biology Annual Spring Symposia*. Springer US, pp. 109–112.

Georgieva, E.R., Ramlall, T.F., Borbat, P.P., Freed, J.H., & Eliezer, D. (2008) Membrane-bound alpha-synuclein forms an extended helix: long-distance pulsed ESR measurements using vesicles, bicelles, and rodlike micelles. *J. Am. Chem. Soc.*, **130**, 12856–12857.

Ghosh, A., Pithadia, A.S., Bhat, J., Bera, S., Midya, A., Fierke, C.A., Ramamoorthy, A., & Bhunia, A. (2015) Self-Assembly of a Nine-Residue Amyloid-Forming Peptide Fragment of SARS Corona Virus E-Protein: Mechanism of Self Aggregation and Amyloid-Inhibition of hIAPP. *Biochemistry*, **54**, 2249–2261.

Ghosh, D. & Maji, S.K. (2015) Preparation of aggregate-free α -synuclein for _in vitro_ aggregation study. *Protocol Exchange*, DOI:10.1038/protex.2015.037.

Ghosh, D., Mondal, M., Mohite, G.M., Singh, P.K., Ranjan, P., Anoop, A., Ghosh, S., Jha, N.N., Kumar, A., & Maji, S.K. (2013) The Parkinson's disease-associated H50Q mutation accelerates α-Synuclein aggregation in vitro. *Biochemistry*, **52**, 6925–6927.

Ghosh, D., Sahay, S., Ranjan, P., Salot, S., Mohite, G.M., Singh, P.K., Dwivedi, S., Carvalho, E., Banerjee, R., Kumar, A., & Maji, S.K. (2014) The newly discovered parkinson's disease associated finnish mutation (A53E) attenuates α-synuclein aggregation and membrane binding. *Biochemistry*, **53**, 6419–6421.

Ghosh, D., Singh, P.K., Sahay, S., Jha, N.N., Jacob, R.S., Sen, S., Kumar, A., Riek, R., & Maji, S.K. (2015) Structure based aggregation studies reveal the presence of helix-rich intermediate during α-Synuclein aggregation. *Sci Rep*, **5**.

Giasson, B.I., Uryu, K., Trojanowski, J.Q., & Lee, V.M.-Y. (1999) Mutant and Wild Type Human α-Synucleins Assemble into Elongated Filaments with Distinct Morphologies in Vitro. *J. Biol. Chem.*, **274**, 7619–7622.

Gilead, S., Wolfenson, H., & Gazit, E. (2006) Molecular mapping of the recognition interface between the islet amyloid polypeptide and insulin. *Angew. Chem. Int. Ed. Engl.*, **45**, 6476–6480.

Glenner, G.G., Eanes, E.D., & Wiley, C.A. (1988) Amyloid fibrils formed from a segment of the pancreatic islet amyloid protein. *Biochem. Biophys. Res. Commun.*, **155**, 608–614.

Glenner, G.G. & Wong, C.W. (1984) Alzheimer's disease and Down's syndrome: sharing of a unique cerebrovascular amyloid fibril protein. *Biochem. Biophys. Res. Commun.*, **122**, 1131–1135.

Goldsbury, C., Goldie, K., Pellaud, J., Seelig, J., Frey, P., Müller, S.A., Kistler, J., Cooper, G.J., & Aebi, U. (2000) Amyloid fibril formation from full-length and fragments of amylin. *J. Struct. Biol.*, **130**, 352–362.

Gordon, D.J., Tappe, R., & Meredith, S.C. (2002) Design and characterization of a membrane permeable N-methyl amino acid-containing peptide that inhibits Abeta1-40 fibrillogenesis. *J. Pept. Res.*, **60**, 37–55.

Green, J., Goldsbury, C., Mini, T., Sunderji, S., Frey, P., Kistler, J., Cooper, G., & Aebi, U. (2003) Full-length Rat Amylin Forms Fibrils Following Substitution of Single Residues from Human Amylin. *Journal of Molecular Biology*, **326**, 1147–1156.

Greenbaum, E.A., Graves, C.L., Mishizen-Eberz, A.J., Lupoli, M.A., Lynch, D.R., Englander, S.W., Axelsen, P.H., & Giasson, B.I. (2005) The E46K mutation in alpha-synuclein increases amyloid fibril formation. *J. Biol. Chem.*, **280**, 7800–7807.

Guvench, O. & Brooks, C.L. (2005) Tryptophan side chain electrostatic interactions determine edge-to-face vs parallel-displaced tryptophan side chain geometries in the designed beta-hairpin "trpzip2." *J. Am. Chem. Soc.*, **127**, 4668–4674.

Gwinn-Hardy, K. & Farrer, M. (2002) Parkinson's genetics: An embarrassment of riches. *Ann Neurol.*, **51**, 7–8.

Hamilton, B.A. (2004) alpha-Synuclein A53T substitution associated with Parkinson disease also marks the divergence of Old World and New World primates. *Genomics*, **83**, 739–742.

Hamley, I.W. (2012) The amyloid beta peptide: a chemist's perspective. Role in Alzheimer's and fibrillization. *Chem. Rev.*, **112**, 5147–5192.

Hancock, R.E.W. & Sahl, H.-G. (2006) Antimicrobial and host-defense peptides as new anti-infective therapeutic strategies. *Nat Biotech*, **24**, 1551–1557.

Haque, T.S., Little, J.C., & Gellman, S.H. (1994) "Mirror image" reverse turns promote .beta.-hairpin formation. *J. Am. Chem. Soc.*, **116**, 4105–4106.

Hartl, F.U. & Hayer-Hartl, M. (2009) Converging concepts of protein folding in vitro and in vivo. *Nat Struct Mol Biol*, **16**, 574–581.

Harwig, S.S., Waring, A., Yang, H.J., Cho, Y., Tan, L., & Lehrer, R.I. (1996) Intramolecular disulfide bonds enhance the antimicrobial and lytic activities of protegrins at physiological sodium chloride concentrations. *Eur. J. Biochem.*, **240**, 352–357.

Hayden, M.R. & Tyagi, S.C. (2001) "A" is for amylin and amyloid in type 2 diabetes mellitus. *JOP*, **2**, 124–139.

He, K., Ludtke, S.J., Huang, H.W., & Worcester, D.L. (1995) Antimicrobial Peptide Pores in Membranes Detected by Neutron In-Plane Scattering. *Biochemistry*, **34**, 15614–15618.

He, K., Ludtke, S.J., Worcester, D.L., & Huang, H.W. (1996) Neutron scattering in the plane of membranes: structure of alamethicin pores. *Biophys. J.*, **70**, 2659–2666.

He, Y., Prieto, L., & Lazaridis, T. (2013) Modeling peptide binding to anionic membrane pores. *J. Comput. Chem.*, **34**, 1463–1475.

Hiddinga, H.J. & Eberhardt, N.L. (1999) Intracellular amyloidogenesis by human islet amyloid polypeptide induces apoptosis in COS-1 cells. *Am. J. Pathol.*, **154**, 1077–1088.

Higham, C.E., Jaikaran, E.T., Fraser, P.E., Gross, M., & Clark, A. (2000) Preparation of synthetic human islet amyloid polypeptide (IAPP) in a stable conformation to enable study of conversion to amyloid-like fibrils. *FEBS Lett.*, **470**, 55–60.

Hirsch, J.G. (1956) Phagocytin: a bactericidal substance from polymorphonuclear leucocytes. *J. Exp. Med.*, **103**, 589–611.

Hoogwerf, B.J., Doshi, K.B., & Diab, D. (2008) Pramlintide, the synthetic analogue of amylin: physiology, pathophysiology, and effects on glycemic control, body weight, and selected biomarkers of vascular risk. *Vasc Health Risk Manag*, **4**, 355–362.

Hooper, D.C. (1999) Mechanisms of fluoroquinolone resistance. *Drug Resistance Updates*, **2**, 38–55.

Hopping, G., Kellock, J., Caughey, B., & Daggett, V. (2013) Designed Trpzip-3 β-Hairpin Inhibits Amyloid Formation in Two Different Amyloid Systems. *ACS Med. Chem. Lett.*, **4**, 824–828.

Howard, C.F. (1978) Insular amyloidosis and diabetes mellitus in Macaca nigra. *Diabetes*, **27**, 357–364.

Hoyer, W., Cherny, D., Subramaniam, V., & Jovin, T.M. (2004) Impact of the acidic C-terminal region comprising amino acids 109-140 on alpha-synuclein aggregation in vitro. *Biochemistry*, **43**, 16233–16242.

Hu, R., Ren, B., Zhang, M., Chen, H., Liu, Y., Liu, L., Gong, X., Jiang, B., Ma, J., & Zheng, J. (2017) Seed-Induced Heterogeneous Cross-Seeding Self-Assembly of Human and Rat Islet Polypeptides. *ACS Omega*, **2**, 784–792.

Huang, C., Gurlo, T., Haataja, L., Costes, S., Daval, M., Ryazantsev, S., Wu, X., Butler, A.E., & Butler, P.C. (2010) Calcium-activated calpain-2 is a mediator of beta cell dysfunction and apoptosis in type 2 diabetes. *J. Biol. Chem.*, **285**, 339–348.

Huggins, K.N.L., Bisaglia, M., Bubacco, L., Tatarek-Nossol, M., Kapurniotu, A., & Andersen, N.H. (2011) Designed hairpin peptides interfere with amyloidogenesis pathways: fibril formation and cytotoxicity inhibition, interception of the preamyloid state. *Biochemistry*, **50**, 8202–8212.

Islam, M.R., Nagao, J.-I., Zendo, T., & Sonomoto, K. (2012) Antimicrobial mechanism of lantibiotics. *Biochem. Soc. Trans.*, **40**, 1528–1533.

Jaikaran, E.T. & Clark, A. (2001) Islet amyloid and type 2 diabetes: from molecular misfolding to islet pathophysiology. *Biochim. Biophys. Acta*, **1537**, 179–203.

Janciauskiene, S. & Ahrén, B. (1998) Different sensitivity to the cytotoxic action of IAPP fibrils in two insulin-producing cell lines, HIT-T15 and RINm5F cells. *Biochem. Biophys. Res. Commun.*, **251**, 888–893.

Janson, J., Ashley, R.H., Harrison, D., McIntyre, S., & Butler, P.C. (1999) The mechanism of islet amyloid polypeptide toxicity is membrane disruption by intermediate-sized toxic amyloid particles. *Diabetes*, **48**, 491–498.

Jao, C.C., Der-Sarkissian, A., Chen, J., & Langen, R. (2004) Structure of membrane-bound alpha-synuclein studied by site-directed spin labeling. *Proc. Natl. Acad. Sci.U. S. A.*, **101**, 8331–8336.

Jao, C.C., Hegde, B.G., Chen, J., Haworth, I.S., & Langen, R. (2008) Structure of membrane-bound α-synuclein from site-directed spin labeling and computational refinement. *Proc. Natl. Acad. Sci. U.S.A.*, **105**, 19666–19671.

Jiang, P., Li, W., Shea, J.-E., & Mu, Y. (2011) Resveratrol inhibits the formation of multiple-layered β-sheet oligomers of the human islet amyloid polypeptide segment 22-27. *Biophys. J.*, **100**, 1550–1558.

Jin, F., Wu, Q., Lu, Y.-F., Gong, Q.-H., & Shi, J.-S. (2008) Neuroprotective effect of resveratrol on 6-OHDA-induced Parkinson's disease in rats. *European Journal of Pharmacology*, **600**, 78–82.

Jin, Y., Hammer, J., Pate, M., Zhang, Y., Zhu, F., Zmuda, E., & Blazyk, J. (2005) Antimicrobial Activities and Structures of Two Linear Cationic Peptide Families with Various Amphipathic β-Sheet and α-Helical Potentials. *Antimicrob Agents Chemother*, **49**, 4957–4964.

Joly, S., Maze, C., McCray, P.B., & Guthmiller, J.M. (2004) Human β-Defensins 2 and 3 Demonstrate Strain-Selective Activity against Oral Microorganisms. *J. Clin. Microbiol.*, **42**, 1024–1029.

Kajava, A.V., Aebi, U., & Steven, A.C. (2005) The parallel superpleated beta-structure as a model for amyloid fibrils of human amylin. *J. Mol. Biol.*, **348**, 247–252.

Kang, L., Janowska, M.K., Moriarty, G.M., & Baum, J. (2013) Mechanistic Insight into the Relationship between N-Terminal Acetylation of α-Synuclein and Fibril Formation Rates by NMR and Fluorescence. *PLoS ONE*, **8**, e75018.

Kang, L., Moriarty, G.M., Woods, L.A., Ashcroft, A.E., Radford, S.E., & Baum, J. (2012) N-terminal acetylation of α-synuclein induces increased transient helical propensity and decreased aggregation rates in the intrinsically disordered monomer. *Protein Sci.*, **21**, 911–917.

Kapurniotu, A. (2001) Amyloidogenicity and cytotoxicity of islet amyloid polypeptide. *Biopolymers*, **60**, 438–459.

Kapurniotu, A., Schmauder, A., & Tenidis, K. (2002) Structure-based design and study of non-amyloidogenic, double N-methylated IAPP amyloid core sequences as inhibitors of IAPP amyloid formation and cytotoxicity1. *J Mol Biol*, **315**, 339–350.

Karpinar, D.P., Balija, M.B.G., Kügler, S., Opazo, F., Rezaei-Ghaleh, N., Wender, N., Kim, H.-Y., Taschenberger, G., Falkenburger, B.H., Heise, H., Kumar, A., Riedel, D., Fichtner, L., Voigt, A., Braus, G.H., Giller, K., Becker, S., Herzig, A., Baldus, M., Jäckle, H., Eimer, S., Schulz, J.B., Griesinger, C., & Zweckstetter, M. (2009) Pre-fibrillar alpha-synuclein variants with impaired beta-structure increase neurotoxicity in Parkinson's disease models. *EMBO J.*, **28**, 3256–3268.

Kawano, K., Yoneya, T., Miyata, T., Yoshikawa, K., Tokunaga, F., Terada, Y., & Iwanaga, S. (1990) Antimicrobial peptide, tachyplesin I, isolated from hemocytes of the horseshoe crab (Tachypleus tridentatus). NMR determination of the beta-sheet structure. *J. Biol. Chem.*, **265**, 15365–15367.

Kayed, R., Bernhagen, J., Greenfield, N., Sweimeh, K., Brunner, H., Voelter, W., & Kapurniotu, A. (1999) Conformational transitions of islet amyloid polypeptide (IAPP) in amyloid formation in vitro. *J. Mol. Biol.*, **287**, 781–796.

Kayed, R., Sokolov, Y., Edmonds, B., McIntire, T.M., Milton, S.C., Hall, J.E., & Glabe, C.G. (2004) Permeabilization of lipid bilayers is a common conformation-dependent activity of soluble amyloid oligomers in protein misfolding diseases. *J. Biol. Chem.*, **279**, 46363–46366.

Kiely, A.P., Asi, Y.T., Kara, E., Limousin, P., Ling, H., Lewis, P., Proukakis, C., Quinn, N., Lees, A.J., Hardy, J., Revesz, T., Houlden, H., & Holton, J.L. (2013) α-Synucleinopathy associated with G51D SNCA mutation: a link between Parkinson's disease and multiple system atrophy? *Acta Neuropathologica*, **125**, 753.

Kier, B., Anderson, J.M., & Andersen, N.H. (2015) Disulfide-Mediated β-Strand Dimers: Hyperstable β-Sheets Lacking Tertiary Interactions and Turns. *J. Am. Chem. Soc.*, **137**, 5363–5371.

Kier, B.L., Shu, I., Eidenschink, L.A., & Andersen, N.H. (2010) Stabilizing capping motif for β-hairpins and sheets. *Proc. Natl. Acad. Sci. U.S.A.*, **107**, 10466–10471.

Kogire, M., Ishizuka, J., Thompson, J.C., & Greeley, G.H. (1991) Inhibitory action of islet amyloid polypeptide and calcitonin gene-related peptide on release of insulin from the isolated perfused rat pancreas. *Pancreas*, **6**, 459–463.

Kokkoni, N., Stott, K., Amijee, H., Mason, J.M., & Doig, A.J. (2006) N-Methylated peptide inhibitors of beta-amyloid aggregation and toxicity. Optimization of the inhibitor structure. *Biochemistry*, **45**, 9906–9918.

Kolterman, O.G. (1997) Amylin and glycaemic regulation: a possible role for the human amylin analogue pramlintide. *Diabet. Med.*, **14 Suppl 2**, S35-38.

Kolterman, O.G., Gottlieb, A., Moyses, C., & Colburn, W. (1995) Reduction of postprandial hyperglycemia in subjects with IDDM by intravenous infusion of AC137, a human amylin analogue. *Diabetes Care*, **18**, 1179–1182.

Konarkowska, B., Aitken, J.F., Kistler, J., Zhang, S., & Cooper, G.J.S. (2006) The aggregation potential of human amylin determines its cytotoxicity towards islet β-cells. *FEBS Journal*, **273**, 3614–3624.

Krebs, M.R.H., Bromley, E.H.C., & Donald, A.M. (2005) The binding of thioflavin-T to amyloid fibrils: localisation and implications. *J. Struct. Biol.*, **149**, 30–37.

Kruger, D.F., Gatcomb, P.M., & Owen, S.K. (1999) Clinical implications of amylin and amylin deficiency. *Diabetes Educ*, **25**, 389–397; quiz 398.

Krüger, R., Kuhn, W., Müller, T., Woitalla, D., Graeber, M., Kösel, S., Przuntek, H., Epplen, J.T., Schöls, L., & Riess, O. (1998) Ala30Pro mutation in the gene encoding alpha-synuclein in Parkinson's disease. *Nat. Genet.*, **18**, 106–108.

Kuhl, M.M. (2014) Foxfeed Blog. *Parkinson's Vaccine Safe in Phase I Trial*,.

Kuhl, M.M. (2016) Foxfeed Blog. *Vaccine for Parkinson's Reports Positive Results from Boost Study*,.

Kushibiki, T., Kamiya, M., Aizawa, T., Kumaki, Y., Kikukawa, T., Mizuguchi, M., Demura, M., Kawabata, S., & Kawano, K. (2014) Interaction between tachyplesin I, an antimicrobial peptide derived from horseshoe crab, and lipopolysaccharide. *Biochim. Biophys. Acta*, **1844**, 527–534.

Laederach, A., Andreotti, A.H., & Fulton, D.B. (2002) Solution and Micelle-Bound Structures of Tachyplesin I and Its Active Aromatic Linear Derivatives†,‡. *Biochemistry*, **41**, 12359–12368.

Larson, J.L. & Miranker, A.D. (2004) The mechanism of insulin action on islet amyloid polypeptide fiber formation. *J. Mol. Biol.*, **335**, 221–231.

Latorre, R. & Alvarez, O. (1981) Voltage-dependent channels in planar lipid bilayer membranes. *Physiol. Rev.*, **61**, 77–150.

Lecerf, J.M., Shirley, T.L., Zhu, Q., Kazantsev, A., Amersdorfer, P., Housman, D.E., Messer, A., & Huston, J.S. (2001) Human single-chain Fv intrabodies counteract in situ huntingtin aggregation in cellular models of Huntington's disease. *Proc. Natl. Acad. Sci. U.S.A.*, **98**, 4764–4769.

Lee, H.-J., Bae, E.-J., Jang, A., Ho, D.-H., Cho, E.-D., Suk, J.-E., Yun, Y.-M., & Lee, S.-J. (2011) Enzyme-linked immunosorbent assays for alpha-synuclein with species and multimeric state specificities. *J. Neurosci. Meth.*, **199**, 249–257.

Lee, H.-J., Suk, J.-E., Patrick, C., Bae, E.-J., Cho, J.-H., Rho, S., Hwang, D., Masliah, E., & Lee, S.-J. (2010) Direct transfer of alpha-synuclein from neuron to astroglia causes inflammatory responses in synucleinopathies. *J. Biol. Chem.*, **285**, 9262–9272.

Lesage, S., Anheim, M., Letournel, F., Bousset, L., Honoré, A., Rozas, N., Pieri, L., Madiona, K., Dürr, A., Melki, R., Verny, C., Brice, A., & French Parkinson's Disease Genetics

Study Group (2013) G51D α-synuclein mutation causes a novel parkinsonian-pyramidal syndrome. *Ann. Neurol.*, **73**, 459–471.

Leung, T.C.H., Lui, C.N.P., Chen, L.W., Yung, W.H., Chan, Y.S., & Yung, K.K.L. (2012) Ceftriaxone ameliorates motor deficits and protects dopaminergic neurons in 6-hydroxydopamine-lesioned rats. *ACS Chem Neurosci*, **3**, 22–30.

LeVine, H. (1993) Thioflavine T interaction with synthetic Alzheimer's disease beta-amyloid peptides: detection of amyloid aggregation in solution. *Protein Sci*, **2**, 404–410.

LeVine, H. (1995) Thioflavine T interaction with amyloid β-sheet structures. *Amyloid*, **2**, 1–6.

LeVine III, H. (1999) [18] Quantification of β-sheet amyloid fibril structures with thioflavin T. In Enzymology, B.-M. in (ed), *Amyloid, Prions, and Other Protein Aggregates*. Academic Press, pp. 274–284.

Li, J., Uversky, V.N., & Fink, A.L. (2001) Effect of Familial Parkinson's Disease Point Mutations A30P and A53T on the Structural Properties, Aggregation, and Fibrillation of Human α-Synuclein. *Biochemistry*, **40**, 11604–11613.

Li, W., West, N., Colla, E., Pletnikova, O., Troncoso, J.C., Marsh, L., Dawson, T.M., Jäkälä, P., Hartmann, T., Price, D.L., & Lee, M.K. (2005) Aggregation promoting C-terminal truncation of α-synuclein is a normal cellular process and is enhanced by the familial Parkinson's disease-linked mutations. *PNAS*, **102**, 2162–2167.

Liang, G., Zhao, J., Yu, X., & Zheng, J. (2013) Comparative Molecular Dynamics Study of Human Islet Amyloid Polypeptide (IAPP) and Rat IAPP Oligomers. *Biochemistry*, **52**, 1089–1100.

Ling, Y.L., Strasfeld, D.B., Shim, S.-H., Raleigh, D.P., & Zanni, M.T. (2009) Two-dimensional infrared spectroscopy provides evidence of an intermediate in the membrane-catalyzed assembly of diabetic amyloid. *J Phys Chem B*, **113**, 2498–2505.

Liu, B. & Pop, M. (2009) ARDB--Antibiotic Resistance Genes Database. *Nucleic Acids Res.*, **37**, D443-447.

Liu, C.-W., Giasson, B.I., Lewis, K.A., Lee, V.M., DeMartino, G.N., & Thomas, P.J. (2005) A Precipitating Role for Truncated α-Synuclein and the Proteasome in α-Synuclein Aggregation: Implications for Pathogenesis of Parkinson Disease. *J. Biol. Chem.*, **280**, 22670–22678.

Liu, Y., Carver, J.A., Calabrese, A.N., & Pukala, T.L. (2014) Gallic acid interacts with α-synuclein to prevent the structural collapse necessary for its aggregation. *Biochim. Biophys. Acta*,.

Lockwood, N.A., Haseman, J.R., Tirrell, M.V., & Mayo, K.H. (2004) Acylation of SC4 dodecapeptide increases bactericidal potency against Gram-positive bacteria, including drug-resistant strains. *Biochem. J.*, **378**, 93–103.

Loeffler, J.M., Nelson, D., & Fischetti, V.A. (2001) Rapid killing of Streptococcus pneumoniae with a bacteriophage cell wall hydrolase. *Science*, **294**, 2170–2172.

Lopes, D.H.J., Meister, A., Gohlke, A., Hauser, A., Blume, A., & Winter, R. (2007) Mechanism of islet amyloid polypeptide fibrillation at lipid interfaces studied by infrared reflection absorption spectroscopy. *Biophys. J.*, **93**, 3132–3141.

Lorenzen, N., Nielsen, S.B., Yoshimura, Y., Vad, B.S., Andersen, C.B., Betzer, C., Kaspersen, J.D., Christiansen, G., Pedersen, J.S., Jensen, P.H., Mulder, F.A.A., & Otzen, D.E. (2014) How epigallocatechin gallate can inhibit α-synuclein oligomer toxicity in vitro. *J. Biol. Chem.*, jbc.M114.554667.

Lorenzo, A., Razzaboni, B., Weir, G.C., & Yankner, B.A. (1994) Pancreatic islet cell toxicity of amylin associated with type-2 diabetes mellitus. *Nature*, **368**, 756–760.

Lorenzo, A. & Yankner, B.A. (1994) Beta-amyloid neurotoxicity requires fibril formation and is inhibited by congo red. *Proc. Natl. Acad. Sci. U.S.A.*, **91**, 12243–12247.

Luca, S., Yau, W.-M., Leapman, R., & Tycko, R. (2007) Peptide conformation and supramolecular organization in amylin fibrils: constraints from solid-state NMR. *Biochemistry*, **46**, 13505–13522.

Ludtke, S.J., He, K., Heller, W.T., Harroun, T.A., Yang, L., & Huang, H.W. (1996) Membrane pores induced by magainin. *Biochemistry*, **35**, 13723–13728.

Luk, K.C., Kehm, V., Carroll, J., Zhang, B., O'Brien, P., Trojanowski, J.Q., & Lee, V.M.-Y. (2012) Pathological α-Synuclein Transmission Initiates Parkinson-like Neurodegeneration in Nontransgenic Mice. *Science*, **338**, 949–953.

Lutz, T.A. (2012) Control of energy homeostasis by amylin. *Cell. Mol. Life Sci.*, **69**, 1947–1965.

Madani, F., Lindberg, S., Langel, U., Futaki, S., & Gräslund, A. (2011) Mechanisms of cellular uptake of cell-penetrating peptides. *J Biophys*, **2011**, 414729.

Madine, J., Doig, A.J., & Middleton, D.A. (2008) Design of an N-methylated peptide inhibitor of alpha-synuclein aggregation guided by solid-state NMR. *J. Am. Chem. Soc.*, **130**, 7873–7881.

Mak, D.O. & Webb, W.W. (1995) Two classes of alamethicin transmembrane channels: molecular models from single-channel properties. *Biophys. J.*, **69**, 2323–2336.

Mak, P., Pohl, J., Dubin, A., Reed, M.S., Bowers, S.E., Fallon, M.T., & Shafer, W.M. (2003) The increased bactericidal activity of a fatty acid-modified synthetic antimicrobial peptide of human cathepsin G correlates with its enhanced capacity to interact with model membranes. *Int. J. Antimicrob. Agents*, **21**, 13–19.

Mandard, N., Bulet, P., Caille, A., Daffre, S., & Vovelle, F. (2002) The solution structure of gomesin, an antimicrobial cysteine-rich peptide from the spider. *European Journal of Biochemistry*, **269**, 1190–1198.

Mandler, M., Valera, E., Rockenstein, E., Weninger, H., Patrick, C., Adame, A., Santic, R., Meindl, S., Vigl, B., Smrzka, O., Schneeberger, A., Mattner, F., & Masliah, E. (2014) Next-generation active immunization approach for synucleinopathies: implications for Parkinson's disease clinical trials. *Acta Neuropathol*, **127**, 861–879.

Mangoni, M.E., Aumelas, A., Charnet, P., Roumestand, C., Chiche, L., Despaux, E., Grassy, G., Calas, B., & Chavanieu, A. (1996) Change in membrane permeability induced by protegrin 1: implication of disulphide bridges for pore formation. *FEBS Lett.*, **383**, 93–98.

Marcelino, A.M.C. & Gierasch, L.M. (2008) Roles of β-Turns in Protein Folding: From Peptide Models to Protein Engineering. *Biopolymers*, **89**, 380–391.

Marek, P., Abedini, A., Song, B., Kanungo, M., Johnson, M.E., Gupta, R., Zaman, W., Wong, S.S., & Raleigh, D.P. (2007) Aromatic Interactions Are Not Required for Amyloid Fibril Formation by Islet Amyloid Polypeptide but Do Influence the Rate of Fibril Formation and Fibril Morphology. *Biochemistry*, **46**, 3255–3261.

Martin, C. (2006) The physiology of amylin and insulin: maintaining the balance between glucose secretion and glucose uptake. *Diabetes Educ*, **32 Suppl 3**, 101S–104S.

Martinez, J.L. & Baquero, F. (2000) Mutation Frequencies and Antibiotic Resistance. *Antimicrob. Agents Chemother.*, **44**, 1771–1777.

Martinez-Freijo, P., Fluit, A.C., Schmitz, F.J., Grek, V.S., Verhoef, J., & Jones, M.E. (1998) Class I integrons in Gram-negative isolates from different European hospitals and association with decreased susceptibility to multiple antibiotic compounds. *J Antimicrob Chemother*, **42**, 689–696.

Masliah, E., Rockenstein, E., Mante, M., Crews, L., Spencer, B., Adame, A., Patrick, C., Trejo, M., Ubhi, K., Rohn, T.T., Mueller-Steiner, S., Seubert, P., Barbour, R., McConlogue, L., Buttini, M., Games, D., & Schenk, D. (2011) Passive Immunization Reduces Behavioral and Neuropathological Deficits in an Alpha-Synuclein Transgenic Model of Lewy Body Disease. *PLoS ONE*, **6**, e19338.

Masters, C.L., Multhaup, G., Simms, G., Pottgiesser, J., Martins, R.N., & Beyreuther, K. (1985) Neuronal origin of a cerebral amyloid: neurofibrillary tangles of Alzheimer's disease

contain the same protein as the amyloid of plaque cores and blood vessels. *EMBO J.*, **4**, 2757–2763.

Masters, C.L., Simms, G., Weinman, N.A., Multhaup, G., McDonald, B.L., & Beyreuther, K. (1985) Amyloid plaque core protein in Alzheimer disease and Down syndrome. *Proc. Natl. Acad. Sci. U.S.A.*, **82**, 4245–4249.

Matsuzaki, K., Murase, O., Tokuda, H., Funakoshi, S., Fujii, N., & Miyajima, K. (1994) Orientational and Aggregational States of Magainin 2 in Phospholipid Bilayers. *Biochemistry*, **33**, 3342–3349.

Matsuzaki, K., Nakamura, A., Murase, O., Sugishita, K., Fujii, N., & Miyajima, K. (1997) Modulation of Magainin 2−Lipid Bilayer Interactions by Peptide Charge. *Biochemistry*, **36**, 2104–2111.

Matsuzaki, K., Yoneyama, S., Fujii, N., Miyajima, K., Yamada, K., Kirino, Y., & Anzai, K. (1997) Membrane Permeabilization Mechanisms of a Cyclic Antimicrobial Peptide, Tachyplesin I, and Its Linear Analog. *Biochemistry*, **36**, 9799–9806.

Matsuzaki, K., Yoneyama, S., & Miyajima, K. (1997) Pore formation and translocation of melittin. *Biophys. J.*, **73**, 831–838.

Mattson, M.P. & Goodman, Y. (1995) Different amyloidogenic peptides share a similar mechanism of neurotoxicity involving reactive oxygen species and calcium. *Brain Res.*, **676**, 219–224.

Mazor, Y., Gilead, S., Benhar, I., & Gazit, E. (2002) Identification and characterization of a novel molecular-recognition and self-assembly domain within the islet amyloid polypeptide. *J. Mol. Biol.*, **322**, 1013–1024.

Meier, J.J., Kayed, R., Lin, C.-Y., Gurlo, T., Haataja, L., Jayasinghe, S., Langen, R., Glabe, C.G., & Butler, P.C. (2006) Inhibition of human IAPP fibril formation does not prevent beta-cell death: evidence for distinct actions of oligomers and fibrils of human IAPP. *Am. J. Physiol. Endocrinol. Metab.*, **291**, E1317-1324.

Melo, M.N., Ferre, R., & Castanho, M.A.R.B. (2009) Antimicrobial peptides: linking partition, activity and high membrane-bound concentrations. *Nat Rev Micro*, **7**, 245–250.

Meng, F., Abedini, A., Plesner, A., Middleton, C.T., Potter, K.J., Zanni, M.T., Verchere, C.B., & Raleigh, D.P. (2010) The Sulfated Triphenyl Methane Derivative Acid Fuchsin is a Potent Inhibitor of Amyloid Formation by Human Islet Amyloid Polypeptide and Protects Against the Toxic Effects of Amyloid Formation. *J Mol Biol*, **400**, 555–566.

Meng, F., Abedini, A., Plesner, A., Verchere, C.B., & Raleigh, D.P. (2010) The Flavanol (−)-Epigallocatechin 3-Gallate Inhibits Amyloid Formation by Islet Amyloid Polypeptide,

Disaggregates Amyloid Fibrils, and Protects Cultured Cells against IAPP-Induced Toxicity. *Biochemistry*, **49**, 8127–8133.

Meng, X., Munishkina, L.A., Fink, A.L., & Uversky, V.N. (2009) Molecular Mechanisms Underlying the Flavonoid-Induced Inhibition of α-Synuclein Fibrillation. *Biochemistry*, **48**, 8206–8224.

Midura-Nowaczek, K. & Markowska, A. (2014) Antimicrobial Peptides and Their Analogs: Searching for New Potential Therapeutics. *Perspect Medicin Chem*, **6**, 73–80.

Minor, D.L. & Kim, P.S. (1994) Measurement of the beta-sheet-forming propensities of amino acids. *Nature*, **367**, 660–663.

Mirecka, E.A., Shaykhalishahi, H., Gauhar, A., Akgül, Ş., Lecher, J., Willbold, D., Stoldt, M., & Hoyer, W. (2014) Sequestration of a β-Hairpin for Control of α-Synuclein Aggregation. *Angew. Chem. Int. Ed.*, **53**, 4227–4230.

Mirzabekov, T.A., Lin, M., & Kagan, B.L. (1996) Pore Formation by the Cytotoxic Islet Amyloid Peptide Amylin. *J. Biol. Chem.*, **271**, 1988–1992.

Mishra, R., Sellin, D., Radovan, D., Gohlke, A., & Winter, R. (2009) Inhibiting Islet Amyloid Polypeptide Fibril Formation by the Red Wine Compound Resveratrol. *ChemBioChem*, **10**, 445–449.

Moore, C.X. & Cooper, G.J. (1991) Co-secretion of amylin and insulin from cultured islet beta-cells: modulation by nutrient secretagogues, islet hormones and hypoglycemic agents. *Biochem. Biophys. Res. Commun.*, **179**, 1–9.

Moriarty, D.F. & Raleigh, D.P. (1999) Effects of sequential proline substitutions on amyloid formation by human amylin20-29. *Biochemistry*, **38**, 1811–1818.

Murphy, M.P. & LeVine, H. (2010) Alzheimer's Disease and the β-Amyloid Peptide. *J Alzheimers Dis*, **19**, 311.

Murphy, R.C. & Messer, A. (2004) A single-chain Fv intrabody provides functional protection against the effects of mutant protein in an organotypic slice culture model of Huntington's disease. *Brain Res. Mol. Brain Res.*, **121**, 141–145.

Murray, I.V.J., Giasson, B.I., Quinn, S.M., Koppaka, V., Axelsen, P.H., Ischiropoulos, H., Trojanowski, J.Q., & Lee, V.M.-Y. (2003) Role of α-Synuclein Carboxy-Terminus on Fibril Formation in Vitro. *Biochemistry*, **42**, 8530–8540.

Naiki, H., Higuchi, K., Hosokawa, M., & Takeda, T. (1989) Fluorometric determination of amyloid fibrils in vitro using the fluorescent dye, thioflavin T1. *Anal. Biochem.*, **177**, 244–249.

Nakamura, K., Mori, F., Kon, T., Tanji, K., Miki, Y., Tomiyama, M., Kurotaki, H., Toyoshima, Y., Kakita, A., Takahashi, H., Yamada, M., & Wakabayashi, K. (2015) Filamentous aggregations of phosphorylated α-synuclein in Schwann cells (Schwann cell cytoplasmic inclusions) in multiple system atrophy. *Acta Neuropathologica Communications*, **3**, 29.

Nakamura, K., Nemani, V.M., Azarbal, F., Skibinski, G., Levy, J.M., Egami, K., Munishkina, L., Zhang, J., Gardner, B., Wakabayashi, J., Sesaki, H., Cheng, Y., Finkbeiner, S., Nussbaum, R.L., Masliah, E., & Edwards, R.H. (2011) Direct membrane association drives mitochondrial fission by the Parkinson disease-associated protein alpha-synuclein. *J. Biol. Chem.*, **286**, 20710–20726.

Nakamura, K., Nemani, V.M., Wallender, E.K., Kaehlcke, K., Ott, M., & Edwards, R.H. (2008) Optical reporters for the conformation of alpha-synuclein reveal a specific interaction with mitochondria. *J. Neurosci.*, **28**, 12305–12317.

Nakamura, T., Furunaka, H., Miyata, T., Tokunaga, F., Muta, T., Iwanaga, S., Niwa, M., Takao, T., & Shimonishi, Y. (1988) Tachyplesin, a class of antimicrobial peptide from the hemocytes of the horseshoe crab (Tachypleus tridentatus). Isolation and chemical structure. *J. Biol. Chem.*, **263**, 16709–16713.

Nanga, R.P.R., Brender, J.R., Xu, J., Veglia, G., & Ramamoorthy, A. (2008) Structures of rat and human islet amyloid polypeptide IAPP(1-19) in micelles by NMR spectroscopy. *Biochemistry*, **47**, 12689–12697.

Narhi, L., Wood, S.J., Steavenson, S., Jiang, Y., Wu, G.M., Anafi, D., Kaufman, S.A., Martin, F., Sitney, K., Denis, P., Louis, J.-C., Wypych, J., Biere, A.L., & Citron, M. (1999) Both Familial Parkinson's Disease Mutations Accelerate α-Synuclein Aggregation. *J. Biol. Chem.*, **274**, 9843–9846.

Nath, A., Schlamadinger, D.E., Rhoades, E., & Miranker, A.D. (2015) Structure-Based Small Molecule Modulation of a Pre-Amyloid State: Pharmacological Enhancement of IAPP Membrane-Binding and Toxicity. *Biochemistry*, **54**, 3555–3564.

Nath, S., Meuvis, J., Hendrix, J., Carl, S.A., & Engelborghs, Y. (2010) Early Aggregation Steps in α-Synuclein as Measured by FCS and FRET: Evidence for a Contagious Conformational Change. *Biophys J*, **98**, 1302–1311.

Nemani, V.M., Lu, W., Berge, V., Nakamura, K., Onoa, B., Lee, M.K., Chaudhry, F.A., Nicoll, R.A., & Edwards, R.H. (2010) Increased expression of alpha-synuclein reduces neurotransmitter release by inhibiting synaptic vesicle reclustering after endocytosis. *Neuron*, **65**, 66–79.

Nishi, M., Sanke, T., Seino, S., Eddy, R.L., Fan, Y.S., Byers, M.G., Shows, T.B., Bell, G.I., & Steiner, D.F. (1989) Human islet amyloid polypeptide gene: complete nucleotide sequence, chromosomal localization, and evolutionary history. *Mol. Endocrinol.*, **3**, 1775–1781.

Onuchic, J.N., Luthey-Schulten, Z., & Wolynes, P.G. (1997) Theory of protein folding: the energy landscape perspective. *Annu Rev Phys Chem*, **48**, 545–600.

Opie, E.L. (1901) The Relation of Diabetes Mellitus to Lesions of the Pancreas. Hyaline Degeneration of the Islands of Langerhahns. *J Exp Med*, **5**, 527–540.

Oren, Z., Lerman, J.C., Gudmundsson, G.H., Agerberth, B., & Shai, Y. (1999) Structure and organization of the human antimicrobial peptide LL-37 in phospholipid membranes: relevance to the molecular basis for its non-cell-selective activity. *Biochemical Journal*, **341**, 501–513.

Padrick, S.B. & Miranker, A.D. (2001) Islet amyloid polypeptide: identification of long-range contacts and local order on the fibrillogenesis pathway. *J. Mol. Biol.*, **308**, 783–794.

Padrick, S.B. & Miranker, A.D. (2002) Islet amyloid: phase partitioning and secondary nucleation are central to the mechanism of fibrillogenesis. *Biochemistry*, **41**, 4694–4703.

Paleologou, K.E., Schmid, A.W., Rospigliosi, C.C., Kim, H.-Y., Lamberto, G.R., Fredenburg, R.A., Lansbury, P.T., Fernandez, C.O., Eliezer, D., Zweckstetter, M., & Lashuel, H.A. (2008) Phosphorylation at Ser-129 but Not the Phosphomimics S129E/D Inhibits the Fibrillation of α-Synuclein. *J. Biol. Chem.*, **283**, 16895–16905.

Pasanen, P., Myllykangas, L., Siitonen, M., Raunio, A., Kaakkola, S., Lyytinen, J., Tienari, P.J., Pöyhönen, M., & Paetau, A. (2014) A novel α-synuclein mutation A53E associated with atypical multiple system atrophy and Parkinson's disease-type pathology. *Neurobiol. Aging*, **35**, 2180.e1-5.

Patil, S.M., Xu, S., Sheftic, S.R., & Alexandrescu, A.T. (2009) Dynamic α-Helix Structure of Micelle-bound Human Amylin. *J. Biol. Chem.*, **284**, 11982–11991.

Patrzykat, A., Friedrich, C.L., Zhang, L., Mendoza, V., & Hancock, R.E.W. (2002) Sublethal Concentrations of Pleurocidin-Derived Antimicrobial Peptides Inhibit Macromolecular Synthesis in Escherichia coli. *Antimicrob. Agents Chemother.*, **46**, 605–614.

Perez, R.G., Waymire, J.C., Lin, E., Liu, J.J., Guo, F., & Zigmond, M.J. (2002) A role for alpha-synuclein in the regulation of dopamine biosynthesis. *J. Neurosci.*, **22**, 3090–3099.

Petkova, A.T., Ishii, Y., Balbach, J.J., Antzutkin, O.N., Leapman, R.D., Delaglio, F., & Tycko, R. (2002) A structural model for Alzheimer's β-amyloid fibrils based on experimental constraints from solid state NMR. *Proc. Natl. Acad. Sci. U.S.A.*, **99**, 16742–16747.

Petukhov, M., Tatsu, Y., Tamaki, K., Murase, S., Uekawa, H., Yoshikawa, S., Serrano, L., & Yumoto, N. (2009) Design of stable alpha-helices using global sequence optimization. *J. Pept. Sci.*, **15**, 359–365.

Pieri, L., Madiona, K., Bousset, L., & Melki, R. (2012) Fibrillar α-synuclein and huntingtin exon 1 assemblies are toxic to the cells. *Biophys. J.*, **102**, 2894–2905.

Polymeropoulos, M.H., Lavedan, C., Leroy, E., Ide, S.E., Dehejia, A., Dutra, A., Pike, B., Root, H., Rubenstein, J., Boyer, R., Stenroos, E.S., Chandrasekharappa, S., Athanassiadou, A., Papapetropoulos, T., Johnson, W.G., Lazzarini, A.M., Duvoisin, R.C., Di Iorio, G., Golbe, L.I., & Nussbaum, R.L. (1997) Mutation in the alpha-synuclein gene identified in families with Parkinson's disease. *Science*, **276**, 2045–2047.

Porat, Y., Abramowitz, A., & Gazit, E. (2006) Inhibition of amyloid fibril formation by polyphenols: structural similarity and aromatic interactions as a common inhibition mechanism. *Chem Biol Drug Des*, **67**, 27–37.

Porat, Y., Mazor, Y., Efrat, S., & Gazit, E. (2004) Inhibition of islet amyloid polypeptide fibril formation: a potential role for heteroaromatic interactions. *Biochemistry*, **43**, 14454–14462.

Pouny, Y., Rapaport, D., Mor, A., Nicolas, P., & Shai, Y. (1992) Interaction of antimicrobial dermaseptin and its fluorescently labeled analogs with phospholipid membranes. *Biochemistry*, **31**, 12416–12423.

Powers, J.-P.S. & Hancock, R.E.W. (2003) The relationship between peptide structure and antibacterial activity. *Peptides*, Antimicrobial Peptides II, **24**, 1681–1691.

Profit, A.A., Vedad, J., & Desamero, R.Z.B. (2017) Peptide Conjugates of Benzene Carboxylic Acids as Agonists and Antagonists of Amylin Aggregation. *Bioconjugate Chem.*, **28**, 666–677.

Pronin, A.N., Morris, A.J., Surguchov, A., & Benovic, J.L. (2000) Synucleins Are a Novel Class of Substrates for G Protein-coupled Receptor Kinases. *J. Biol. Chem.*, **275**, 26515–26522.

Proukakis, C., Dudzik, C.G., Brier, T., MacKay, D.S., Cooper, J.M., Millhauser, G.L., Houlden, H., & Schapira, A.H. (2013) A novel α-synuclein missense mutation in Parkinson disease. *Neurology*, **80**, 1062.

Ramakrishnan, M., Jensen, P.H., & Marsh, D. (2003) α-Synuclein Association with Phosphatidylglycerol Probed by Lipid Spin Labels †. *Biochemistry*, **42**, 12919–12926.

Ramamoorthy, A., Thennarasu, S., Tan, A., Gottipati, K., Sreekumar, S., Heyl, D.L., An, F.Y.P., & Shelburne, C.E. (2006) Deletion of All Cysteines in Tachyplesin I Abolishes Hemolytic Activity and Retains Antimicrobial Activity and Lipopolysaccharide Selective Binding†. *Biochemistry*, **45**, 6529–6540.

Rao, A.G. (1999) Conformation and Antimicrobial Activity of Linear Derivatives of Tachyplesin Lacking Disulfide Bonds. *Archives of Biochemistry and Biophysics*, **361**, 127–134.

Rao, J.N., Kim, Y.E., Park, L.S., & Ulmer, T.S. (2009) Effect of pseudorepeat rearrangement on alpha-synuclein misfolding, vesicle binding, and micelle binding. *J. Mol. Biol.*, **390**, 516–529.

Ravussin, E., Smith, S.R., Mitchell, J.A., Shringarpure, R., Shan, K., Maier, H., Koda, J.E., & Weyer, C. (2009) Enhanced weight loss with pramlintide/metreleptin: an integrated neurohormonal approach to obesity pharmacotherapy. *Obesity (Silver Spring)*, **17**, 1736–1743.

Richardson, J.S. & Richardson, D.C. (2002) Natural β-sheet proteins use negative design to avoid edge-to-edge aggregation. *Proc. Natl. Acad. Sci. U. S. A.*, **99**, 2754–2759.

Rink, T.J., Beaumont, K., Koda, J., & Young, A. (1993) Structure and biology of amylin. *Trends Pharmacol. Sci.*, **14**, 113–118.

Ritzel, R.A., Meier, J.J., Lin, C.-Y., Veldhuis, J.D., & Butler, P.C. (2007) Human islet amyloid polypeptide oligomers disrupt cell coupling, induce apoptosis, and impair insulin secretion in isolated human islets. *Diabetes*, **56**, 65–71.

Roberts, A.N., Leighton, B., Todd, J.A., Cockburn, D., Schofield, P.N., Sutton, R., Holt, S., Boyd, Y., Day, A.J., & Foot, E.A. (1989) Molecular and functional characterization of amylin, a peptide associated with type 2 diabetes mellitus. *Proc. Natl. Acad. Sci. U. S. A.*, **86**, 9662–9666.

Robinson, J.A., Shankaramma, S.C., Jetter, P., Kienzl, U., Schwendener, R.A., Vrijbloed, J.W., & Obrecht, D. (2005) Properties and structure–activity studies of cyclic β-hairpin peptidomimetics based on the cationic antimicrobial peptide protegrin I. *Bioorganic & Medicinal Chemistry*, **13**, 2055–2064.

Rochet, J.C. & Lansbury, P.T. (2000) Amyloid fibrillogenesis: themes and variations. *Curr. Opin. Struct. Biol.*, **10**, 60–68.

Rössger, K., Charpin-El-Hamri, G., & Fussenegger, M. (2013) A closed-loop synthetic gene circuit for the treatment of diet-induced obesity in mice. *Nat Commun*, **4**, 2825.

Rothstein, D.M., Spacciapoli, P., Tran, L.T., Xu, T., Roberts, F.D., Serra, M.D., Buxton, D.K., Oppenheim, F.G., & Friden, P. (2001) Anticandida Activity Is Retained in P-113, a 12-Amino-Acid Fragment of Histatin 5. *Antimicrob. Agents Chemother.*, **45**, 1367–1373.

Ruschak, A.M. & Miranker, A.D. (2007) Fiber-dependent amyloid formation as catalysis of an existing reaction pathway. *Proc. Natl. Acad. Sci. U. S. A.*, **104**, 12341–12346.

Ruzza, P., Siligardi, G., Hussain, R., Marchiani, A., Islami, M., Bubacco, L., Delogu, G., Fabbri, D., Dettori, M.A., Sechi, M., Pala, N., Spissu, Y., Migheli, R., Serra, P.A., & Sechi, G. (2014) Ceftriaxone blocks the polymerization of α-synuclein and exerts neuroprotective effects in vitro. *ACS Chem Neurosci*, **5**, 30–38.

Sajjan, U.S., Tran, L.T., Sole, N., Rovaldi, C., Akiyama, A., Friden, P.M., Forstner, J.F., & Rothstein, D.M. (2001) P-113d, an Antimicrobial Peptide Active againstPseudomonas aeruginosa, Retains Activity in the Presence of Sputum from Cystic Fibrosis Patients. *Antimicrob. Agents Chemother.*, **45**, 3437–3444.

Salomón, R.A. & Farías, R.N. (1992) Microcin 25, a novel antimicrobial peptide produced by Escherichia coli. *J. Bacteriol.*, **174**, 7428–7435.

Salveson, P.J., Spencer, R.K., & Nowick, J.S. (2016) X-ray Crystallographic Structure of Oligomers Formed by a Toxic β-Hairpin Derived from α-Synuclein: Trimers and Higher-Order Oligomers. *J. Am. Chem. Soc.*, **138**, 4458–4467.

Samsom, M., Szarka, L.A., Camilleri, M., Vella, A., Zinsmeister, A.R., & Rizza, R.A. (2000) Pramlintide, an amylin analog, selectively delays gastric emptying: potential role of vagal inhibition. *Am. J. Physiol-Gastr. L.*, **278**, G946–G951.

Samuel, F., Flavin, W.P., Iqbal, S., Pacelli, C., Sri Renganathan, S.D., Trudeau, L.-E., Campbell, E.M., Fraser, P.E., & Tandon, A. (2016) Effects of Serine 129 Phosphorylation on α-Synuclein Aggregation, Membrane Association, and Internalization. *J. Biol. Chem.*, **291**, 4374–4385.

Sanke, T., Bell, G.I., Sample, C., Rubenstein, A.H., & Steiner, D.F. (1988) An islet amyloid peptide is derived from an 89-amino acid precursor by proteolytic processing. *J. Biol. Chem.*, **263**, 17243–17246.

Sato, H., Arawaka, S., Hara, S., Fukushima, S., Koga, K., Koyama, S., & Kato, T. (2011) Authentically phosphorylated α-synuclein at Ser129 accelerates neurodegeneration in a rat model of familial Parkinson's disease. *J. Neurosci.*, **31**, 16884–16894.

Sawaya, M.R., Sambashivan, S., Nelson, R., Ivanova, M.I., Sievers, S.A., Apostol, M.I., Thompson, M.J., Balbirnie, M., Wiltzius, J.J.W., McFarlane, H.T., Madsen, A.Ø., Riekel, C., & Eisenberg, D. (2007) Atomic structures of amyloid cross-beta spines reveal varied steric zippers. *Nature*, **447**, 453–457.

Scherbaum, W.A. (1998) The role of amylin in the physiology of glycemic control. *Experimental and Clinical Endocrinology & Diabetes*, **106**, 97–102.

Schneeberger, A., Mandler, M., Mattner, F., & Schmidt, W. (2010) AFFITOME® technology in neurodegenerative diseases: The doubling advantage. *Human Vaccines*, **6**, 948–952.

Schubert, D., Behl, C., Lesley, R., Brack, A., Dargusch, R., Sagara, Y., & Kimura, H. (1995) Amyloid peptides are toxic via a common oxidative mechanism. *Proc. Natl. Acad. Sci. U. S. A.*, **92**, 1989–1993.

Scrocchi, L.A., Chen, Y., Waschuk, S., Wang, F., Cheung, S., Darabie, A.A., McLaurin, J., & Fraser, P.E. (2002) Design of Peptide-based Inhibitors of Human Islet Amyloid Polypeptide Fibrillogenesis. *Journal of Molecular Biology*, **318**, 697–706.

Searle, M.S., Williams, D.H., & Packman, L.C. (1995) A short linear peptide derived from the N-terminal sequence of ubiquitin folds into a water-stable non-native beta-hairpin. *Nat. Struct. Biol.*, **2**, 999–1006.

Serpell, L.C., Berriman, J., Jakes, R., Goedert, M., & Crowther, R.A. (2000) Fiber diffraction of synthetic α-synuclein filaments shows amyloid-like cross-β conformation. *Proc. Natl. Acad. Sci. U.S.A.*, **97**, 4897–4902.

Serrano, L. & Fersht, A.R. (1989) Capping and alpha-helix stability. *Nature*, **342**, 296–299.

Shai, Y. (1999) Mechanism of the binding, insertion and destabilization of phospholipid bilayer membranes by α-helical antimicrobial and cell non-selective membrane-lytic peptides. *Biochim. Biophys. Acta*, **1462**, 55–70.

Shai, Y. (2002) Mode of action of membrane active antimicrobial peptides. *Biopolymers*, **66**, 236–248.

Shankaramma, S.C., Athanassiou, Z., Zerbe, O., Moehle, K., Mouton, C., Bernardini, F., Vrijbloed, J.W., Obrecht, D., & Robinson, J.A. (2002) Macrocyclic Hairpin Mimetics of the Cationic Antimicrobial Peptide Protegrin I: A New Family of Broad-Spectrum Antibiotics. *ChemBioChem*, **3**, 1126–1133.

Shim, S.-H., Gupta, R., Ling, Y.L., Strasfeld, D.B., Raleigh, D.P., & Zanni, M.T. (2009) Two-dimensional IR spectroscopy and isotope labeling defines the pathway of amyloid formation with residue-specific resolution. *Proc. Natl. Acad. Sci. U.S.A.*, **106**, 6614–6619.

Sibanda, B.L. & Thornton, J.M. (1991) [5] Conformation of β hairpins in protein structures: Classification and diversity in homologous structures. In Enzymology, B.-M. in (ed), *Molecular Design and Modeling: Concepts and Applications Part A: Proteins, Peptides, and Enzymes*. Academic Press, pp. 59–82.

Silva, P.I., Daffre, S., & Bulet, P. (2000) Isolation and Characterization of Gomesin, an 18-Residue Cysteine-rich Defense Peptide from the Spider Acanthoscurria gomesiana Hemocytes with Sequence Similarities to Horseshoe Crab Antimicrobial Peptides of the Tachyplesin Family. *J. Biol. Chem.*, **275**, 33464–33470.

Silvestre, R.A., Rodríguez-Gallardo, J., Jodka, C., Parkes, D.G., Pittner, R.A., Young, A.A., & Marco, J. (2001) Selective amylin inhibition of the glucagon response to arginine is extrinsic to the pancreas. *Am. J. Physiol. Endocrinol. Metab.*, **280**, E443-449.

Silvestro, L., Weiser, J.N., & Axelsen, P.H. (2000) Antibacterial and Antimembrane Activities of Cecropin A in Escherichia coli. *Antimicrob. Agents Chemother.*, **44**, 602–607.

Sivanesam, K., Byrne, A., Bisaglia, M., Bubacco, L., & Andersen, N. (2015) Binding interactions of agents that alter α-synuclein aggregation. *RSC Adv.*, **5**, 11577–11590.

Sivanesam, K., Kier, B.L., Whedon, S.D., Chatterjee, C., & Andersen, N.H. (2016) Hairpin structure stability plays a role in the activity of two antimicrobial peptides. *FEBS Lett.*, **590**, 4480–4488.

Sivanesam, K., Shu, I., Huggins, K.N.L., Tatarek-Nossol, M., Kapurniotu, A., & Andersen, N.H. (2016) Peptide Inhibitors of the amyloidogenesis of IAPP: verification of the hairpin-binding geometry hypothesis. *FEBS Lett.*, **590**, 2575–2583.

Smith, T.J., Stains, C.I., Meyer, S.C., & Ghosh, I. (2006) Inhibition of β-Amyloid Fibrillization by Directed Evolution of a β-Sheet Presenting Miniature Protein. *J. Am. Chem. Soc.*, **128**, 14456–14457.

Spear, G.S., Caple, M.V., & Sutherland, L.R. (1984) The pancreas in the degu. *Exp. Mol. Pathol.*, **40**, 295–310.

Subbalakshmi, C. & Sitaram, N. (1998) Mechanism of antimicrobial action of indolicidin. *FEMS Microbiol Lett*, **160**, 91–96.

Suk, J.-E., Lokappa, S.B., & Ulmer, T.S. (2010) The clustering and spatial arrangement of beta-sheet sequence, but not order, govern alpha-synuclein fibrillogenesis. *Biochemistry*, **49**, 1533–1540.

Susa, A.C., Wu, C., Bernstein, S.L., Dupuis, N.F., Wang, H., Raleigh, D.P., Shea, J.-E., & Bowers, M.T. (2014) Defining the molecular basis of amyloid inhibitors: human islet amyloid polypeptide-insulin interactions. *J. Am. Chem. Soc.*, **136**, 12912–12919.

Sveinbjörnsdottir, S., Hicks, A.A., Jonsson, T., Pétursson, H., Guğmundsson, G., Frigge, M.L., Kong, A., Gulcher, J.R., & Stefansson, K. (2000) Familial aggregation of Parkinson's disease in Iceland. *N. Engl. J. Med.*, **343**, 1765–1770.

Tam, J.P., Wu, C., & Yang, J.-L. (2000) Membranolytic selectivity of cystine-stabilized cyclic protegrins. *Eur. J. Biochem.*, **267**, 3289–3300.

Taniguchi, S., Suzuki, N., Masuda, M., Hisanaga, S., Iwatsubo, T., Goedert, M., & Hasegawa, M. (2005) Inhibition of heparin-induced tau filament formation by phenothiazines, polyphenols, and porphyrins. *J. Biol. Chem.*, **280**, 7614–7623.

Tatarek-Nossol, M., Yan, L.-M., Schmauder, A., Tenidis, K., Westermark, G., & Kapurniotu, A. (2005) Inhibition of hIAPP amyloid-fibril formation and apoptotic cell death by a designed hIAPP amyloid- core-containing hexapeptide. *Chem. Biol.*, **12**, 797–809.

Telfer, S.G., McLean, T.M., & Waterland, M.R. (2011) Exciton coupling in coordination compounds. *Dalton Trans.*, **40**, 3097–3108.

Tenidis, K., Waldner, M., Bernhagen, J., Fischle, W., Bergmann, M., Weber, M., Merkle, M.-L., Voelter, W., Brunner, H., & Kapurniotu, A. (2000) Identification of a penta- and hexapeptide of islet amyloid polypeptide (IAPP) with amyloidogenic and cytotoxic properties1. *J. Mol. Biol.*, **295**, 1055–1071.

Thompson, R.G., Gottlieb, A., Organ, K., Koda, J., Kisicki, J., & Kolterman, O.G. (1997) Pramlintide: a human amylin analogue reduced postprandial plasma glucose, insulin, and C-peptide concentrations in patients with type 2 diabetes. *Diabet. Med.*, **14**, 547–555.

Tomiyama, T., Kaneko, H., Kataoka, K. i, Asano, S., & Endo, N. (1997) Rifampicin inhibits the toxicity of pre-aggregated amyloid peptides by binding to peptide fibrils and preventing amyloid-cell interaction. *Biochem. J.*, **322 (Pt 3)**, 859–865.

Tracz, S.M., Abedini, A., Driscoll, M., & Raleigh, D.P. (2004) Role of Aromatic Interactions in Amyloid Formation by Peptides Derived from Human Amylin. *Biochemistry*, **43**, 15901–15908.

Tripathi, P., Beaussart, A., Andre, G., Rolain, T., Lebeer, S., Vanderleyden, J., Hols, P., & Dufrêne, Y.F. (2012) Towards a nanoscale view of lactic acid bacteria. *Micron*, **43**, 1323–1330.

Tu, L.-H. & Raleigh, D.P. (2013) Role of Aromatic Interactions in Amyloid Formation by Islet Amyloid Polypeptide. *Biochemistry*, **52**, 333–342.

Tu, L.-H., Young, L.M., Wong, A.G., Ashcroft, A.E., Radford, S.E., & Raleigh, D.P. (2015) Mutational analysis of the ability of resveratrol to inhibit amyloid formation by islet amyloid polypeptide: critical evaluation of the importance of aromatic-inhibitor and histidine-inhibitor interactions. *Biochemistry*, **54**, 666–676.

Turner, J., Cho, Y., Dinh, N.N., Waring, A.J., & Lehrer, R.I. (1998) Activities of LL-37, a cathelin-associated antimicrobial peptide of human neutrophils. *Antimicrob. Agents Chemother.*, **42**, 2206–2214.

Ulmer, T.S., Bax, A., Cole, N.B., & Nussbaum, R.L. (2005) Structure and dynamics of micelle-bound human alpha-synuclein. *J. Biol. Chem.*, **280**, 9595–9603.

Ulrih, N.P., Barry, C.H., & Fink, A.L. (2008) Impact of Tyr to Ala mutations on alpha-synuclein fibrillation and structural properties. *Biochim. Biophys. Acta*, **1782**, 581–585.

Vassar, P.S. & Culling, C.F. (1959) Fluorescent stains, with special reference to amyloid and connective tissues. *Arch Pathol*, **68**, 487–498.

Velander, P., Wu, L., Ray, W.K., Helm, R.F., & Xu, B. (2016) Amylin Amyloid Inhibition by Flavonoid Baicalein: Key Roles of Its Vicinal Dihydroxyl Groups of the Catechol Moiety. *Biochemistry*, **55**, 4255–4258.

Venkatachalam, C.M. (1968) Stereochemical criteria for polypeptides and proteins. V. Conformation of a system of three linked peptide units. *Biopolymers*, **6**, 1425–1436.

Verkleij, A.J., Zwaal, R.F., Roelofsen, B., Comfurius, P., Kastelijn, D., & van Deenen, L.L. (1973) The asymmetric distribution of phospholipids in the human red cell membrane. A combined study using phospholipases and freeze-etch electron microscopy. *Biochim. Biophys. Acta*, **323**, 178–193.

Vilar, M., Chou, H.-T., Luhrs, T., Maji, S.K., Riek-Loher, D., Verel, R., Manning, G., Stahlberg, H., & Riek, R. (2008) The fold of alpha-synuclein fibrils. *Proc. Natl. Acad. Sci.U. S. A.*, **105**, 8637–8642.

Wang, H., Ridgway, Z., Cao, P., Ruzsicska, B., & Raleigh, D.P. (2015) Analysis of the Ability of Pramlintide To Inhibit Amyloid Formation by Human Islet Amyloid Polypeptide Reveals a Balance between Optimal Recognition and Reduced Amyloidogenicity. *Biochemistry*, **54**, 6704–6711.

Westermark, P. (1973) Fine structure of islets of Langerhans in insular amyloidosis. *Virchows Arch A Pathol Pathol Anat*, **359**, 1–18.

Westermark, P., Andersson, A., & Westermark, G.T. (2011) Islet amyloid polypeptide, islet amyloid, and diabetes mellitus. *Physiol. Rev.*, **91**, 795–826.

Westermark, P., Engström, U., Johnson, K.H., Westermark, G.T., & Betsholtz, C. (1990) Islet amyloid polypeptide: pinpointing amino acid residues linked to amyloid fibril formation. *Proc. Natl. Acad. Sci. U.S.A.*, **87**, 5036–5040.

Westermark, P., Li, Z.C., Westermark, G.T., Leckström, A., & Steiner, D.F. (1996) Effects of beta cell granule components on human islet amyloid polypeptide fibril formation. *FEBS Lett.*, **379**, 203–206.

Westermark, P., Wernstedt, C., O'Brien, T.D., Hayden, D.W., & Johnson, K.H. (1987) Islet amyloid in type 2 human diabetes mellitus and adult diabetic cats contains a novel putative polypeptide hormone. *Am. J. Pathol.*, **127**, 414–417.

Westermark, P., Wernstedt, C., Wilander, E., Hayden, D.W., O'Brien, T.D., & Johnson, K.H. (1987) Amyloid fibrils in human insulinoma and islets of Langerhans of the diabetic cat are derived from a neuropeptide-like protein also present in normal islet cells. *Proc. Natl. Acad. Sci. U.S.A.*, **84**, 3881–3885.

Westermark, P., Wernstedt, C., Wilander, E., & Sletten, K. (1986) A novel peptide in the calcitonin gene related peptide family as an amyloid fibril protein in the endocrine pancreas. *Biochem. Biophys. Res. Commun.*, **140**, 827–831.

White, S.H., Wimley, W.C., & Selsted, M.E. (1995) Structure, function, and membrane integration of defensins. *Curr. Opin. Struct. Biol.*, **5**, 521–527.

Williamson, J.A., Loria, J.P., & Miranker, A.D. (2009) Helix Stabilization Precedes Aqueous and Bilayer-Catalyzed Fiber Formation in Islet Amyloid Polypeptide. *J. Mol. Biol.*, **393**, 383–396.

Williamson, J.A. & Miranker, A.D. (2007) Direct detection of transient α-helical states in islet amyloid polypeptide. *Prot. Sci.*, **16**, 110–117.

Wiltzius, J.J.W., Sievers, S.A., Sawaya, M.R., Cascio, D., Popov, D., Riekel, C., & Eisenberg, D. (2008) Atomic structure of the cross-beta spine of islet amyloid polypeptide (amylin). *Prot. Sci.*, **17**, 1467–1474.

Wiltzius, J.J.W., Sievers, S.A., Sawaya, M.R., & Eisenberg, D. (2009) Atomic structures of IAPP (amylin) fusions suggest a mechanism for fibrillation and the role of insulin in the process. *Prot. Sci.*, **18**, 1521–1530.

Winner, B., Jappelli, R., Maji, S.K., Desplats, P.A., Boyer, L., Aigner, S., Hetzer, C., Loher, T., Vilar, M., Campioni, S., Tzitzilonis, C., Soragni, A., Jessberger, S., Mira, H., Consiglio, A., Pham, E., Masliah, E., Gage, F.H., & Riek, R. (2011) In vivo demonstration that α-synuclein oligomers are toxic. *Proc. Natl. Acad. Sci. U.S.A.*, **108**, 4194–4199.

Woods, W.S., Boettcher, J.M., Zhou, D.H., Kloepper, K.D., Hartman, K.L., Ladror, D.T., Qi, Z., Rienstra, C.M., & George, J.M. (2007) Conformation-specific binding of alpha-synuclein to novel protein partners detected by phage display and NMR spectroscopy. *J. Biol. Chem.*, **282**, 34555–34567.

Wright, G.D. (2000) Resisting resistance: new chemical strategies for battling superbugs. *Chemistry & Biology*, **7**, R127–R132.

Wu, C., Wang, Z., Lei, H., Duan, Y., Bowers, M.T., & Shea, J.-E. (2008) The binding of thioflavin T and its neutral analog BTA-1 to protofibrils of the Alzheimer's disease Abeta(16-22) peptide probed by molecular dynamics simulations. *J. Mol. Biol.*, **384**, 718–729.

Wu, Y., Li, X., Zhu, J.X., Xie, W., Le, W., Fan, Z., Jankovic, J., & Pan, T. (2011) Resveratrol-Activated AMPK/SIRT1/Autophagy in Cellular Models of Parkinson's Disease. *Neurosignals*, **19**, 163–174.

Yan, L.-M., Tatarek-Nossol, M., Velkova, A., Kazantzis, A., & Kapurniotu, A. (2006) Design of a mimic of nonamyloidogenic and bioactive human islet amyloid polypeptide (IAPP) as

nanomolar affinity inhibitor of IAPP cytotoxic fibrillogenesis. *Proc. Natl. Acad. Sci. U.S.A.*, **103**, 2046–2051.

Yan, L.-M., Velkova, A., Tatarek-Nossol, M., Andreetto, E., & Kapurniotu, A. (2007) IAPP mimic blocks Abeta cytotoxic self-assembly: cross-suppression of amyloid toxicity of Abeta and IAPP suggests a molecular link between Alzheimer's disease and type II diabetes. *Angew. Chem. Int. Ed. Engl.*, **46**, 1246–1252.

Yanagi, K., Ashizaki, M., Yagi, H., Sakurai, K., Lee, Y.-H., & Goto, Y. (2011) Hexafluoroisopropanol Induces Amyloid Fibrils of Islet Amyloid Polypeptide by Enhancing Both Hydrophobic and Electrostatic Interactions. *J. Biol. Chem.*, **286**, 23959–23966.

Yang, L., Harroun, T.A., Weiss, T.M., Ding, L., & Huang, H.W. (2001) Barrel-stave model or toroidal model? A case study on melittin pores. *Biophys J*, **81**, 1475–1485.

Yang, L., Weiss, T.M., Harroun, T.A., Heller, W.T., & Huang, H.W. (1999) Supramolecular Structures of Peptide Assemblies in Membranes by Neutron Off-Plane Scattering: Method of Analysis. *Biophys. J.*, **77**, 2648–2656.

Yang, L., Weiss, T.M., Lehrer, R.I., & Huang, H.W. (2000) Crystallization of Antimicrobial Pores in Membranes: Magainin and Protegrin. *Biophysical Journal*, **79**, 2002–2009.

Yano, B.L., Hayden, D.W., & Johnson, K.H. (1981) Feline insular amyloid: association with diabetes mellitus. *Vet. Pathol.*, **18**, 621–627.

Yonemoto, I.T., Kroon, G.J.A., Dyson, H.J., Balch, W.E., & Kelly, J.W. (2008) Amylin Proprotein Processing Generates Progressively More Amyloidogenic Peptides that Initially Sample the Helical State. *Biochemistry*, **47**, 9900–9910.

Yonezawa, A., Kuwahara, J., Fujii, N., & Sugiura, Y. (1992) Binding of tachyplesin I to DNA revealed by footprinting analysis: significant contribution of secondary structure to DNA binding and implication for biological action. *Biochemistry*, **31**, 2998–3004.

Young, A.A., Vine, W., Gedulin, B.R., Pittner, R., Janes, S., Gaeta, L.S.L., Percy, A., Moore, C.X., Koda, J.E., Rink, T.J., & Beaumont, K. (1996) Preclinical pharmacology of pramlintide in the rat: Comparisons with human and rat amylin. *Drug Dev. Res.*, **37**, 231–248.

Yu, L., Fan, Q., Yue, X., Mao, Y., & Qu, L. (2015) Activity of a novel-designed antimicrobial peptide and its interaction with lipids. *J. Pept. Sci.*, **21**, 274–282.

Yu, L., Ran, Y., Bai, X.-X., Li, A.-R., Zhu, Y.-Y., Qin, Y., & Qu, L.-B. (2012) Design and Bioactivity of Novel Antimicrobial Peptides and Its Computer Simulation with Phospholipid. *Chem. J. Chinese U.*, **33**, 2681–2687.

Zarranz, J.J., Alegre, J., Gómez-Esteban, J.C., Lezcano, E., Ros, R., Ampuero, I., Vidal, L., Hoenicka, J., Rodriguez, O., Atarés, B., Llorens, V., Gomez Tortosa, E., del Ser, T., Muñoz, D.G., & de Yebenes, J.G. (2004) The new mutation, E46K, of alpha-synuclein causes Parkinson and Lewy body dementia. *Ann. Neurol.*, **55**, 164–173.

Zhang, S., Liu, H., Yu, H., & Cooper, G.J.S. (2008) Fas-associated death receptor signaling evoked by human amylin in islet beta-cells. *Diabetes*, **57**, 348–356.

Zhang, S., Liu, J., MacGibbon, G., Dragunow, M., & Cooper, G.J.S. (2002) Increased expression and activation of c-Jun contributes to human amylin-induced apoptosis in pancreatic islet beta-cells. *J. Mol. Biol.*, **324**, 271–285.

Zhang, S., Liu, J., Saafi, E.L., & Cooper, G.J. (1999) Induction of apoptosis by human amylin in RINm5F islet beta-cells is associated with enhanced expression of p53 and p21WAF1/CIP1. *FEBS Lett.*, **455**, 315–320.

Zhang, X., St. Clair, J.R., London, E., & Raleigh, D.P. (2017) Islet Amyloid Polypeptide Membrane Interactions: Effects of Membrane Composition. *Biochemistry*, **56**, 376–390.

Zhao, X., Wu, H., Lu, H., Li, G., & Huang, Q. (2013) LAMP: A Database Linking Antimicrobial Peptides. *PLoS ONE*, **8**, e66557.

Zheng, Z. & Diamond, M.I. (2012) Huntington disease and the huntingtin protein. *Prog Mol Biol Transl Sci*, **107**, 189–214.

Zhou, C., Emadi, S., Sierks, M.R., & Messer, A. (2004) A human single-chain Fv intrabody blocks aberrant cellular effects of overexpressed alpha-synuclein. *Mol. Ther.*, **10**, 1023–1031.

Zhu, M., Rajamani, S., Kaylor, J., Han, S., Zhou, F., & Fink, A.L. (2004) The flavonoid baicalein inhibits fibrillation of alpha-synuclein and disaggregates existing fibrils. *J. Biol. Chem.*, **279**, 26846–26857.

Appendix A

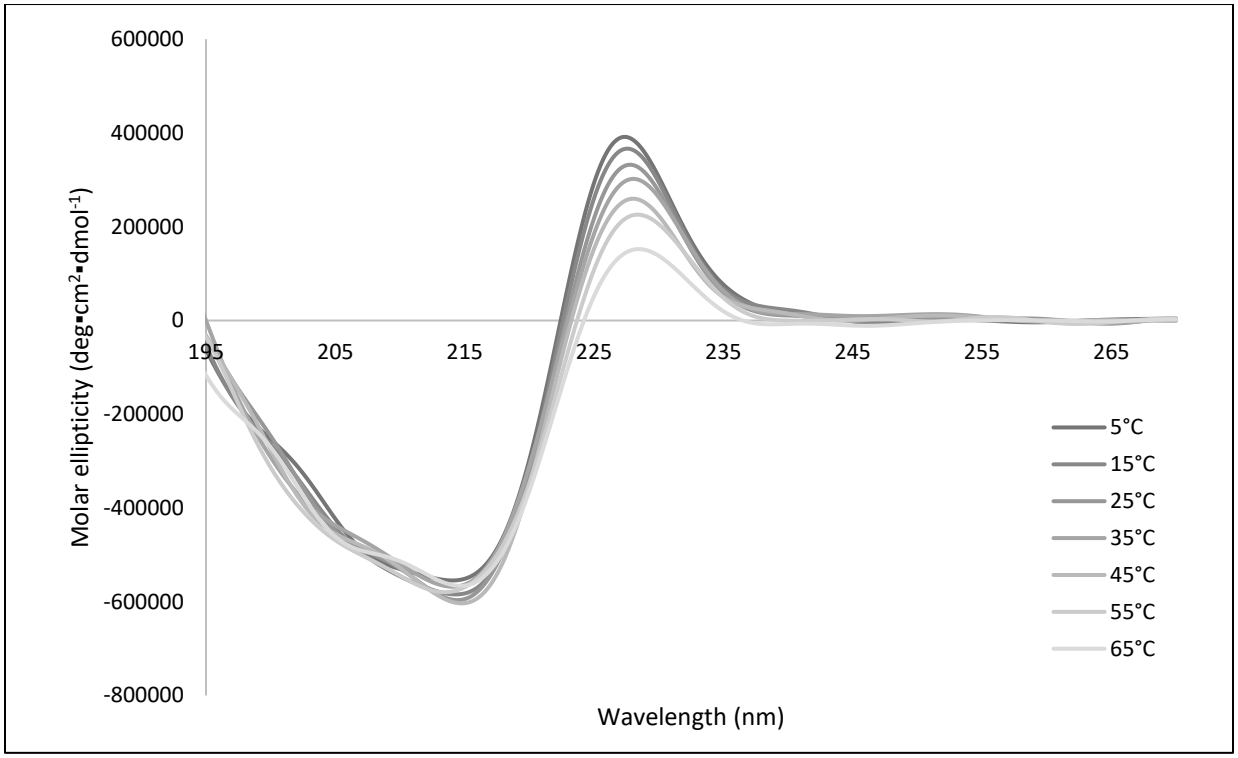

Appendix A1. CD spectrum of Ac-cap-WW taken from 5 °C to 65 °C at 10 °C intervals.

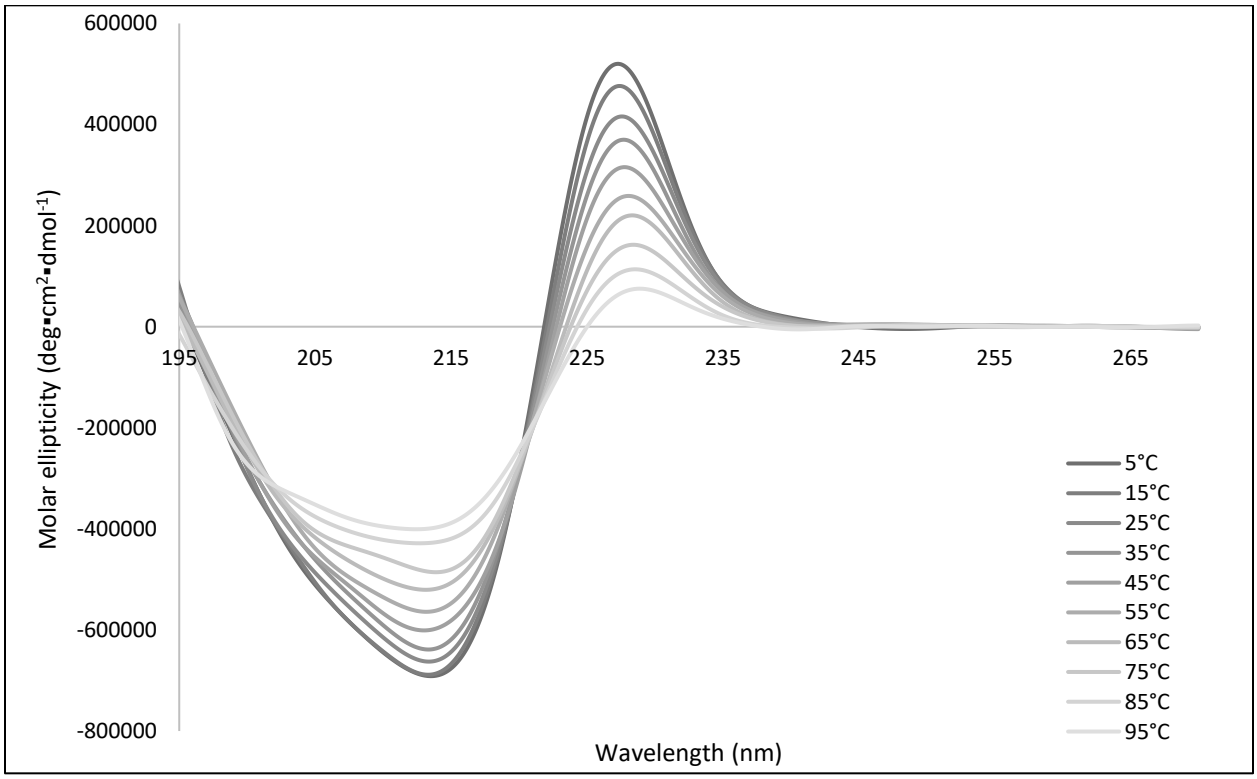

Appendix A2. CD spectrum of Bz-cap-WW taken from 5 °C to 95 °C at 10 °C intervals.

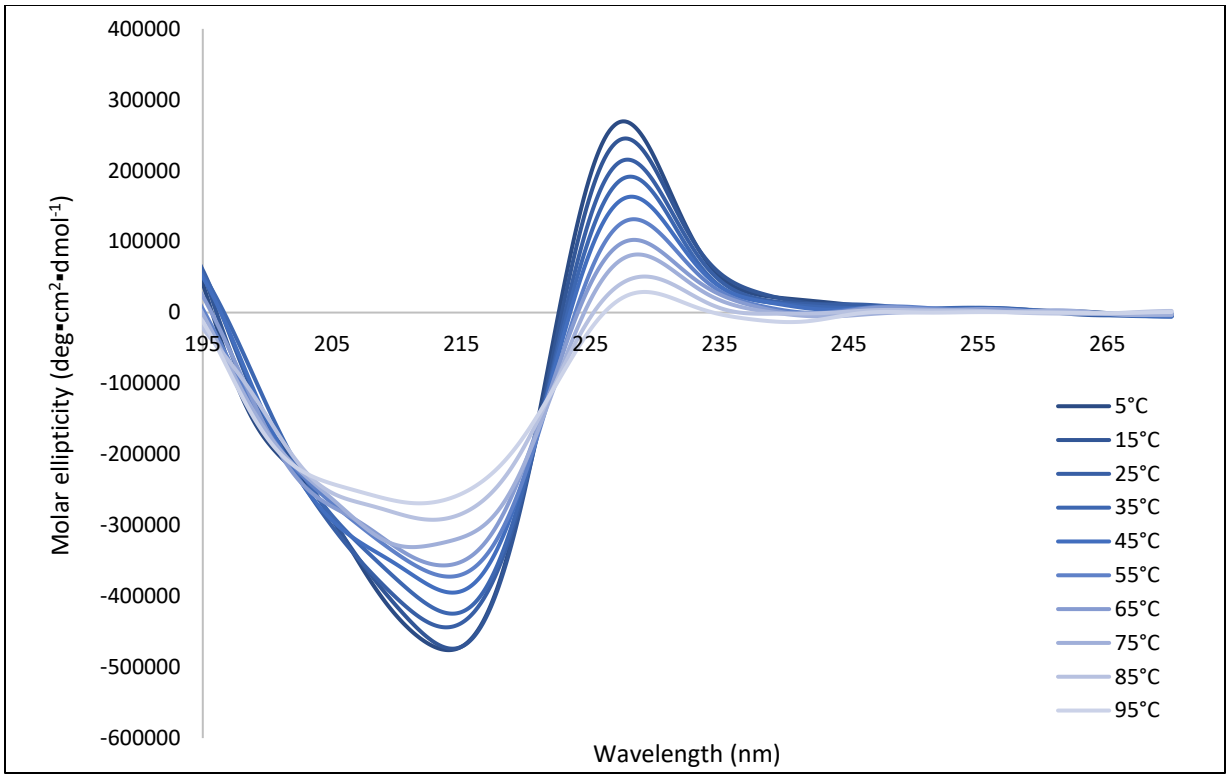

Appendix A3. CD spectrum of Gal-cap-WW taken from 5 °C to 95 °C at 10 °C intervals.

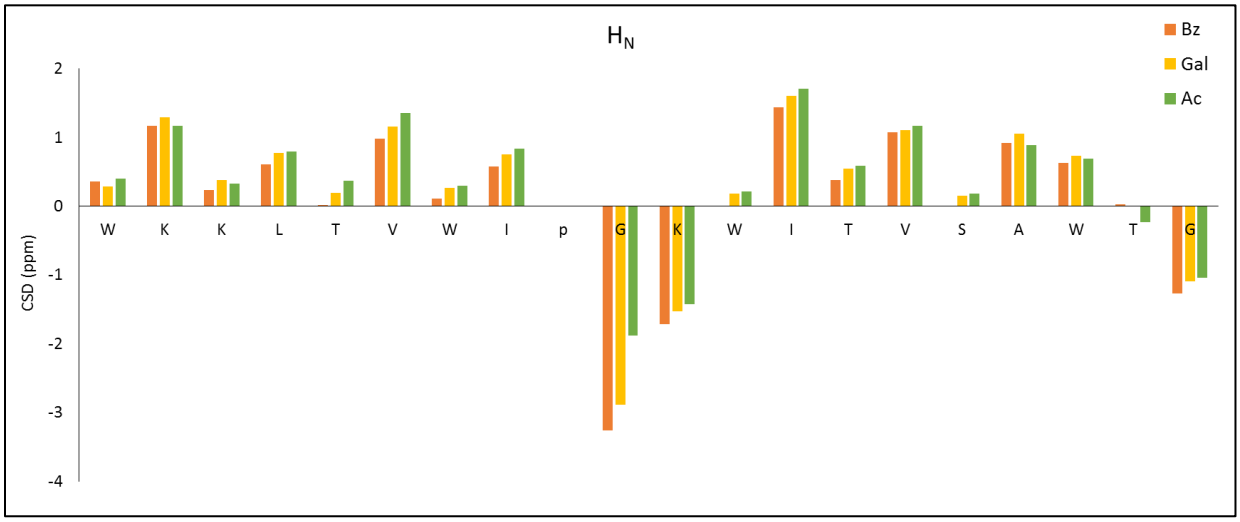

Appendix A4. Chemical shift deviations of backbone H_N for 3 peptides: Ac-cap-WW, Bz-cap-WW and Gal-cap-WW.

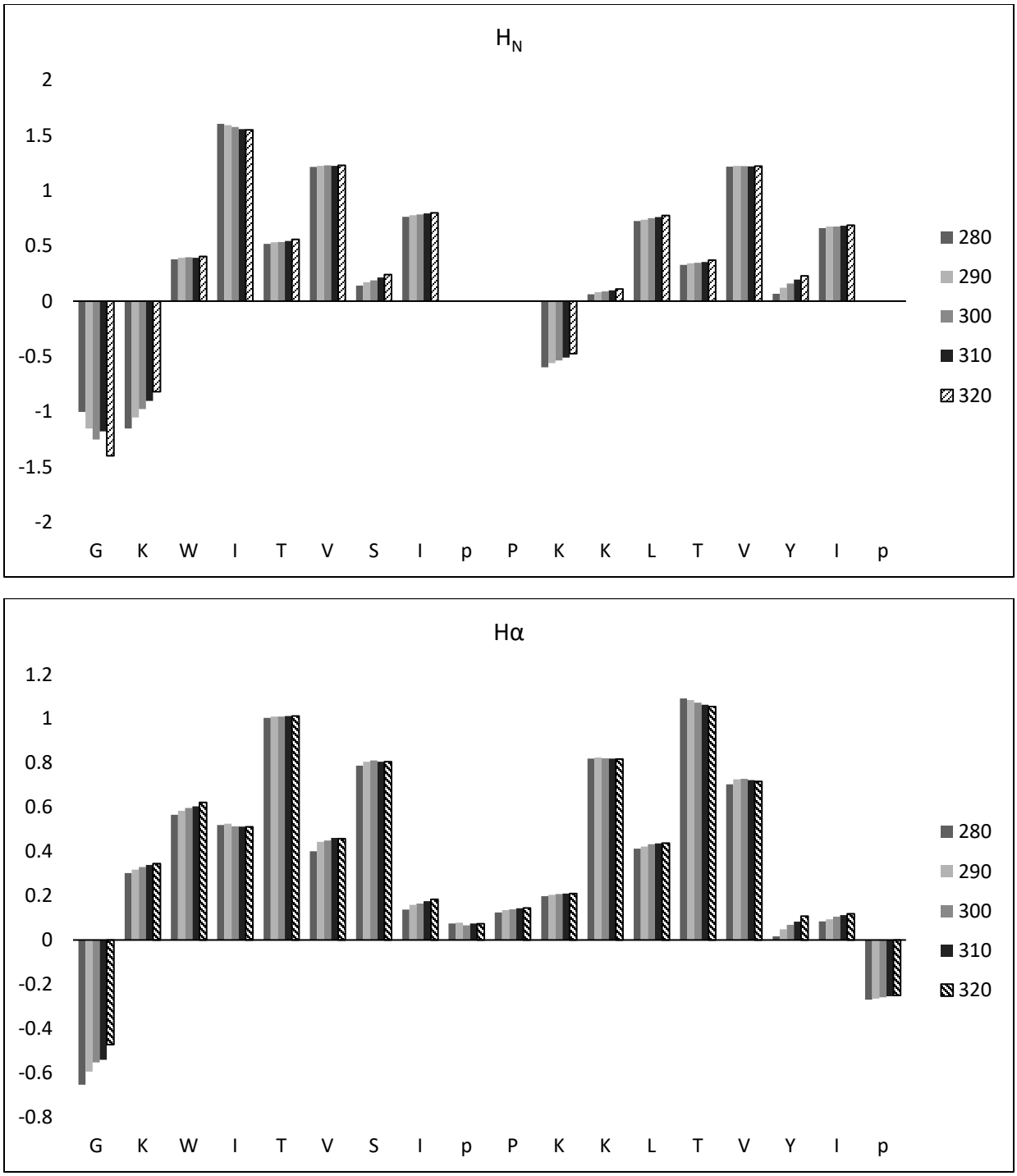

Appendix A5. Chemical shifts deviation for the backbone H_N and Hα of cyclo-WY at 280K, 290K, 300K, 310K and 320K. The lack of change in CSDs with temperature change indicates that the peptide has a highly stable hairpin structure.

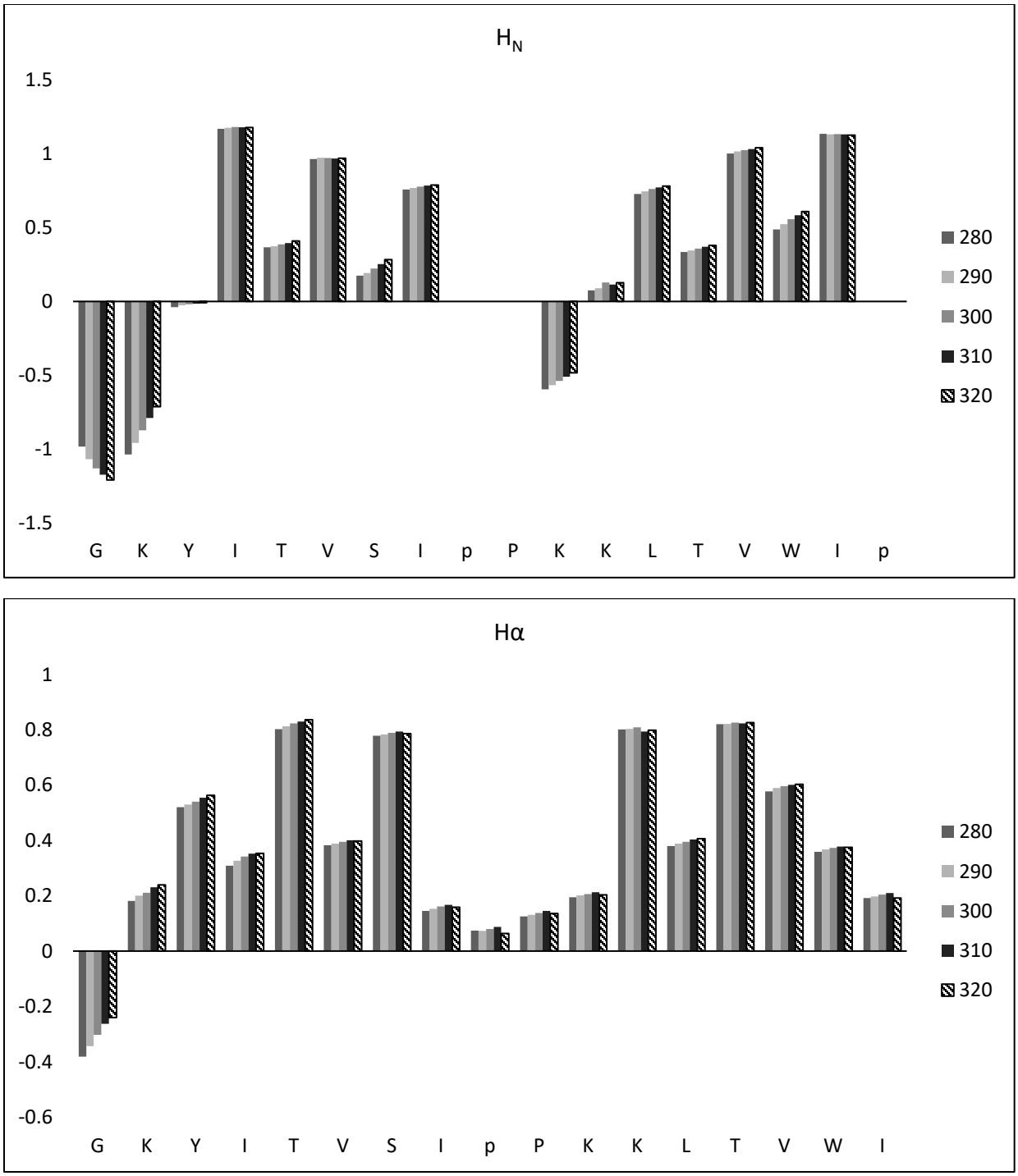

Appendix A6. Chemical shifts deviation for the backbone H_N and Hα of cyclo-YW at 280K, 290K, 300K, 310K and 320K. The lack of change in CSDs with temperature change indicates that the peptide has a highly stable hairpin structure.

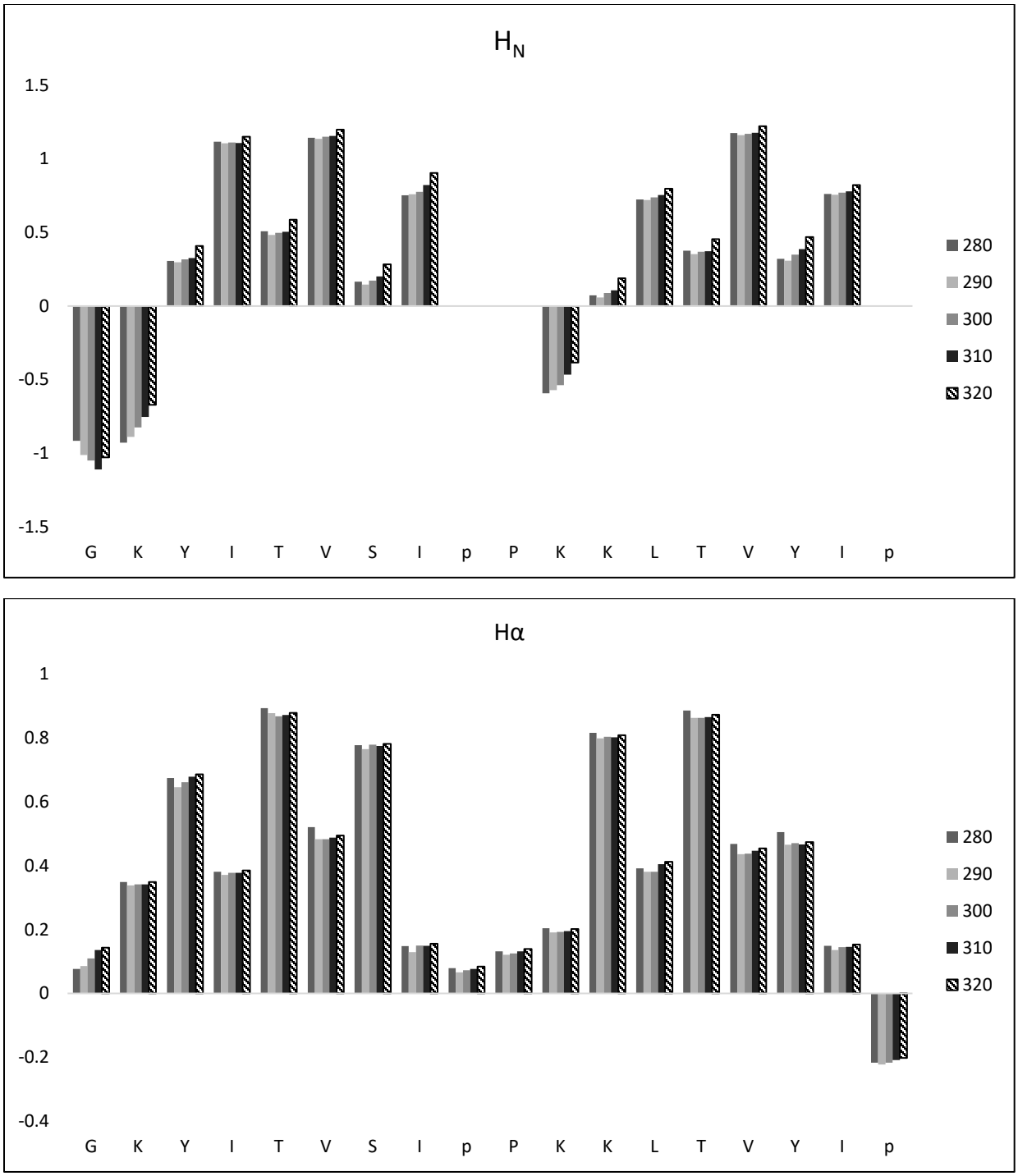

Appendix A7. Chemical shifts deviation for the backbone H_N and Hα of cyclo-YY at 280K, 290K, 300K, 310K and 320K. The lack of change in CSDs with temperature change indicates that the peptide has a highly stable hairpin structure.

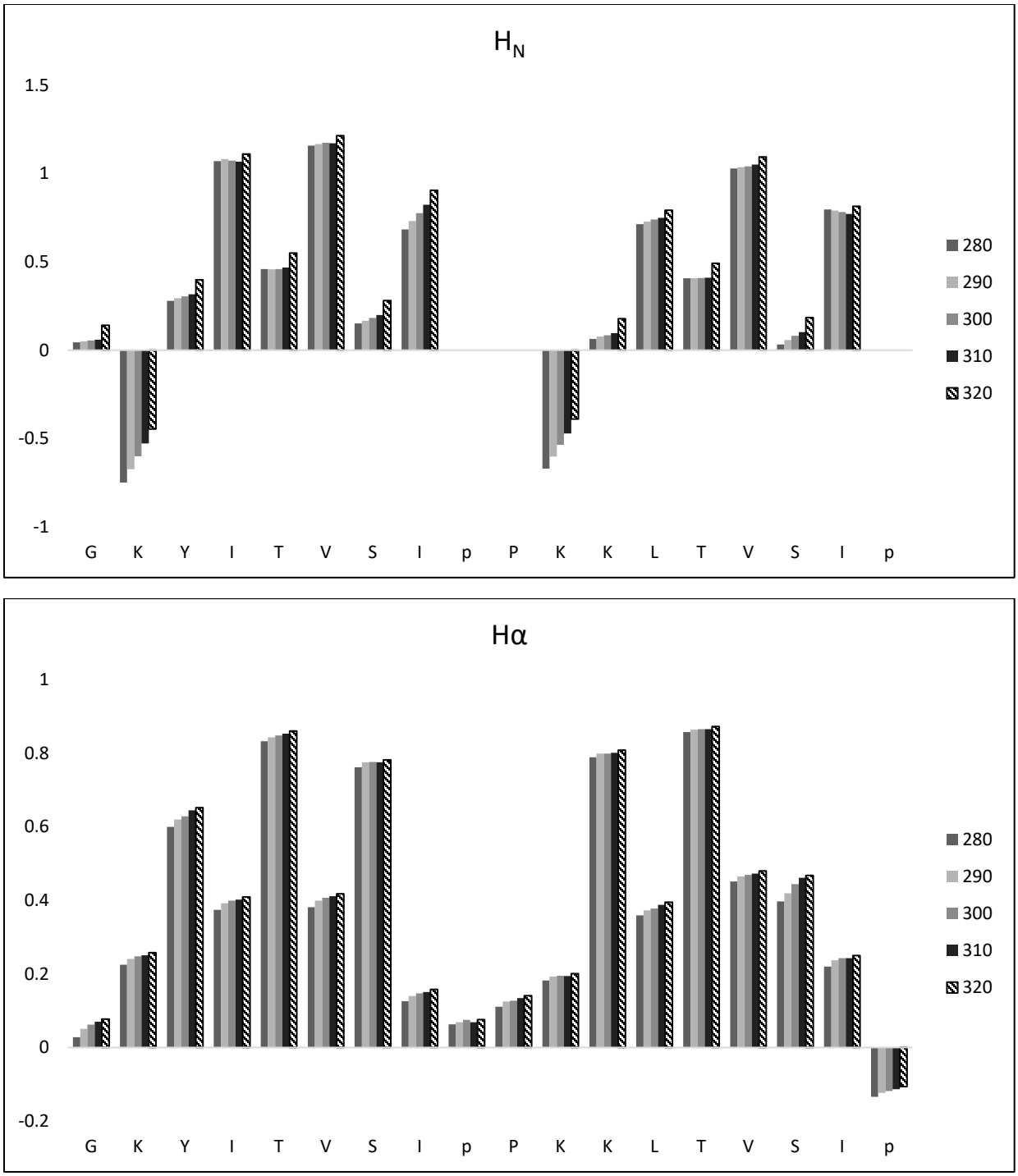

Appendix A8. Chemical shifts deviation for the backbone H_N and Hα of cyclo-YS at 280K, 290K, 300K, 310K and 320K. The lack of change in CSDs with temperature change indicates that the peptide has a highly stable hairpin structure.

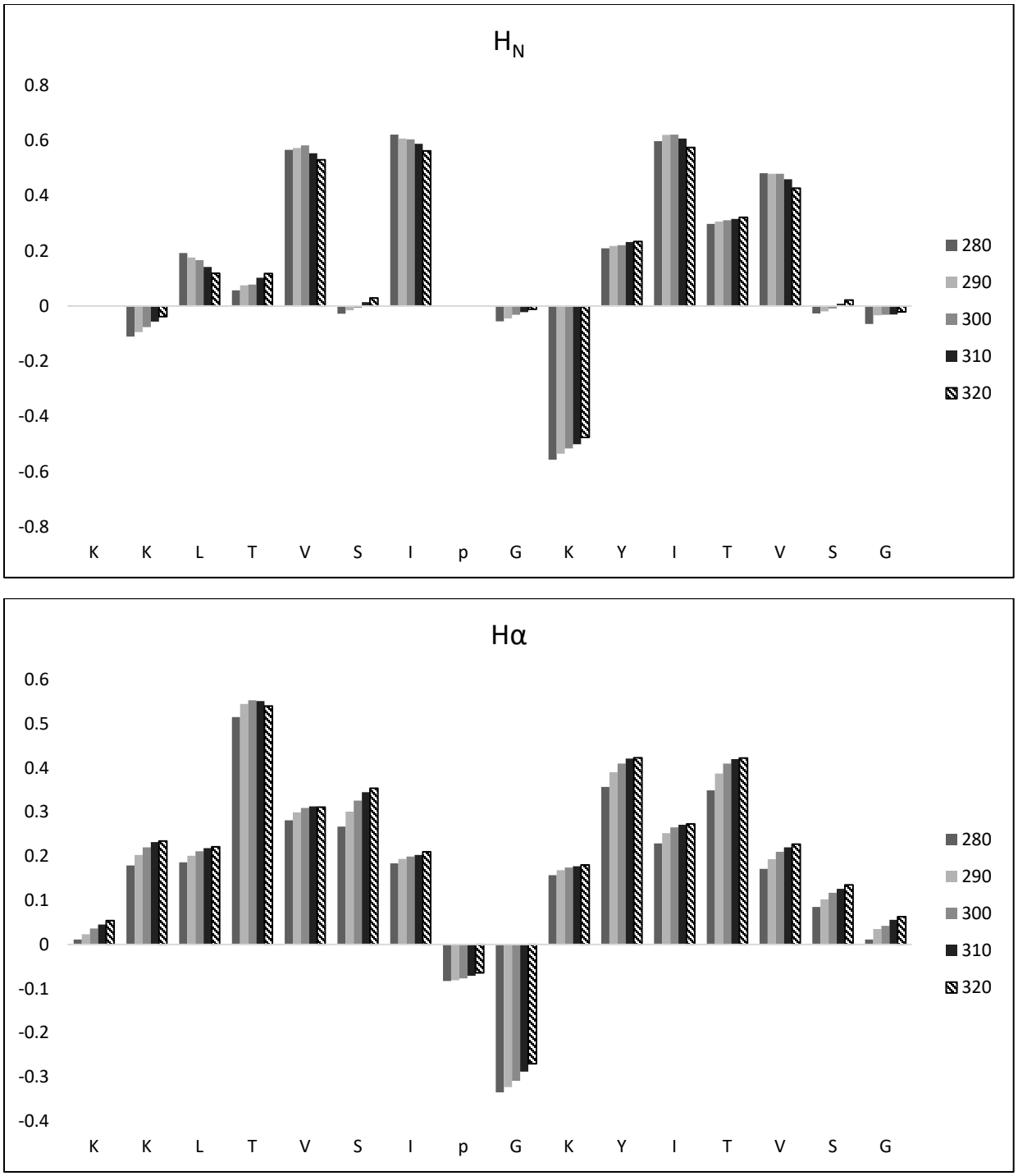

Appendix A9. Chemical shifts deviation for the backbone H_N and Hα of SY (uncyclized, non-circularly permuted analog of cyclo-YS) at 280K, 290K, 300K, 310K and 320K. The relatively small change in the CSDs as temperature is increased indicates that the fold population is not much changed over this temperature range, quite stable at up to 300K, but the smaller absolute CSD values compared to previous figure herein suggest that the hairpin population is smaller.

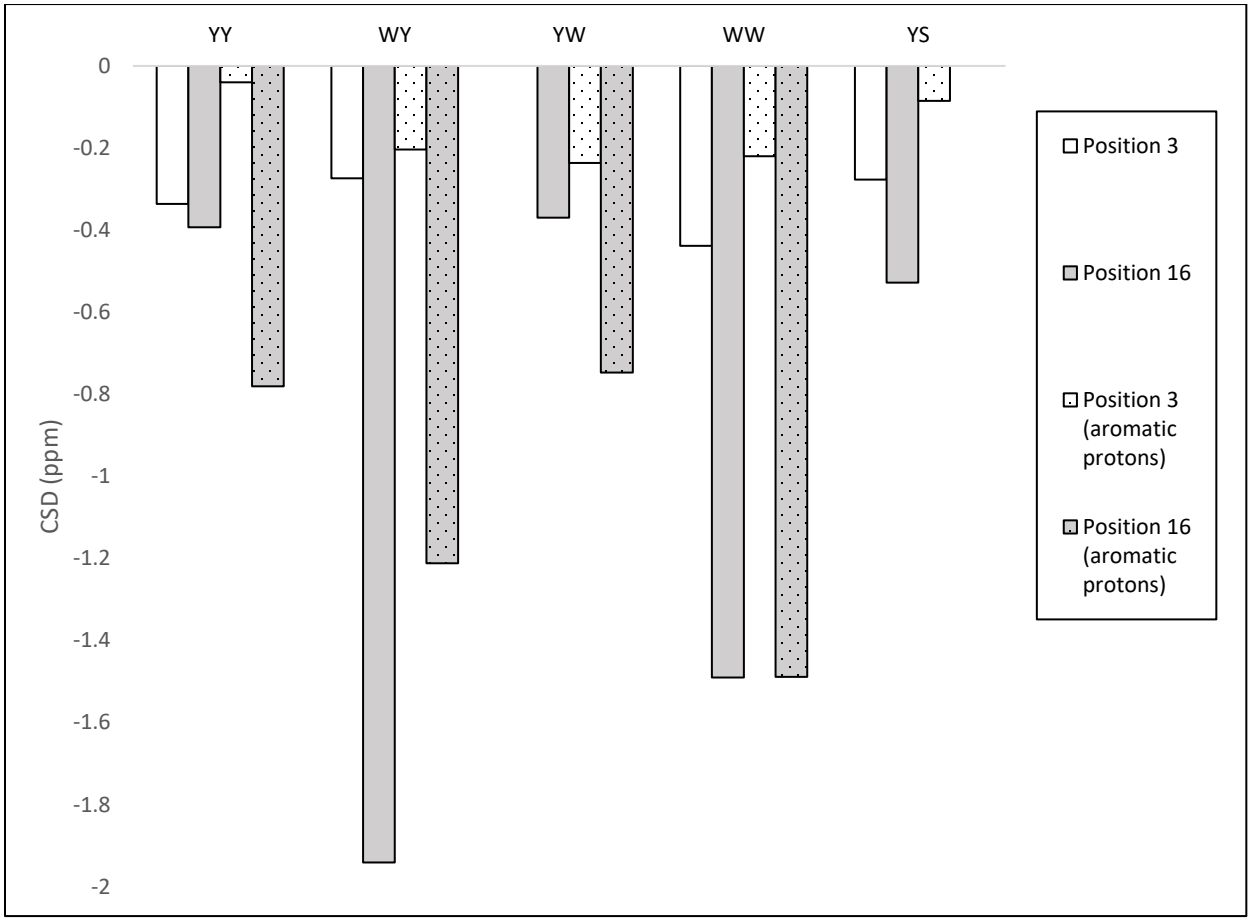

Appendix A10. Chemical shift deviations of select protons in all the cyclic peptides tested. Hβ3 and/ or the aromatic protons [Hδ -tyrosine residues; Hε3 - tryptophan residues] can be used to determine the edge-ring and the face-ring of an edge-to-face orientation. The data indicates that all four peptides with aromatic amino acids at both positions 3 and positions 16 have a strong edge-to-face interaction with the edge-ring at position 16 and the face-ring at position 3. For cyclo-YS, incapable of forming an edge-to-face aryl/aryl interaction, there is still a small amount of shielding experienced by serine, Hβ3 due to the cross-strand tyrosine aromatic ring. (See Chapter 1.4.2 for more details).

Appendix B

Note: All overlaid HSQC spectra shown here are zeroed by aligning the A140 peak at 130.6 ppm (ω_1-^{15}N) and 7.942 ppm (ω_2-^{1}H) since this peak shows no signs of peak attenuation or shifting in the presence of most inhibitors or over the course of time.

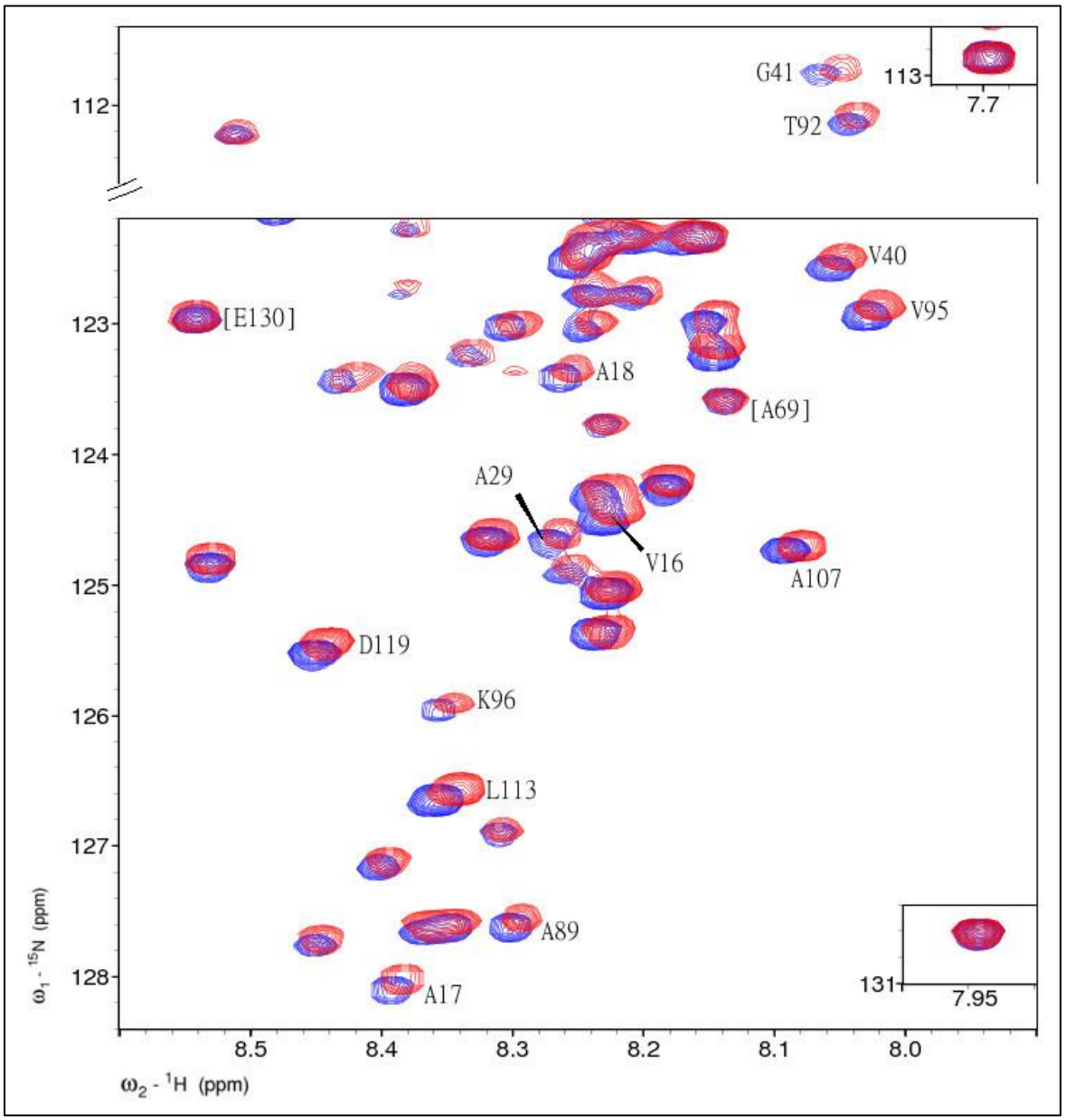

Appendix B1. 200 μM α-syn (dissolved in 50 mM phosphate buffer, pH 6.5) in the presence of 5 molar eq of EGCG (red) overlaid on a spectrum of α-syn collected in the absence of inhibitor (blue). Select peaks are labeled to show that shifting is occurring throughout the protein and is not confined to the C-terminus. (*Image adapted from Sivanesam* et al., *2015)*

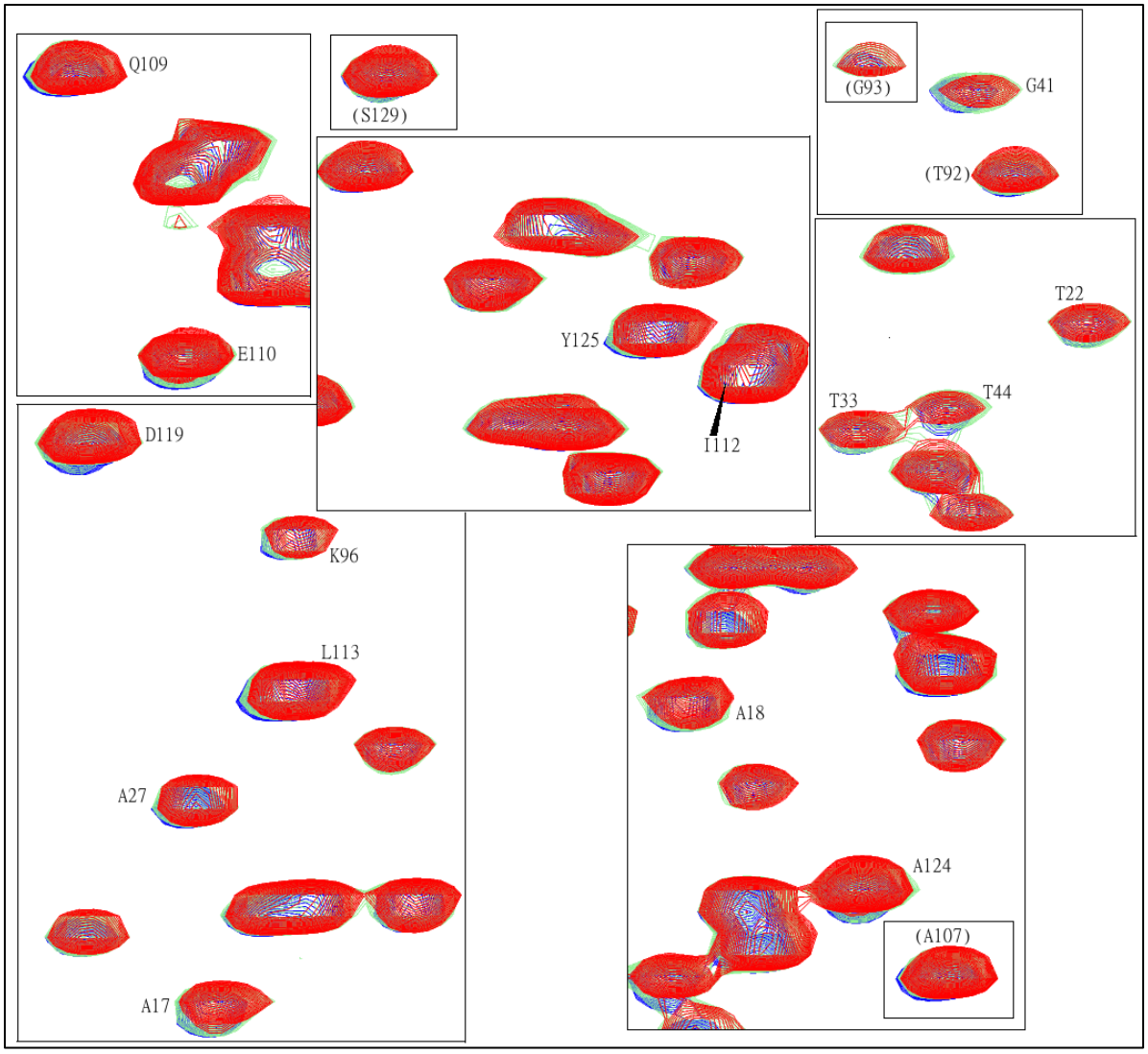

Appendix B2. Titration of EGCG into a 200 µM sample of α-syn (in 50 mM phosphate, pH 6.5). Panels have been selected that contain residues with titration related shifts. The changing of peak shape over the course of time (such as in the case of G93) can give the impression ofa change in chemical shift even when none actually occurs. Blue: no inhibitor; cyan: 1 eq inhibitor; red: 1.5 eq inhibitor. (*Image adapted from Sivanesam* et al., *2015)*

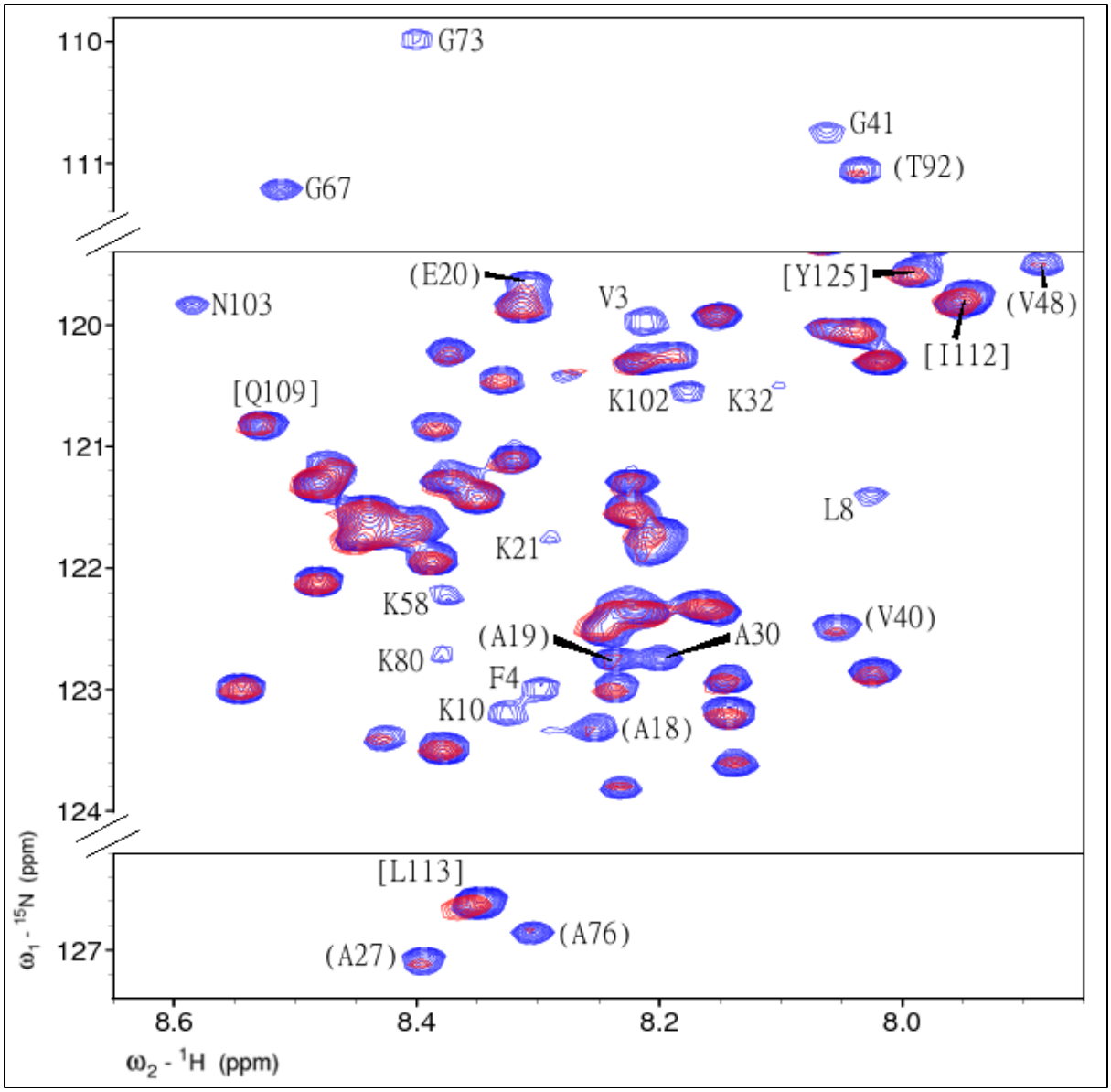

Appendix B3. Spectra of α-syn (in 50 mM phosphate, pH 6.5) taken before (blue) and after (red) a 96-hour incubation with 1.5 eq EGCG in the presence of 2 vol-% HFIP. Peaks that have disappeared at 96 hours are labeled. (*Image adapted from Sivanesam* et al., *2015)*

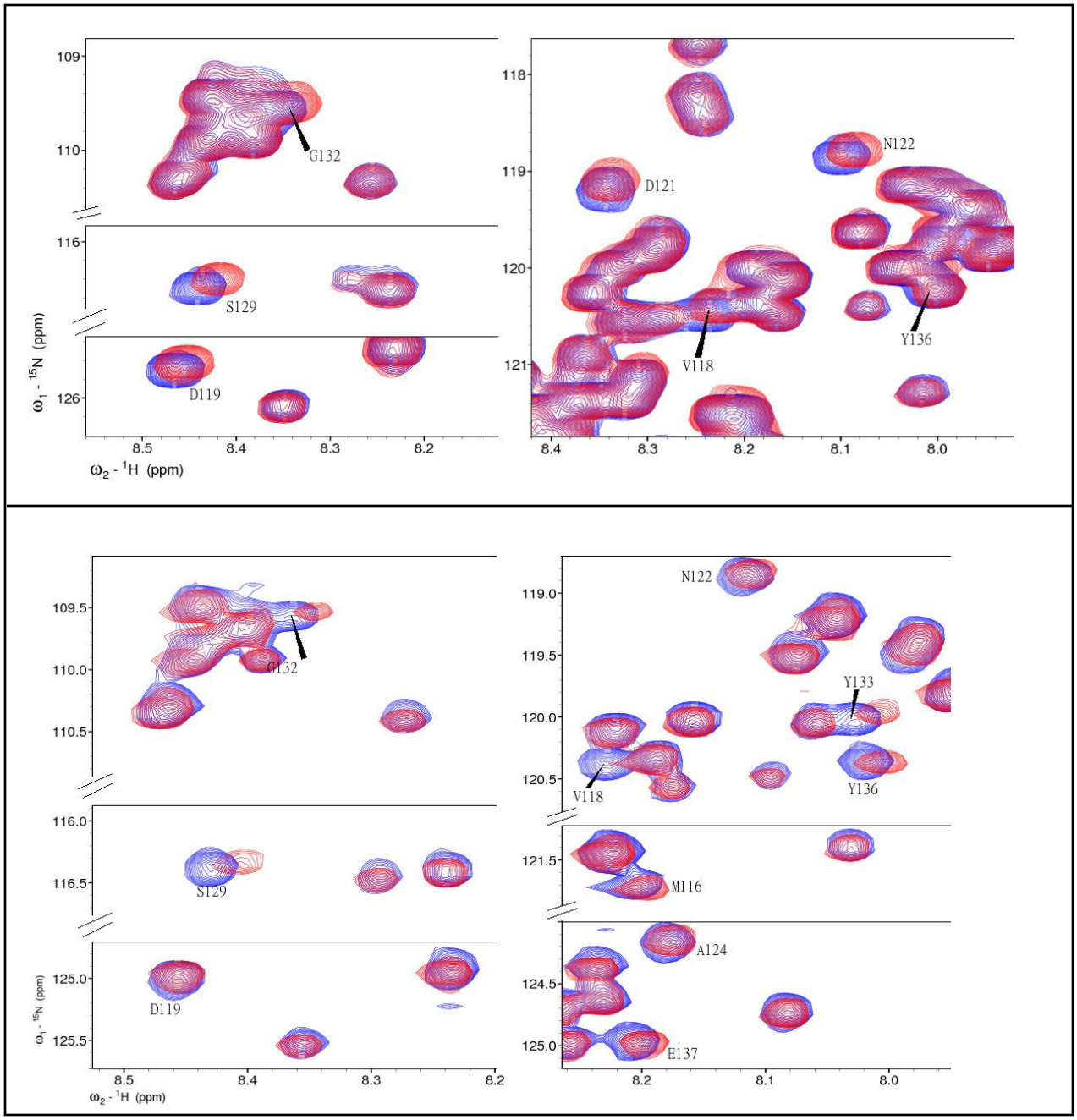

Appendix B4. TOP: Segments of the α-syn spectrum that displayed the largest titration shifts in the presence of 0.6 eq (blue) and 1.5 eq (red) WW. BOTTOM: Segments of the α-syn spectrum that displayed the largest titration shifts in the presence of 0 eq (blue) and 0.6 eq (red) cp-WW. Experiment carried out by Dr. Aimee Byrne using 400 μM α-syn dissolved in 50 mM phosphate buffer, pH 6.5. Peaks that show titration related shifts are labeled. (*Image adapted from Sivanesam* et al., *2015)*

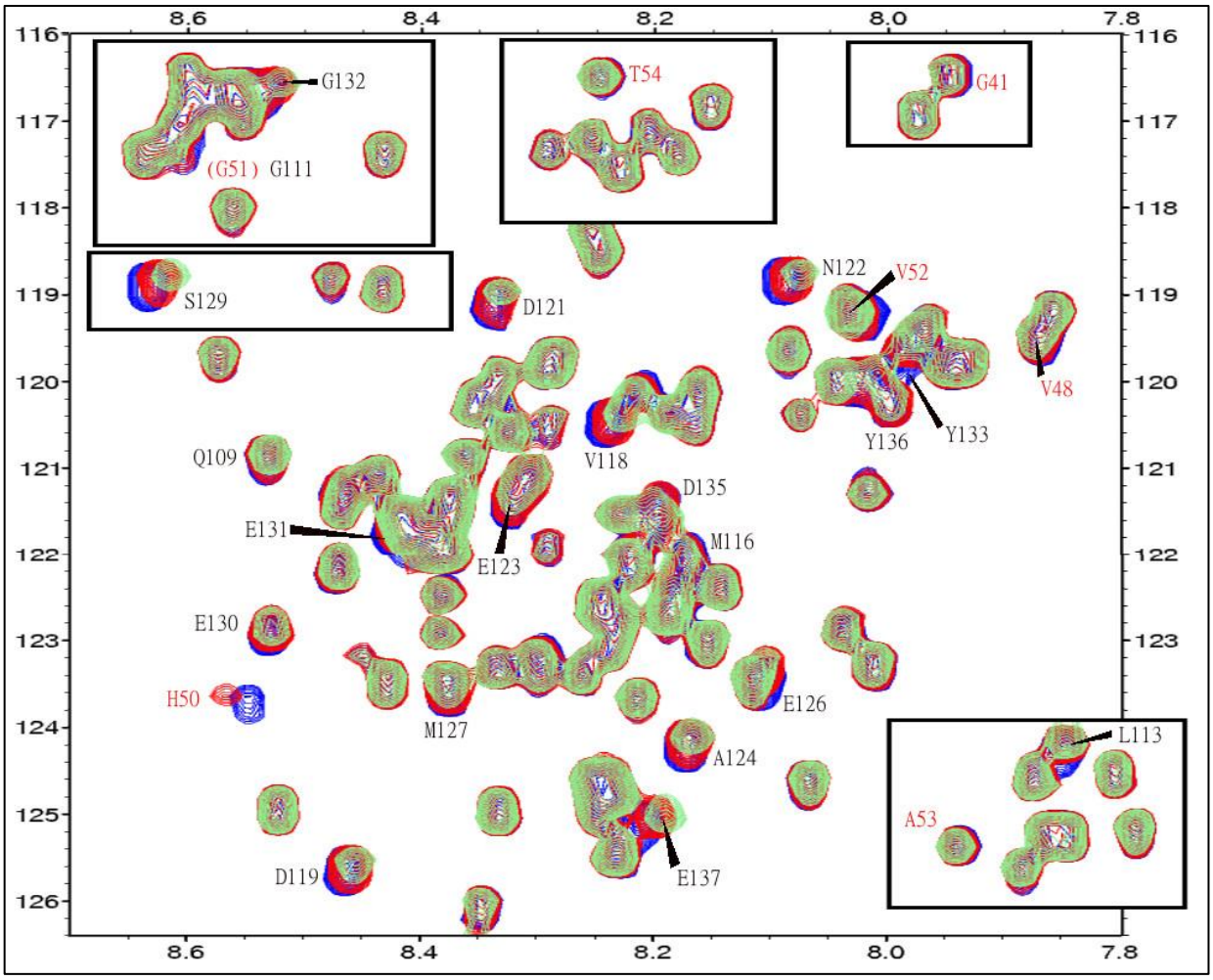

Appendix B5. Titration shifts of α-syn in the presence of 0.6 eq (red) and 1.2 eq (green) cyclo-WW. 200 μM α-syn (in 50 mM phosphate pH 6.5) before the addition of inhibitor is shown in blue. Peaks that are labeled in red represent those peaks that are outside the C-terminal segment of α-syn. (*Image adapted from Sivanesam* et al., *2015)*

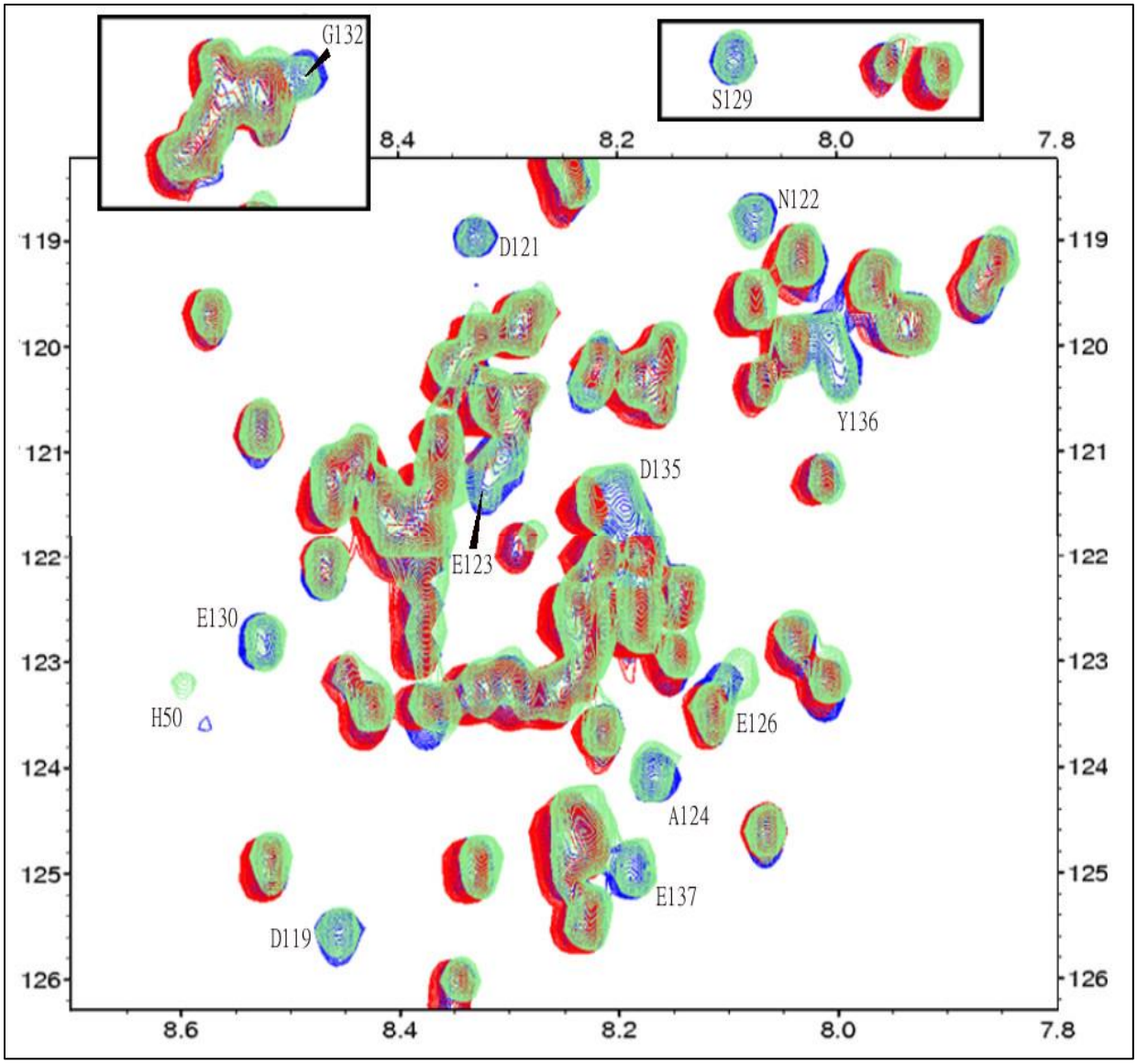

Appendix B6. Titration shifts for α-syn (dissolved in 50 mM phosphate buffer, pH 6.5) in the presence of 1.2 eq cyclo-WW (blue) and 2.2 eq cyclo-WW (red) as well as after the addition of 1.5 vol-% HFIP (green). Peaks that are labeled are those that were completely attenuated in the presence of 2.2 eq of cyclo-WW but reappeared upon addition of HFIP. (*Image adapted from Sivanesam* et al., *2015)*

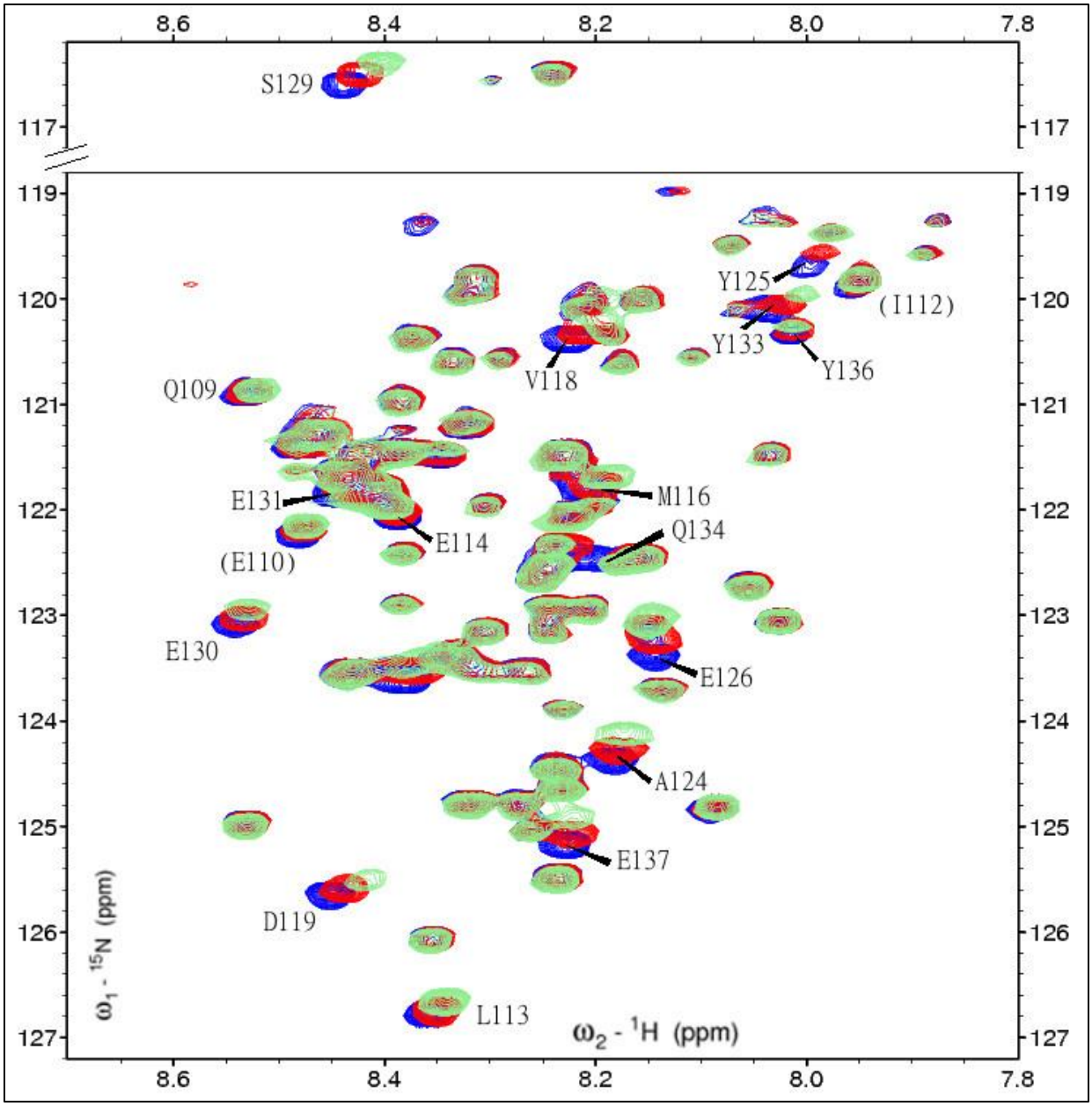

Appendix B7. Titration shifts associated with the addition of 0.5 eq (red) and 1.5 eq (green) of RW-HCH-WE to α-syn (dissolved in 50 mM phosphate buffer, pH 6.5) peaks prior to addition are shown in blue. Peaks that show the largest chemical shifts have been labeled. (*Image adapted from Sivanesam* et al., *2015)*

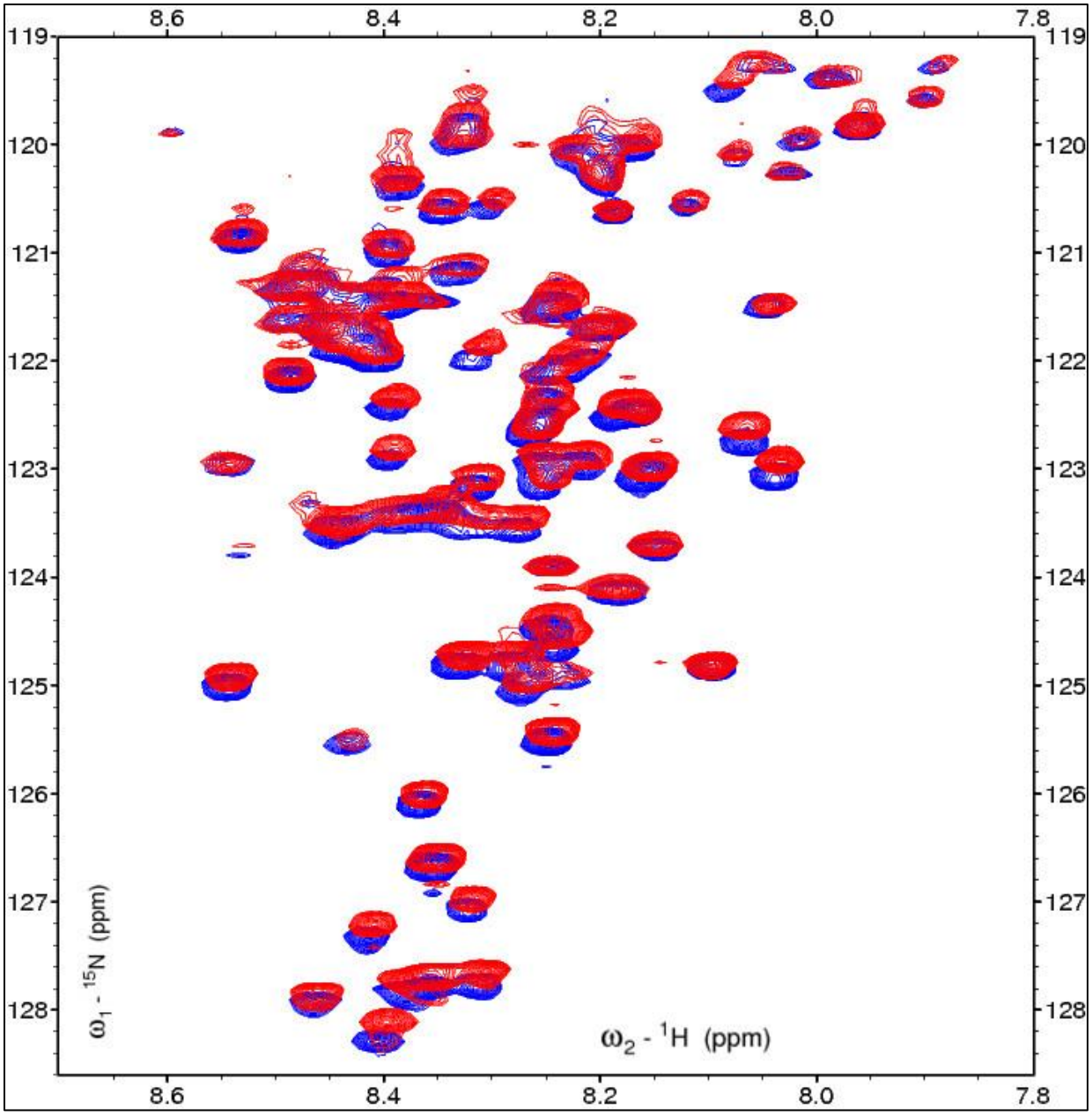

Appendix B8. General upfield shift observed upon addition of 1.5 vol-% HFIP (red) to an α-syn sample (dissolved in 50 mM phosphate buffer, pH 6.5) containing 1.5 eq RW-HCH-WE (blue). (*Image adapted from Sivanesam* et al.*, 2015)*

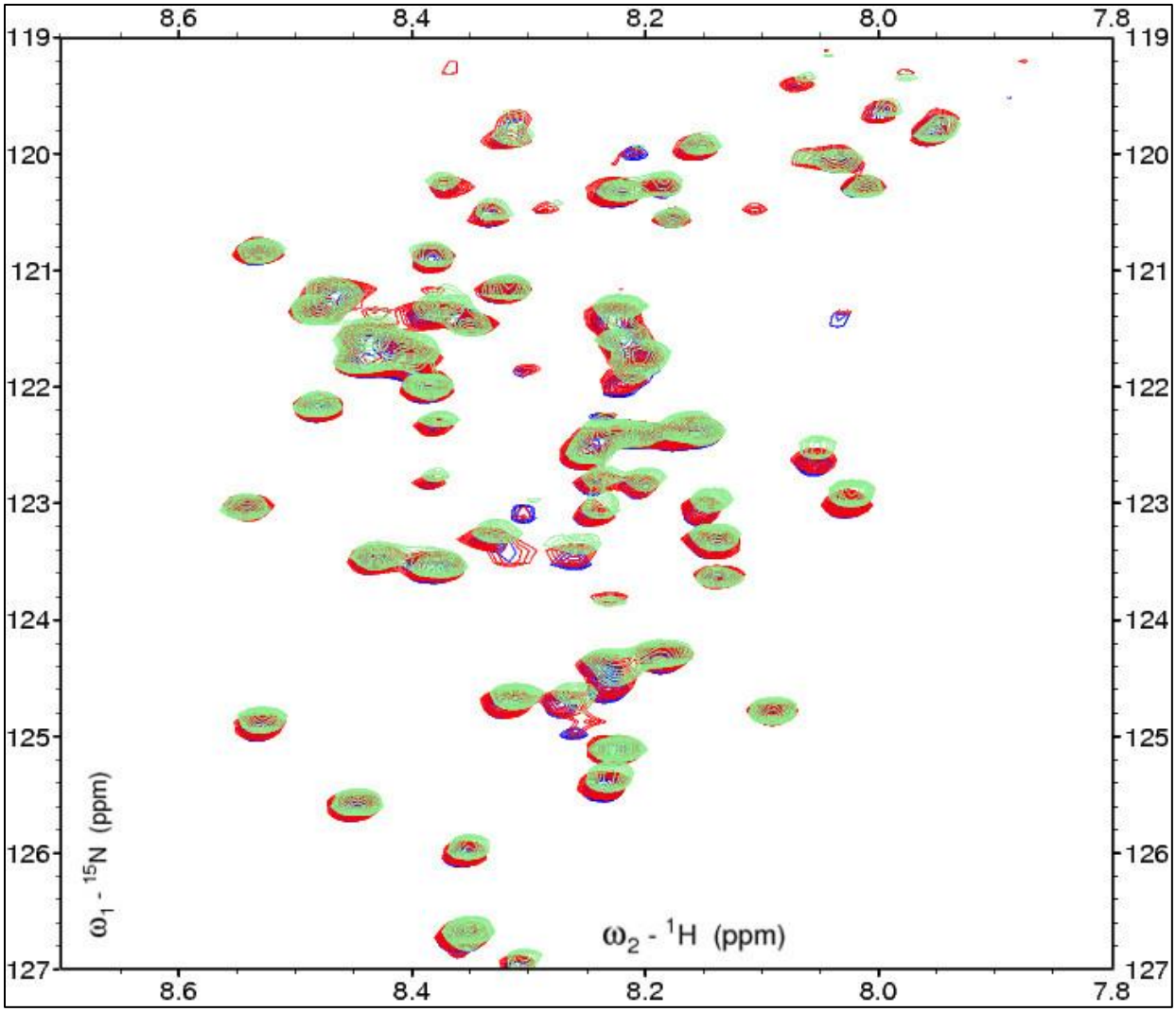

Appendix B9. Addition of 1.5 eq YY-µPro (red) to a 200 µM sample of α-syn (blue) (dissolved in 50 mM phosphate buffer, pH 6.5) resulted in no prominent binding related chemical shifts. The addition of 1.5 vol-% HFIP (green) resulted in a general upfield shift as seen in Appendix B8. (*Image adapted from Sivanesam* et al.*, 2015)*

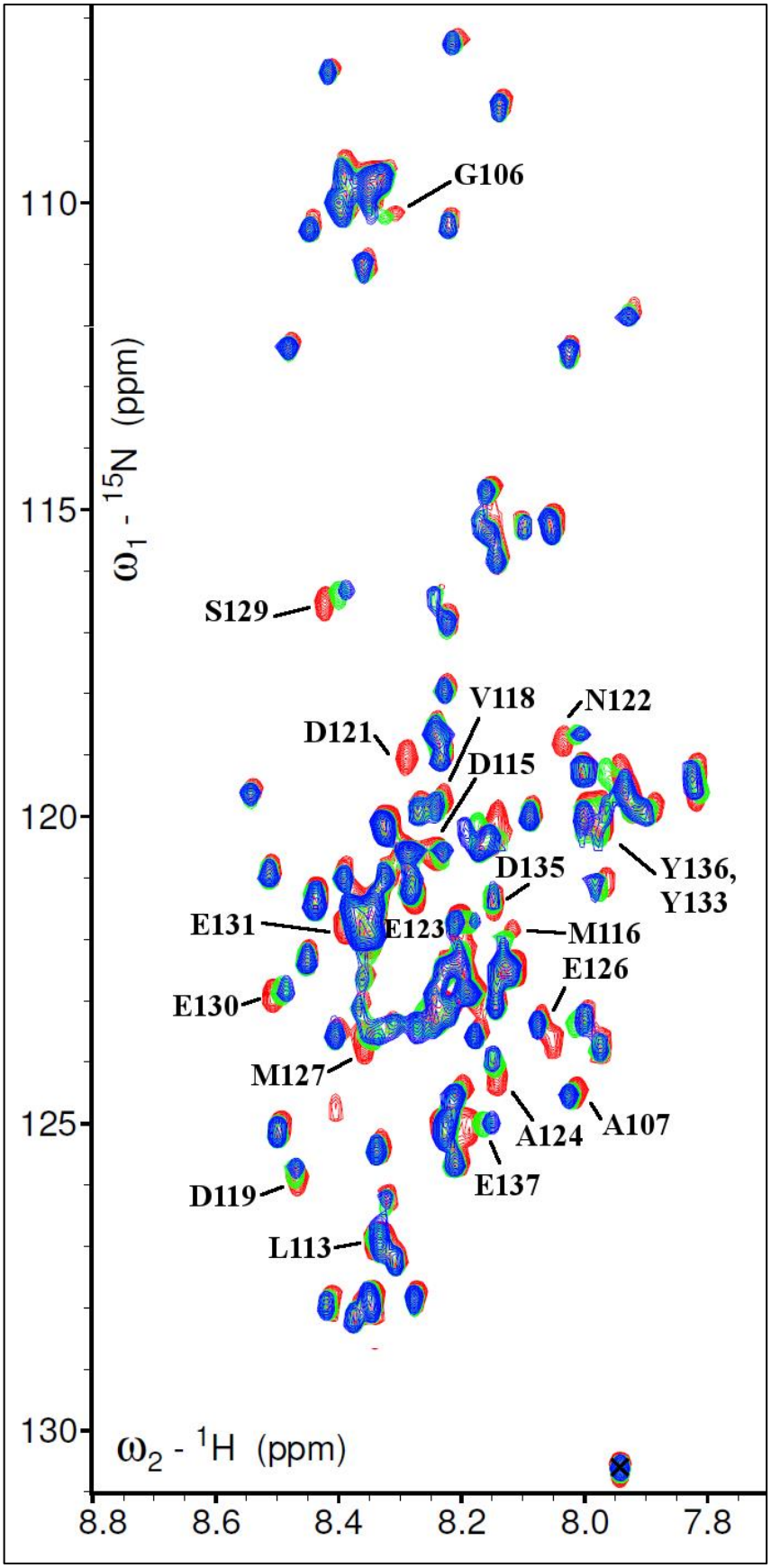

Appendix B10. Titration of cyclo-WW into 100 µM α-syn in 20 mM Tris.HCl, pH 7.2 buffer. The spectrum for α-syn in the absence of inhibitor (red) is overlaid with the spectra of α-syn in the presence of 0.6 eq cyclo-WW (green) and 1.2 eq cyclo-WW (blue). Binding shifts for residues within the C-terminus are labeled. The peak for A140 is indicated with an 'X'.

The peak for D121, E131 and M127 are completely attenuated with the addition of 0.6 eq cyclo-WW. This peak attenuation is seen to a lesser extent with residues N122, S129 and G106 with attenuation increasing as cyclo-WW is titrated in. The peak attenuation possibly indicates strong interaction with cyclo-WW that immobilizes these residues, the strength of which increases for G106, N122 and S129 as ratio of inhibitor to α-syn is increased.

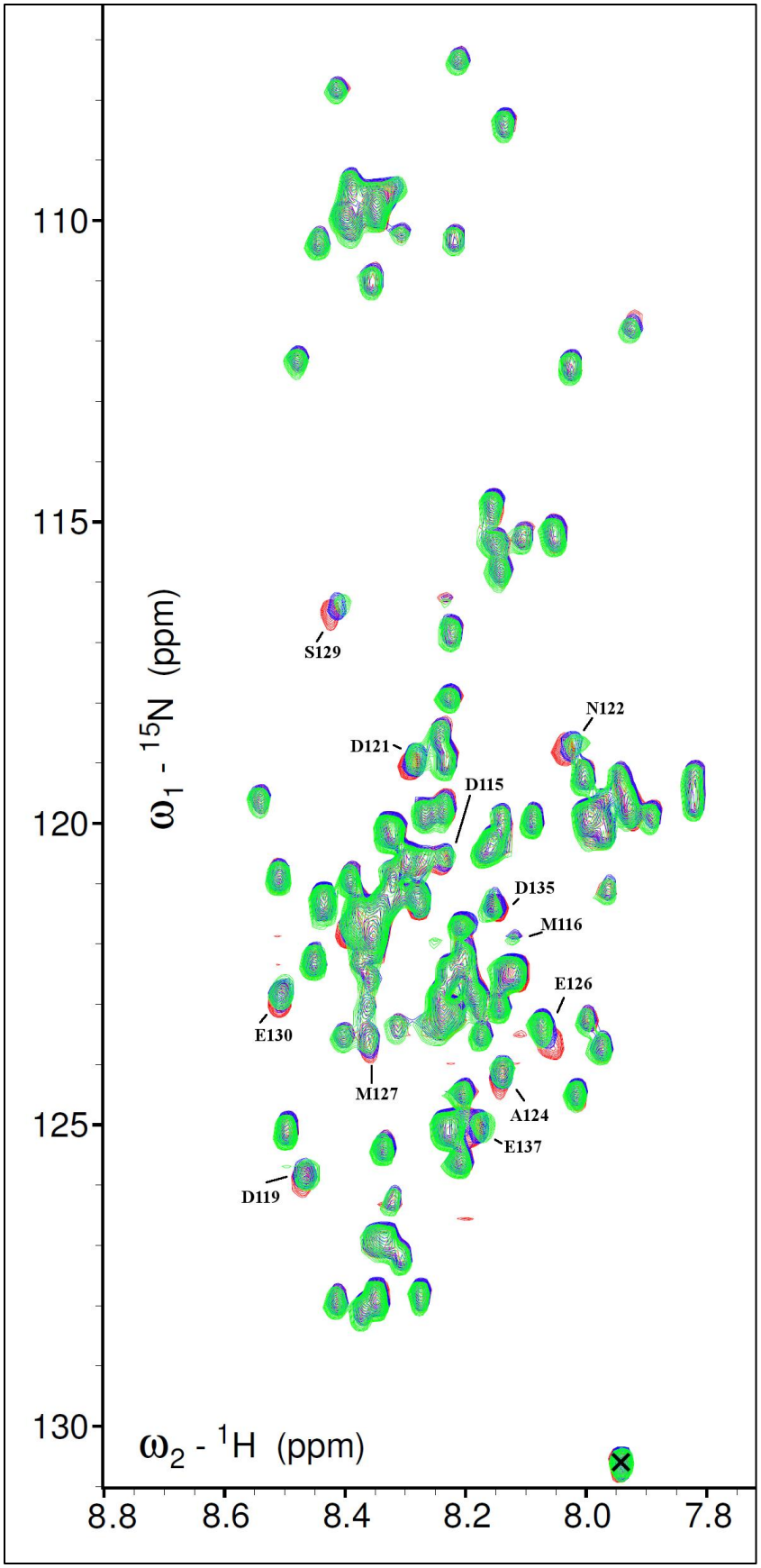

Appendix B11. Titration of cyclo-WY to 100 µM α-syn in 20 mM Tris.HCl, pH 7 buffer. The spectrum for α-syn in the absence of inhibitor (red) is overlaid with the spectra of α-syn in the presence of 0.6 eq cyclo-WY (blue) and 1.2 eq cyclo-WY (green). Binding shifts for residues within the C-terminus are labeled. The peak for A140 is indicated with an 'X'.

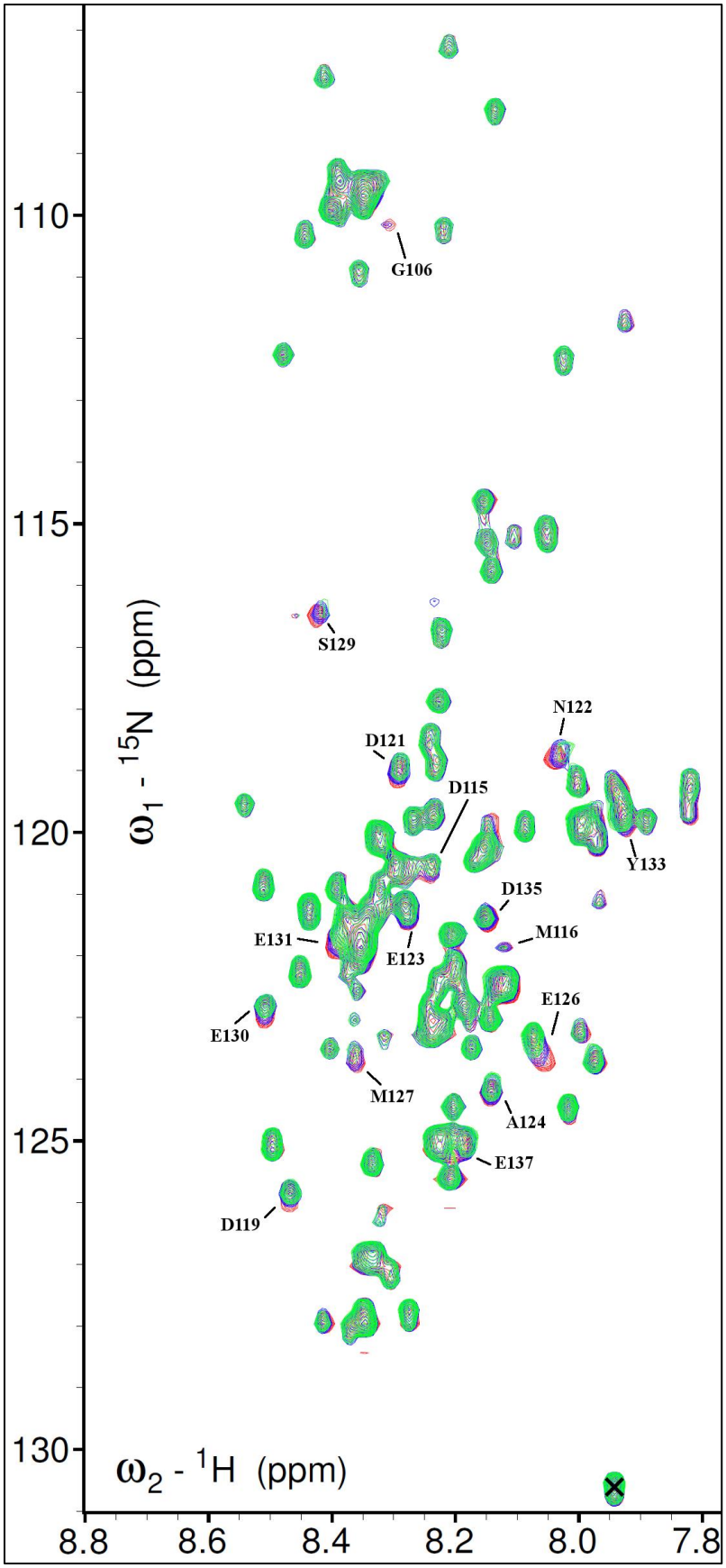

Appendix B12. Titration of cyclo-YW to 100 µM α-syn in 20 mM Tris.HCl, pH 7 buffer. The spectrum for α-syn in the absence of inhibitor (red) is overlaid with the spectra of α-syn in the presence of 0.6 eq cyclo-YW (blue) and 1.2 eq cyclo-YW (green). Binding shifts for residues within the C-terminus are labeled. The peak for A140 is indicated with an 'X'.

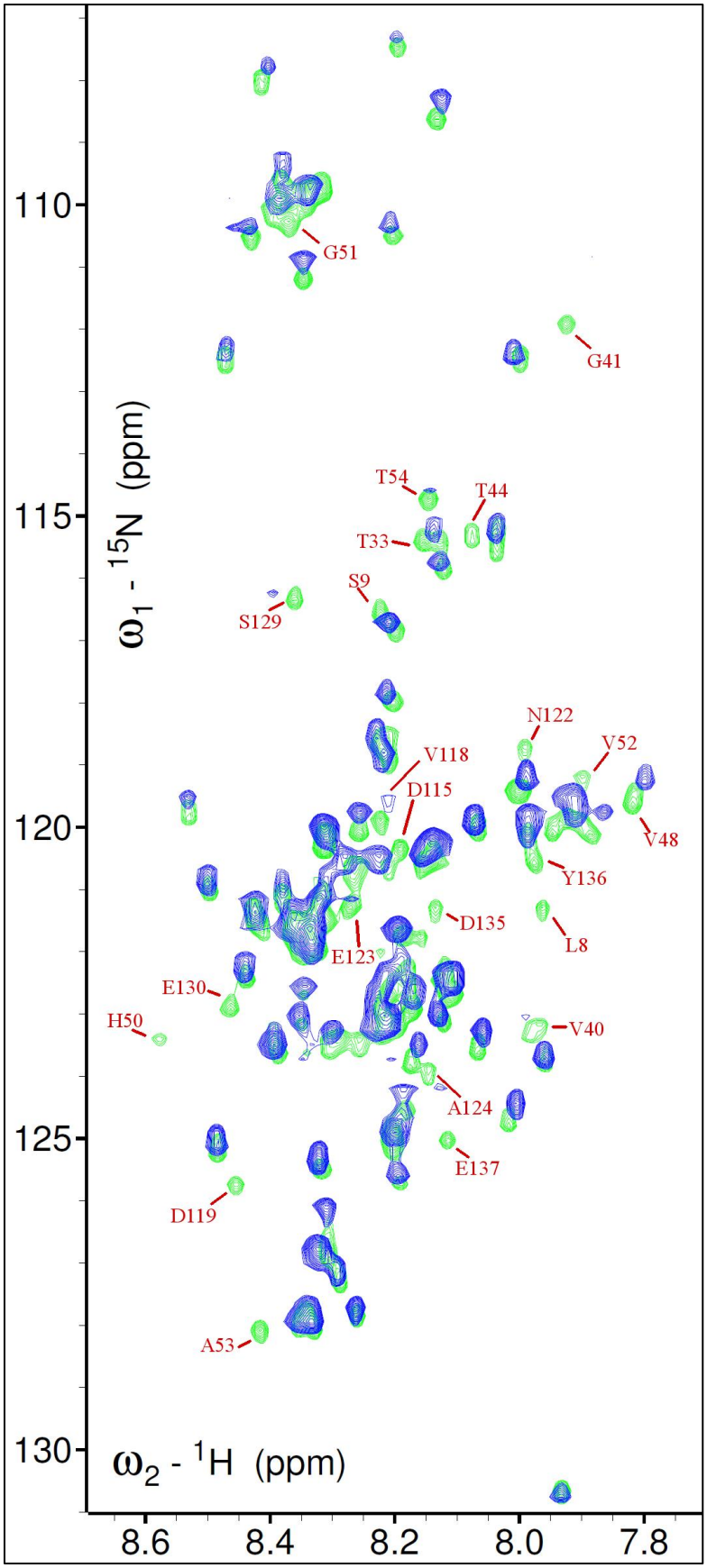

Appendix B13. Spectrum of α-syn with 2.0 eq gal-cap-WW in the absence (blue) and presence (green) of 2 vol-% HFIP. Peaks that are visible only in the presence of HFIP are labeled.

Appendix C

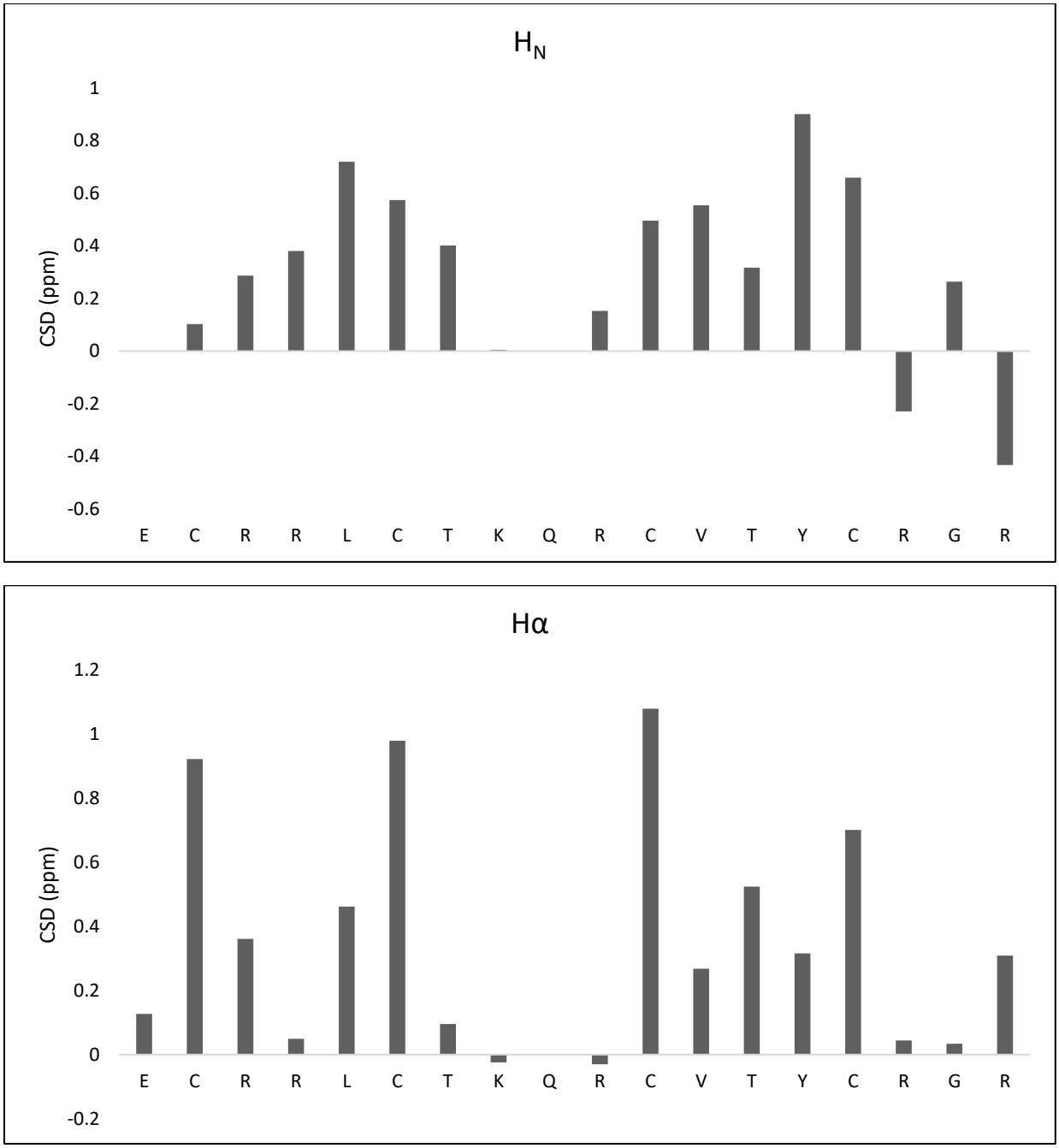

Appendix C1. NMR spectra for backbone H_N and Hα of gomesin taken at 280K in 20 mM phosphate buffer, pH 6.5.

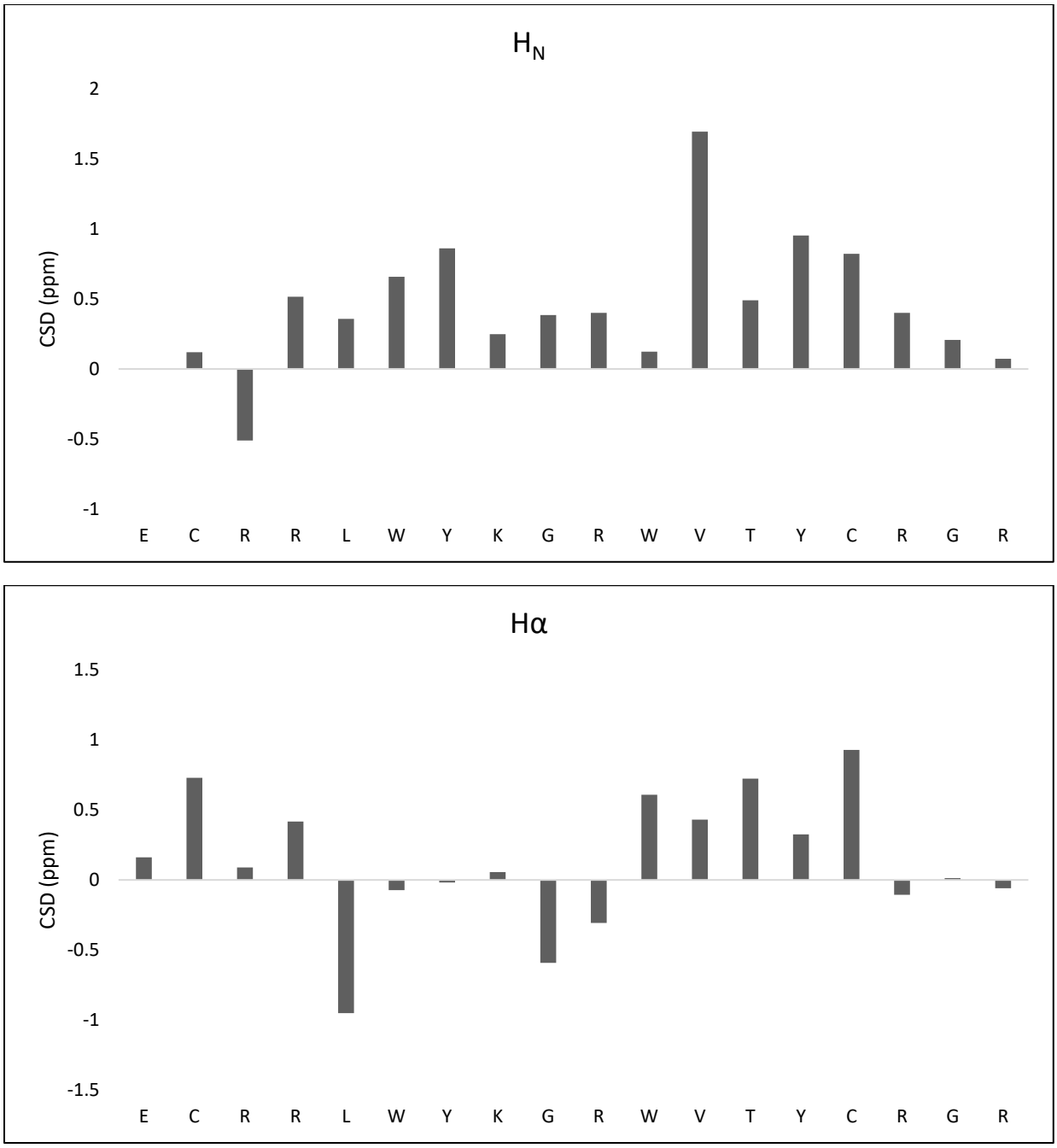

Appendix C2. NMR spectra for backbone H_N and Hα of gommut-1 taken at 280K in 20 mM phosphate buffer, pH 6.5.

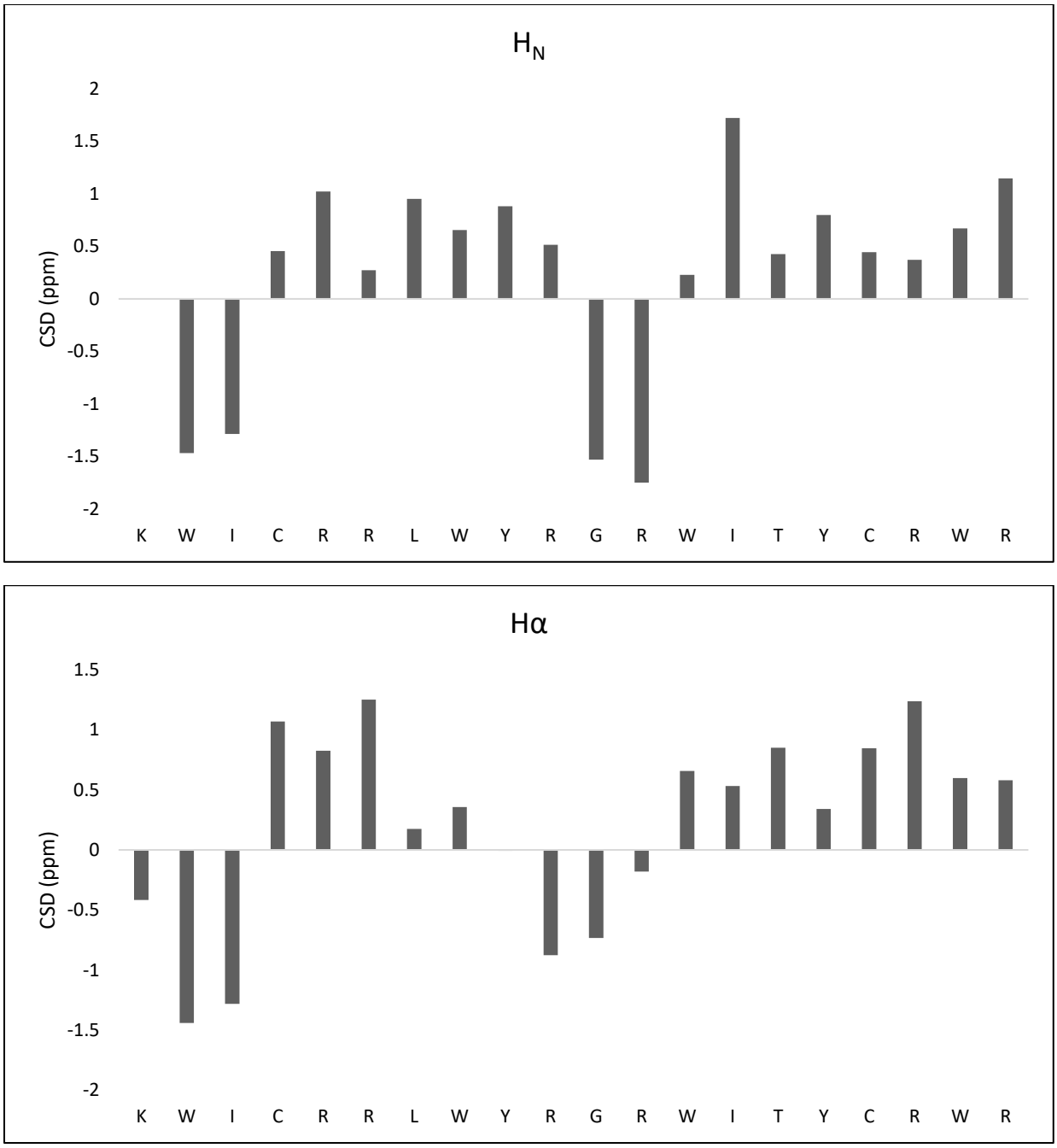

Appendix C3. NMR spectra for backbone H_N and Hα of gommut-2 taken at 280K in 20 mM phosphate buffer, pH 6.5.

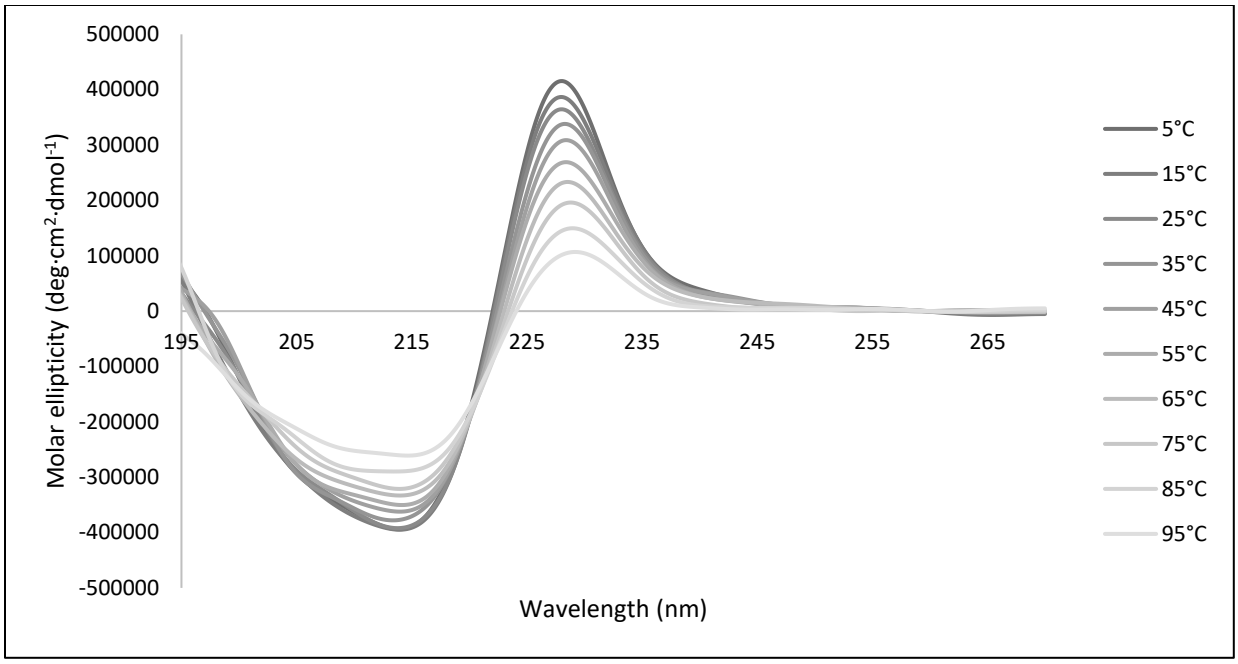

Appendix C4. CD spectra of gommut-1 taken in 20 mM phosphate buffer, pH 6.5 at 5°C to 95°C (at every 10°C interval).

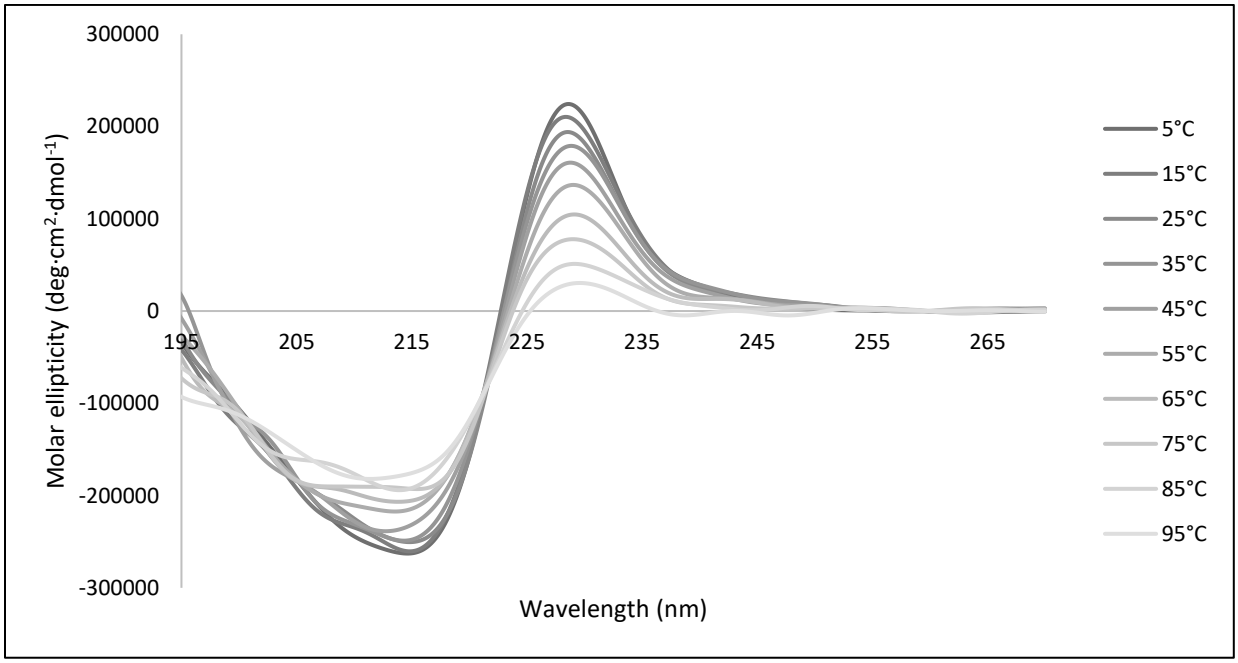

Appendix C5. CD spectra of gommut-2 taken in 20 mM phosphate buffer, pH 6.5 at 5°C to 95°C (at every 10°C interval).

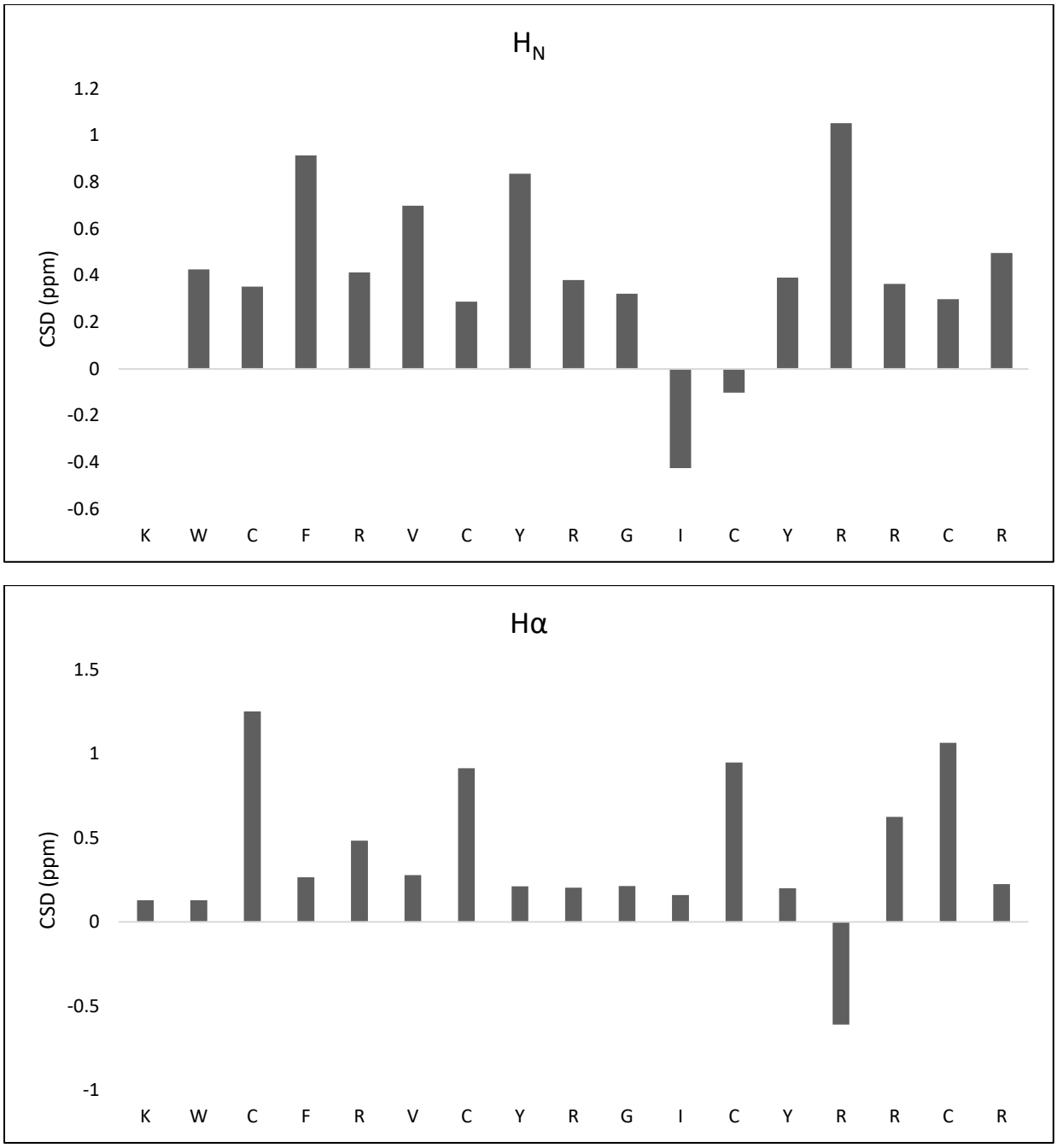

Appendix C6. NMR spectra for backbone H_N and Hα of tachyplesin I taken at 280K in 20 mM phosphate buffer, pH 6.5.

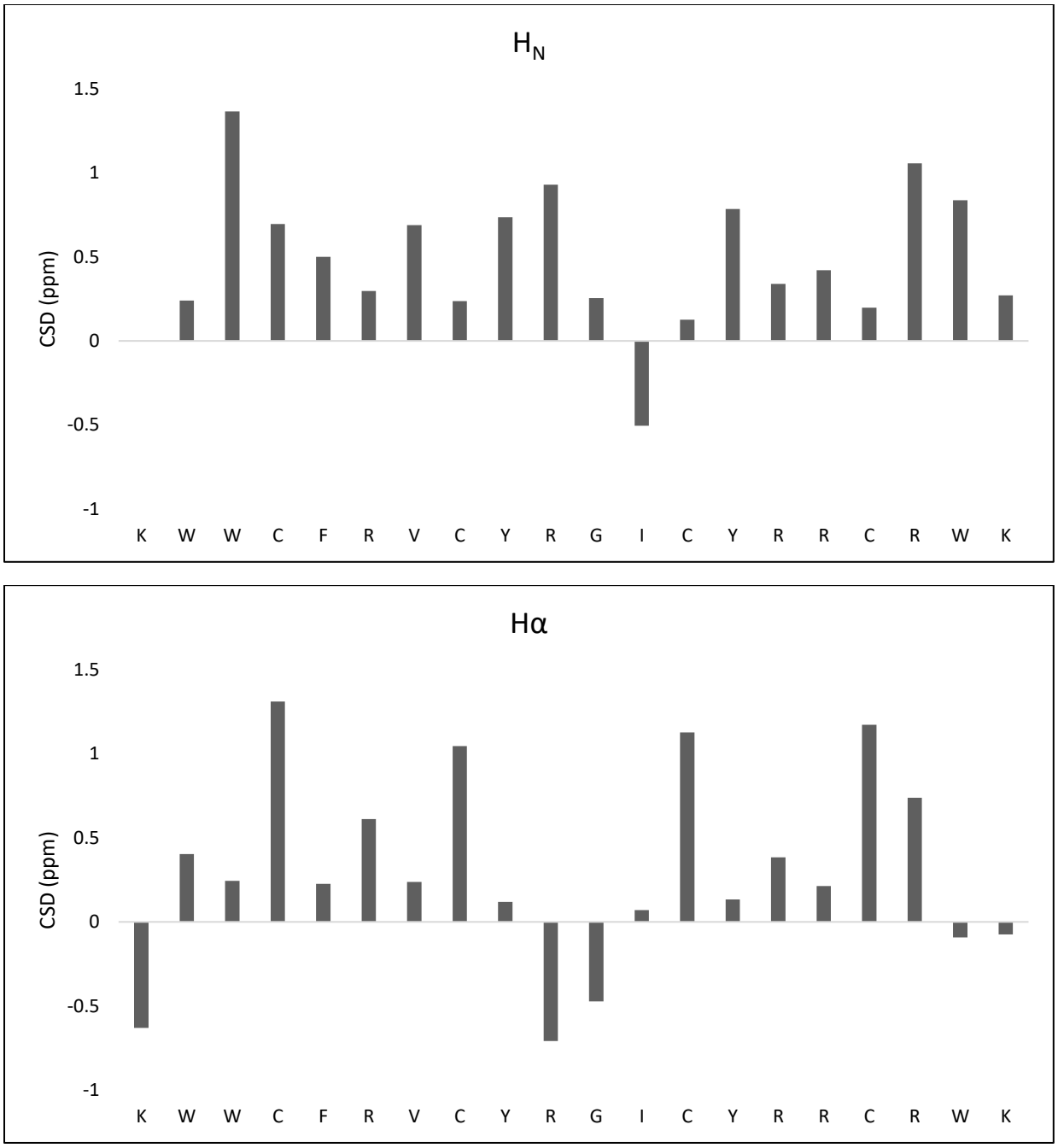

Appendix C7. NMR spectra for backbone H_N and Hα of tachymut 1 taken at 280K in 20 mM phosphate buffer, pH 6.5.

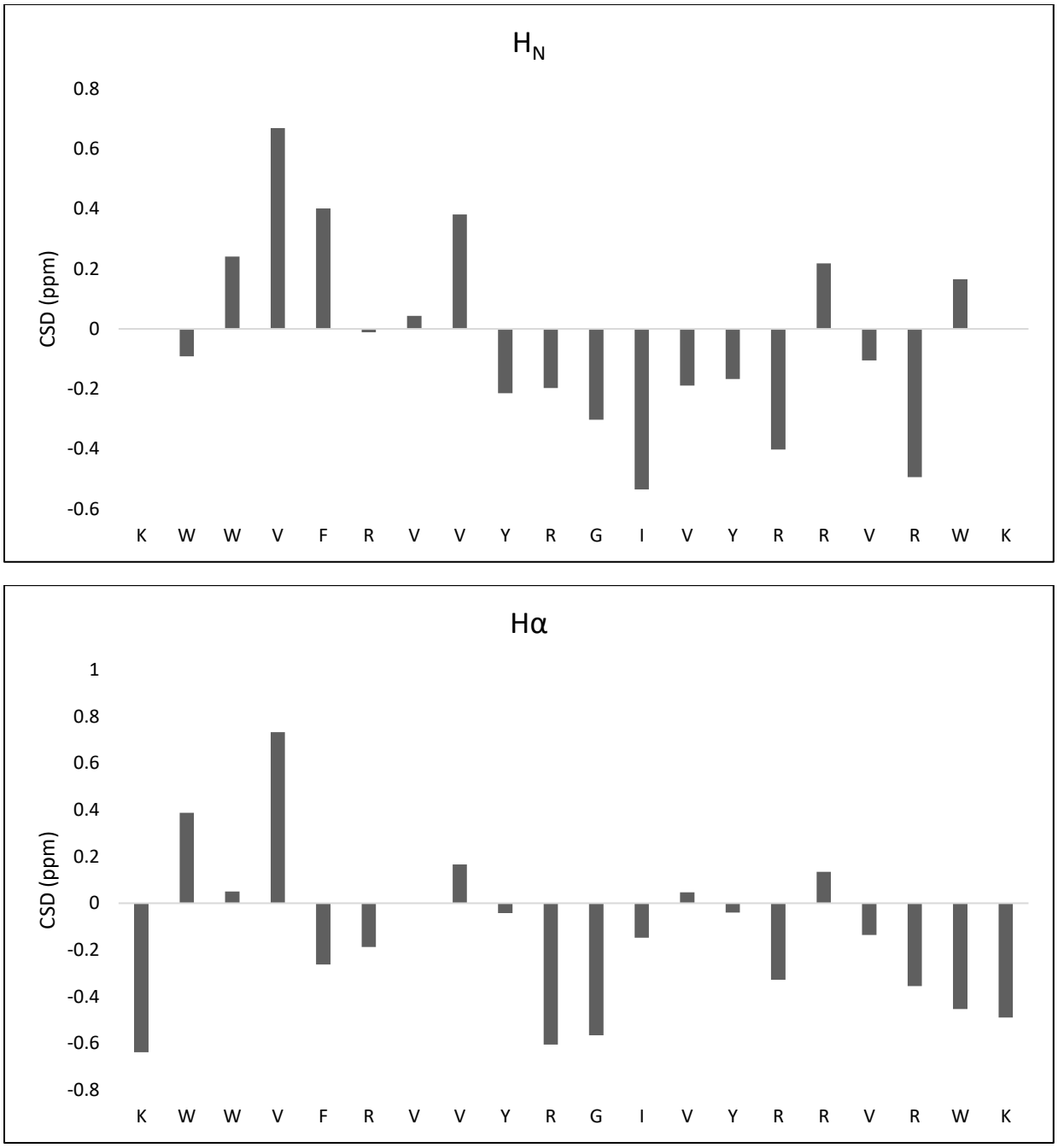

Appendix C8. NMR spectra for backbone H_N and Hα of tachymut 2 taken at 280K in 20 mM phosphate buffer, pH 6.5.

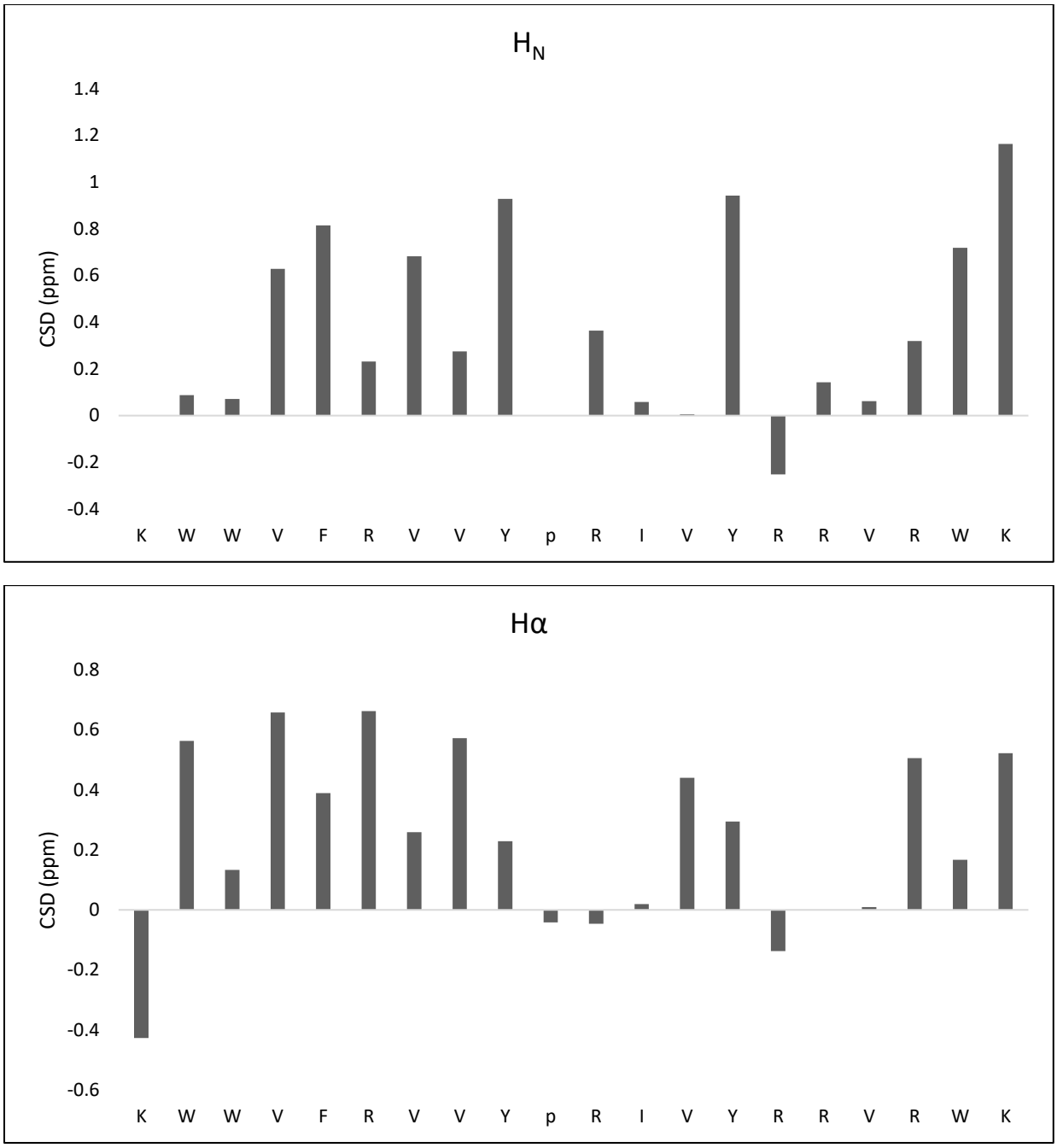

Appendix C9. NMR spectra for backbone H_N and Hα of tachymut 3 taken at 280K in 20 mM phosphate buffer, pH 6.5.

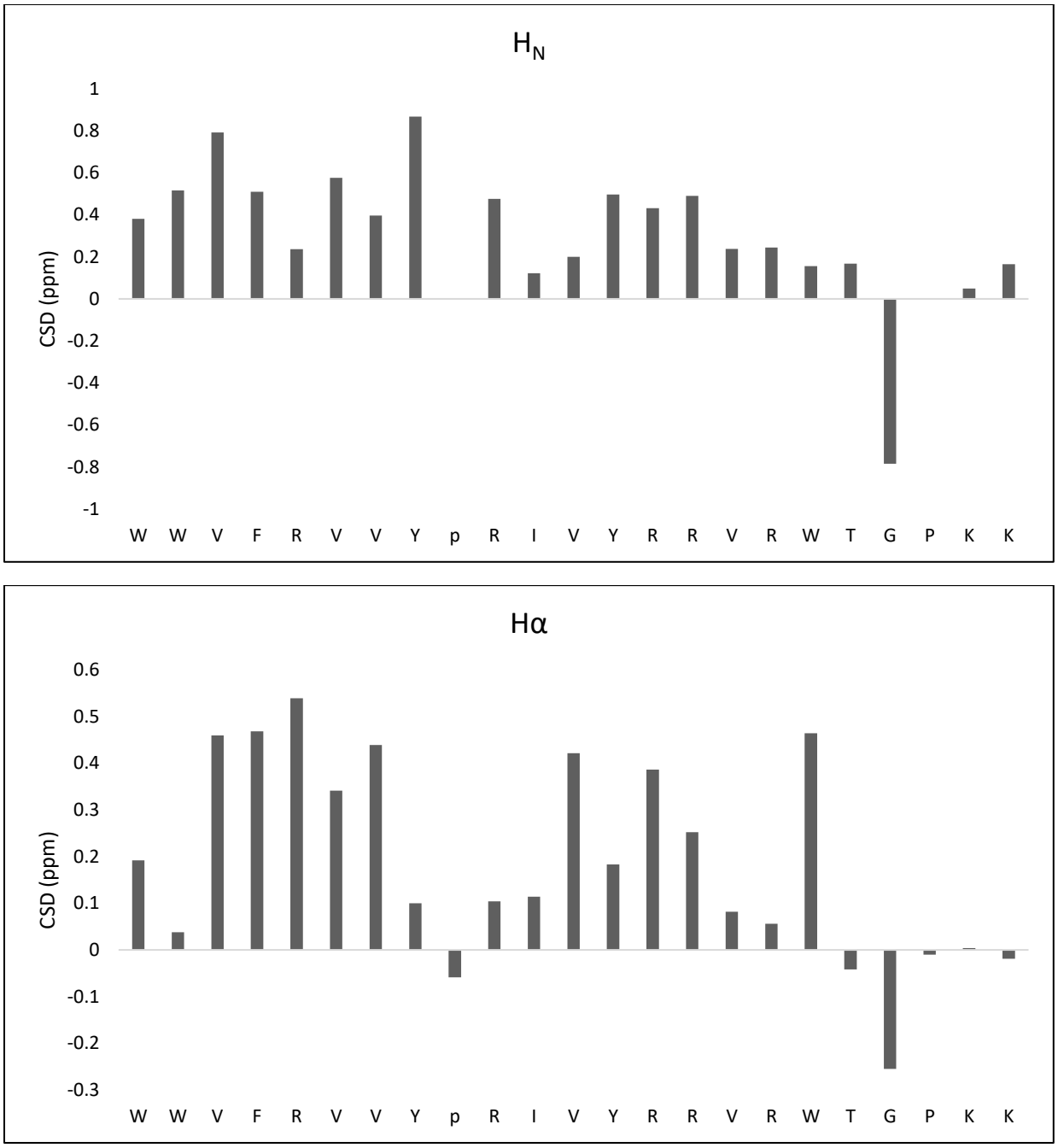

Appendix C10. NMR spectra for backbone H_N and Hα of tachymut 5-bz taken at 280K in 20 mM phosphate buffer, pH 6.5.

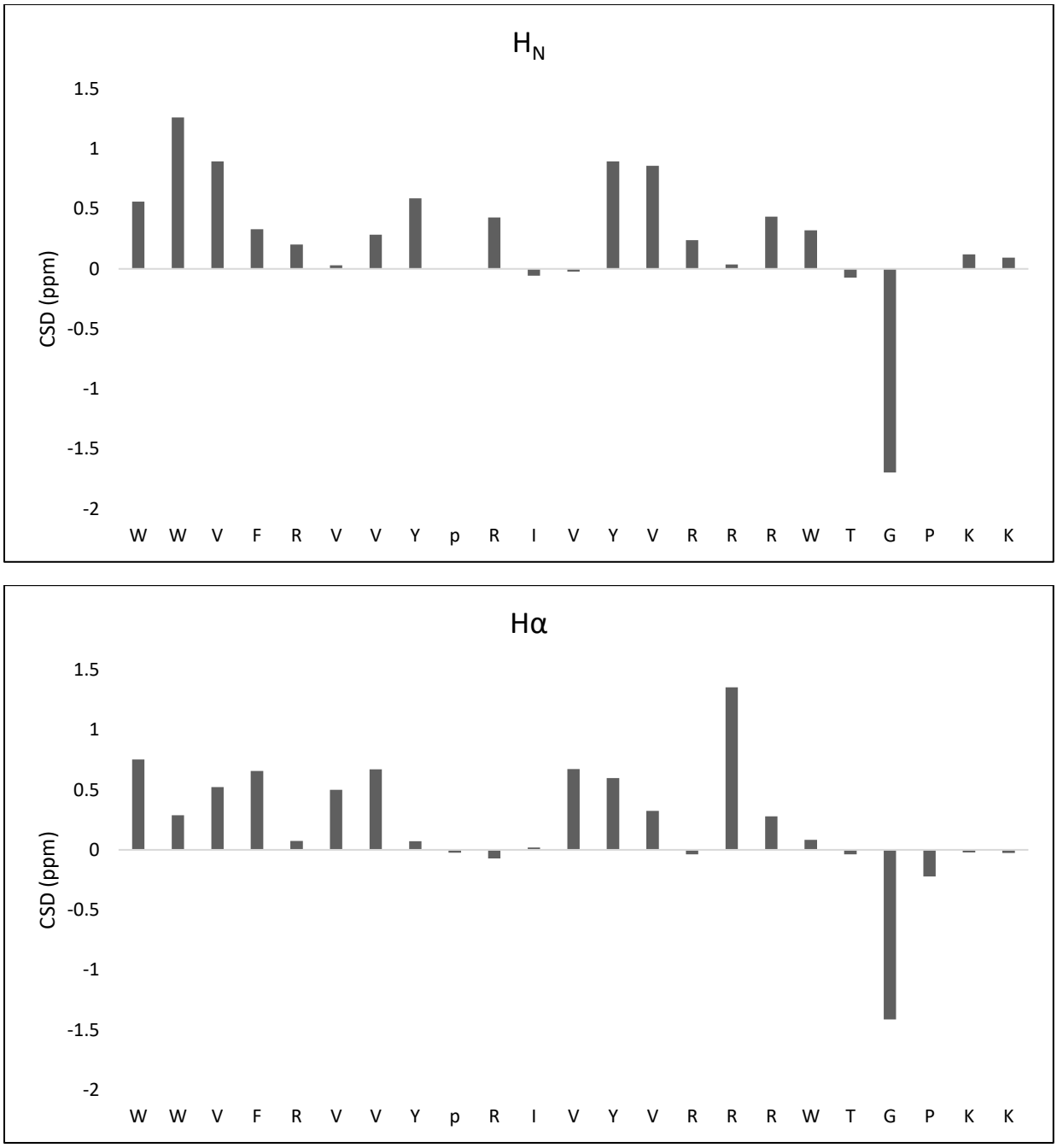

Appendix C11. NMR spectra for backbone H_N and Hα of tachymut 6 taken at 280K in 20 mM phosphate buffer, pH 6.5.

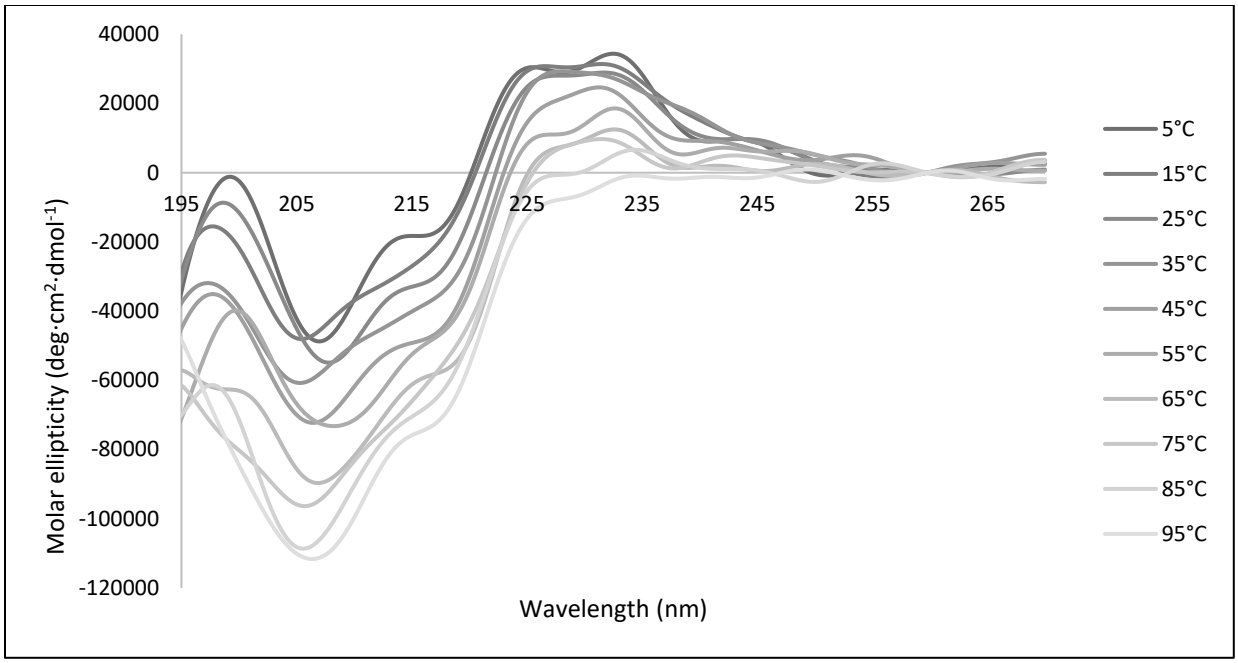

Appendix C12. CD spectra of tachyplesin I taken in 20 mM phosphate buffer, pH 6.5 at 5°C to 95°C (at every 10°C interval). Kushibiki *et al.* report that at 25°C, CD spectra of 30 µM tachyplesin I in 10 mM phosphate buffer, pH 7.4 has 2 maxima at 198 nm and 232 nm as well as a minimum at 211 nm. (Kushibiki *et al.*, 2014) The CD spectra shown here does show the beginnings of a small maximum at 198 nm at low temperatures. However, there are two maxima between 225 nm and 235 nm as opposed to one. There is also two minima as opposed to one between 205 nm and 215 nm.

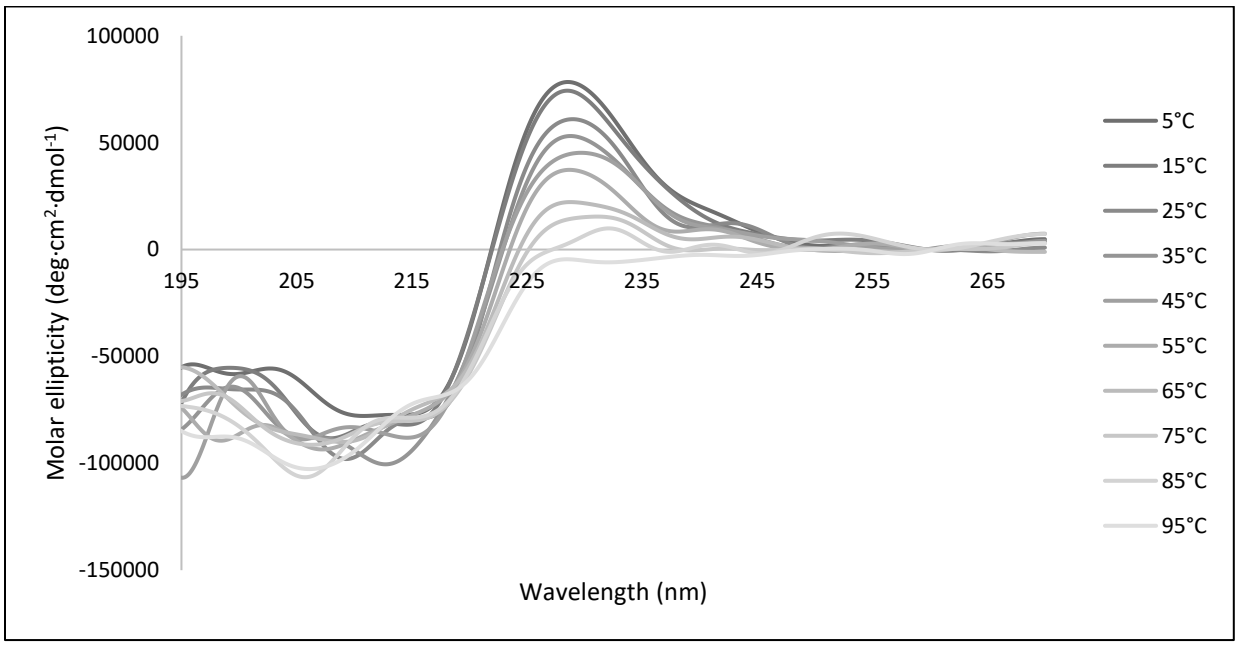

Appendix C13. CD spectra of tachymut 1 (TM1) taken in 20 mM phosphate buffer, pH 6.5 at 5°C to 95°C (at every 10°C interval).

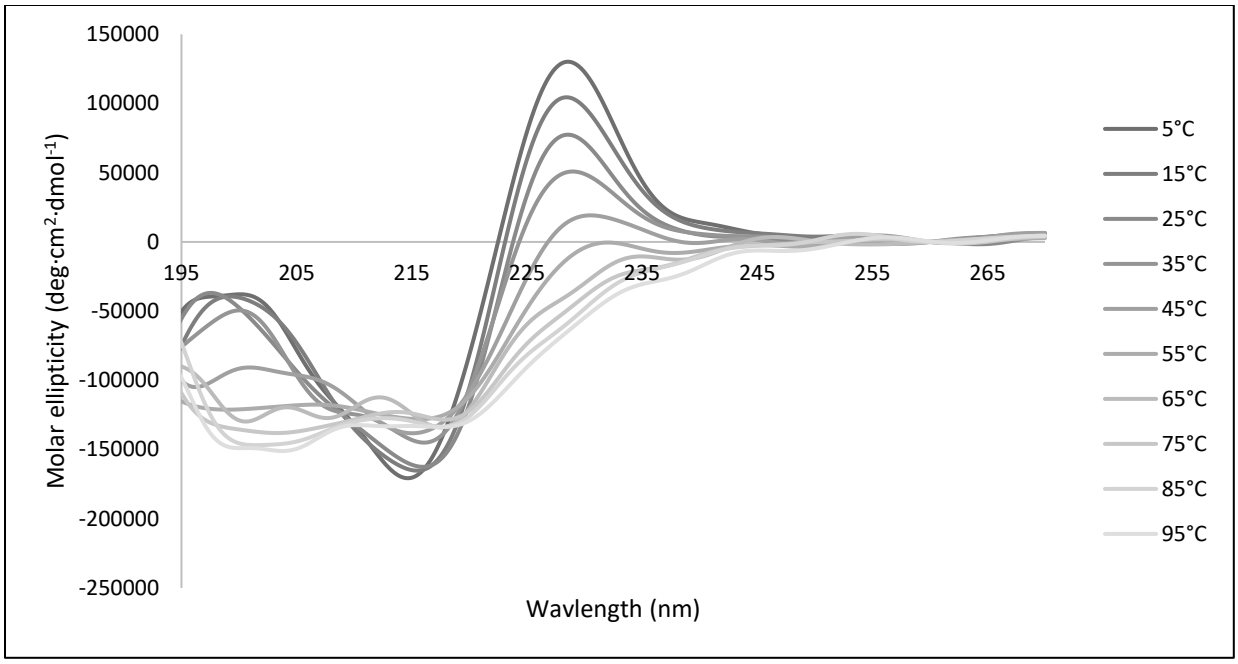

Appendix C14. CD spectra of tachymut 2 (TM2) taken in 20 mM phosphate buffer, pH 6.5 at 5°C to 95°C (at every 10°C interval).

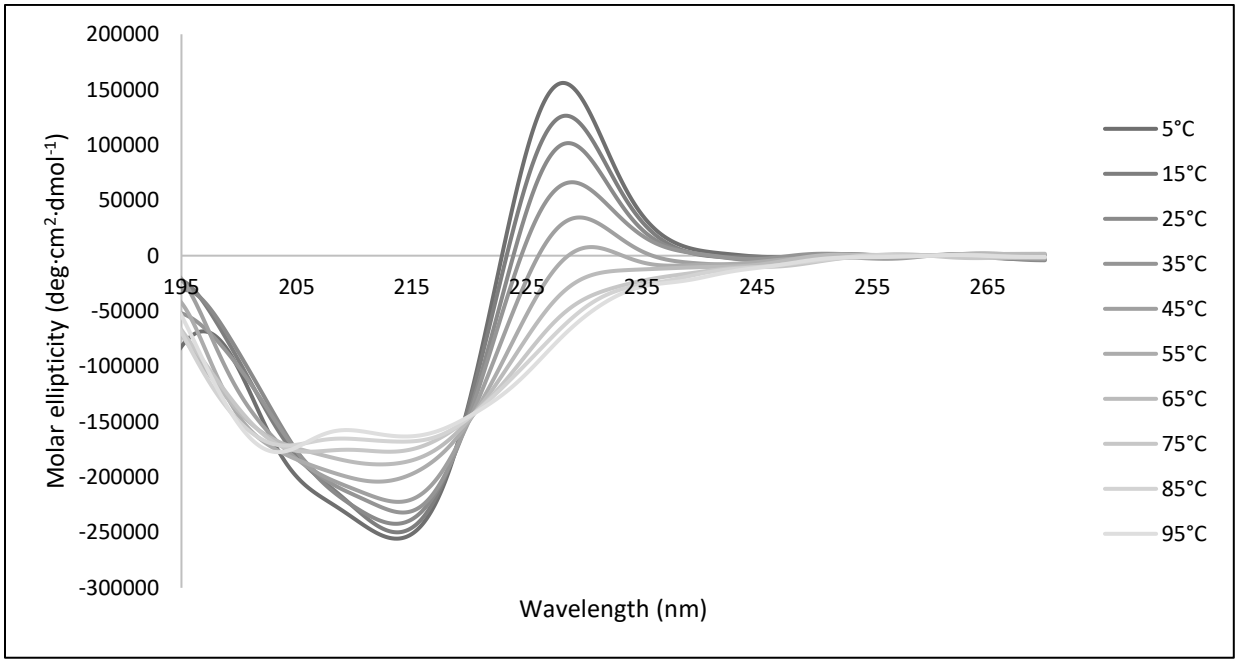

Appendix C15. CD spectra of tachymut 3 (TM3) taken in 20 mM phosphate buffer, pH 6.5 at 5°C to 95°C (at every 10°C interval).

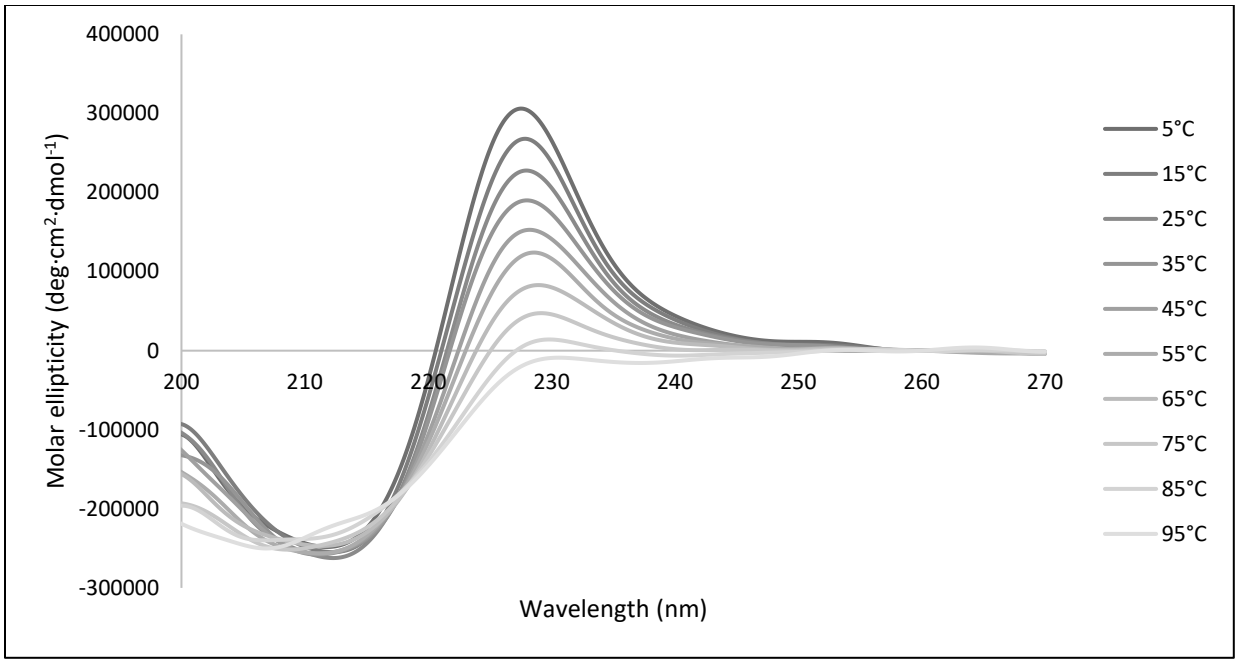

Appendix C16. CD spectra of tachymut 4 (TM4) taken in 20 mM phosphate buffer, pH 6.5 at 5°C to 95°C (at every 10°C interval).

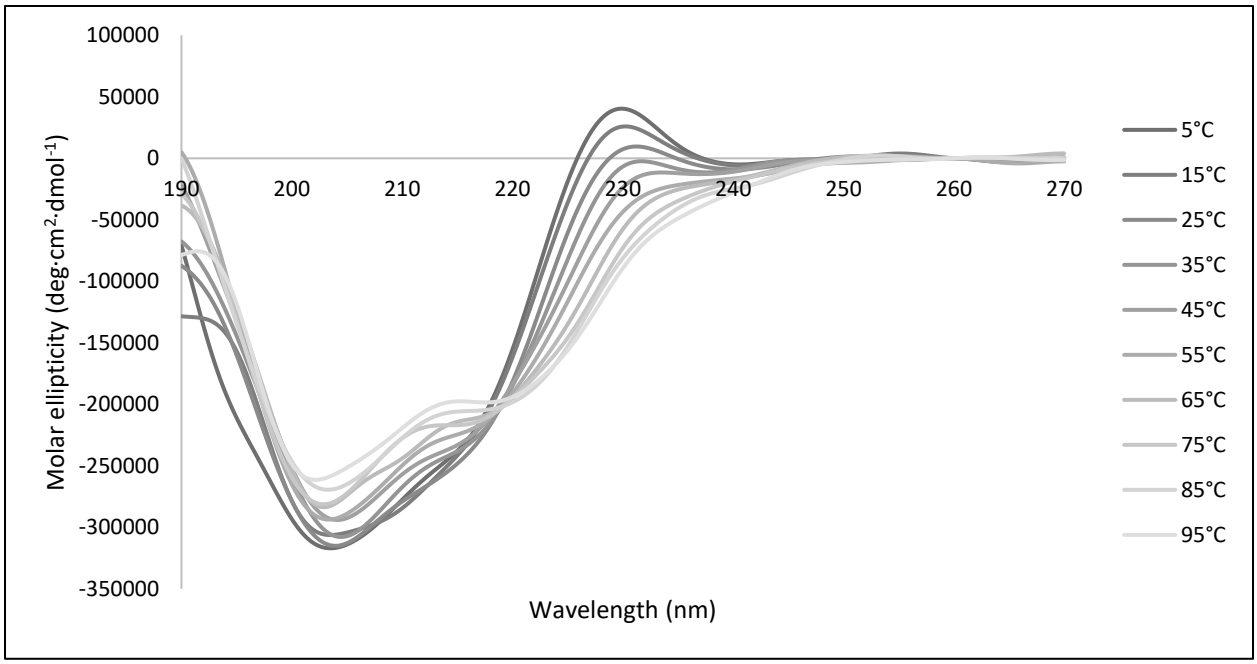

Appendix C17. CD spectra of tachymut 5-ac (TM5-ac) taken in 20 mM phosphate buffer, pH 6.5 at 5°C to 95°C (at every 10°C interval).

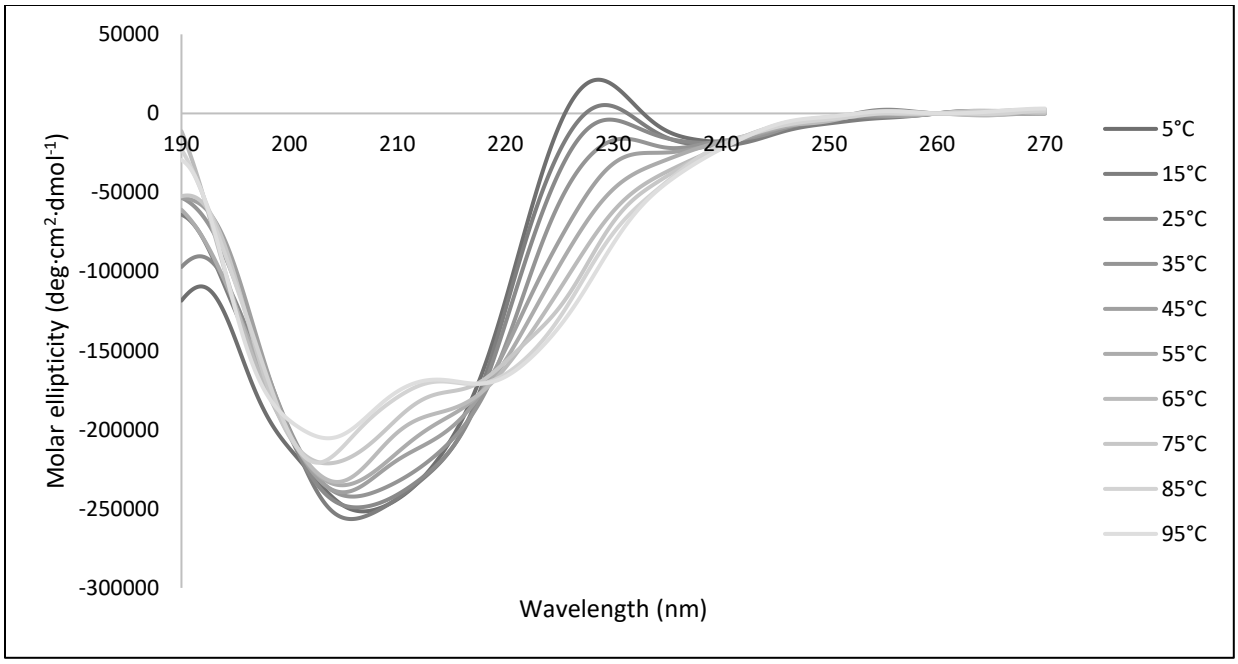

Appendix C18. CD spectra of tachymut 5-bz (TM5-bz) taken in 20 mM phosphate buffer, pH 6.5 at 5°C to 95°C (at every 10°C interval).

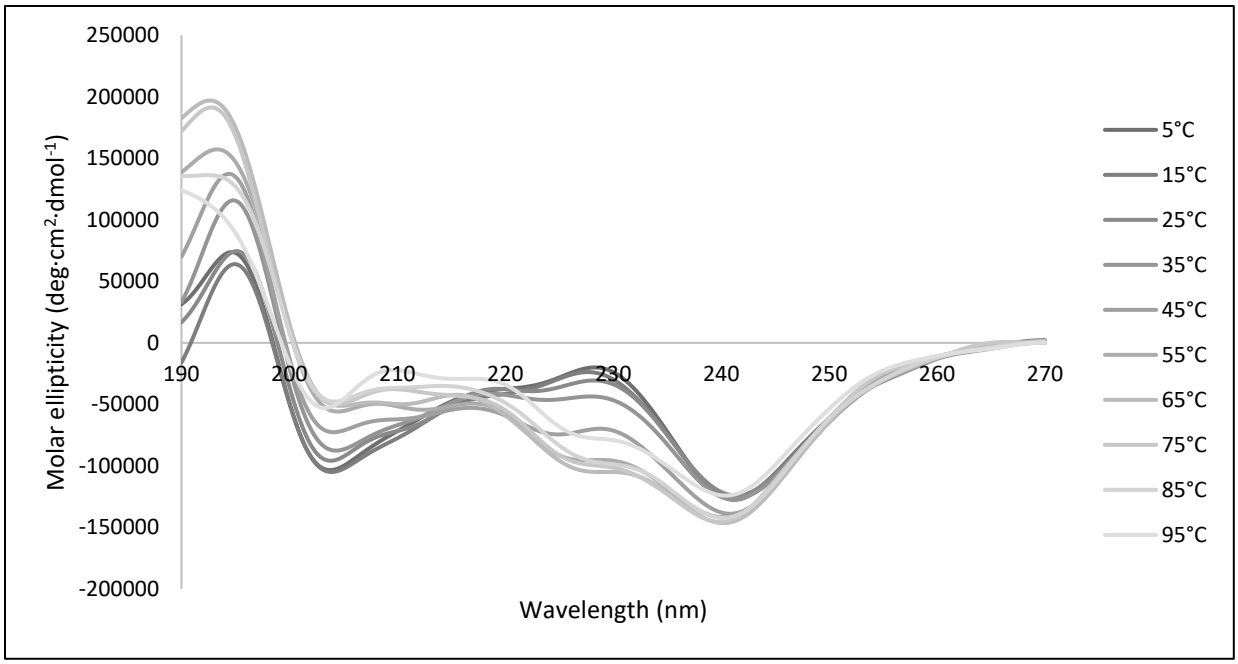

Appendix C19. CD spectra of tachymut 5-py (TM5-py) taken in 20 mM phosphate buffer, pH 6.5 at 5°C to 95°C (at every 10°C interval).

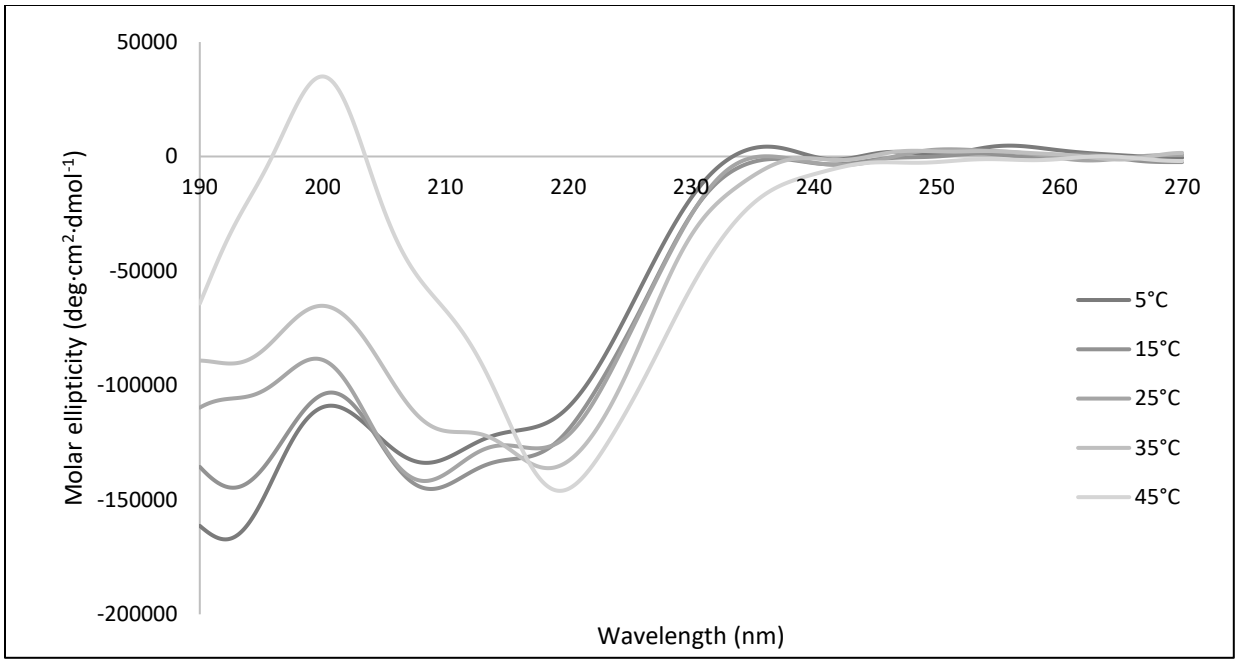

Appendix C20. CD spectra of tachymut 5-my (TM5-my) taken in 20 mM phosphate buffer, pH 6.5 at 5°C to 45°C (at every 10°C interval).

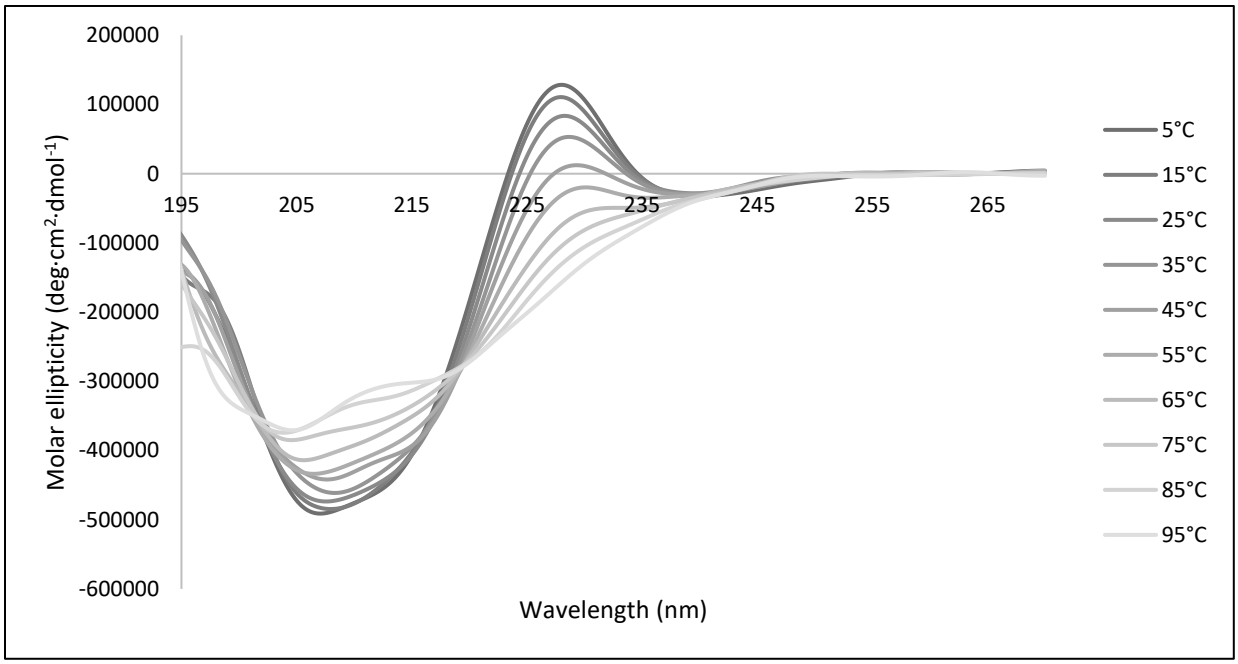

Appendix C21. CD spectra of tachymut 6 (TM6) taken in 20 mM phosphate buffer, pH 6.5 at 5°C to 95°C (at every 10°C interval).

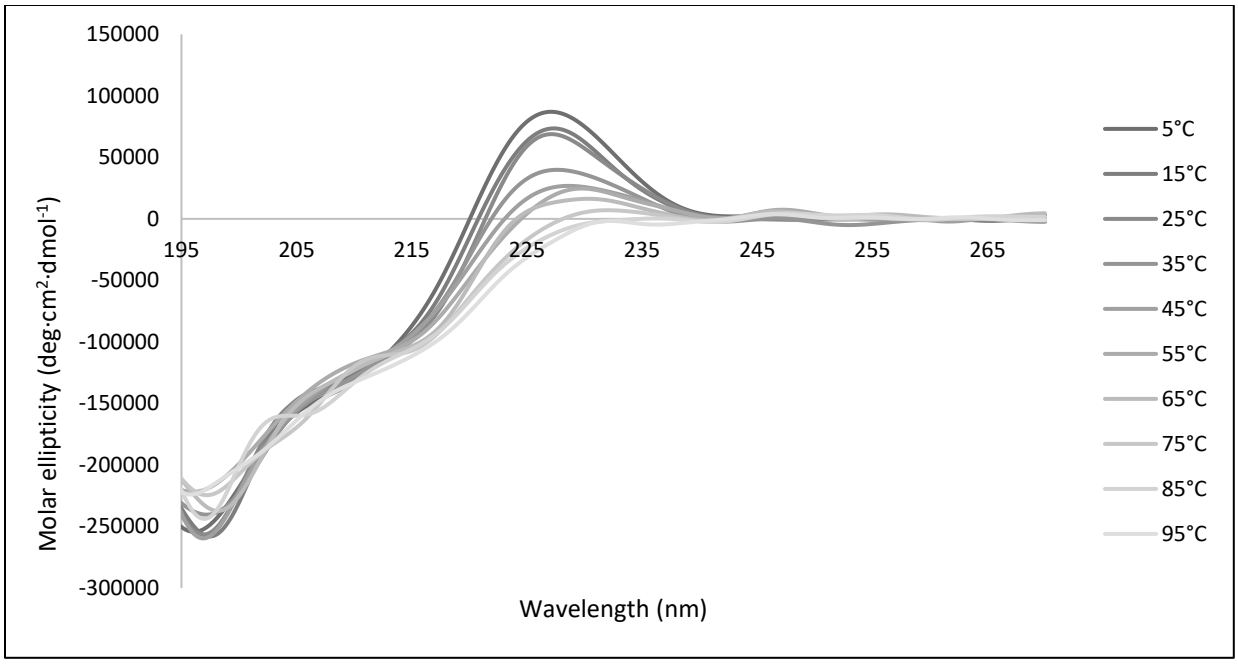

Appendix C22. CD spectra of acyclin 1 taken in 20 mM phosphate buffer, pH 6.5 at 5°C to 95°C (at every 10°C interval).

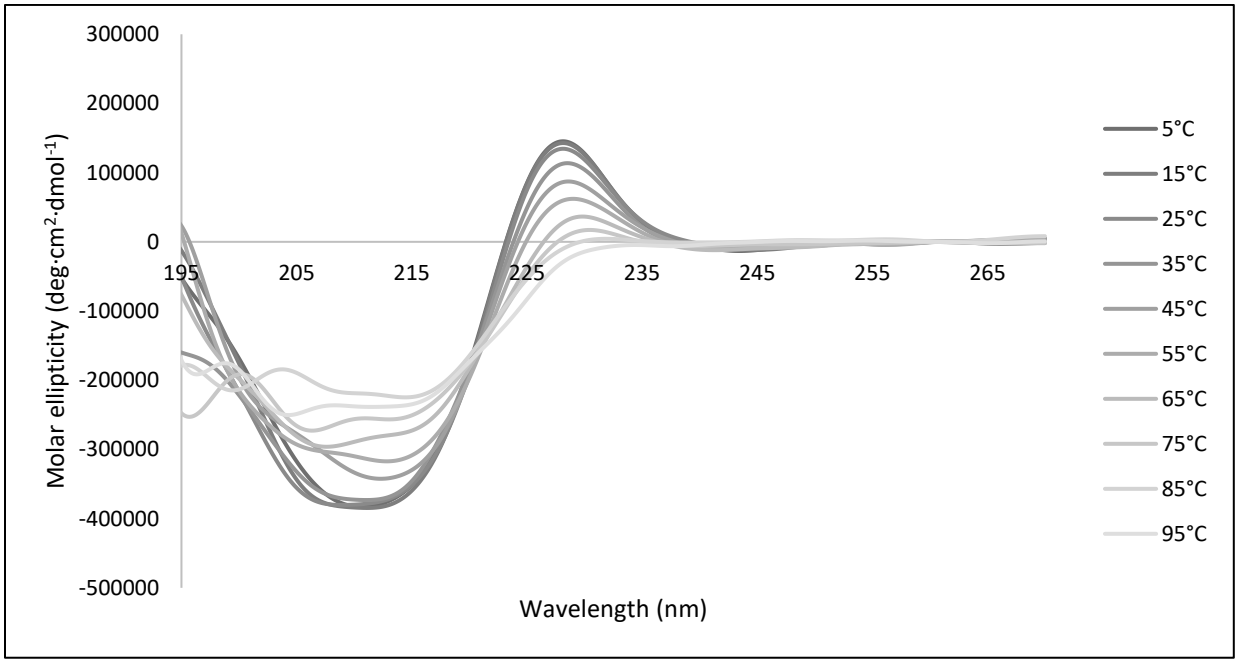

Appendix C23. CD spectra of acyclin 2 taken in 20 mM phosphate buffer, pH 6.5 at 5°C to 95°C (at every 10°C interval).

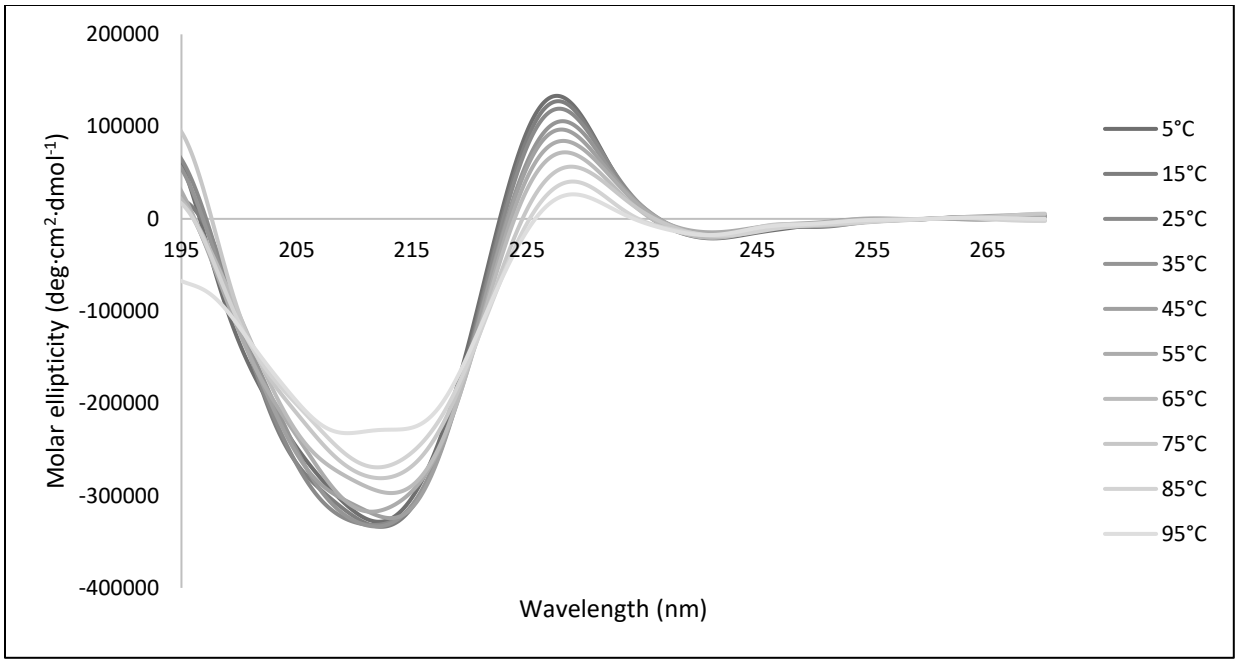

Appendix C24. CD spectra of acyclin 3 taken in 20 mM phosphate buffer, pH 6.5 at 5°C to 95°C (at every 10°C interval).

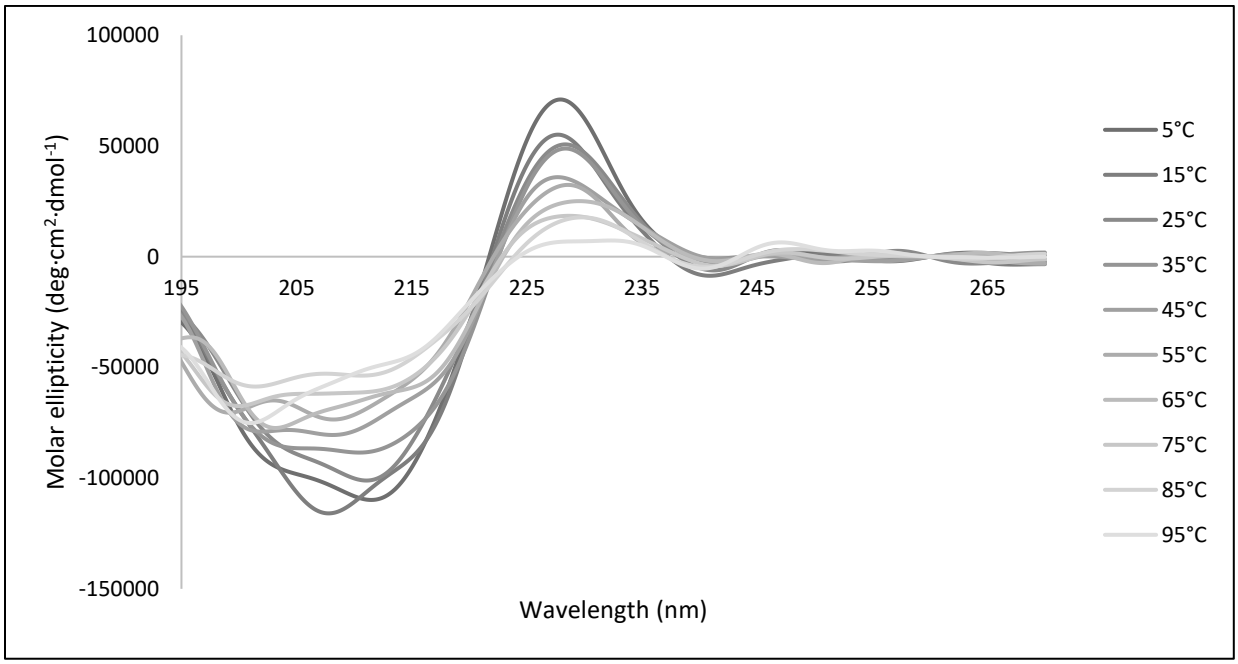

Appendix C25. CD spectra of acyclin 4 taken in 20 mM phosphate buffer, pH 6.5 at 5°C to 95°C (at every 10°C interval).

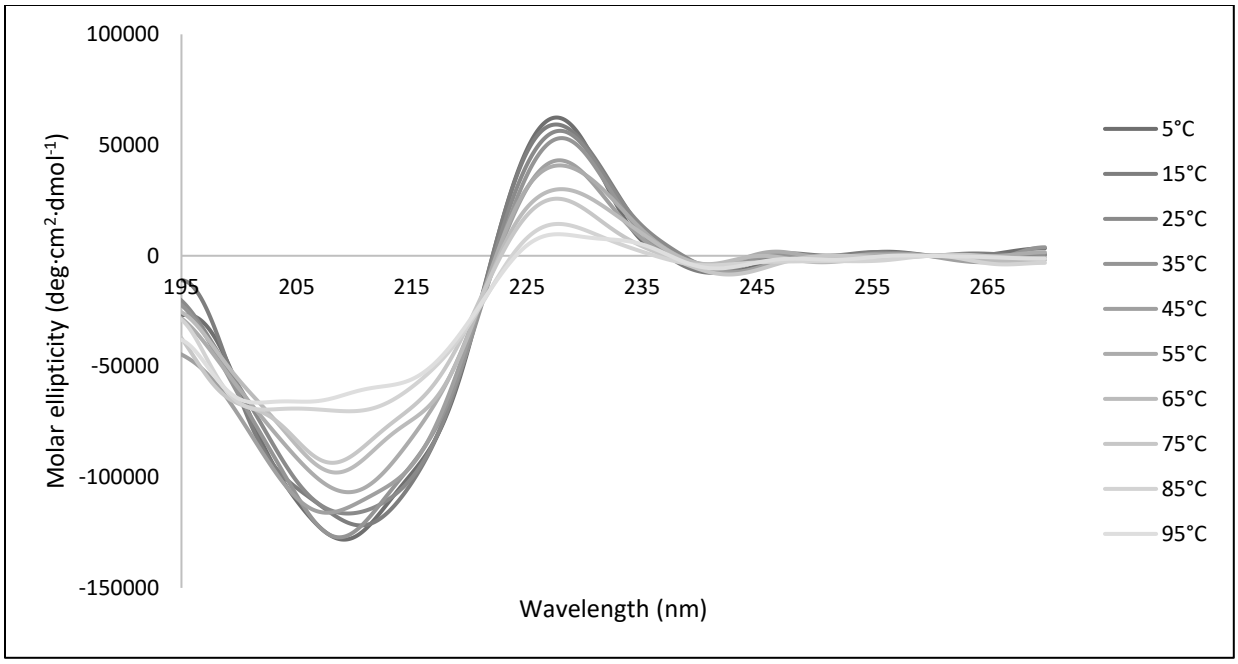

Appendix C26. CD spectra of acyclin 5 taken in 20 mM phosphate buffer, pH 6.5 at 5°C to 95°C (at every 10°C interval).

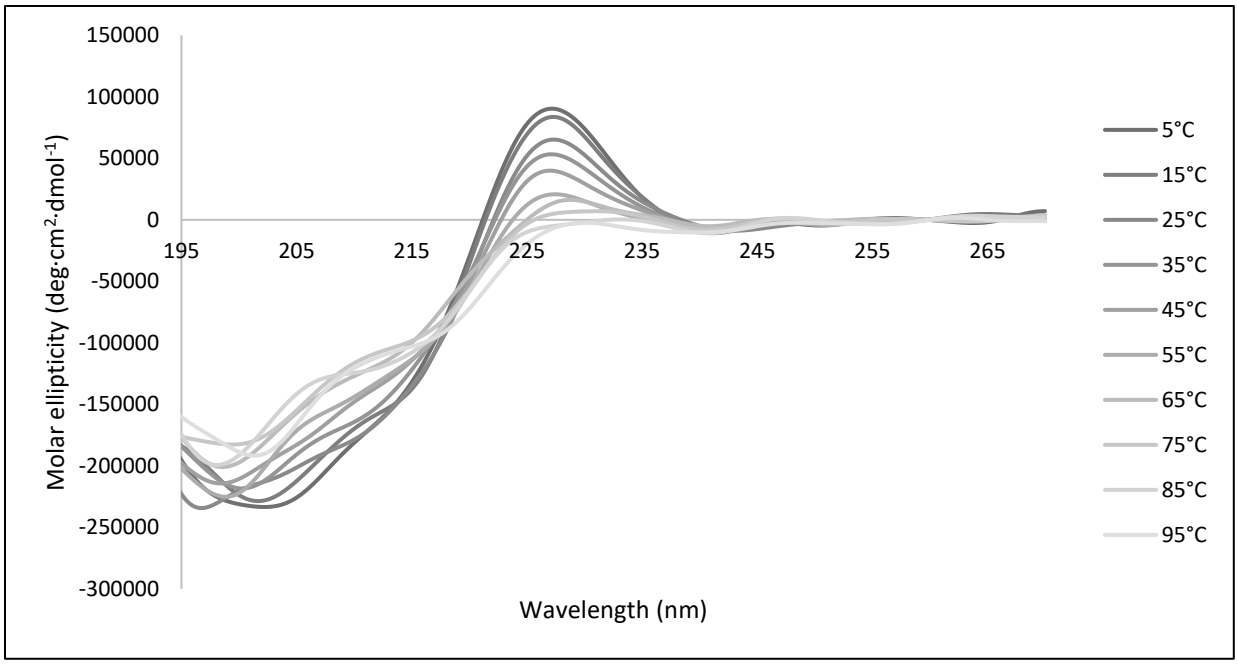

Appendix C27. CD spectra of acyclin 6 taken in 20 mM phosphate buffer, pH 6.5 at 5°C to 95°C (at every 10°C interval).

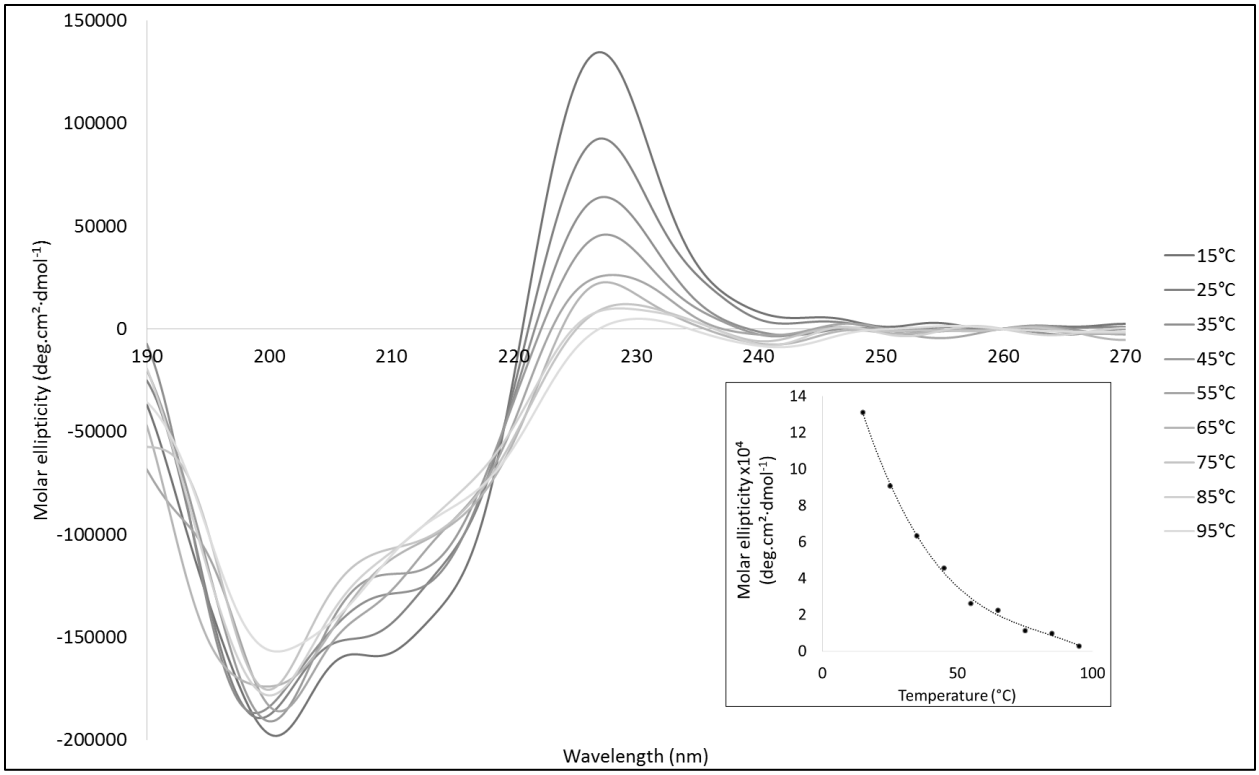

Appendix C28. CD spectra of I-RW taken in 20 mM phosphate buffer, pH 6.5 at 15°C to 95°C (at every 10°C interval). Inset: Molar ellipticity at 228 nm measured at 15°C to 95°C (at every 10°C interval) with a third-degree polynomial trend line.

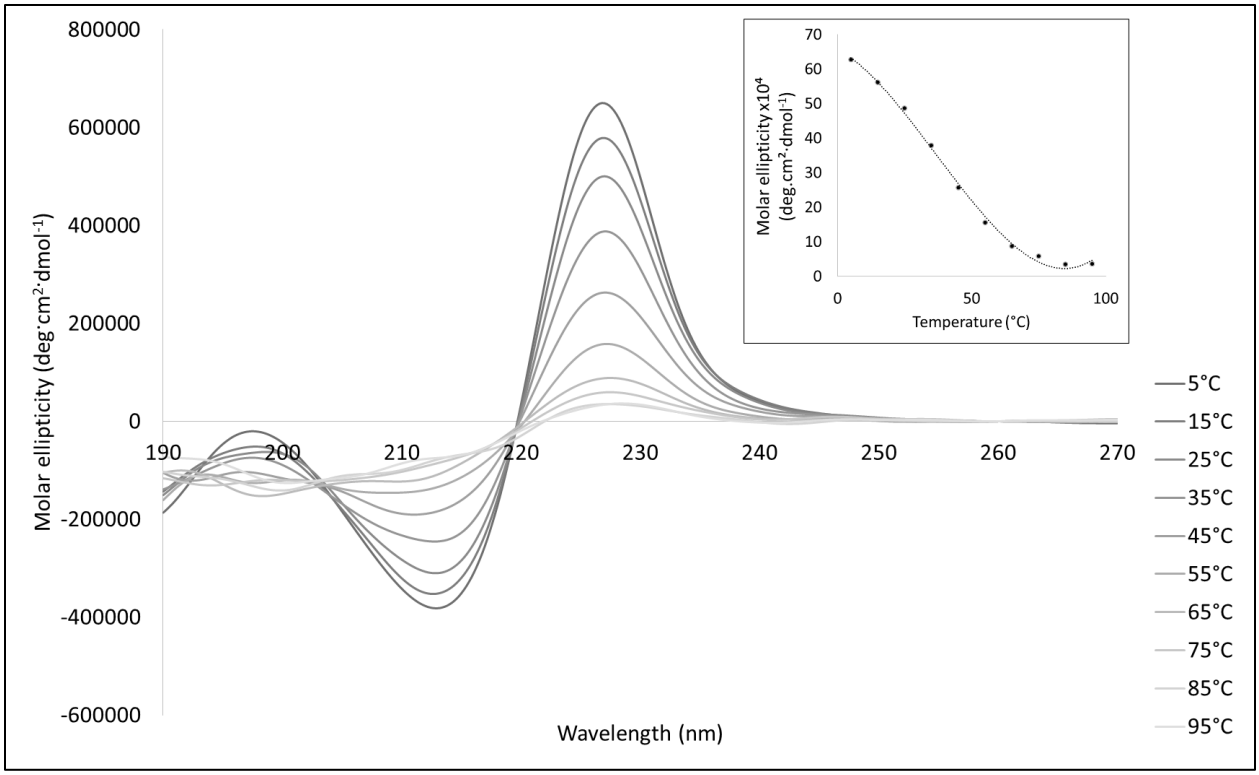

Appendix C29. CD spectra of 2-RW taken in 20 mM phosphate buffer, pH 6.5 at 5°C to 95°C (at every 10°C interval). Inset: Molar ellipticity at 228 nm measured at 5°C to 95°C (at every 10°C interval) with a third-degree polynomial trend line.

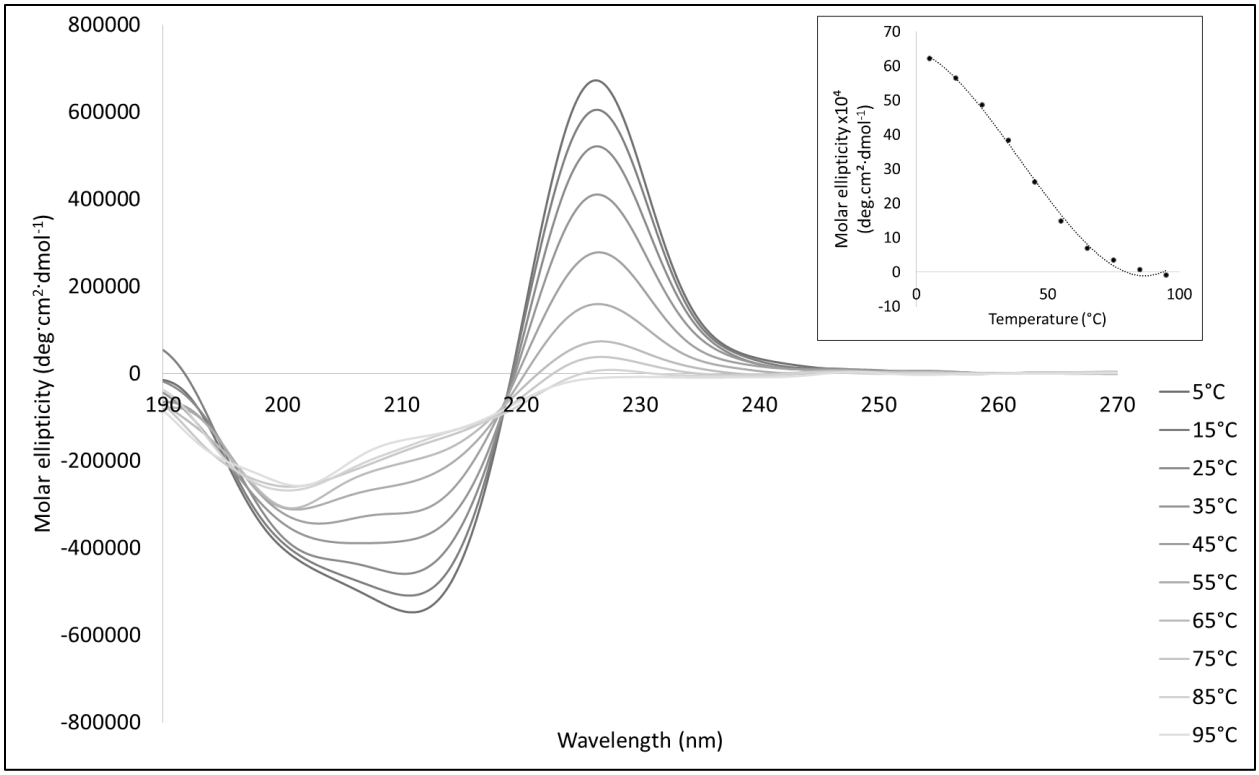

Appendix C30. CD spectra of 3-RW taken in 20 mM phosphate buffer, pH 6.5 at 5°C to 95°C (at every 10°C interval). Inset: Molar ellipticity at 228 nm measured at 5°C to 95°C (at every 10°C interval) with a third-degree polynomial trend line.

Vita

Kalkena Sivanesam

Education

Doctor of Philosophy, Chemistry, 2017
University of Washington
Seattle. WA

Masters of Science, Chemistry, 2015
University of Washington
Seattle, WA

Bachelor of Science, Chemistry, 2012
University of Washington
Seattle, WA

Bachelor of Arts, History & Biochemistry, 2012
University of Washington
Seattle, WA

Publications

Smirnov, D., Dhall, A., Sivanesam, K., Sharar, R.J. & Chatterjee, C. (2013) Fluorescent probes reveal a minimal ligase recognition motif in the prokaryotic ubiquitin-like protein from Mycobacterium tuberculosis. *Journal of the American Chemical Society*, **135**, 2887–2890.

Sivanesam, K., Byrne, A., Bisaglia, M., Bubacco, L. & Andersen, N. (2015) Binding interactions of agents that alter α-synuclein aggregation. *RSC Advances*, **5**, 11577–11590.

Sivanesam, K. & Andersen, N.H. (2016) Modulating the Amyloidogenesis of α-Synuclein. *Current Neuropharmacology*, **14**, 226–237.

Sivanesam, K., Shu, I., Huggins, K.N.L., Tatarek-Nossol, M., Kapurniotu, A. & Andersen, N.H. (2016) Peptide Inhibitors of the amyloidogenesis of IAPP: verification of the hairpin-binding geometry hypothesis. *FEBS letters*, **590**, 2575–2583.

Sivanesam, K., Kier, B.L., Whedon, S.D., Chatterjee, C. & Andersen, N.H. (2016) Hairpin structure stability plays a role in the activity of two antimicrobial peptides. *FEBS letters*, **590**, 4480–4488.